Fabrication of (bio)molecular patterns with contact printing techniques

Juan Pablo Agusil Antonoff

Tesis doctoral

FABRICATION OF (BIO)MOLECULAR PATTERNS WITH CONTACT PRINTING TECHNIQUES

Memoria presentada por

JUAN PABLO AGUSIL ANTONOFF

Para optar al grado de **Doctor en Nanociencias**

Universitat de Barcelona
Departament d'Electrònica

Programa de doctorado de Nanociencias
2010 – 2014

Tesis doctoral dirigida por
Prof. Josep Samitier Martí

Barcelona, 2015

Juan Pablo Agusil Antonoff: *Fabrication of (bio)molecular patterns with contact printing techniques*, 2015 i. e.

"Think of and look at your work as though it were done by your enemy.
If you look at it to admire it, you are lost."
— Improvement in Art – The Note-Books of Samuel Butler (1912)

We have a habit in writing articles published in scientific journals to make the work as finished as possible, to cover all the tracks, to not worry about the blind alleys or to describe how you had the wrong idea first, and so on. So there isn't any place to publish, in a dignified manner, what you actually did in order to get to do the work [...]

— Richard P. Feynman

ACKNOWLEDGMENTS

Pocas cosas en la vida son tan individuales, tan personales e íntimas como escribir una tesis. Al momento de ponerme a escribir, me di cuenta de todo el trabajo, esfuerzo, frustraciones y alegrías que me han guiado por este camino. Un camino en el que siempre he estado acompañado por gente maravillosa, apoyándome tanto emocionalmente como profesionalmente. Sé que es el final del camino al momento de buscar las palabras más sinceras para mostrar mi más eterno agradecimiento a todos los que han estado caminando conmigo.

Muchos años han pasado desde que entré por primera vez al laboratorio. Por lo mismo, me gustaría seguir estos agradecimientos cronológicamente y de ser posible ubicando a todos geográficamente dentro del laboratorio. Evidentemente mi primer y más sincero agradecimiento es para mi director y tutor de esta tesis, el Prof. Josep Samitier. Muchísimas gracias por recibirme y mantenerme bajo tu tutela. Me has dado la oportunidad de crecer profesionalmente en unas instalaciones vanguardistas y rodeado de los mejores medios para desarrollar este trabajo. Igualmente, me has permitido crecer emocionalmente al permitirme resolver los conflictos y retos que se presentaron durante mi estancia en tu laboratorio. Muchas gracias por darme esta oportunidad. Estoy infinitamente agradecido.

Continúo agradeciendo a Christian Sporer, quién me introdujo al mundo de la ciencia al momento de aceptar dirigir el proyecto para terminar mi carrera que posteriormente se convertiría en este trabajo, que felizmente, ha finalizado. Muchas gracias por darme esta oportunidad y por todos los consejos que me diste. Muy a tu manera, Elena, muchas gracias por echarme una mano cuando la necesitaba, por no dudar en invitarme a discutir alguna duda y ayudarme cuando estaba atascado en algún protocolo. A Anna Lagunas, muchas gracias por las risas, bromas y uno que otro consejo de química, ya que los consejos de moda *trash* no me aplicaban. Igualmente, muchas gracias Mònica por ayudarme cuando lo necesitaba. También me encantaría agradecer a Bea. Bea es admirable tu paz interior, tranquilidad e inmensa energía para que las cosas salgan, y salgan bien. Muchas gracias por los consejos dentro y fuera del laboratorio. Patrizia, gracias

por alegrarme el día con tu manera plácida de ver la vida. Al rey de la lluvia, del frío y de la paciencia, Juanjo, eres una gran persona. Y de igual manera me gustaría gradecer las charlas con Xavi.

Sin duda alguna los dos grandes pilares que mantienen este laboratorio son Míriam y David. Míriam, tienes un encanto y energía sin límites. Muchísimas gracias por ayudarme y enseñarme tanto, has sido una gran maestra. Espero que yo haya sido un alumno a tu nivel. De la misma manera, David, gracias por ocuparte de todos nosotros, por sentarte y discutir y por llegar a la mejor solución ante cualquier incertidumbre.

No podría haber llegado a ser uno de los "viejos" del laboratorio sin la ayuda de los que yo veía como "viejos". Por lo mismo, agradezco a la alegre y desenfrenada chamaquita Ivón, recordándome de mis orígenes. Agradezco al Dr. Caballero por su ayuda y contribución científica, por los ratos de risas y más risas. Igualmente al pragmático Jordi, con una capacidad de enfoque y de desarrollo espectaculares y con una visión única del mundo que nos rodea. Y aún estando a medio mundo de distancia, jamás olvidaré a la Evita con su alegre espíritu contagioso, al igual que la fortaleza y ayuda de Lorena y Sam. Indiscutiblemente mis ingenieros favoritos son Sergio y Óscar. Sergio, hacía falta alguien con el que pudiera comunicarme en lenguaje ingenieril dentro del laboratorio. Y Óscar, muchas gracias por toda la ayuda científica y personal que me diste, al final encontré el camino. A *frau* Stuttgart, Sabine, siempre súper atenta conmigo, compartiendo tanto tus conocimientos como opiniones que siempre valoraré. Y por supuesto, a la mujer con las mejores rodillas: Maruxa. Eres una persona espectacular y única, y nunca dudaste en echarme una mano cuando la necesitaba.

A mi "jefa" Marília, ejemplo de perseverancia y dedicación, de seriedad y de humor al mismo tiempo. Enigmática y encantadora, pero sobre todo, una maravillosa persona. Gracias por compartir conmigo tu conocimiento y maneras de ver la vida, así como hacer de cada día en el laboratorio una aventura. Como portadora del estandarte de valentía está Coco, la más fuerte y animosa del laboratorio, que constantemente me recuerda que la fuerza que necesitamos para afrontar los retos del mundo, viene de dentro de nosotros mismos.

En este maravilloso sumario de memorias incluyo a Marta, muy atenta y siempre cariñosa, dispuesta a hablar de cualquier tema. Echaré de menos a las gaviotas de bienvenida de la divertida Rossella y sus historias espectaculares regularmente rodeadas de conflictos involucrando perros. Historias que rivalizan con la intensidad y la pasión de Reyes, siempre buscando la manera de transmitir su buen humor o de aliviar tus penas, todo esto manteniendo constantemente el mejor estilo. Muchas gracias Vero, eres una chica encantadora y que constantemente me alegras. Eres un gran ejemplo a seguir, la primera en alzar la voz y buscar la solución, convenciendo al mismo

tiempo a los demás a hacer lo correcto. Recordaré siempre a los Reyes en Burgos. Maria, gracias por los ánimos y por transmitirme constantemente tranquilidad y paciencia. Y Albert, que día tras día buscabas la manera de hacerlo más divertido. Agradezco la ayuda de Juanma y los comentarios de Toni, César, Wilmer, Bogachan y José Luis que de alguna manera contribuyeron para que terminara este trabajo.

Igualmente muchísimas gracias Mateu por expresar tu interés en el trabajo que realizaba, por darme consejos y trucos y por tu apoyo en el laboratorio. Al igual que a Gizem por ayudarme en muchos experimentos. It was great to share a slice of life with you Tommy, and I hope that you find the best place to take root, you might as well run to find it. Y aunque ahora parezca un poco difícil, yo sé que tú, Margarita, saldrás siempre exitosa en todo momento. Muchísimas gracias por tus charlas tanto científicas como personales.

No me puedo olvidar el gran fichaje que eres Luis para mantener el estandarte de este laboratorio, que queda es tus manos y en las de Roberto.

Aprovecho para agradecer profundamente a la Dra. Maria Lluïsa Pérez de la Facultad de Farmacia de la Universitat de Barcelona por su incalculable ayuda tanto en conceptos de química de superficie como en temas personales. Igualmente quiero extender mi agradecimiento al Dr. José Antonio Plaza y a la recientemente graduada Dra. Núria Torras ambos del Centre Nacional de Microelectrònica por la colaboración laboral y por compartir su experiencia científica y personal contribuyendo en la finalización de este trabajo. También extiendo los agradecimientos a la Dra. María Teresa Suárez, al Dr. Alberto Hernández y a la Dra. Patricia Vázquez del Centro de Investigaciones Biológicas. I would like to thank Dr. André Bernard and collaborators from the Institute for Micro and Nanotechnology, for the development of the automatized printing tool. Muchas gracias a Isabel Oliveira y a Marina Cazorla por su flexibilidad y ayuda en la sala blanca. Finalmente agradezco al Institut de Bioenginyeria de Catalunya por la beca para realizar este trabajo.

Aunque el trabajo es vida, también hay vida fuera del trabajo. Por eso quisiera agradecer a todos mis amigos que han estado conmigo durante estos años, dándome su amor y apoyo incondicional, los fundadores de Can Rocafort: a tí Carolina, Adolfo, Edgar, Lalo, Gloria, Javi y especialmente a Alex, *vielen herzlichen Dank*, muchísimas gracias por estar en todo momento, apoyándome y dándome la bienvenida a casa.

Y finalmente, agradezco de todo corazón a mi familia, José Manuel y Mireille, mis padres y a Esteban y Sebastián, mis hermanos, que me han acompañado constantemente en los momentos más alegres y más duros de este camino. Gracias por las largas conversaciones trasatlánticas, las ideas, el apoyo y la educación y valores para así

poder terminar este gran camino. Gracias, muchas gracias. Los quiero muchísimo.

Ha sido un verdadero placer compartir tantas horas con todos trabajando en el laboratorio, asi como rodearme de esos grandes momentos fuera del mismo. Sólo espero que nuestros caminos vuelvan a cruzarse en el futuro.

INDEX

GLOSSARY

αCP	Affinity Contact printing
AEE	2-(2-Aminoethoxy)-ethanol
AFM	Atomic force microscopy
AF488	Alexa Fluor® 488
AF555	Alexa Fluor® 555
AF647	Alexa Fluor® 647
AMCA	Aminomethyl coumarin acetate
APTES	(3-Aminopropyl)triethoxysilane
BAT	Biotin alkyl thiol
BSA	Bovine serum albumin
CCD	Charge-coupled device
CMOS	Complementary metal-oxide-semiconductor
Cy3	Cyanine dye 3
DMSO	Dimethyl sulfoxide
DNA	Deoxyribonucleic acid
DPN	Dip-pen nanolithography
DWL	Direct write laser lithography
E. coli	*Escherichia coli*
EDC	1-Ethyl-3-(3-dimethylaminopropyl)carbodiimide
EDTA	Ethylenediaminetetraacetic acid
EG2OMS	2-(1-hydroxy)-ethoxy-eth-1-yl methanesulfonate
ELISA	Enzyme-linked immunosorbent assay
FITC	Fluorescein isothiocyanate
FWHM	Full width at half maximum
GOPDMS	3-Glycidoxypropyldimethoxymethylsilane
IgG	Immunoglobulin G

ITO	Indium tin oxide
μCP	Microcontact printing
MCH	6-Mercapto-1-hexanol
MHDA	16-Mercaptohexadecanoic acid
NAV	Neutravidin
NHS	N-Hydroxysuccinimide
ODT	1-Octadecanethiol
OG_{488}	Oregon Green® 488
PBS	Phosphate buffered saline
PCR	Polymerase chain reaction
PDMS	Poly(dimethyl siloxane)
PEG	Poly(ethylene glycol)
PEG_3-thiol	Triethylene glycol mono-11-mercaptoundecyl ether
PEI	Poly(ethyleneimine)
PFOTCS	1H,1H,2H,2H-Perfluoroctyltrichlorosilane
PHA	Phytohaemagglutinin
pHrodo	pHrodo™ Red
PLL	Poly-L-lysine
PMMA	Poly(methyl methacrylate)
PPL	Polymer pen lithography
PVA	Polyvinyl alcohol
RNA	Ribonucleic acid
ROI	Region of interest
SAM	Self-assembled monolayer
SAV	Streptavidin
SDS	Sodium dodecyl sulfate
SEM	Scanning electron microscopy
SiOx	Silicon oxide
SP-PCR	Solid-phase polymerase chain reaction

SPR	Surface plasmon resonance
SSC	Saline-sodium citrate
ssDNA	Single-stranded DNA
TAMRA	Tetramethylrhodamine
TRIS	Tris(hydroxymethyl)aminomethane
Tween 20	Polyoxyethylenesorbitan monolaurate
TxR	Texas Red®
UV	Ultra violet
WGA	Wheat germ agglutinin

1 GENERAL INTRODUCTION

1.1 BACKGROUND

Patterns. A pattern is a collection of forming units predictably repeated over a defined magnitude. To easily understand the reaches of such vast definition, we can rely on the information obtained by our senses. At a defined sight, our eyes and brains have been trained to recognize similar or repeated objects. The vast tiles forming the floor in a cathedral or the simple action of reading these words have been developed based on repetition. The same occurs when listening to music. The structural level forming the rhythm follows standardized and repeated units, developing the tempo. Therefore, one could argue that following such examples, patterns are a man-made inception. Yet, it comes at no surprise that most natural phenomena follows a repetition, a pattern.[1] The seasons, the leaves on the trees, the electromagnetic radiation, and even life itself follows predetermined milestones. It is quite impressive that simple shapes are repeated in nature at vastly different scales, as shown in Figure 1.1, where huge basaltic rocks, resulted from cooling lava have a near perfect alignment as the wax cells formed by the bees in a beehive, mimicking the disposition of carbon atoms in a monoatomic graphene sheet.

Figure 1.1: **Tessellation in nature.** From larger to smaller, (A) basalt columns forming the Giant's Causeway on the coast of Northern Ireland, (B) honeycomb, and (C) graphene. Scale bars = 2 nm on (C) and 0.3 nm in the inset. Adapted from [2–4].

Two main approaches have been developed to take advantage of repeated units. In science, researchers use cumulative data to guarantee the functionality and repeatability of their approach. The data is obtained by repeating the same experiment under the same conditions in hope that the results are comparable. The first approach uses a single substrate derivatized with repeated units to create multiple testing sites, hence, obtaining a repeated multi-analysis system on

a single platform. The second approach uses repeated localizations with different testing elements, creating a diverse multi-analysis platform. In the case of biochemical assays, the approach to detect the presence of certain antigens has been traditionally done with Enzyme-linked immunosorbent assay (ELISA). This assay uses antibodies fixed to the walls of a well plate which are later inundated with the solution carrying the antigen. After the binding event, a secondary enzyme-conjugated antibody is added to the grafted antigen. A colorimetry reaction is usually produced after the substrate is added to the reaction well, obtaining a direct relationship between the amount of antigen and the resulting color. This assay requires repetitions as well as controls, accounting for a large amount of materials and reagents needed to test a single antigen.

The miniaturization of such assays provides an alternative to reduce cost, maximize efficiency, and increase repeatability. An alternative would require smaller wells for the assays, yet hydrophobic and hydrophilic interactions would provide physical limitations. An alternative was found with patterns, miniaturized patterns. Today, these miniaturized patterns, referred to as microarrays, consist on immobilized (bio)molecular motifs constrained in minuscule areas on a solid substrate. These fixed spots provide up to thousands of reaction sites for parallel detection. Micropatterns were first developed to study the interaction between Deoxyribonucleic acid (DNA) strands and the study of the genome. Afterwards, this technology was used to create miniaturized protein patterns.[5] Today, this technology is essential for large-scale and high-throughput biological and biochemical studies.

Figure 1.2 summarizes the broad range of applications based using functional or analytical microarrays. Immobilized antibodies or antigens provide reaction sites to detect the presence of proteins when inundated with a solution. The repeated addressable motifs on these analytical microarrays help confirm the presence of such protein, while different features allow the detection of multiple proteins on a single substrate. While antibodies and antigens are specific to reduced number of complementary elements, a protein microarray provides a wider range of target identification, including other proteins, lipids, drugs, enzymes or nucleic acids. Alternatively, small molecule and carbohydrate arrays have also been developed to understand their interaction with proteins.[6]

Single-feature microarrays are routinely reproduced at many laboratories using various contact, non-contact, or alternatively methods. The foundation is to transfer a biomolecule in a solution onto a solid substrate obtaining a defined feature shape. Two main anchoring formats have been established to define the feature size. Either the biomolecule is placed with a transporting mechanism on the exact position, coupled with the correct surface chemistry, or the substrate

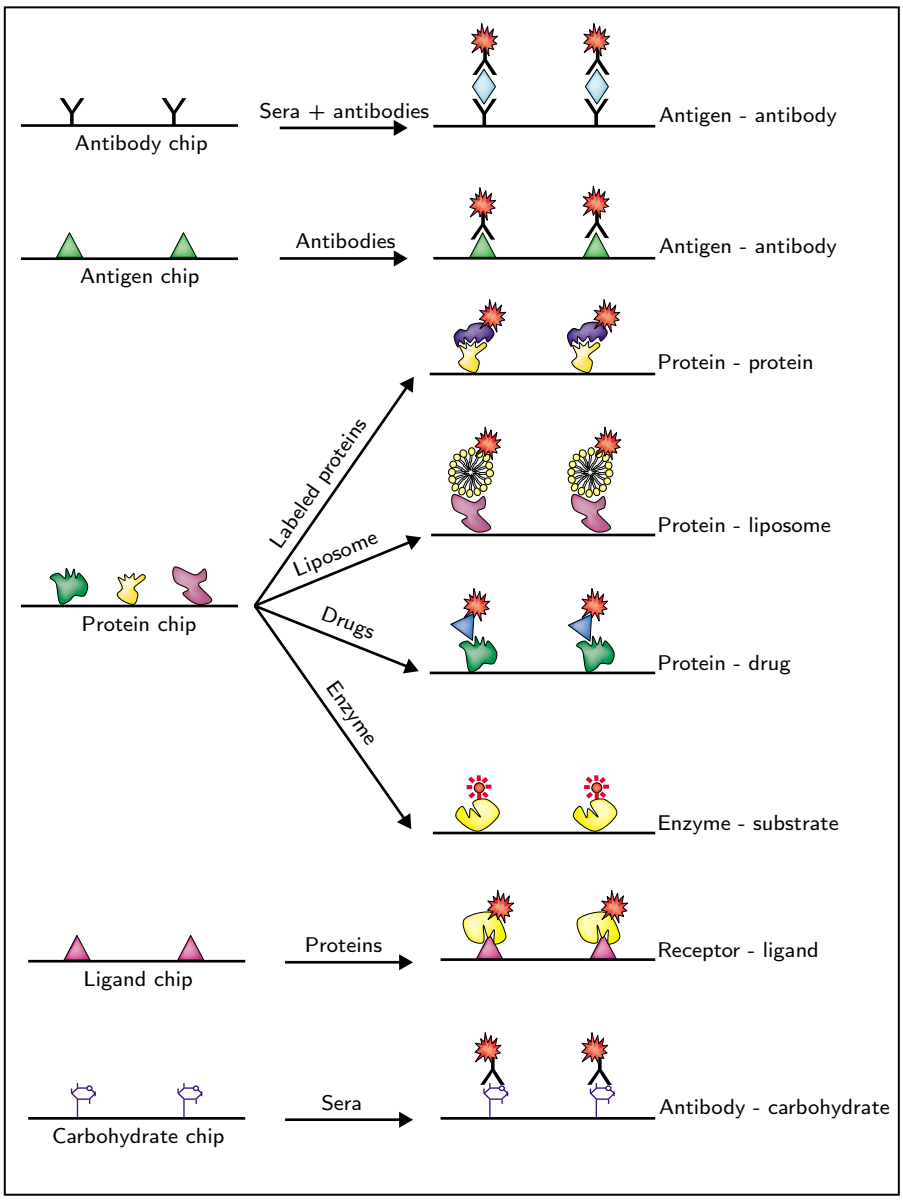

Figure 1.2: **Functional and analytical protein arrays.** Functional arrays are used to assay biochemical interactions between proteins and various other reagents. Analytical arrays are simply used to detected proteins in a complex sample. Adapted from [6].

is previously derivatized into selective zones where the biomolecule later binds. Both formats have advantages and disadvantages.

Three fabrication methods are described in Figure 1.3. The initial approach shown in Figure 1.3A results from the direct placement of fluorescent-labeled antibody over glass using a previously coated stamp. The resulting patterns mimic the protruding features from the stamp, translating the spatial distribution towards the microarray. This patterning technique called Microcontact printing (μCP) will we discussed in depth in Chapter 2. The fluorescent images in Fig-

ure 1.3B and C were obtained by limiting the contact between different protein solutions and the substrate using a thin polymeric stencil. By interchanging the stencils, Zhao *et al.*[7] were able to create complex patterns. Finally in Figure 1.3D, spots of reactive groups were deposited on selected coordinates and were later left to react with a selective molecule. The interesting point of this experiment is the direction of the chemical reaction towards the selected site. This type of reactions will be thoroughly explained in Chapter 3.

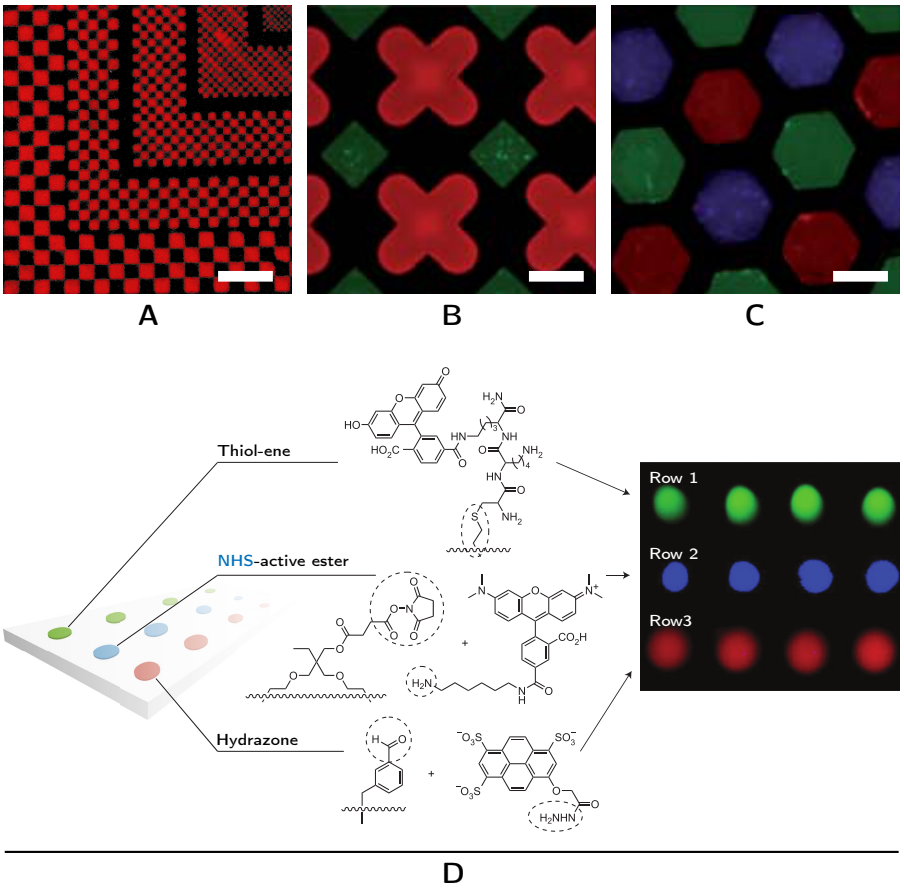

Figure 1.3: **From single to multiplexed protein arrays.** (A) Direct placement of rhodamine-labeled antibodies over glass by contact printing. (B) Two albumin proteins conjugated with green and red fluorophores, patterned using an elastomeric stencil. (C) Both, red and green albumins, along with an avidin derivative labeled with a blue fluorophore, again immobilized using a stencil. (D) Multiplexed array obtained using either thiol-ene, hydrazone or NHS-active ester chemistries. The orthogonality directs the reaction of either rhodamine-NH_2, fluorescein-alkyne, and Cascade Blue-$NHNH_2$ represented in red, green, and blue, respectively, towards the desired moiety. Scale bars = 50 µm in (A) and 100 µm in (B) and (C). Adapted from [7–9].

1.2 GENERAL OBJECTIVES

This thesis, entitled Fabrication of (bio)molecular patterns with contact printing techniques, aims to expand the current contact replication techniques for microarray fabrication. To achieve this purpose, the research was based on the improvement and maturation of current patterning techniques such as μCP and Polymer pen lithography (PPL), and the development of new replication methodologies. Several (bio)molecules were patterned on multiple substrates to fabricate complex and functional microarrays. The spatial distribution as well as the functionality of such features were extensively characterized to guarantee a robust platform for further studies.

This work is structured in three experimental chapters on three independent subjects. Each chapter contains a thorough introduction to situate the reader on the correct basis and current state-of-the-art, followed by an experimental section describing all the protocols and methodologies followed to achieve the objective. The results are presented and discussed extensively before arriving to an independent conclusion for each chapter. To avoid confusion, the terms printing, patterning or stamping were used indefinitely to refer to the same action: the transport of an ink to a substrate via a printing mechanism. The thesis ends with a section presenting the overall achievements and conclusions obtained during this work.

In addition, Appendix A presents all the fabrication and characterizations techniques, coupled with the DNA strands and software codes for data analysis to guide the reader.

1.3 BRIEF DESCRIPTION AND SPECIFIC OBJECTIVES EACH CHAPTER

Each chapter followed a unique objective, yet the backbone of this thesis resides on the extrapolation and approaches of a single subject: micropatterns.

Chapter 2 presents the basic parameters and applications of μCP, a micropatterning method, along with its main limitations. An automatized printing tool was assembled to expand the applications of this technique as well as overtaking the main limitations. Alkanethiols, alkylsilanes, proteins, antibodies, and DNA were patterned on various substrates and characterized with fluorescence and Atomic force microscopy (AFM). The objective of this Chapter is to expand the applications of μCP by developing an automatized printing tool and characterize the entire patterning process.

In Chapter 3, the improvements found in the previous chapter were applied to fabricate miniaturized protein microarrays on anchored microparticles. An alternatively patterning process, PPL, was implemented using the automatized printing tool to print various proteins onto constricted areas. A novel liberation method was explored to free the anchored microparticles, maintaining protein functionality. Fluorescence microscopy was extensively used to characterize every fabrication step. The main goal of this Chapter is the development of a robust miniaturization method to fabricate biomolecule microarrays on anchored microparticles and their subsequent liberation, safeguarding the localization and functionality of the printed motifs.

Finally, in Chapter 4, two contact replication methods were developed and expanded to copy DNA master arrays. The first approach transported complementary hybridized DNA strands to an intermediate substrate, to be rehybridized and replicated onto a third substrate, transferring the information and distribution from the master array. The second approach synthesized *in situ* long DNA chains, which were subsequently transferred to an intermediate substrate and reconstructed via enzymatic growth. Afterwards, the newly built strands were transferred to a third substrate, obtaining a replica of the initial array. The purpose of this chapter is to transport both, the chemical information and spatial distribution of DNA features present on various microarrays. Hybridization and *in situ* synthesis were used to transport the coded information.

1.4 REFERENCES

[1] Ball, P. *Nature's patterns: a tapestry in three parts. 1: Shapes*. Oxford University Press, Oxford (2009). URL http://scholar.google.com/scholar?hl=en&btnG=Search&q=intitle:Nature's+Pattens:+a+tapastry+in+three+parts#2

[2] Dolya, S. 'Giants - a real miracle of nature' (2011). URL http://sergeydolya.livejournal.com/

[3] Ball, P. 'How honeycombs can build themselves'. *Nature*. URL http://www.nature.com/doifinder/10.1038/nature.2013.13398

[4] Xue, J; Sanchez-Yamagishi, J; Bulmash, D; Jacquod, P; Deshpande, A; Watanabe, K; Taniguchi, T; Jarillo-Herrero, P; and LeRoy, BJ. 'Scanning tunnelling microscopy and spectroscopy of ultra-flat graphene on hexagonal boron nitride.' *Nature materials*, 10 (4) (2011) 282–5. URL http://www.ncbi.nlm.nih.gov/pubmed/21317900

[5] Inerowicz, H; Howell, S; Regnier, F; and Reifenberger, R. 'Multiprotein immunoassay arrays fabricated by microcontact printing'. *Langmuir*, 18 (13) (2002) 5263–5268. URL http://pubs.acs.org/doi/abs/10.1021/la0157216

[6] Zhu, H and Snyder, M. 'Protein chip technology'. *Current Opinion in Chemical Biology*, 7 (1) (2003) 55–63. URL http://linkinghub.elsevier.com/retrieve/pii/S1367593102000054

[7] Zhao, S; Chen, A; Revzin, A; and Pan, T. 'Stereomask lithography (SML): a universal multi-object micro-patterning technique for biological applications.' *Lab on a chip*, 11 (2) (2011) 224–30. URL http://www.ncbi.nlm.nih.gov/pubmed/21113523

[8] Bernard, A; Renault, JP; Michel, B; Bosshard, HR; and Delamarche, E. 'Microcontact Printing of Proteins'. *Advanced Materials*, 12 (14) (2000) 1067–1070. URL http://doi.wiley.com/10.1002/1521-4095%28200007%2912%3A14%3C1067%3A%3AAID-ADMA1067%3E3.3.CO%3B2-D

[9] Gupta, N; Lin, BF; Campos, LM; Dimitriou, MD; Hikita, ST; Treat, ND; Tirrell, MV; Clegg, DO; Kramer, EJ; and Hawker, CJ. 'A versatile approach to high-throughput microarrays using thiol-ene chemistry.' *Nature chemistry*, 2 (2) (2010) 138–45. URL http://www.ncbi.nlm.nih.gov/pubmed/21124405

2

PATTERNING WITH AN AUTOMATIZED MICROCONTACT PRINTING TOOL

This Chapter presents a general overview of the Microcontact printing of (bio)molecules onto different substrates. The main focus is to state the current technological achievements as well as the limitations of the technique. Further on, the development of an automatized Microcontact printing tool presented the opportunity to create multiplexed patterns over large areas and different substrates overcoming some of the inherent limitations of the technique.

2.1 BACKGROUND

The creation of miniaturized patterns on diverse substrates has been an important goal in current material science research. Each feature of the pattern presents an individual active site to study interactions when the entire pattern is exposed to different environments. Miniaturized patterns present great advantages in their fabrication and function compared to macroscopic functional surfaces. Multiple and independent probes, less reagent use, and low waste production are some of the most interesting properties these patterns have.

Traditionally, miniaturized patterns have been fabricated using photolithographic techniques. This top-down method uses a beam of Ultra violet (UV) light and a photomask to fabricate a pattern on a substrate previously coated with a photoresist.[1] The spatial and sequential distribution of the pattern is controlled by the design of the photomask. The miniaturized pattern is fabricated in a single exposition to light. This technology has proven the best approach in the fabrication of miniaturized circuits for the microelectronics industry. Yet, it is worth mentioning that photolithography is a rather expensive technique, requiring specialized equipment and clean room facilities. This fabrication technique limits the size due to aberrations and diffusion of the UV light, and restricts the chemistry of the patterned features.

Limitations apart, with the great leap in the microelectronics industry, scientist borrowed several steps in photolithography and applied them in the fabrication of biomolecular micropatterns. So far, DNA and simple-peptide microarrays have been the only biomolecular features synthesized using photolithography.[2, 3] This limited range of biomolecular applications is due to the inherent process of photolithography. UV light and the photoresist, coupled with organic solvents and developers, may jeopardize the functionality or structure of other biomolecules.[4]

Today, direct placement is the alternative to create biomolecular microarrays. This technique consists in the transportation of adsorbed (bio)molecules on a solid base with the desired geometry to the substrate to be patterned. This approach descends from the work of Kumar and Whitesides[5]. In their work, a rubber stamp with several features ranging from the centi- to the micrometer scale was loaded with an alkanethiol solution. Afterwards, the stamp was brought in contact with a gold surface and the adsorbed alkanethiol molecules were transfered in the areas where the stamp contacted the surface. The final gold features were obtained after the etching of the unpatterned areas the gold substrate. The micrometer scale of the obtained features, coupled with the printing mechanism helped coined the term Microcontact printing.

2.2 PRINCIPLES OF MICROCONTACT PRINTING

Microcontact printing (μCP) was developed as an alternative to photolithography. This fast, easy, and straightforward fabrication method uses an elastomeric stamp with protruding features to transport an adsorbed (bio)molecule onto a desired substrate. The entire μCP process is represented in Figure 2.1. First, a master with the chosen features is fabricated. Photolithography and micromachining are the main fabrication methods to create the master, usually from a silicon substrate. Then, a prepolymer mixture is poured over the master. The liquid nature of the material allows it to reach even the smallest features, creating an exact replica of the master. After the polymerization of the prepolymer, the stamp can be peeled from the master. The flexibility of the material allows it to be bended and separated without damaging the replicated features. Afterwards, the stamp is exposed to the "ink". It is imperative to take into account the physical properties of the elastomeric stamp, as this influences the adsorption of the ink on its surface. Hydrophobicity and hydrophilicity play a major role on the solvent that can be used with the desired (bio)molecule. The inked stamp is rinsed with the same solvent used as carrier of the ink and dried afterwards. This removes any multilayers formed during the inking process, leaving a single layer of adsorbed (bio)molecules on the surface of the stamp. Finally, the stamp is brought in contact with the chosen substrate.

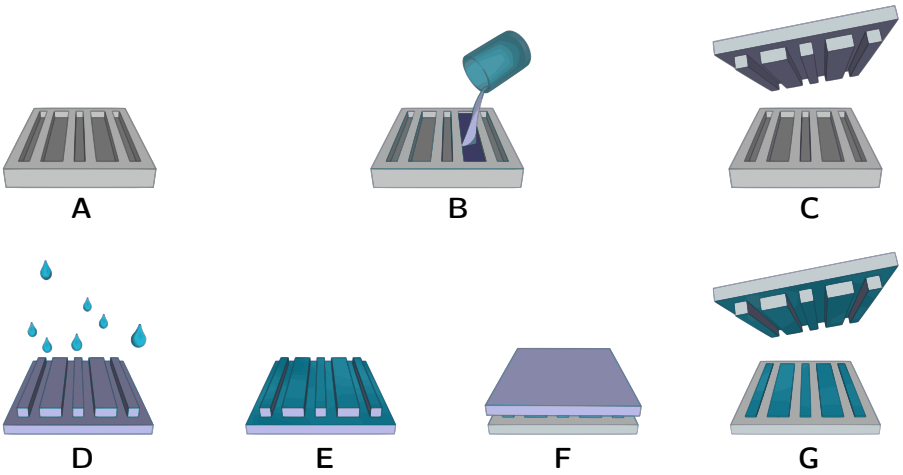

Figure 2.1: **Sequential steps in μCP.** (A) A microfabricated master with the desired features is selected and liquid prepolymer mixture is poured over it (B). (C) Once solidified, the stamp is peeled from the master, and inked with an ink solution (D). The excess of the ink is removed from the stamp (E), and it is brought in contact with the appropriate substrate (F). (G) The obtained pattern replicates the protruding features of the stamp. The stamp can be inked again and used to print more substrates (D - G).

The areas where the stamp contacts the substrate will interact with the adsorbed ink. If the substrate presents a higher affinity to the ink than the stamp, the ink will transfer. This substrate-ink affinity is the result of electrostatic forces, van der Waals interactions or the creation of chemical bonds.

2.2.1 *Elastomeric stamps*

Taking in consideration the substrate-ink affinity, the next important element of μCP is the stamp. The stamp must be flexible enough to form conformal contact with the substrate yet maintain sufficient mechanical stiffness to preserve its shape and pattern distribution at the micro- and nanoscale. Many organic polymers have been used to fabricate stamps for μCP, yet the most widely used is Poly(dimethyl siloxane) (PDMS).[6]

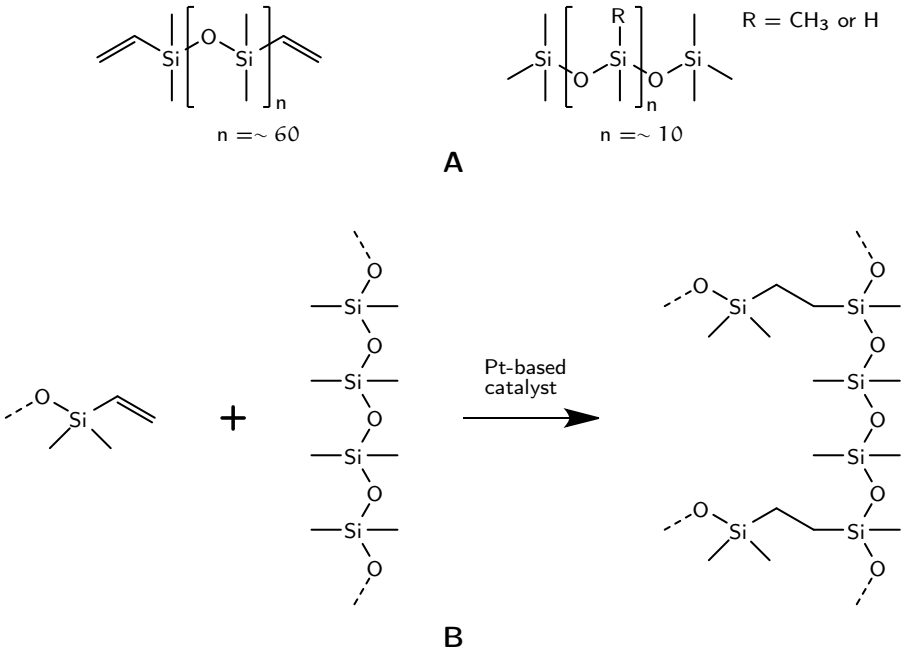

Figure 2.2: **Molecular structure of the PDMS polymer.** (A) The polymer precursor is formed by a mixture of siloxane oligomers of different lengths terminated with vinyl groups. (B) The platinum-based catalyst is added to cross-link the oligomer mixture.[7]

PDMS is a flexible elastomer prepared by the reaction of a vinyl-terminated prepolymer and a poly(dimethylhydrosilane) cross-linker with the regulation of a platinum-based catalyst.[7] Figure 2.2 shows the molecular structure and binding sites of the prepolymer to form the final polymer. The polymerization occurs at elevated temperatures or at long periods of time after mixing. Typically, a mixing ratio of 1:10 *w/w* catalyst and siloxane mixture is used. The resulting prod-

uct is a transparent material with a Young's modulus, (E), ranging from 1.32 MPa to 2.97 MPa depending on the curing temperature.[8] With this, the PDMS stamp can deform and adapt to the irregularities of the substrate over areas of cm^2, yet maintain the mechanical integrity of the replicated pattern. The flexibility of the material allows the stamp to be peeled from the substrate after printing without damaging the patterned features.

An important physical property is the hydrophobicity of the bulk and the surface of PDMS. This limits the inks or carrier solutions that can be used during μCP. When Kumar and Whitesides[5] printed the alkanethiol on gold, the carrier solvent was ethanol, a non-polar organic solvent. For that same reason, ethanol was able to coat the entire PDMS stamp. Non-polar solvents also permeate the PDMS, dragging the molecules into the bulk of the stamp. This feature creates an ink reservoir in the stamp and permit the flow of ink molecules to the substrate while printing. Even if the choice of ink solution is based on an organic solvent, one has to be careful to choose the correct one, as PDMS swells in some organic solvents, modifying the size and distribution of the replicated patterns, which will be inevitably transfered to the substrate when printing.[9]

On the contrary, water-soluble inks do not wet the surface of the stamp and do not permeate the bulk of the stamp. Many biological compounds are repulsed by the PDMS, creating an inhomogeneous monolayer on top of the stamp; hence, the printed patterns will be incomplete. Another interesting effect of the hydrophobic surface of the PDMS is the denaturation and irreversible adsorption of proteins.[6] To create a suitable stamp to pattern polar inks, the surface of the PDMS can be modified. Oxidizing the first layer of the stamp to form hydoxyl groups is the first choice to produce a hydrophilic stamp. This can be done with standard oxygen-plasma oxidation, forming a glass-like layer on the PDMS stamp. This procedure opens many routes to tune the surface of the stamp.[10]

2.2.2 *Printing and fabrication of patterns*

μCP masters fabricated with photolithography can create a vast number of feature geometry and distribution. Once the PDMS stamp is peeled from the master, it is inked with the solution to be printed. The ink molecules will be adsorbed on the surface of the stamp, and with certain inks, the molecules flow towards the bulk of the stamp. To print the molecules, the surface of the substrate must be more energetically favorable than staying adsorbed on the surface of the stamp.[11] Successful μCP depends on the optimization of the immobilization of the probed (bio)molecules taking into account their chemical and biochemical differences, and their interaction with the

chosen substrate. Gold, glass, Silicon oxide (SiOx), and polymeric substrates are widely used in μCP.

When printing thiols on gold, the *quasi*-covalent bond created between the sulfhydryl group and the gold form a strong and stable interaction.[12] In the case of proteins, different approaches have to be followed. For example, in Figure 2.3 the Fluorescein isothiocyanate (FITC)-Poly-L-lysine (PLL) and laminin A patterns were formed with several PDMS stamps previously coated with a 10% Sodium dodecyl sulfate (SDS) solution, an anionic surfactant which prevents the repulsion of the proteins due to the hydrophobic nature of the PDMS.[13]

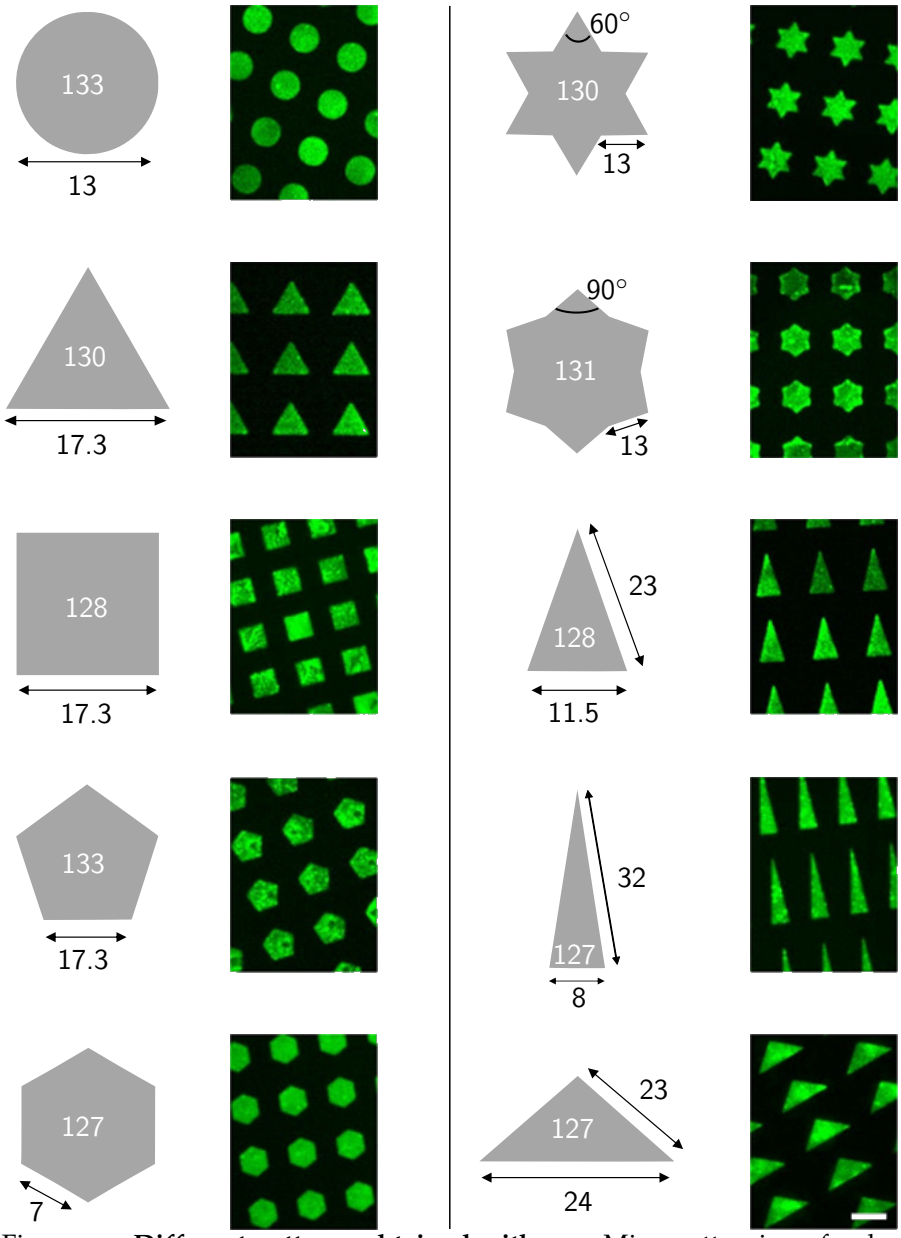

Figure 2.3: **Different patterns obtained with μCP.** Micropatterning of polygon arrays of FITC-PLL and laminin A with various feature shape and length. Dimension units are μm (black) and μm^2 (white). Scale bar = 20 μm. Adapted from [13].

Figure 2.3 also presents several patterns in which the stamps can be fabricated. Jang and Nam[13] required features with different geometries maintaining a similar contact area. Bench-top μCP provided the best alternative to create the vast number of arrays required for their work.

Although μCP is a straightforward and simple technique, several considerations have to be taken into account to obtain the best patterns with the maximum reproducibility.

2.2.2.1 *Main Limitations of Microcontact printing*

The quality of the pattern is limited by two main elements: the configuration of the stamp and the spread of the ink across the surface while printing. A PDMS stamp can replicate single ionic steps ranging from $3-5$ Å in height[17], yet in practice, μCP requires a stamp designed to withstand its own weight and pressure applied during printing. Any deformation of the stamp will result in a modified pattern and decrease reproducibility.

The design of the stamp is decisive in obtaining a desired pattern, this prevents the deformation of the stamp under normal μCP conditions. The design must follow the parameters represented in Figure 2.4A. The height, (h), of the protruding features divided by their width, (w), defines the aspect ratio of a pattern. If the height, (h), is greater than the distance, (d), between features $(h \gg d)$, pairing and buckling of the features might occur (Figure 2.4B). Pairing occurs when the features clump together after peeling the stamp due to electrostatic forces or during the inking process due to capillary actions. Buckling results when the features collapse towards the substrate while printing. On the contrary, sagging (Figure 2.4C) arises when the height is much smaller than the distance between features $(d \gg h)$. In this case, the roof of the stamps crashes towards the substrate transferring the ink (bio)molecules on regions where patterning is not intended.

A correct design guarantees the mechanical integrity of the of the stamp during μCP, however, the pattern may be affected if a correctly designed stamp is used under high printing pressure. In Figure 2.5A the force applied to a stamp of 8000 inverted pyramids show a profound correlation with the feature size. In the graph, two compression regimes were found depending of the applied force. The feature size change radically from ~0.5 μm when 1.25 mN were applied to a feature size of ~2.0 μm under a force of 17.5 mN.[18] Taking advantage of this, Xia and Whitesides[20] used high pressure during μCP to increase the lateral size of the printed features while at the same time, decrease the gap between the them.

Ink compatibility and the correct stamp have been discussed previously, yet another parameter affects the pattern: the flow of the ink when the stamp contacts the surface of the substrate. It is important

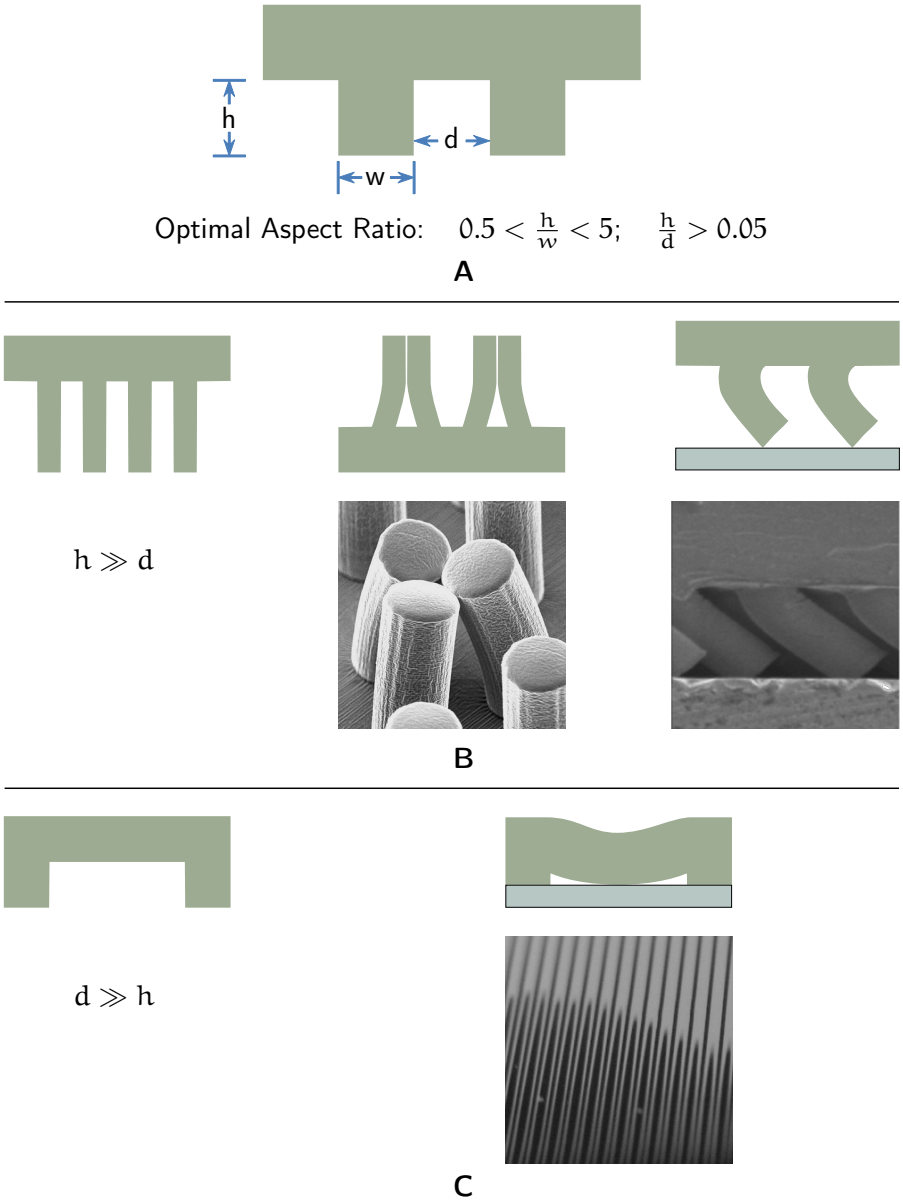

Figure 2.4: **Schematic representation of a PDMS stamp.** (A) The correct aspect ratio is crucial in the design of a PDMS stamp.[1] (B) Pairing[14] or buckling[15] can occur with high aspect ratios. (C) Sagging occurs with low aspect ratios.[16]

to note that not all molecules get adsorbed on the PDMS stamp the same way. Small non-polar molecules such as alkanethiols and alkylsilanes can travel within the polymeric matrix shortly after the stamp is exposed to the ink. This flowing mechanism is repeated outwards when the stamp contacts the substrate. The molecules diffuse at the stamp-substrate interface. Bergmair *et al.*[19] obtained various feature sizes from the same rigid stamp inked with a 1-octadecanethiol solution when printing at different times (Figure 2.5B). The size of the gold rings increases for longer contact times.

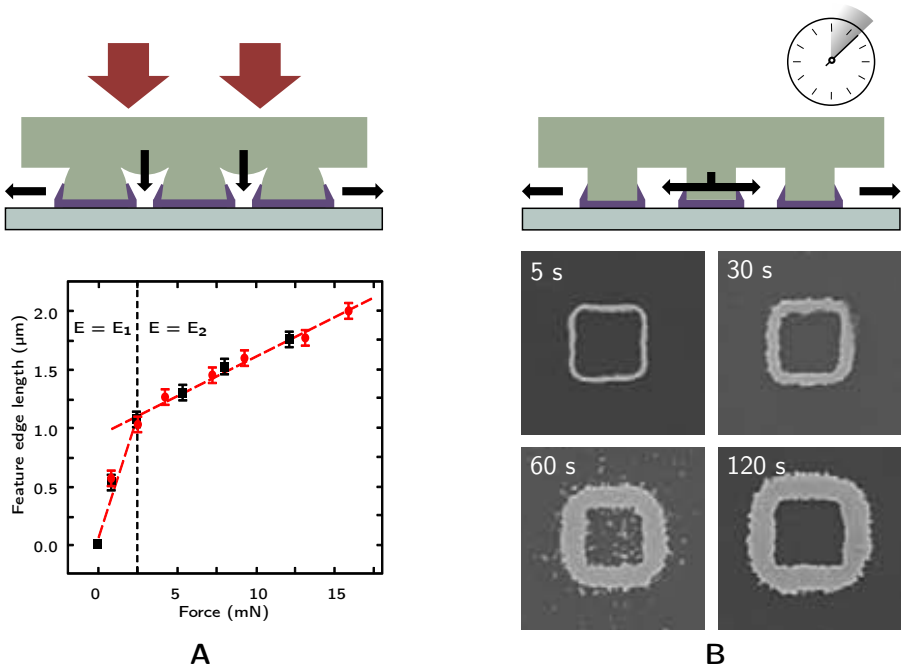

Figure 2.5: **Pressure and printing dwell times affect the printed pattern.** (A) Soft elastomeric stamps deform under pressure, transferring an altered pattern to the substrate. [18] (B) The stored ink in the stamp flows towards the substrate when printing.[19] Scale bar = 1 µm.

On the other hand, molecules with higher molecular mass remain adsorbed solely on the surface of the stamp. Once in contact with the substrate, the pattern is defined by direct placement as diffusion is greatly limited.

Several proposals have been presented to overcome the limitations of µCP. Bessueille *et al.*[21] developed submerged microcontact printing. This approach uses elastomeric stamps with high aspect ratios and limited to non-water-soluble inks to create patterns that otherwise would collapse during patterning. The patterning process follows the same steps as in traditional µCP, but with an aqueous media functioning as a support for the roof of the stamp. Their findings suggest the possibility of stamps with an aspect ratio of 100:1.

Another interesting approach to prevent collapsing or diffusion is the use of flat stamps.[22] This technique creates the final pattern form a previously patterned PDMS slab. This approach has produced submicrometric protein patterns.[23]

Although these two approaches solve some of the problems associated with traditional µCP, their limitations, whether they use non-water-soluble inks or molecules that only attach to the surface of the stamp reduce their applications. For such reasons, the design and deformation of the stamp, together with the spread of the ink during

patterning have to be studied and standardized when using traditional μCP.

2.2.3 *Patterning of various inks*

μCP exploits the spontaneous adsorption of molecules from a solution or ink pad to a stamp, and the transport of such molecules to a substrate. The main goal is to create a single, ordered, and homogeneous layer of the chosen molecules and its uses thereafter. The most widely used molecules in μCP are those which form a Self-assembled monolayer (SAM).

2.2.3.1 *Self-Assembled Monolayers*

SAMs are semi-crystalline, single-molecule films over a two dimensional plane. The molecules that form SAMs have two elements used to form the film: a head domain that binds to the substrate and an oriented tail that form structures away from the substrate.[11] The head group must have a strong affinity to the substrate to keep the film anchored in its place. This affinity results in the electrostatic or chemical bonds between molecules. Contrarily to the head, the tail group must be less energetically favored to attach to the substrate. Tail groups are commonly formed by alkyl chains with a functional moiety at the end. This moiety can regulate the properties of the substrate where the SAM is attached (Figure 2.6A).

The wetting, bio-compatibility, adhesion, or passivation of the substrate can be tailored with the functional moiety.[24] SAMs are easy to prepare as they form spontaneously and ordered on the substrate. This configuration grants them robustness and decreases the formation of defects. The tail allows the control of the film thickness by ~1 Å by tuning the length of the alkyl chain.[25]

Patterning SAMs opened the way for μCP, and continue to be a powerful choice to control the properties of the patterned substrates. Starting with Kumar and Whitesides[5], alkanethiols remain the most widely used SAM producing molecules.

The head group of these molecules consists of a carbon-bonded sulfhydryl ($-C-SH$). When in contact with noble metals, such as gold or silver, the sulfhydryl group looses the hydrogen and creates a coordinated bond with the substrate (Figure 2.6B). If the availability of SAM-forming molecules is high, the monolayer will continue to grow until the substrate is completely covered (Figure 2.6C) conferring it with different physical and chemical properties. The initial and most common application of alkanethiols SAMs is the creation of a protective film to fabricate patterns of gold on a surface. This film forms a barrier between the underlying gold and any chemical enchant, resulting in features of gold with a micro- and nanoresolution with demonstrated biosensing and microelectronics applications.[26]

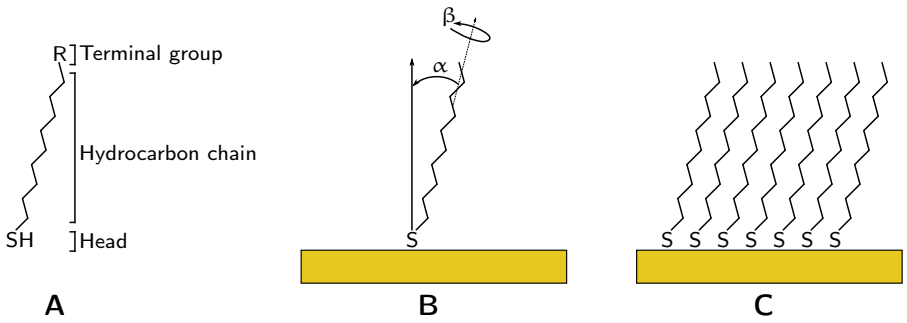

Figure 2.6: **Alkanethiol self-assembled monolayer.** (A) Basic structure of a alkanethiol molecule with the head formed by carbon-bonded sulfhydryl, followed by a hydrocarbon chain and a terminal group which can contain a reactive moiety. Please refer to Figure 2.7 for examples. (B) Orientation of a decanethiol molecule adsorbed on gold in a standing up conformation where $\alpha = 30°$ and $\beta = 55°$.[27] (C) The SAM can adopt a close-packed configuration.

Alkylsilanes also form SAMs.[28] As with alkenethiols, alkylsilanes have two main structural elements: head and tail. In this case, the head is formed by a tetravalent single bonded silicon atom. As represented in Figure 2.7A, three of the four single bonds of the silicon atom are alkoxy groups (X). The most used are the methoxy $(-O-CH_3)$ and the ethoxy $(-O-CH_2-CH_3)$ groups. The last single bond of the silicon atom forms the anchoring location for the tail. The tail consist in an aliphatic carbon chain which ends with a functional group.[29] The length of the tail can be tailored as with alkenethiols to tune the thickness of the monolayer.

To form an alkylsilane SAM, the substrate requires active moieties to substitute the alkoxy groups and create a bond. Glass, SiOx, and metal oxides present hydroxyl $(-OH)$ groups on their surface (Figure 2.7B). This group reacts with the alkoxy moiety from the alkylsilane molecule creating a covalent $-Si-O-Si-$ bond (Figure 2.7C). It is worth noting that the alkoxy groups between different molecules may react creating a bridge independent from the substrate. This can lead to the formation of multiple alkylsilanes layers on the substrate.

Both, alkanethiols and alkylsilanes are widely used in μCP. This patterning technique generates a SAM when the inked PDMS features of the stamp contact the substrate. With this, only the contacted regions are covered with the SAM and the unstamped areas remain unmodified. The new functional groups grafted on the substrate, apart of providing new chemical and physical properties, can work as anchoring platforms for subsequent funtionalization. The reactive groups can create covalent bonds with other organic and inorganic compounds, some of the most interesting: biomolecules.

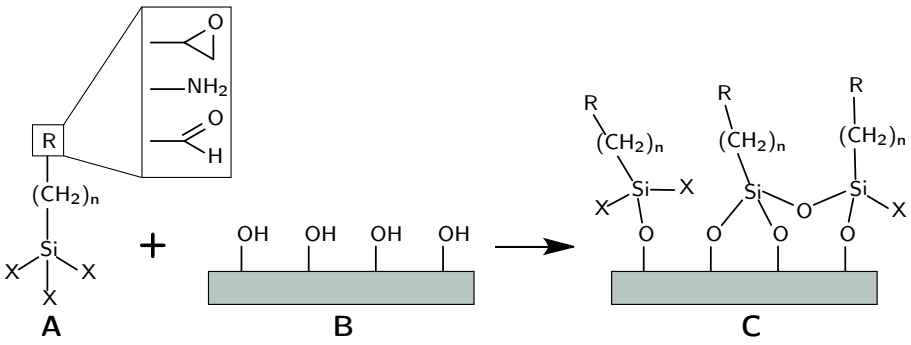

Figure 2.7: **Alkylsilane self-assembled monolayer.** (A) Basic structure of an alkylsilane with at least one carbon to silicon bond. The aliphatic carbon chain can contain a terminal functional group as a place for further reactivity. The scheme shows three possible reactive groups (R) epoxy, amine, or aldehyde. (B) SiOx, glass or metal oxide surfaces contain hydroxyl groups which replace the alkoxy moiety (X), forming a close-packed monolayer with a covalent bond (C).

2.2.3.2 *Biomolecular inks*

Biomolecular patterns on solid substrates have been used in a wide range of biomedical applications. Proteins, antibodies or DNA are excellent candidates for μCP. Their large molecular mass helps form and maintain well-defined patterns since the diffusion during the patterned process is exiguous. Still, several important parameters have to be taken into consideration in advance. First, depending on the characteristics of the biomolecule, the surface of the stamp must be customized so that the affinity of the biomolecule is higher to the substrate than to the stamp. Secondly, the temporary binding of the biomolecule to the stamp should not cause conformational changes or denaturation. And lastly, the active sites of the biomolecules should remain exposed towards the surface of the substrate. This promotes the anchoring of the biomolecule to the when contacting the substrate.

James *et al.*[30] introduced in 1998 the μCP of proteins directly on a substrate. A PLL ink was used to coat a plasma-activated PDMS stamp which was later used to print an activated glass cover slip. The electrostatic interaction between the protein and glass proved sufficient to hold it on site. When the PDMS stamp is covered with a protein ink, the non-polar dependencies of the proteins reversibly bind to the stamp, forming a monolayer. When the inked stamp contacts the substrate, the proteins transfer.

Proteins have been printed on diverse substrates to study their interaction with other biomolecules or more complex systems as live cells. Schmalenberg *et al.*[31] used plasma activation to graft laminin lines to Poly(methyl methacrylate) (PMMA). The initial surface acti-

vation was necessary for the physisorption or the proteins to the stamp to obtain a correct transfer of the biomolecules. Rozkiewicz *et al.*[32] developed various spatially and geometrically controlled patterns with collagen-like proteins onto aldehyde-terminated SAMs. The SAMs were produced to create active regions for the proteins to bind over Au or SiOx substrates. Renault *et al.*[33] developed Affinity Contact printing (αCP). This printing technique permits the simultaneous capture of different proteins on a single stamp, then, the stamp is contacted with the desired substrate to create a multiple-protein array. The transfered proteins had a 95% recognition signal, opening the way for high-throughput, protein screening systems.

In the case of the Immunoglobulin G (IgG) antibody complexes, the biomolecules adsorb to the surface of the PDMS stamp through van der Waals interactions. Electrostatic forces guide the transfer from stamp to substrate with an efficiency in the contact zones greater than 99%.[34] Rabbit IgGs were patterned on a cover glass as the foundation of a specific immunoreaction. The pattern was exposed to europium-doped gadolinium oxide ($Eu{:}Gd_2O_3$) nanoparticles coated with anti-rabbit IgG. Fluorescence and Scanning electron microscopy (SEM) demonstrated the use of these nanoparticles as biolabels. [35] In another study, μCP was used to patten parallel lines of anti-mouse and anti-human IgGs to create a biosensing immunoassays platform. Both lines were rotated by 90° creating a checkered pattern. Immunofluorescence was used to characterize the assay.[36] LaGraff and Chu-LaGraff[37] compared the amount of IgGs grafted via μCP or by submerging the substrate in the IgG solution. Their results show a greater transfer of IgGs when using μCP, and the IgGs retained their functionality. Reaching the limits of μCP, Renault *et al.*[38] used precise location to probe single antibodies on surfaces. High-resolution μCP generated FITC labelled rabbit IgGs patterns from 600 nm down to 40 nm.

The electrostatic interactions between DNA and PDMS allow the patterning of such biomolecule. Xu *et al.*[39] used surfactant-modified DNA to create patterns on glass cover slips. The hydrophobic interactions between surfactant and substrate proved sufficient to maintain the biomolecules grafted in place. Hybridization with a fluorescent complementary strand was used to characterize the pattern. Thibault *et al.*[40] fabricated easy to implement, low cost DNA patterns by direct μCP. The hybridization signals from the μCPed arrays proved 10-times more sensitive compared with other arrays constructed via conventional spotting technology.

Many immobilization and patterning strategies have been developed, creating systems to fabricate and develop protein, antibody, and DNA microarrays, as well as biosensors, and cell, drug, and biocompatibility studies. The strategy must take into account effectiveness, cost, repeatability, and biomolecular compatibility. Bench-top

Microcontact printing offers various advantages to generate these patterns, yet several challenges still remain in this patterning field. For instance, the deformation of the stamp under loads and the spread of the ink while printing pose big obstacles. Multiple ordered patterns in the same substrate is rather limited, and the alignment between stamp and substrate is non-existent.

The goal of this part of the thesis is to face some of these challenges with the aid of an automatized Microcontact printing tool to create multiplexed patterns over large areas on various substrates.

2.3 AUTOMATIZED MICROCONTACT PRINTING

2.3.1 *The need of automatized Microcontact printing*

There are huge interests in the development of automatized patterning techniques to easily reproduce the results obtained with benchtop μCP. These interests include the transferring the printed patterns during basic scientific research towards industrial applications or as bases to create complex patterns for advanced research. As μCP has been traditionally a manual process, the application of the chosen ink to the stamp, the guidance of the stamp into contact with the substrate, and the exertion of pressure are all affected by human imprecision. This imprecision leads to errors.

The automation pursuits the standardization of the several critical parameters affecting the quality of the patterns obtained during μCP. The printing pressure and time, the stamp loading and the localization of the substrate are the most complex parameters to control during the printing process. Several groups have developed different μCP tools depending on their particular needs. The complexity of these systems vary greatly, hence, three main parameters were chosen to compare the tools (Figure 2.8A):

1. Printing requirements: In this section, the characteristics of the stamps and aligning machinery are presented. Many tools require complex PDMS stamps to print. Four fabrication methods are presented. The first one includes the use of a casting tool to shape a backbone directly on stamp where it is fixed in the tool. The second method, describe the design and fabrication of patterned PDMS membranes. A third method calls for a magnetized stamp fabricated with iron powder. The last one requires no modification of the stamps. Also in this section, the different methods to align the stamp and substrate are presented. Some tools use Moiré patterns, others physical grooves, and a last one, a printing head fixed on a ball-joint.

2. Actuating systems: The actuation is defined by the mechanism in which the tool locates and drives the stamp towards the substrate. Fluid mechanics, direct mechanical force, magnetic field, and weight are the four printing mechanisms described throughout the bibliography.

3. Monitoring systems: Several schemes were developed to track the position and pressure while the tool is printing. Adapted microscopes and cameras represent the optical monitoring mechanisms. Vacuum and direct contact between substrate and stamp embody the force actuation. The controlled force actuation generated the pressure between substrate and stamp. Thus, the pressure could be inherently regulated.

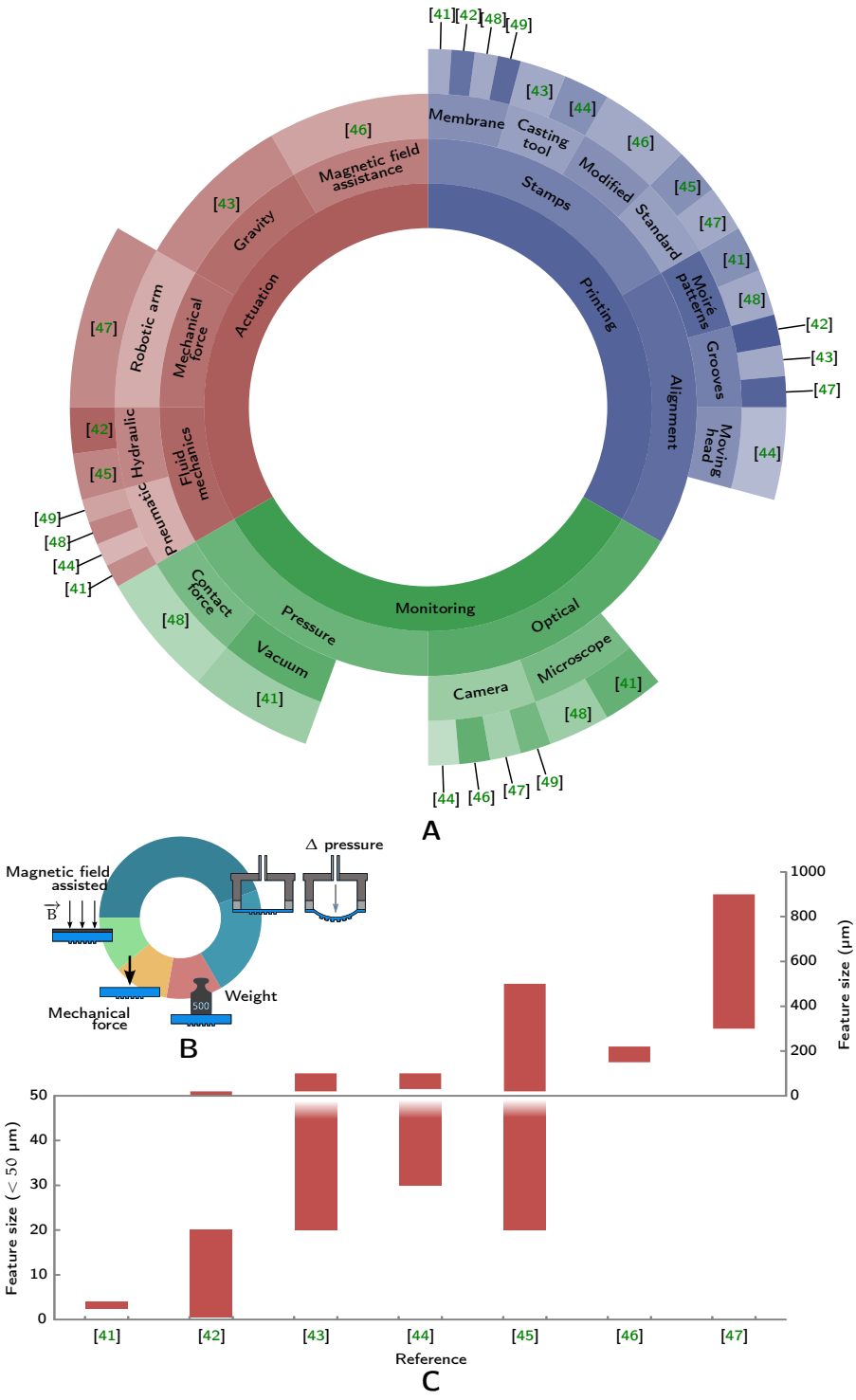

Figure 2.8: **Comparison between different µCP tools.** (A) Chart presenting the characteristics of the published and commercial µCP tools following three main classifications: Actuating system, printing requirements, and monitoring systems. (B) Of the nine tools, six use fluid mechanics to create the force to print. Magnetic fields, direct mechanical force, and applied weight are the other actuating mechanisms. (C) Minimum and maximum printed feature size at different scales.

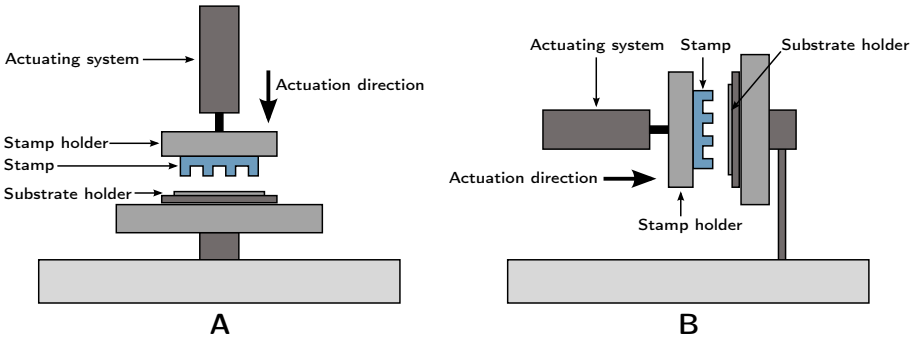

Figure 2.9: **Basic automatized μCP mechanisms.** (A) Vertical and (B) horizontal designs for automatized printing tools. Different actuation mechanisms exert the force to direct a fixed stamp towards an immobilized substrate.

Figure 2.9 presents a simple schematic summarizing the function of a vertical and a horizontal automatized μCP tools. Several actuating mechanisms have been developed and their function is to transport a fixed stamp towards an immobilized substrate. The actuation mechanisms can be group into two groups: manual or automatized actuation. This moving part is often denominated as the printing head. Hydraulic and pneumatic presses, weight, and magnetic fields have been used to accomplish the translation. Regularly, all of the automatized printing systems rely on PDMS stamps to create the patterns. To fix the stamp to the printing head, vacuum, machined holders or simple glue have been used in some systems. Alternatively, some stamps are fabricated directly into the printing head, minimizing any lateral displacement. Similar approaches have been developed to immobilize the substrate to a required position on a dedicated holder. Finally, some automatized patterning tools also include sensing peripherals to monitor the printing force using pressure sensors or by regulating the actuation. Coupled microscopes or cameras are also reported, and their use is to monitor the real-time position of the stamp.

Elloumi-Hannachi *et al.*[45] developed a simple approach. Their work presents a portable, easy to sterilize device. It consists on a fabricated syringe plunger with an enlarged head connected to another commercial syringe through a silicon tube filled with water. A 40 mm petri dish with the PDMS stamp is fixed under the mobile head. The user manually actuates the syringe, pushing the plunger of the second syringe with the stamp towards the substrate. No pressure or imaging system is present. Various volumes of water were injected to compare their results. With this system, the authors patterned fibronectin lines from 20 μm to 500 μm on a petri dish.

Another manual arrangement is presented by Trinkle and Lee.[43] This μCP tool uses a system that uses exact constrains and small contact area to fabricate highly repeatable positions. This system is called kinematic coupling. This same system is used to fabricate and fix the

PDMS directly in the plate of a complementary mold. Fluorescent IgGs were patterned with a resolution of ~50 µm on glass slides. The printing pressure was produced with a weight placed on top of the system. As the stamps are fabricated directly into the complementary chuck, the possible patterns are limited.

Choonee and Syms[42] developed a straightforward hydraulic µCP system. It consisted of a molded PDMS membrane with the desired pattern sandwiched between a two-piece ring holder. The membrane-holder assembly was placed on top of a hydraulic chuck and water was injected. The pressure was applied on the back side of the membrane which caused it to balloon towards a substrate located on top of the set-up. 1-hexadecanethiol was used to pattern gold with a resolution of 10 µm. It is worth mentioning that the ballooning effect creates distortions on the pattern as the contact between stamp and substrate is not constant. This mechanism had neither optical nor pressure monitoring systems.

More complex systems have been created. Cau *et al.*[46] assembled a µCP system with automated stamp loading, inking, drying, and cleaning all controlled with a magnetic field perpendicular to the stamp. The PDMS was mixed with iron powder to create a magnetic stamp. A dynamometer was used to calibrate the printing pressure and a two-camera system provided simultaneous visualization of the stamp and the substrate. Cyanine dye 3 (Cy3) was printed in features of ranging 150 to 200 µm.

Bou Chakra *et al.*[44] assembled an elaborate printer that consists on a mobile head fixed on a flexible coupler with a ball-joint. This spherical bearing allows the stamp to be located parallel to the substrate. The printing head is directed towards the substrate with a pneumatic actuator. The contact is regulated with screws sticking out between the stamp and substrate. The PDMS stamp is directly fabricated on the stamp holder and inked with an implemented spray nozzle. A fixed camera with zoom constitute the imaging system. Cy3 features between 30 to 100 µm were printed.

Instead of building a printer form scratch, Takulapalli *et al.*[41] modified a photolithography mask aligner. The stage of the device was altered to hold a PDMS membrane with lines of 1.5 µm. Using a microfluidic inking cartridge the stamp was exposed to fluorescein labeled thymidine phosphoramidite. Afterwards, a nanomachined substrate with pillars ranging from 500 to 50 nm was aligned using Moiré patterns. The interior of the printing stage was vacuumed to bend the stamp towards the substrate. When in contact, air at 20 psi was injected on the backside of the stamp to finish the printing process.

The most complex system was recently published. Using a selectively compliant articulated robotic arm, McNulty *et al.*[47] printed ω-mercaptoundecyl bromoisobutyrate on gold to obtain features ranging from 300 to 900 µm. The robotic arm had a mobile camera to rec-

ognize etch marks on the substrate and alignment marks of $\geqslant 50$ µm on interchangeable stamps. These marks were used to guide and print. This system required simple PDMS stamps with uniform thickness glued on a holder fixed with vacuum to the robotic arm. An inking and drying station was used to ink the stamp.

It is interesting to mention that Kim *et al.*[50] use a µCP tool to locate quantum dots on flexible and conducting surfaces to create a fully functional display. Unfortunately, the specifications of such printing system are not mentioned.

Lastly, two commercial µCP tools are currently available, the EVG© 6200 µContact Printer[48] and the GeSim© µContact Printer[49]. Both use the same PDMS membrane approach, are pneumatically actuated, and have dedicated inking and drying stations. Optical microscopes are used to align the stamp and the substrate. Resolutions from 5 µm sown to 50 nm have been achieved.

Figure 2.8B summarizes the different actuating systems of the µCP tools. It is important to note that most of the printing tools rely heavily on fluid mechanics (hydraulic or pneumatic) to print. The fluid was used either to move a piston or to bloat a PDMS membrane. In the second case, the resulted patterns may suffer distortions due to the non-constant contact between stamp and substrate. Pressure is also applied by the direct position of weight on top of the ensemble. This method is quite simple yet the placement and removal of the weight is controlled by the user. Unintended errors might occur while handling the system.

The maximum and minimum size of the printed features of the published µCP tools are compared in Figure 2.8C. The scale of the $y-$axis in the graph is separated to differentiate the range in which the tools can work. The lower chart is a zoom of the top chart showing a range from 0 up to 50 µm. The top chart has the whole range from 0 to 1000 µm.

To assure a homogeneous transfer of the pattern, the elastomeric stamp has to be brought into conformal contact with the substrate. One important difficulty consists in doing so without trapping air bubbles and avoiding the collapse of the stamp by applying high pressure. Since µCP is usually a manual process, the results depend on the experience of the researcher, hence, the process is difficult to standardize. These difficulties set the bases to develop an automatized µCP tool. The prototype was developed in collaboration with Prof. Dr. André Bernard and colleagues at the Institute for Micro and Nanotechnology from NTB Interstate University of Applied Sciences in Buchs, Switzerland (`http://institute.ntb.ch`).

2.3.2 *Description of the automatized Microcontact printing tool*

Three main pillars were identified and the prototype was shaped around the inherent requirements of each one:

1. Stamps: A flexible, inert, easy to pattern, and transparent elastomeric polymer was required. The best material was found to be PDMS. This polymer would be used to create stamps of a total patterned area of $\sim 10 \times 10$ mm^2.

2. Inks: A broad range of inks were selected, including hydrophobic alkylthiols, biotinylated inks or biomolecules.

3. Substrates: The stamping area was defined from 10×10 mm^2 up to 25×75 mm^2. Gold, glass, SiOx, and polymers represented the predominant materials.

Some other technical parameters to facilitate the use of the prototype were established. First, the stamps and substrates had to be easy to mount and interchangeable, yet the relative position between stamp and substrate should remain fixed during the patterning process. These characteristics allowed the creation of a wide range of patterns in a single substrate, or the replication of the same pattern along many substrates. To pattern at the precise position, a transparent stamp was preferred to ensure the possibility to coordinate samples during consecutive patterning processes. The alignment can be facilitated with alignment marks on both, the stamp and the substrate.

The pressure and the printing time had to be controlled. With this, the pressure had to be applied homogeneously over the whole substrate excluding air bubbles, with a printing time adjustable from a few seconds to hours. Finally, the printing reproducibility had to be better than 5 µm during consecutive printings, guarantying high reproducibility.

2.3.2.1 *Description of the mechanical parts*

The prototype was designed as a bench-top equipment composed of two main parts: the actuating and monitoring elements. A scheme of the tool with the main parts is presented in Figure 2.10. The entire set-up was fixed on a bulky platform. A rotation stage and a pillar with the printing head, were fixed directly onto the platform. The stamp holder was located on top of the rotation stage and the printing head had the stamp holder and a Complementary metal-oxide-semiconductor (CMOS) camera. The printing head and the substrate were vertically aligned. All the set-up rested on a vibration absorbing base, to prevent smearing of the ink while printing due to external fluctuations.

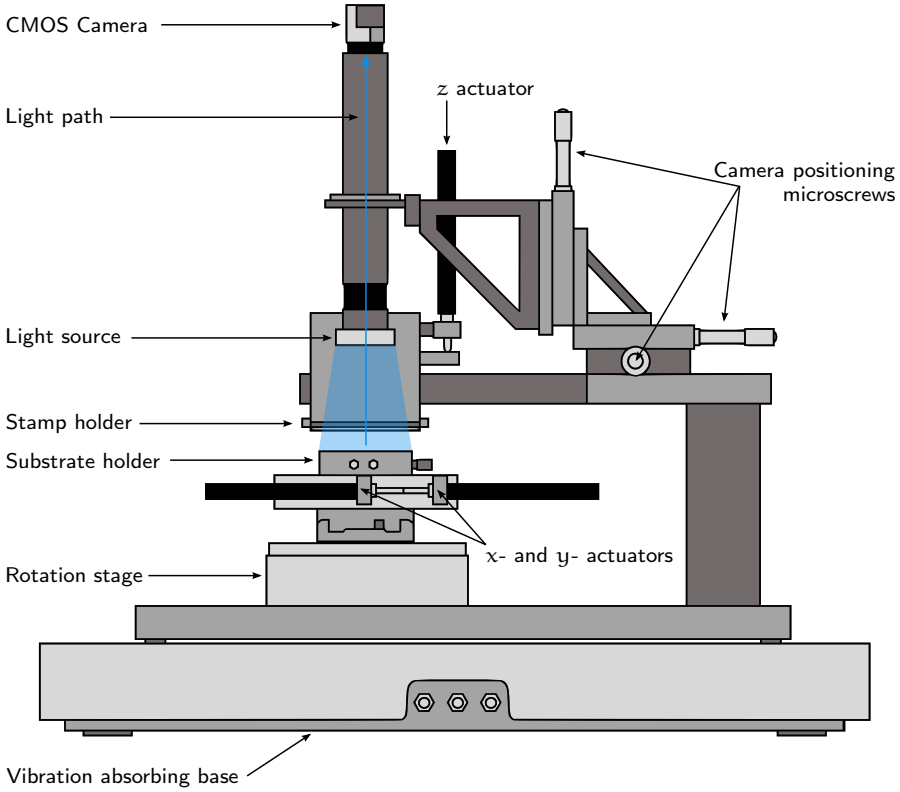

Figure 2.10: **Schematic of the basic μCP Tool.** Three stages, two on the x– and y– directions, and one on the z– direction, formed the actuating part. A CMOS camera with a light source manipulated with microscrews, composed the monitoring part

A printing process started when the stamp and substrate were loaded onto the tool. First, the stamp was bound to a microscope slide, which was later immobilized on the stamp holder with vacuum. This holder was fixed on a vertical motorized translation stage with a servo motor identified as z– actuator, which pushed the stamp holder towards the substrate. Then, the substrate was fixed with vacuum on the substrate holder facing the stamp. The holder had a two-dimension motorized stage controlled by the x– and y– actuators. With this stage, the substrate was located at the exact position with a resolution of <1 μm. All servo motors and stages were obtained from Thorlabs, Inc., and were connected to a central system, controlled by a computer.

2.3.2.2 *Description of the monitoring systems*

Once the stamp and substrate were loaded on the tool, both had to be aligned to pattern the correct areas with the precise pressure. To do so, real-time optical and pressure monitoring systems were included in the prototype.

The optical monitoring system consisted on a CMOS camera fixed on the print head. A simple LED-based light source illuminated the stamp and substrate. The $x-$, $y-$, and $z-$ position of the camera relative to the substrate was controlled by three microscrews. The light path was directly above the substrate and the capture image was constantly monitored via a computer.

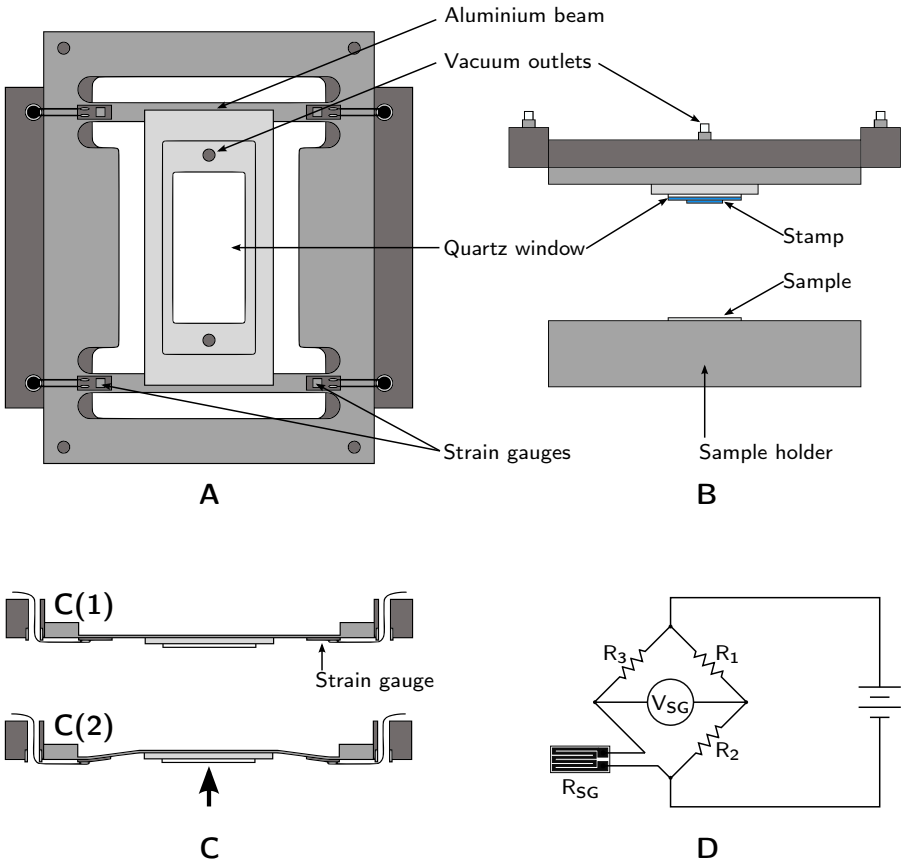

Figure 2.11: **Description of the pressure sensors integrated in the stamp holder.** (A) Bottom, (B) lateral, and (C) axial views of the stamp holder. A quartz window with two vacuum outlets is suspended between two aluminum beams. Four strain gauges, one on each beam fixture, are independently connected to one of four Wheatstone bridges to record any load exerted on the suspended quartz window. (D) Wheatstone bridge to calculate the value of the R_{SG} with the measurement of V_{SG}.

With the aligned substrate, the printing process could continue. The stamp was brought into contact with the substrate. The constant monitoring of the pressure was a central parameter on the entire process. To fulfill such requirement, an active pressure sensor system was mounted on the stamp holder. The microscope slide where the stamp is mounted was vacuum-fixed on a suspended quartz window. This window was fixed onto two aluminium beams on its both ends. Four strain gauges were independently glued on each end of the beams.

Strain gauges are sensors used to measure the deformation of an object. The most common type consists on a metallic foil pattern bonded to a carrier. Usually, these sensors are tightly fixed or glued to the object to measure. When the object is deformed, the electrical resistance of the gauge changes. Measuring the change of the resistance, the strain of the object can be calculated.

Figure 2.11A-B present a bottom and lateral views of the holder. The bending of the beams provided the measurement of the force applied to the stamp, hence, obtaining the printing pressure. The black arrow in Figure 2.11C represents a load applied vertically to the beam. As the strain gauges are glued to the beam, the deformation of the beam is translated to the them. To measure the change on the pressure, the strain gauges are connected to a Wheatstone bridge, an electrical circuit used to measure an unknown electrical resistance.

In Figure 2.11D, R_1 was set to match R_3, and R_2 was adjusted at a value equal to the resistance of the strain gauge (R_{SG}) without applied force. With no load on the beam, the ratios $\frac{R_2}{R_1} = \frac{R_{SG}}{R_3}$, the bridge will be symmetrically balanced, thus $V_{SG} = 0$ V. When compressed or tensed, R_{SG} will decrease or increase unbalancing the bridge, obtainging a measuremente $V_{SG} \neq 0$ V. The constant monitoring of V_{SG} gives a real-time measurement of the deformation of the beam. A relationship between the deformation of the beam and applied force had to be calculated. To calculate this, a weighting balance was placed under the stamp holder. Then, the stamp holder was lowered until it contacted the weighting plate. The mass (m) was registered along the value of V_{SG}. The applied force ($\vec{F}$) was calculated using the relationship $\vec{F} = m \cdot \vec{a}$, replacing the value of $\vec{g}$ for $\vec{a}$, and introducing the value of m. The stamp was lowered slightly again, and the new m and V_{SG} were recorded. At least 10 different mass measurements were measured to obtain the calibration curve. This values presented the relationship between the calculated $\vec{F}$ and the measured V_{SG}.

2.3.2.3 *Description of the software functions*

All the functions of the μCP tool are controlled by a dedicated program based on LabVIEW© from National Instruments (Austin, TX, USA). The program runs a state-machine following a set of states with independent instructions, data input, or output. Figure 2.12 presents the simplified state diagram of the μCP tool. The first step when running the program is the initialization of the sensing and actuating mechanisms. This first step is referred to as the **Init** state. Immediately afterwards, the program advances to the **Main Menu** state, and remains in a constant loop returning to this state until a different instruction is received. Most of the states represent a single step before returning back to the **Main Menu** state.

All information and instructions are introduced via the front panel shown in Figure 2.13. Some states do not require inputs, the only

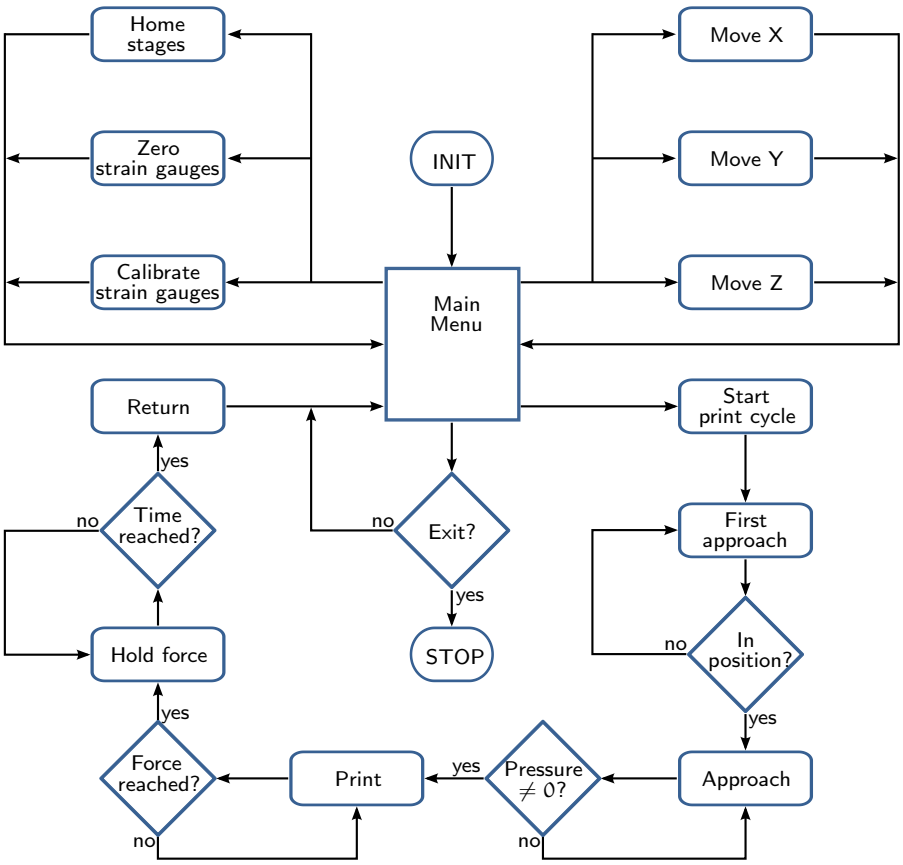

Figure 2.12: **Simplified state machine of the μCP Tool.** The program starts with a first state where the sensing and actuating mechanisms are initialized. The program remains in a constant loop returning to the **Main Menu** state, until it receives a different instruction.

instruction is to change the state. In Figure 2.13A, the **Home X-Y-Z Motors** button instructs the actuators to return to their original position, while the **Zero Strain Gauges** button is a tare function for the strain gauges, finally **Quit Program** ends the program. The absolute position of the actuators is controlled in Figure 2.13B with the **Move X**, **Move Y**, and **Move Z** buttons as well the toggle function in Figure 2.13E. Figure 2.13C, G, and H present information of the current state, the position in real-time of the actuators, and the actual contact force between stamp and substrate, respectively. Figure 2.13D is a graphical display presenting the measured force throughout a period of time. The values presented in this graph can be recorded for future experiments. If anything goes wrong, the emergency stop button in Figure 2.13F stops the program and brings the actuators to their initial position.

An automatized printing cycle was also integrated within the program. The complete cycle is presented in Figure 2.12 and it relies on actual contact force measured during the process. A **First Approach**

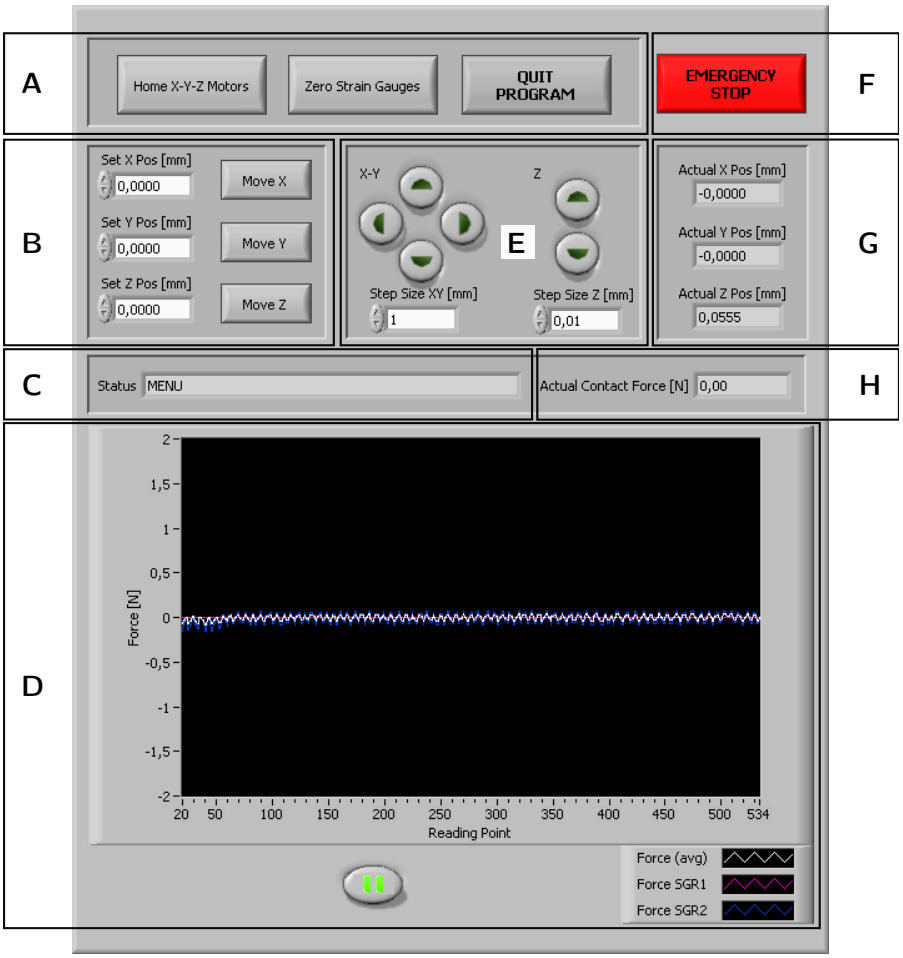

Figure 2.13: **Front panel with the controls and displays required to work with the µCP Tool.** (A) Controls with no parameter input. (B) Controls to set the position of the x−, y−, and z− actuators. (C) Current state of the program. (D) Graphical display showing the measured force throughout a period of time. (E) Toggle of the x−, y−, and z− actuators. (F) An emergency stop button to return every actuator to its original position. (G) Displays showing the real-time position of the x−, y−, and z− actuators. (H) Numerical display showing the actual contact force.

state brings the stamp to a pre-defined position. Subsequently, the stamp is lowered until the measured force crosses the value of the introduced force. At this moment, the program maintained the pressure until the selected time was reached. To prevent the damage of the stamp or the substrate, as well as an incorrect stamping, the pressure was constantly measured. Any change in the value was corrected by the µCP tool.

2.4 EXPERIMENTAL PROCEDURES FOR THE AUTOMATED PATTERNING ON DIVERSE SUBSTRATES

While μCP offers unique alternatives to create (bio)molecular patterns on a wide range of substrates, this inherently manually technique possesses a plethora of weaknesses. The lack of standardized protocols presents a huge opportunity to create an automatized mechanism to diminish the limitations and explore the strengths present in this technique.

The purpose of this Chapter was to characterize the patterns fabricated with the described prototype. The patterns were assembled first, to help study and understand the fundamental limitations of μCP, and then, to standardize the patterning protocols for the next Chapters of this Thesis. Several different (bio)molecules were patterned on various substrates. Initially, thiols, were used to study the effects of the printing pressure and dwell time. Furthermore, complex patterns were fabricated with multiple printing series of thiols on gold. The functionalization of different substrates allowed the patterning of more complex entities such as proteins, antibodies, and DNA.

2.4.1 *Fabrication of PDMS stamps*

To study the characteristics of the automatized μCP tool, stamps with different features were fabricated. The shape of the patterns are defined by the configuration of the master, hence, various masters with different geometries were required. Direct write laser lithography (DWL) was used to manufacture several features on a SiOx wafer from NTB (Buchs, Switzerland). The diffracted light shown in the localized zones of Figure 2.14A indicates the microstructured areas. Figure 2.14B shows a microscopic photography of one of the fabricated geometries which consisted on two positive (posts) and two negative (holes) square patterns of 5 μm and 10 μm. Figure 2.14C shows rhomboidal depressions at different orientations.

Afterwards, the surface of the master was activated in a Harrick plasma cleaner (Ithaca, NY, USA) at 30 *W* for 1 min, and vapour-coated with 1H,1H,2H,2H-Perfluoroctyltrichlorosilane (PFOTCS) from Fluka (Buchs, Switzerland) in a vacuum desiccator for 1h. After baking for 1 h at 80 °C the masters were ready for replication. The PFOTCS prevented the adhesion of the elastomer to the master during the stamp fabrication.

Various PDMS stamps with different patterns were fabricated using the Sylgard© 184 Silicone Elastomer Kit from Dow Corning (Midland, MI, USA). The stamps were obtained mixing a 10:1 ratio (w/w) of the siloxane mixtures and catalyst. Then, the mixture was degassed under vacuum to extract all the air bubbles, poured onto the PFOTCS-coated SiOx wafer, and afterwards, baked at 75 °C during 1 h. Finally,

the solidified polymer was peeled form the wafer. After rinsing with absolute ethanol obtained from Panreac (Barcelona, Spain), the wafer could be reused indefinitely.

Some PDMS stamps were fabricated directly on 75×25 mm microscope glass slides from Corning Inc. (Corning, NY, USA) using smaller SiOx masters provided by the Centre Nacional de Microelectrònica (CNM) (Barcelona, Spain). A stamp on the microscope slide and two SiOx masters are presented in Figure 2.14D. This design provided a manageable system to load and unload the stamps from the stamp holder of the μCP tool. The stamp was later characterized with a Dimension 3100 AFM equipment from Veeco Instruments (Plainview, NY, USA) in tapping mode using a rectangular NSC15/AIBS silicon tip with a spring constant of 40 N m^{-1} and resonance frequency of 325 kHz purchased from MikroMasch (Wetzlar, Germany). The resulting topography image is depicted in Figure 2.14E, and to obtain the profile of the stamp Figure 2.14F, the data was analyzed with the WSxM 5.0 software from Nanotec Electrónica (Madrid, Spain)[51].

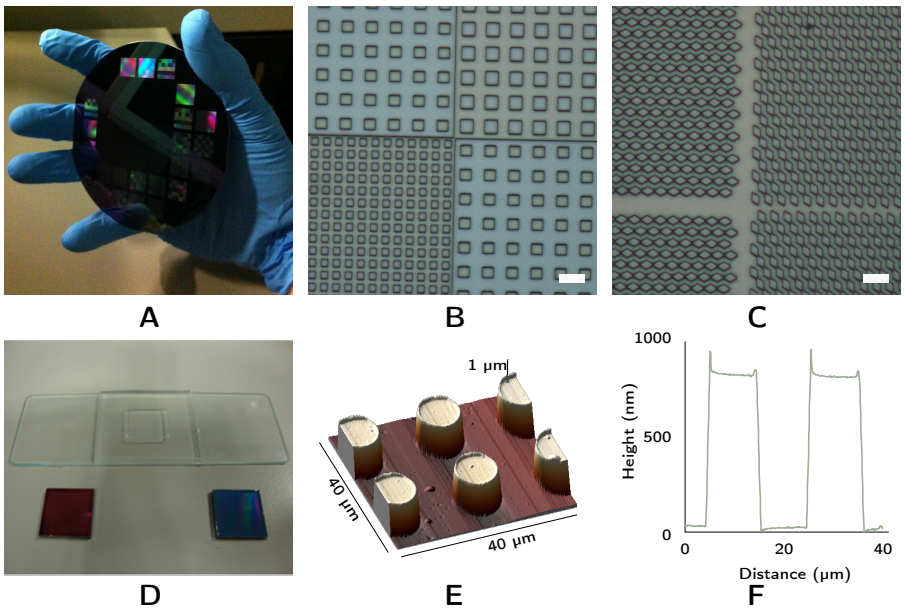

Figure 2.14: **Fabrication and characterization of the PDMS stamps.** Macroscopic (A) and microscopic (B-C) photographies of various SiOx masters for the fabrication of PDMS stamps. Scale bars = 20 μm. (D) Digital photography of a PDMS stamp fabricated on a microscope slide with two SiOx masters measuring 1×1 cm^2. (E) AFM topography image and profile (F) of the PDMS stamp. The protruding cylindrical posts are 10.00 ± 0.03 μm in diameter with a height of 800 nm.

2.4.2 *Materials and methods to print thiols*

Different thiol inks were used to pattern various gold substrates purchased from NTB (Buchs, Switzerland). The substrates were fabricated by evaporating a 2 nm chromium adhesion layer over glass and the subsequent evaporation of a 50 nm gold layer. As thiols diffuse to the bulk of the PDMS stamp, each thiol ink requires an unique and independent stamp. Three inks, Triethylene glycol mono-11-mercaptoundecyl ether (PEG_3-thiol), 16-Mercaptohexadecanoic acid (MHDA), and 1-Octadecanethiol (ODT) from Sigma-Aldrich (St. Louis, MO, USA) were diluted in ethanol to obtain three independent 2 mM solutions. Each PDMS stamp was inked independently for 15 min with a different thiol solution and dried afterwards under a stream of N_2.

A negative stamp with cylindrical holes was utilized to pattern PEG_3-thiol on a Au substrate. The inked PDMS stamp was loaded on the μCP tool and patterned the Au substrate for 2 min with a force of 1 N distributed along the stamp. The same procedure was follow to pattern the MHDA ink using a positive stamp with cylindrical posts with a diameter of 10 μm. The printing dwell time was again 2 min. Finally, using a same copy as the previous stamp, ODT was printed onto a new Au substrate for 2 min and 1 N. Subsequently, it was submerged into a Au etchant consisting on a 30 mM thiourea (CH_4N_2S) and 20 mM Iron(III) nitrate nonahydrate ($Fe(NO_3)_3 \cdot 9H_2O$) aqueous solution. Both reagents were obtained from Panreac (Barcelona, Spain). The etch rate of Au with the etchant is ~3 nm min^{-1}, so the substrate was left to react fo ~16 min to etch the $50-$ nm Au film. During etching, the SAM formed by the ODT acts as a barrier, preventing the dissolution of the Au beneath the patterned areas.[52] After etching, the substrate was rinsed with Milli-Q water from Millipore (Billerica, MA, USA) and blown-dry under a stream of N_2. AFM was used to characterize the thiol SAMs as well as the etched substrate.

Lastly, a Biotin alkyl thiol (BAT) derivate obtained from the work of Prats-Alfonso *et al.*[53], and formed by a thiol, an aliphatic chain ($n = 11,\ 16$), a Poly(ethylene glycol) (PEG) linker, and a biotin, was patterned on a Au substrate. This molecules creates a linker between Au and any molecule bearing any avidin conjugate such as Neutravidin (NAV) or Streptavidin (SAV). The avidin and biotin interaction forms rapidly and is the strongest, non-covalent, biological bond, stable over wide ranges of pH and temperatures interesting for many scientific fields.[54] The BAT pattern was fabricated as previously mentioned and subsequently incubated in a 40 μg ml^{-1} SAV labeled with Texas Red® (TxR) solution from Invitrogen (Eugene, OR, USA) in Phosphate buffered saline (PBS) obtained from Sigma-Aldrich (St. Louis, MO, USA) for 1 h. Afterwards, the substrate was washed multiple times with PBS with 0.5% Polyoxyethylenesorbitan monolaurate (Tween 20) from Sigma Aldrich (St. Louis, MO, USA), then Milli-Q water, and

characterized with an Eclipse E1000 Fluorescence microscope from Nikon (Chiyoda, Tokyo, Japan).

Having successfully patterned various thiols on Au, more in depth characterization of the entire protocol was necessary. To understand some of the factors that shape the pattern when printing, a series of different stamping procedures varying the printing pressure and the printing dwell time were defined.

2.4.2.1 *Patterning thiols at different printing pressures*

As presented previously, the Young's modulus (E) of PDMS varies in the range between 1.32 MPa to 2.97 MPa[8], making it an elastic material which can deform easily under strain. The PDMS stamp from Figure 2.14E was inked for 15 min with a 2 mM MHDA ethanolic solution and was used to pattern Au substrates at different pressures. The printing force was introduced in the printing program and the inked stamp was loaded in the μCP tool. The patterning process followed the path defined by the **Print Cycle** presented in Figure 2.12. In the first state, **Approach**, the stamp holder is lowered constantly until the measured force $\geqslant$ 50% of the defined force. After crossing this mark, the **Print** state takes control and continues to lower the stamp holder until the measured force $\geqslant$ the defined force. At this moment, the program changes to the **Hold Force** state and the timer starts. When the defined time is reached, the program jumps automatically to the **Return** state which brings the substrate holder to its initial position and finally, the program returns to the **Main Menu** state.

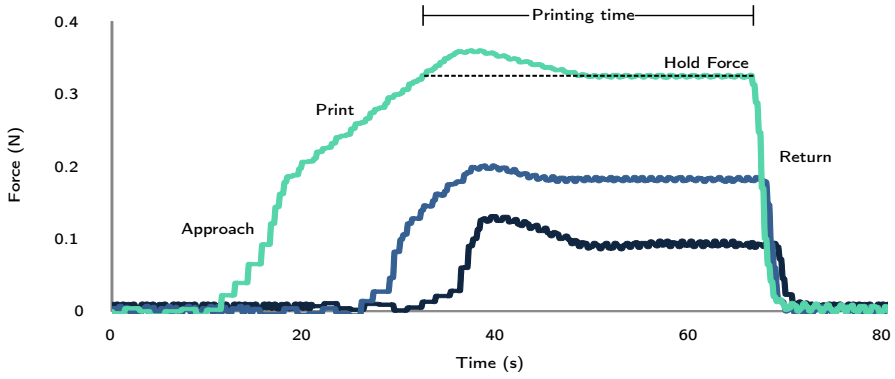

Figure 2.15: **Recorded force curves during μCP.** Different forces were applied during three 30 s printing subroutines: 0.1 N, 0.2 N, and 0.3 N. The curves show a similar profile following the automated printing states shown in Figure 2.12.

The printing subroutine was recorded for three different forces, 0.1 N, 0.2 N, and 0.3 N obtaining the profiles shown in Figure 2.15. A wider range of forces from 0.2 N to 5.0 N was selected to patten the Au substrates at a constant time of 1 min. For a correct statistical analysis, three different substrates were patterned for each pressure.

To minimize artifacts, the stamp was washed thoughtfully between printing cycles first by sonicating in absolute ethanol for 15 min, and a subsequent rinse with absolute ethanol. After drying with compressed N_2 the stamp was inked with the thiol solution and the entire printing cycle was repeated. To prevent the diffusion of the printed thiols, all the substrates were etched with the previously discussed solution and were later characterized using AFM.

As a proof of concept, a PDMS stamp was fabricated replicating a TGT-1500 triangular test grating for AFM from Ted Pella, Inc. (Redding, CA, USA). This grating is formed by parallel-running triangular features. When replicated, the valleys between features formed the ridges of the stamp with maximum width of 500 nm. This value is the limit of the smallest feature printed with standard PDMS.[55] To decrease the patterned feature size, the stamp was inked with the MHDA solution, loaded in to the printer and lowered until the stamp barely contacted the Au substrate. Immediately afterwards, the substrate was etched as previously stated.

2.4.2.2 *Patterning thiols with various printing dwell times*

The diffusion of thiols during the μCP process is well documented and pose big opportunities and drawbacks. For such reasons, it was necessary to understand the effects of the time while patterning Au substrates. The pattering protocol included the same stamp with cylindrical posts with a diameter of 10 μm. The stamp was inked for 15 min with a 2 mM MHDA ethanolic solution, dried under a stream of N_2, and loaded to the μCP tool. The **Print Cycle** was set for 1, 2, 5, 10, and 15 min with a constant printing force of 0.5 N. Three Au substrates per printing time were stamped and subsequently etched. AFM was used to characterize the patterns.

2.4.2.3 *Controlling the printing position*

Chen *et al.*[56] manually printed patterns of ω-mercaptoundecyl bromoisobutyrate on Au substrates by moving or jumping the stamp during the stamping process. They called this process "dynamic μCP". It is interesting to notice that the position and alignment of their patterns was completely random across the substrate and the same distribution of the patterns cannot be repeated. The process is illustrated in Figure 2.16.

Controlling the exact position of the pattern could bring greater advantages in terms of repeatability and standardization of the technique. Taking the dynamic μCP idea, the tool was used to create complex patterns using the same principle of repeated printing. This patterning approach allows the design and creation of specialized features without the need of new stamps with those geometries.

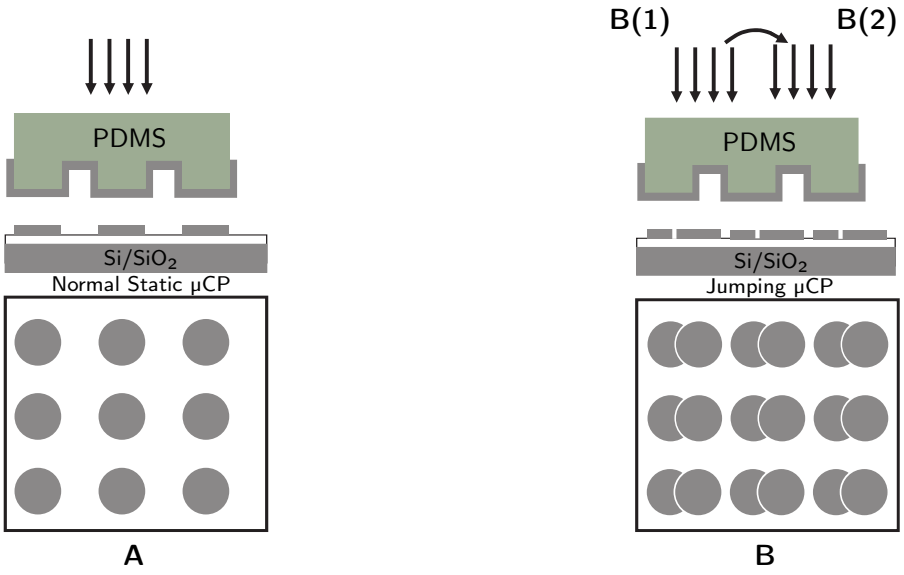

Figure 2.16: **Steps involved in dynamic µCP.** (A) Normal µCP, obtaining a regular array of printed spots. (B) Dynamic or jumping µCP refers to consecutive printings with the same stamp of a first (B1) and second printing (B2) displaced only by a few µm. Adapted from [56].

Two approaches were defined to test the positioning capabilities of the µCP tool. The first one was to fabricate aligned features which were larger that the protruding traits of the stamp. The second one, proposed a combination of features of different sizes in the same substrate. In both cases, the bigger patterns were fabricated by the multiple printing of the pattern following a specified design. To accomplish this, a 2 mM MHDA ethanolic solution was used to pattern Au substrates with the same stamp.

Three patterns were fabricated following the coordinates presented in Table 2.1. These positions are absolute, this means that the µCP received the final coordinate, not distance the substrate holder had to travel to reach the desired position. Every pattern started in a random position (x_0, y_0) on the Au substrate defined as the center $(0, 0)$ of the Cartesian plane. The µCP tool had a substrate holder able to translate from $(-2.5, -2.5)$ to $(2.5, 2.5)$ cm on the $x-$ and $y-$ directions of the horizontal plane, hence, a total translation of 5 cm. The pat-

Table 2.1: Absolute positions of the designed patterns in µm.

	DESIGNS		
STEPS	DIAGONAL	TRIANGULAR	COMBINATION
Position (x_0, y_0)	$(0.0, 0.0)$	$(0.0, 0.0)$	$(0.0, 0.0)$
Position (x_1, y_1)	$(5.0, 2.5)$	$(-8.0, 0.0)$	$(10.0, 7.5)$
Position (x_2, y_2)	—	$(0.0, -8.0)$	$(10.0, 12.5)$

terning followed the same protocol as previously presented just with the defined locations. The stamp was raised between each spot and located on the new coordinate before printing resumed. Finally, the etched samples were characterized with AFM.

2.4.3 *Materials and methods of the direct patterning of biomolecules*

Complex biomolecules like proteins, antibodies, and DNA can be patterned on various substrates to serve different functions. Proteins can coat substrates to form bioactive surfaces. The different patterns create active sites where various (bio)molecules or biological elements can interact. On the other hand, antibodies present mechanisms to create recognition substrates. The interaction between antibodies and their unique antigen open great opportunities to develop biosensing materials. Finally, DNA patterns have been traditionally used in microarrays as recognition elements to extract data from a genetic pool.

The direct placement of biomolecules presents the most reliable method to create patterns on selected substrates. Biomolecules have been traditionally physisorbed on the printed substrate.[34] However, for long term stability of the pattern under chemical or physical attack, the formation of covalent bonds between substrate and biomolecules is recommended.[57] The reactive moieties on these biological complexes introduce exploitable binding sites which can react if the substrate is properly modified. Taking into account this, silanes present interesting choices to modify substrates.

2.4.3.1 *Silanes as molecular glues*

Proteins are a three-dimensional arrangement of linear amino acid residues called polypeptide chains. Primary amine groups ($-NH_2$) are present at the N-terminus of each chain, and their positively-charged nature at physiological pH, locates them regularly on the surface of the protein. This position provides an easy target for any conjugation reagent. The same occurs with antibodies, where amines are numerous and distributed all over its surface.

To bind proteins and antibodies to glass, SiOx, or Indium tin oxide (ITO), a protocol to create active epoxide groups on the substrates was developed. An epoxy-silane was chosen as its active ring reacts easily with amine and thiol moieties. The bonding mechanism is shown in Figure 2.17, creating either a secondary amine bond or a thioether bond.[58]

The fist step in the functionalization protocol was the cleaning and activation of the substrate. To clean the glass slides, the SiOx or the ITO substrates sputtered over glass at the INL (Braga, Portugal), were initially sonicated in absolute ethanol during 15 min, then rinsed with clean ethanol, an finally blown dry with N_2. Two parallel methods were used to create active hydroxyl groups on the surface of the sub-

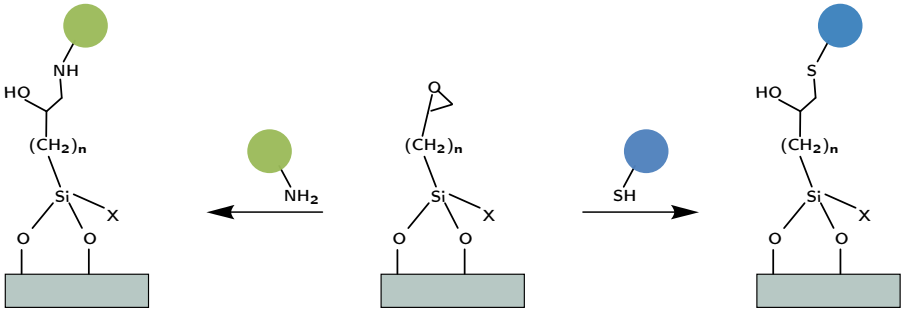

Figure 2.17: **Reaction of epoxide groups.** An epoxy-silane SAM is reactive towards primary amine ($-NH_2$) an thiol ($-SH$) moieties.

strates. The first method, considered the dry method, simply required the clean substrates to be introduced in the plasma cleaner at 30 W for 1 min. The second method, or wet method, called for the samples to be sonicated in a 1 M solution of $NaOH$ obtained from Panreac (Barcelona, Spain) for 15 min, and afterwards, rinsed with Milli-Q water, and immediately submerged in a 1 M HCl solution purchased from Panreac (Barcelona, Spain) for 15 min. To finish, the samples were thoroughly rinsed with Milli-Q water and dried with N_2. After either activation, the dry substrates were submerged in a 2% ethanolic solution of 3-Glycidoxypropyldimethoxymethylsilane (GOPDMS) from Sigma-Aldrich (St. Louis, MO, USA). To form a complete monolayer, yet prevent the creation of multilayers, the reaction time was limited to 20 min. The substrates were subsequently rinsed with clean ethanol and baked at 75 °C for 1 h. After rinsing with ethanol and drying with N_2, the substrates were ready to pattern.

Different proteins, antibodies, and DNA were patterned onto epoxy-modified substrates. Table 2.2 presents a summary of the printed biomolecules along with the substrate in which they were patterned together with the size and geometry of the features from the PDMS stamp used to transfer them. AFM and fluorescence microscopy were used to characterize the transfered patterns. The ImageJ image processing system developed by the NIH (Bethesda, MD, USA) was used to analyze the microscopy images.

Three fluorescent-labeled proteins were patterned several epoxy-modified substrates: Wheat germ agglutinin (WGA), Bovine serum albumin (BSA), and Phytohaemagglutinin (PHA) all acquired from Invitrogen (Eugene, OR, USA). WGA and PHA are naturally occurring lectins present in several plants but at higher concentration in legumes. Both proteins are used to recognize carbohydrates and glycoproteins present in live cells.[59] In the case of BSA, this abundant protein is used in several biochemical applications as blocking agent in Western blots or ELISA or to bind to fatty acids, hormones or drugs.[60] To print, the proteins were individually dissolved in PBS at a concentration of 40 $\mu g\ ml^{-1}$. The stamp was covered by the

Table 2.2: List of patterned biomolecules onto the indicated substrate with the stamp geometry and dimension, where the first number denotes the size of the feature and the second one the pitch.

	BIOMOLECULE	SUBSTRATE	STAMP
Proteins	WGA-TxR	SiOx	○ 10 | 10 µm
	BSA-AF555	Glass	⋘ 5 | 10 µm
	PHA-AF488	SiOx	‖ 1 | 5 µm
Antibodies	anti-*E. coli* O157	ITO	□ 10 | 10 µm
	anti-5C3 IgG	SiOx	□ 5 | 5 µm
	anti-5C3 IgG	SiOx	□ 5 | 5 µm
DNA	FP-NH_2-T	SiOx	◊ 5 | 5 µm
	FP-NH_2-T	Glass	◊ 5 | 5 µm
	5SH-3	SiOx	○ 10 | 10 µm

protein ink for ~15 min, then rinsed with Milli-Q water, and loaded into the µCP tool. Rinsing the stamp prevents the formation of salt crystal on its surface, allowing a correct transfer of the proteins. To prevent the collapse of the stamp, which would inevitably alter the pattern, the printing force was limited to 1 N and the printing time was adjusted to 5 min. This time allows the formation of secondary amine bonds between substrate and protein without compromising its functionality.[58]

Following a similar protocol, mouse anti-*E. coli* O157 from Abcam (Cambridge, UK) and mouse anti-5C3 IgGs fabricated and procured by Leitat (Barcelona, Spain) were patterned over ITO and SiOx respectively with the stamps shown in Table 2.2. The anti-*E. coli* O157 pattern was develop as a collaboration to characterize the binding of *E. coli* on the conductive substrate for biochemical studies. The stamp was inked with a 15 mg ml^{-1} antibody solution in PBS for 15 min, and subsequently rinsed with Milli-Q water. The printing time was fixed at 2 min under a force of 1 N. After letting the pattern react in a humid atmosphere, the sample was incubated with *E. coli* O157 in PBS for 45 min and a second anti-*E. coli* FITC conjugate was used to characterize the specificity of the bacteria to the bound antibodies.

A similar collaboration required the patterning of anti-5C3 IgGs over SiOx. The PDMS stamp was inked with a 40 mg ml^{-1} antibody solution for 15 min. Again, the printing time was 5 min at a force of 1 N. The patterned antibody was left to react for 1 h in a humid chamber. Afterwards, the samples were immersed in a 100 mM 2-(2-Aminoethoxy)-ethanol (AEE) from Sigma-Aldrich (St. Louis, MO,

USA) solution in a 100 mM sodium hydrogen carbonate ($NaHCO_3$) buffer from Panreac (Barcelona, Spain) during 30 min. The amine in the AEE reacted with the unpatterned epoxide groups and rendered them inert. To characterize the patterns, the entire substrates were submerged in a 2 mg ml^{-1} solution of rhu-S100A4 from Leitat (Barcelona, Spain) in PBS, for 1 hr. Subsequently, unbound protein was washed with PBS 0.1%-Tween 20 and the samples were incubated for 30 min with a 4 mg ml^{-1} solution of rabbit anti-S100A4 from Dako (Glostrup, Denmark) in PBS. After several washes, the substrates were lastly incubated with a solution of AF_{488}-conjugated goat-anti-rabbit IgG from Life Technologies (Carlsbad, CA, USA). After a final wash, the substrates were characterized.

Contrarily to proteins and antibodies, DNA lacks the natural occurring amine or thiol groups, yet modified oligos are easily accessible, and the same protocol can be followed to fabricate patterns. The two different strands shown in Table 2.2, FP-NH_2-T labeled with Tetramethylrhodamine (TAMRA) and 5SH-3, were printed from individual solutions at a concentration of 5 µM suspended in a 30 mM sodium phosphate dibasic (Na_2HPO_4) buffer from Sigma-Aldrich (St. Louis, MO, USA). The printing protocol was similar to the one presented by Thibault *et al.*.[40] Briefly, the stamp was inked for 2 min, loaded into the µCP tool, and the substrate was printed for just 1 min. The rest of the substrate was passivated with a 1% (w/v) solution of BSA acquired from Panreac (Barcelona, Spain) in PBS.

As the 5SH-3 strand lacks any label to characterize the transfer, a complementary strand, 5BT-3TR, probed with TxR, was hybridized on the printed spots. The strand was added to a hybridization buffer at a final concentration of 2.5 µM. The buffer was an aqueous solution of 10 mM Tris(hydroxymethyl)aminomethane (TRIS) from Merck, KGaA (Darmstadt, Germany), 1 mM Ethylenediaminetetraacetic acid (EDTA) from Sigma-Aldrich (St. Louis, MO, USA), and 1 M sodium chloride ($NaCl$) from Panreac (Barcelona, Spain). Please refer to Table A.1 for the DNA sequences.

2.4.3.2 *Sequential patterning of biomolecules*

The covalent attachment of biomolecules to epoxy-functionalized substrates forms a robust foundation to create more complex patterns. Using the µCP tool to control the exact printing position, several proteins were printed at defined coordinates with great accuracy.

Table 2.3 summarizes the patterned proteins onto functionalized SiOx substrates, the defined patterns, and the geometry and size of the features of the PDMS stamp. The advanced design of the tool allowed to interchange and align stamps to pattern with multiple inks. This process is more elaborate as compared with Table 2.1, as the initial stamp is removed to leave space for the second one. The alignment is done with the optical monitoring system and the rotating stage.

Table 2.3: Proteins printed with several designs with the indicated stamps.

PATTERN	PROTEIN 1	PROTEIN 2	STAMP
Angled	WGA-TxR	PHA-AF488	||| 5 | 5 µm
Absolute coordinates	SAV-TxR	NAV-OG488	○ 10 | 10 µm
Parallel	WGA-TxR	PHA-AF488	||| 1 | 5 µm
Embeded	WGA-TxR	PHA-AF488	||| 1 | 5 µm

In the **Angled** pattern, the first protein was printed at an intended $\measuredangle = 60°$ from the horizontal plane, while the second pattern with an $\measuredangle = 120°$. These angles would create a crossed pattern with a displacement of 60° from each other. To accomplish this, an initial stamp was inked with a 40 $\mu g\ ml^{-1}$ WGA-TxR solution in PBS for 15 min. After rinsing and drying, the stamp was loaded on the µCP tool. The substrate holder with the vacuum-fixed SiOx sample was rotated to reach the first position. After printing for 5 min, another stamp already inked with a PHA-AF488 solution with the same concentration and time was loaded into the printer. Using the optical monitoring system, the holder was rotated to reach the second position, and subsequently printed.

In the case of the pattern with **Absolute coordinates**, two stamps with the same features were separately inked with SAV-TxR and NAV-OG488 from Invitrogen (Eugene, OR, USA) in PBS, both at a concentration of 40 $\mu g\ ml^{-1}$ and for 15 min. The first stamp was loaded at an initial position $(x_0,\ y_0) = (0,\ 0)\ \mu m$, and the substrate was printed. Afterwards, the next stamp was loaded and localized at the planned second position $(x_1,\ y_1) = (10,\ 10)\ \mu m$ with respect of the first one.

Having characterized the previous results, a standardized protocol was established to create complex designs. To produce the **Parallel** pattern, two stamps with the same design were individually inked with a 40 $\mu g\ ml^{-1}$ WGA-TxR or PHA-AF488 solutions in PBS for 15 min. The idea was to locate the second pattern as closely possible from the first one without overlapping. The chosen stamp was formed by protruding parallel 1 µm lines. The 5 µm separation between the lines presented the best location to print a second set of lines. The first and subsequent stamps were loaded individually to the µCP tool and a SiOx substrate was patterned. These patterns helped measure the aligning capabilities and the error associated with the handling of different stamps.

Finally, taking into account the positioning of the stamp and the correct alignment with the substrate, a last design was conceived. The **Embeded** pattern used the same stamps and printing conditions as the previous one. However, in this case, three patterns were transfered to a new SiOx substrate. Two consecutive printings with the WGA-TxR ink were first stamped on the sample. The initial pattern was located at $\measuredangle = 0°$ with respect of the border of the substrate,

whereas the second one was placed at a $\measuredangle = 90°$. This was done after the sample holder was rotated to the desired angle. The last stamping transfered PHA-AF_{488} after the substrate and the recently loaded stamp were aligned to coordinate the features.

2.5 RESULTS, EVALUATION, AND INFLUENCE OF THE DIFFERENT EXPERIMENTAL PARAMETERS

2.5.1 *Fabrication of thiol patterns on gold*

The primary goal of the thiol patterns was to understand the behaviour of the inks and the characterization methods required to obtain the best foundations for subsequent experiments. Different thiols were printed on Au substrates with the help of the μCP tool. Porter *et al.*[61] measured thiol monolayers on gold with various methods including ellipsometry, infrared spectroscopy, and electrochemistry, and obtained a ratio of 1.3 Å per methylene ($-CH_2-$) group, n, in the chain. Newer reports fix the ratio to 1.2 Å per n.[62] Here, AFM was used to characterize the patterns, and Figure 2.18 presents the initial four printed thiols. Each thiol ink had a different aliphatic chain length and a unique functional terminal moiety.

First, PEG_3-thiol was patterned with a negative stamp, thus, leaving spots of bare Au. The topography image and height profile in Figure 2.18A show the patterned thiol with a measured thickness of 2.38 ± 0.05 nm which confirms the formation of a monolayer since this thiol has a theoretical length of 2.64 nm.

Figure 2.18B presents the topography and profile of the second thiol, MHDA. This double-printed thiol pattern had a measured feature height of 1.96 ± 0.48 nm fitting in the monolayer regime as the theoretical thickness is 2.15 nm.[62] Previous works, also characterized with AFM the transfer of thiols via μCP, arrived to similar monolayer thicknesses.[63]

To maintain the shape and size of the printed feature, the patterned substrate was etched to remove surrounding Au where the thiol could diffuse. Figure 2.18C presents the topography and profile of etched gold features from printed ODT. The 54.31 ± 0.80 nm height of the etched feature is the result of the sum of the thickness of the Au layer given by the supplier (50 nm) and the theoretical monolayer thickness (2.28 nm).

When the Au substrate was patterned with BAT from Prats-Alfonso *et al.*[53], it became an active site to probe with avidin conjugates. In the case of the SAV conjugation, the high dissociation constant creates a robust bond.[54] This tetrameric protein with four biotin binding sites, binds to the surface with one site, serving as an intermediate layer for subsequent biotin bonds. The fluorescent image presented in Figure 2.18D, captured the emission of the TxR conjugated SAV. The printed spots are clearly visible, indicating a successful transfer of thiol and subsequent protein conjugation. The high density of probed protein can be confirmed with the fluorescence emission to background ratio, and the diameter of the spots at the Full width at half maximum (FWHM) was measured at 10.08 ± 0.45 μm.

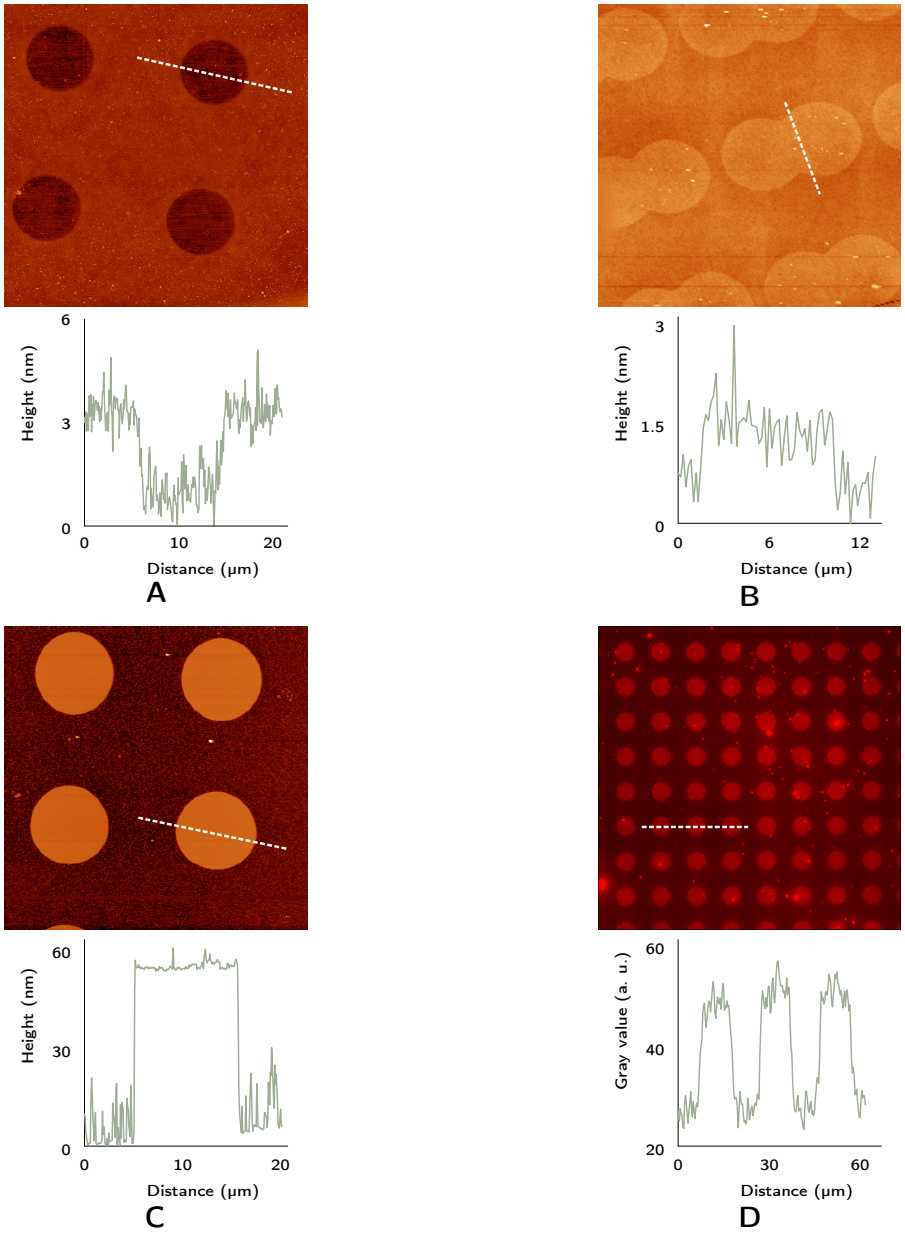

Figure 2.18: **μCP of various thiol inks.** (A-C) AFM topography images and height profile of several thiol patterns on Au. (A) Negative pattern of PEG_3-thiol. (B) Positive double pattern of MHDA. (C) Gold substrate patterned with a positive stamp inked with ODT and subsequently etched. (D) Fluorescence microscopy image presenting a pattern of BAT probed with SAV-TxR

The large availability of thiol inks with different chain length and a diverse array of functional groups, gives the μCP technique a vast library to pattern Au substrates. These functionalized substrates can be applied in many scientific fields, as the functionalized sensor developed by Barreiros dos Santos *et al.*[64] to detect pathogenic bacteria.

2.5.1.1 *Pattern size and morphology under different printing pressures*

One of the nine different measurements (3 from each sample in 3 different samples) from each printing force is presented in Figure 2.19. There, the AFM topographical analyses and profiles of the etched Au features printed with MHDA, are shown, along with the image of etched parallel Au lines printed with very low pressure.

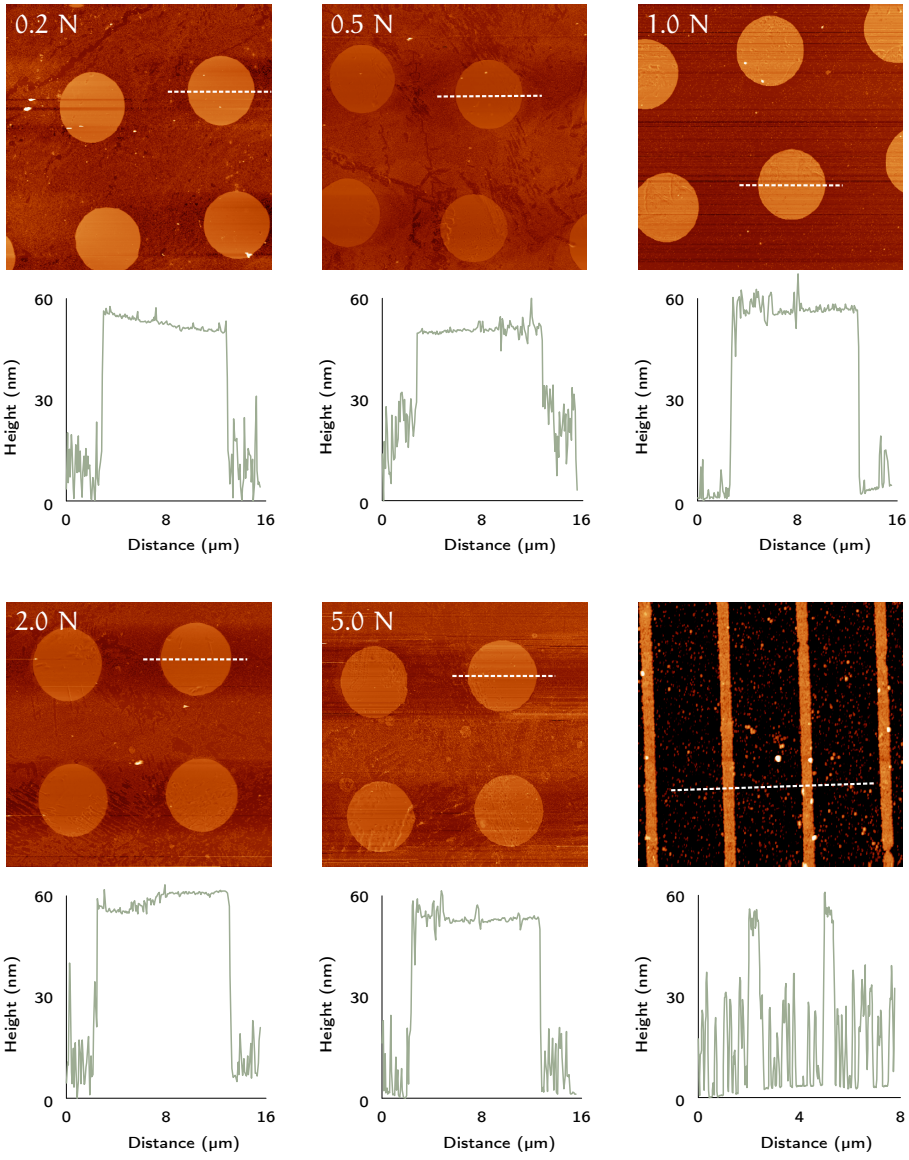

Figure 2.19: **Behaviour of the PDMS stamp under different printing pressures.** AFM topography images of various features obtained by etching of a thiol pattern on Au. The thiol patterns from the first five images were printed at different printing pressures for a printing time of 1 min. The last image shows the lines of 400 nm obtained using a stamp consisting in parallel lines of 500 nm printing under very low pressure.

Here, we have correlated the force applied between stamp and the sample, the mechanical properties of the material, and the geometry of the printing features to explains the relationship between the applied force, $\vec{F}$, and the resulting feature diameter, D, length.

In this presented case, the posts that form the pattern on the stamp suffer a compression and obtain a barreling shape, that is, the compression along the vertical axis of the features, forces the material radially outwards, increasing its diameter, and therefore, the printed pattern. The case assumes that in the tested force range, the deformation of the PDMS stamps is elastic, and that the elastic properties are constant along the feature.

To model the change of D of the contacting PDMS post with the $\vec{F}$, it was necessary to calculate the compression of the post. This compression is governed by the elasticity of the material, obtained by the ratio of stress, σ, to strain, ε, applied to it. This parameter is termed Young's Modulus, E. The scheme in Figure 2.20A associates the length of the radius, R_M, and the compressed height, H, of a post under load. This relation is based on the work of Ebrahimi and Najafizadeh[65], who develop a model to measure the barreling of a cylinder under pressure, which was adapted to understand the behaviour of the PDMS posts:

$$R_T = \sqrt{3\frac{H_0}{H}R_0^2 - 2R_M^2} \tag{2.1}$$

where R_T is the radius of the post at the junction with the bulk, R_0 is the initial radius of the cylinder, here 5 µm, and H_0 is the initial height, which was fixed at 800 nm according to the AFM measurement shown in Figure 2.14. Since the top part of the post cannot change in size, then $R_T \equiv R_0$ can be considered, and the Equation 2.1 can be expressed as:

$$R_0 = \sqrt{3\frac{H_0}{H}R_0^2 - 2R_M^2} \tag{2.2}$$

and isolating H,

$$H = \frac{3H_0R_0^2}{R_0^2 + R_M^2} \tag{2.3}$$

ε can be calculated:

$$\varepsilon = \frac{\delta H}{H_0} = \frac{H_0 - H}{H_0} \tag{2.4}$$

where δH is the change of the height of the post. Once ε was calculated, the sample parameters were introduced in Equation 2.5:

$$\sigma = \frac{\overrightarrow{F_N}}{\pi\left(\frac{D}{2}\right)^2} \tag{2.5}$$

and $\overrightarrow{F_N}$ is the force applied on a single post.

To calculate E, a similar approach as the one used by Liao *et al.*[18] was followed. In their work, the PDMS presents a two-stage compression modulus, therefore, there is a threshold value of $\overrightarrow{F}$ below which $E = E_1$ and above where $E = E_2$. Figure 2.20B presents the plot of σ against ε, where the filled squares represent the measured data and the dashed lines present the two different deformation fitting curves. The presented slopes correspond to the two E values obtained from $\frac{\sigma}{\varepsilon}$ resulting on the first $E_1 = 0.500$ MPa and the second $E_2 = 1.851$ MPa. The values agree with previously published data.[8]

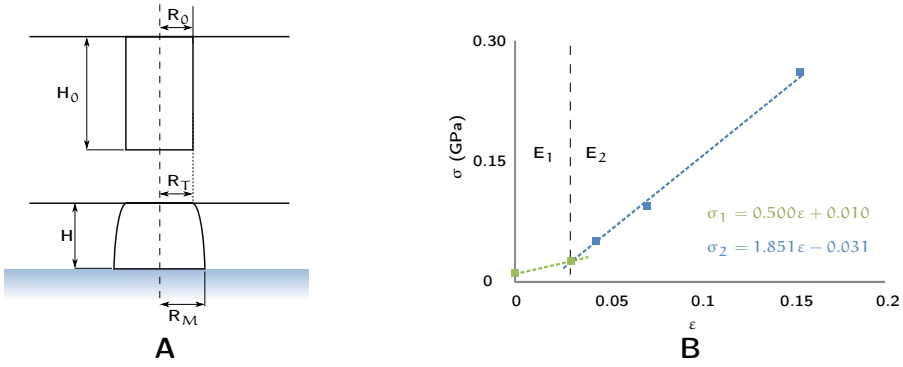

Figure 2.20: **Behaviour of the PDMS stamp under pressure.** (A) The deformation of the PDMS stamp limits the size of the printed features. (B) The calculated Young's Modulus (E) works in two regimes.

The calculated E was used to fit the theoretical radius of the printed features. Figure 2.21A presents a collection of the patterned features along a graph of the measured diameter and the fitting curve. It is clear that the PDMS maintains a two-stage compression which explains the different printed features. Figure 2.21B shows the obtained height of the protruding features of the PDMS stamp under different printing forces calculated from Equation 2.5 and Equation 2.4:

$$\delta H = \frac{\overrightarrow{F_N} H_0}{E\pi\left(\frac{D}{2}\right)^2} \tag{2.6}$$

In the graph, the green dashed line is an approximation when $E = E_1 = 0.500$ MPa. This line then changes to gray to compare the weight of this mechanical property if the stamp was fabricated to maintain a low E value. The blue dashed line is the fitting when

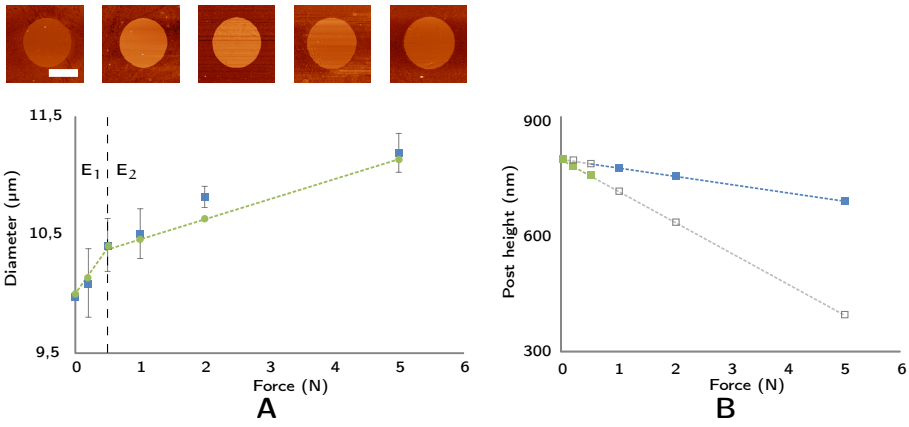

Figure 2.21: **Comparison between printing at different pressures.** (A) The images on top presents the sequential collection of the spots in Figure 2.19. The graph presents the measured diameter $\pm$ σ of the features plotted as a function of the printing force. The green dashed lines are linear fits to the obtained data (R^2>0.96 for both lines). (B) Presents the calculated δH at different printing forces, where the green and blue dashed lines follow the compression obtained with $E = E_1$ and $E = E_2$ respectively. The gray dashed lines represent the calculated compression with the E in intervals where the values were not fitted. Scale bar = 5 µm.

$E = E_2 = 1.851$ MPa. This last value governs the physical properties of the stamp when the $\overrightarrow{F} \geqslant 0.5$ N.

An integrated model was obtained which calculates the final radius of the printed feature, R_M, correlating the applied force, $\overrightarrow{F}$, the number of posts, N, and the initial radius of the features R_0:

$$R_M = R_0 \sqrt{\frac{1}{2}\left(\frac{3}{1-\frac{\overrightarrow{F}}{NE\pi R_0^2}} - 1\right)} \tag{2.7}$$

The final calculated values using Equation 2.7 are presented in Table 2.4. It is interesting to note that the accuracies of the calculations against the actual measurements are >96% in all of the printed features. Also, it is worth mentioning, that the final radius, R_M, is independent from the length of the protruding structure, H_0, as this model requires solely the introduction of the E to calculate the radial increment of the contacting face. The model can be restructured to approximate the size of a printed pattern with a stamp with different printing geometries.

The model does not take into account the diffusion of the ink when the stamp contacts the substrate, for that same reason, different patterns were later fabricated and characterized to asses the change of the printed feature varying the printing dwell time.

Table 2.4: The measured and estimated radius for different forces applied to the polymer stamp.

PRINTING FORCE (N)	PRINTED RADIUS (μm)	ESTIMATED RADIUS (μm)	ACCURACY (%)
0.0	5.00 ± 0.02	—	—
0.2	5.05 ± 0.14	$5.08^{[a]}$	99.41
0.5	5.21 ± 0.11	$5.20^{[a]}$	99.79
1.0	5.26 ± 0.11	$5.10^{[b]}$	97.14
2.0	5.41 ± 0.05	$5.21^{[b]}$	96.35
5.0	5.60 ± 0.08	$5.57^{[b]}$	99.43

$^{[a]}E = E_1 = 0.500 MPa$

$^{[b]}E = E_2 = 1.851 MPa$

2.5.1.2 *Pattern size and morphology under different printing dwell times*

To provide a quantitative measurement of the contribution of the diffusion, C, during the μCP procees, the patterned substrates with different printing dwell times were characterized with AFM. Figure 2.22 presents one example of all the patterns obtained out of 3 individual measurements on 3 independent samples per each indicated amount of time. The topographical images clearly show the increasing effect of the size of the printed spots when patterned at longer contact times. The profiles under each image provide a graphical representation of the final size of the spot.

The coverage rate, C, of the thiol ink, that is, the amount of area covered by the SAM, at any given time, follows the direction represented in Figure 2.23A. Here the C is taken as the absolute value of the change of the measured diameter, D, at predetermined printing times, T_P. Delamarche *et al.*[12] studied a similar system. In their work, a 0.2 mM solution of Eicosanethiol in ethanol was printed with a PDMS stamp for 3 s. The measured feature sizes were correlated to a simulation devised as the discrete coverage of small, finite areas contiguous to the contacting area. This elements were sequentially covered by the advancing SAM. With this approximation, they obtained a $C = 7.00\ \mu m^2\ s^{-1}$. Contrarily, Sharpe *et al.*[66] found very little coverage at the same range of low concentrations of MHDA. Their work situates the $C \approx 0.77\ \mu m^2\ s^{-1}$. It is interesting to note, that the first referenced work, used a longer, and therefore, heavier thiol ink. This opposing results make it difficult to compare the C from this work.

The values that were obtained are plotted in Figure 2.23B along with a collection of some of the analyzed spots. The calculations resulted in a linear relationship between the D of the printed feature and the T_P. The C values were calculated as a function of the change of the area of the feature, obtaining a value for $C = 4.45\ \mu m^2\ min^{-1}$

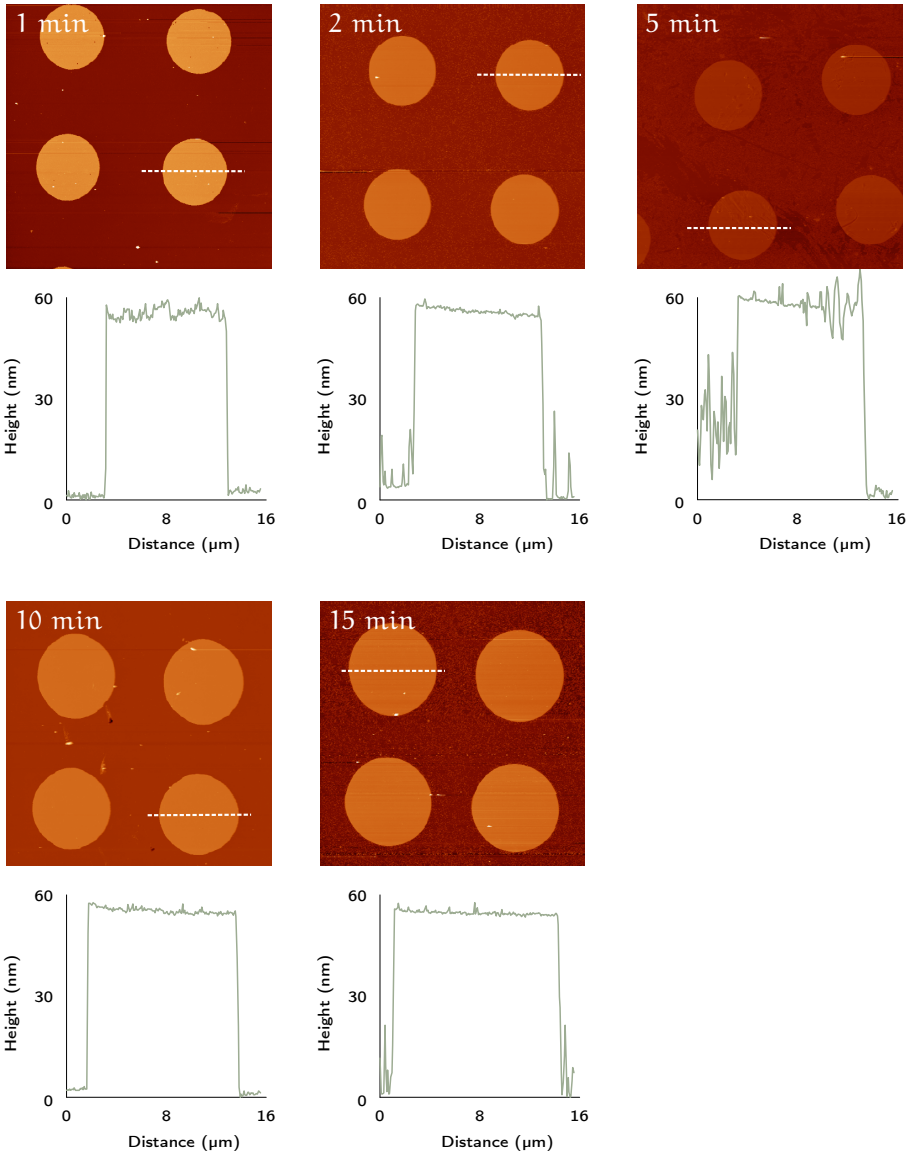

Figure 2.22: **Size of the thiol patterns under different printing dwell times.** AFM topography images of the features obtained after etching a patterned Au substrate. The inked stamp from Figure 2.14 was placed in contact with the substrate for 1, 2, 5, 10, and 15 min to observe the flow of the thiol from the bulk of the stamp to the substrate.

which is equal to 0.25 $\mu m^2\ s^{-1}$. To compare with the published data, the value of C obtained was regressed to represent it as a radially growing circle with a variable D throughout the T_P. Then, the final value can be represented as $C = 0.08\ \mu m\ s^{-1}$. The green dashed line in the graph represents the fitting obtained with the previously mentioned value ($R^2 = 0.97$).

Although the results presented here were obtained with conditions and methods similar to those on the previously published works, the

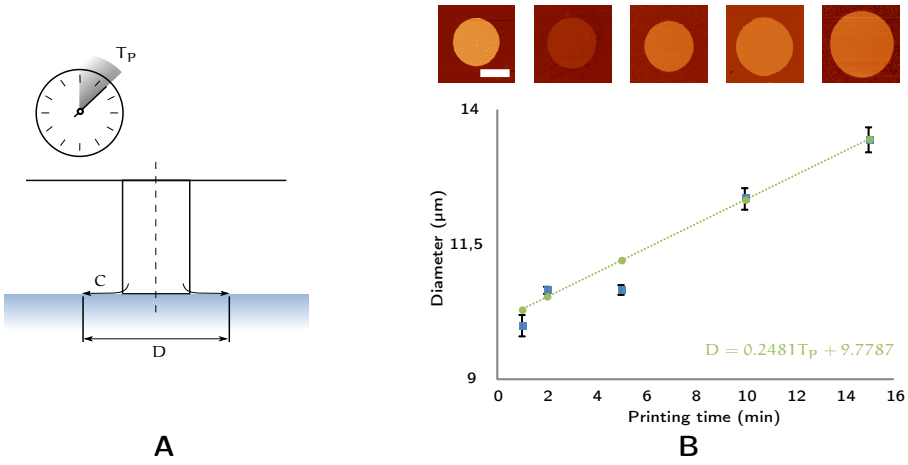

Figure 2.23: **Comparison between printing at different dwell times.** (A) Direction of the coverage, C, of the thiols from the bulk or the stamp to the substrate. (B) The images on top presents the sequential collection of the spots obtained in Figure 2.22. The flow of the thiols from the bulk at different printing dwell times create gradually larger spots. The graph plots the measured diameter different printing dwell times. The green dashed lines follows the fitting equation ($R^2 = 0.97$). Scale bar = 5 µm.

C values have a large variance. From $C = 7.00\ \mu m^2\ s^{-1}$ from Delamarche *et al.*[12], and $C = 0.77\ \mu m^2\ s^{-1}$ from Sharpe *et al.*[66] to the ones presented here, $C = 0.08\ \mu m^2\ s^{-1}$, the wide range of possible values limits the characterization of the printed patterns solely on the coverage of the SAM. It is also worth mentioning that the T_P used is extremely long for many of the applications that require thiol patterning. Subsequent patterns were fabricated with shorter T_P.

2.5.1.3 *Fabrication of complex patterns controlling the printing position*

When printing consecutively with the same stamp, the alignment depends on the accurate positioning of the stage by the actuators. To characterize the difference between the intended and the obtained printing position, a set of complex patterns were designed and printed on Au. The coordinates in Table 2.1 were introduced to the µCP tool and a Au substrate was patterned. A summary of the steps taken to obtain the designs is presented in Figure 2.24. There, the intended positions of every spot for each design is placed on top of the printing scheme. The sequence is presented in the AFM topographic images. To obtain the deviation of the spot from the desired position, the topographic images were transformed into binary bitmaps. With this, the raised features were considered the maximum value, (1) and the depressed areas the minimum (0). A bit-by-bit analysis was performed in every image. The deviation was obtained subtracting the binary topographic image from a binary mask with the intended design. The

relation to obtain the final measurements was 13.42 pixel μm^{-1}, and a theoretical limit of a single pixel representing ~75 nm. The calculated deviation of the intended position with the measured one is presented under the scheme for every printing step for both, the x– and y– axes. The black arrows present the point of the inflection of the spot at the given position for both planar axes. The average inaccuracy of the alignment between the arrows is summarized in Table 2.5 along with the area of the obtained feature.

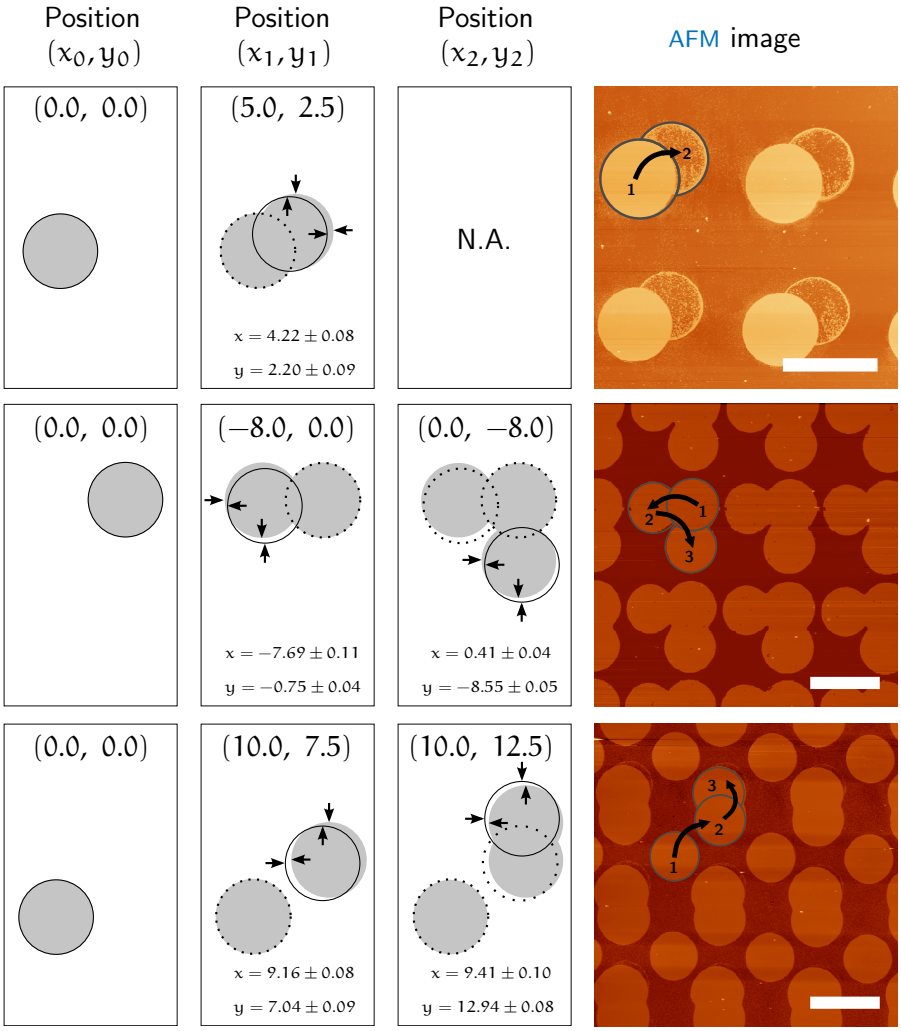

Figure 2.24: **Multiple printings create complex patterns.** A single PDMS stamp loaded with a thiol ink was used to print consecutive spots. The **Diagonal**, **Triangular**, and **Combined** designs are shown. The absolute positions of the design are shown on top of the measured printing positions. The arrows present the deviation between the intended (shadowed) and obtained (clear) spots. The AFM topography images show the patterns after etching the unpatterned Au substrate. Scale bars = 12 μm.

As intended, the printed features were designed to create complex shapes without the need to fabricate a different stamp. By repeating

Table 2.5: Measured area, A, and average deviations, σ, on the x and y axes of the printed patterns.

	DESIGNS		
PARAMETERS	DIAGONAL	TRIANGULAR	COMBINATION
$\sigma_{\overline{x}}$ (μm)	0.78 ± 0.08	0.36 ± 0.06	0.72 ± 0.06
$\sigma_{\overline{y}}$ (μm)	0.30 ± 0.09	0.65 ± 0.03	0.45 ± 0.06
A (μm^2)	76.00 ± 1.39	145.72 ± 1.18	233.01 ± 4.42

the pattern on the surface, larger features or a combination of features with different sizes were achieved. The **Triangular** design had an area 3.07 larger that the area of the features if only one stamping process was carried out. Furthermore, in the **Combined** pattern the complex features were 1.92 larger that original print.

It is important to mention that the lateral alignment of the μCP tool is comparable or better than some of the current existing tools. The average deviations on both axis are between 0.36 and 0.78 μm on the $x-$ axis and 0.30 to 0.65 μm on the $y-$ axis.

Bou Chakra *et al.*[44] developed an instrument with a deviation between 2 and 10 μm along the axes. However, their work only shows a single patterning process, without elaborated designs. Furthermore, the device requires the PDMS stamps to be molded from a custom apparatus. In another publication, Trinkle and Lee[43], produced multiplexed patterns with a deviation of 5 and 15 μm between two printing processes. Still, the location of the stamp cannot be adjusted, and again, the device requires precise fabrication of stamps. The best accuracy so far was reported by Takulapalli *et al.*[41]. They obtained sub-100 nm alignment in Au-Au cold welding. This alignment proved useful to pattern on top of nanofabricated pillars, However, their system is dependent on high precision stamp fabrication.

2.5.2 *Fabrication of biomolecule patterns*

In order to extend the applications of the μCP tool, an important range of biomolecule inks were patterned on various functionalized substrates. The first patterns were produced with proteins.

Proteins conform the largest group of existing biomolecules, thus, most of the functions on living organisms are controlled by these elements. Protein arrays can help understand the function or interaction of different molecules exposed at the same environment. The shape and placement of the spots may affect the effect of the proteins. For such reasons, several protein patterns were fabricated with shape in mind.

Figure 2.25 presents a collection of different biomolecules patterned on various substrates. The first row shows the fluorescent microscopy images of probed proteins. The shape of the pattern can be customized

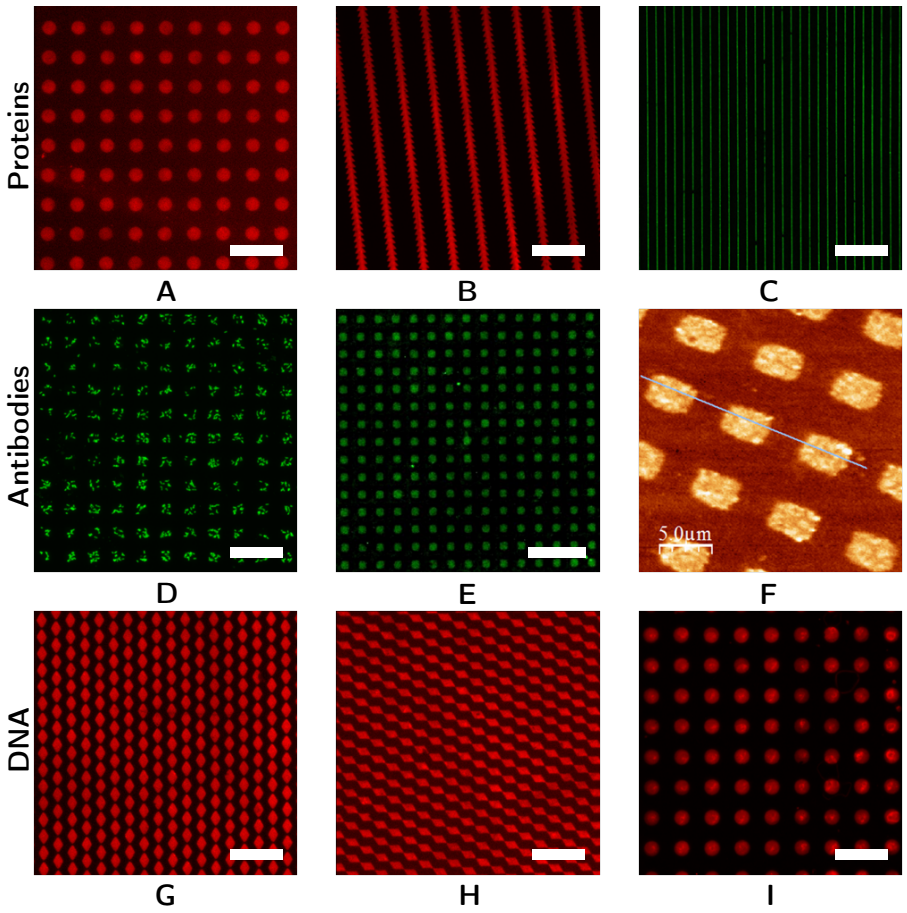

Figure 2.25: **µCP of different biomolecules.** Proteins, antibodies, and DNA can be successfully patterned on different substrates. Fluorescent microscopy images of (A) WGA on SiOx, (B) BSA on glass, and (C) PHA on SiOx. (D) Fluorescence image of an antibody binding assay of an initial pattern of mouse anti-*E. coli* O157 on modified ITO, followed by the incubation of the bacteria, and a final anti-*E. coli* FITC conjugate.[67] (E) Fluorescent microscopy image of a pattern of mouse anti-5C3 IgG, probed with rhu-S100A4 protein, followed by rabbit anti-S100A4, and grafted with AF_{488} goat anti-rabbit IgG (H+L). (F) AFM topography image of a pattern of mouse anti-5C3 IgG.[68] Fluorescent images of stamped DNA: (G) FP-NH_2-T strand patterned on glass, (H) FP-NH_2-T on SiOx, and (I) patterned 5SH-3 hybridized with a complementary 5BT-3TR strand. Scale bars = 30 µm except (F).

for its future use. In Figure 2.25A, WGA-TxR was patterned onto activated SiOx. The shape of the array consists of circles with a diameter of 10 µm. The next pattern, presented in Figure 2.25B, BSA-AF_{555} was patterned on functionalized glass with a stamp with a chain of triangular features running parallel. This type of shapes have been used to guide cells from one area to another.[69] A finer protein pattern is shown in Figure 2.25C. Here, PHA-AF_{488} was directly placed on modified SiOx and create a pattern of parallel lines of 1 µm with a separa-

tion of 5 μm between them. Several cell studies have been developed on similar patterns.[31, 32]

Another important protein group is formed by antibodies. Antibodies work as recognition elements that bind to certain zones on selected antigens. Patterning these biomolecules open a great opportunity to create recognition arrays and parallel immunoassays. When locating antibodies on a restricted zone, a spot on an array, the antigen binds precisely where the antibody is, sequestering it form the rest of the environment. This collocation methods create opportunities for antibody arrays. The second row in Figure 2.25 presents a compilation of several patterned antibodies. In this case, the characterization of the biomolecules was given by a recognition event. The first event consisted on isolating the bacteria *E. coli* from a sample. First, the anti-*E. coli* was patterned on ITO, then the substrate was submerged on the bacteria-loaded sample. The fluorescent microscopy image in Figure 2.25D shows the emission of a secondary FITC conjugated anti-*E. coli* grafted on the sequestered bacteria.

A similar approach was followed for the pattern of anti-SC3 IgG presented in Figure 2.25E. In this case, a complete antibody binding assay was necessary to observe the immobilization of the rhu-S100A4 protein which was recognized by the immobilized antibody. The next layer on the assay was obtained when the antibody-protein complex was exposed to rabbit anti-S100A4, and a final AF_{488} anti-rabbit IgG. With the same patterned antibodies, González *et al.*[68] studied the differences in lateral resolution between tapping and jumping modes in AFM. Figure 2.25F shows the AFM topographic image of the antibody pattern. These images help conclude that the patterned antibodies remained active and functional, and that they provide the a flexible, yet robust foundation for several studies.[35, 37]

Lastly, several DNA micropatterns were fabricated with the μCP tool. The third row in Figure 2.25 presents three different DNA patterns. The first two, Figure 2.25G-H consist on the FP-NH_2-T strand on SiOx and glass respectively. In the last image, the 5SH-3 strand was patterned over epoxy-modified SiOx. This last strand lacked any fluorescent probe. For such reason, a complementary strand 5BT-3TR, conjugated with TxR was hybridized to the immobilized DNA. The successful hybridization confirms the immobilization of the initial strand and its ability to shape around the second strand and bind. Please refer to Table A.1 for the DNA sequences.

It is worth noting that both Lange *et al.*[70] and Xu *et al.*[39] required amino-derivatized PDMS stamps to transfer the DNA from solution to the surface. This modification was not necessary to obtain either pattern previously presented. These results confirm a robust platform similar as the one used by Thibault *et al.*[40] to create functional DNA micropatterns.

Contrarily to small molecules, the interaction between the stamp and the biomolecules create a monolayer only on its surface. The advantage of this phenomena is the creation of patterns that replicate the exact geometry of the stamp without the interference of diffusion.

2.5.2.1 *Multiplexed biomolecule patterns*

Following the positive results with the direct placement of various biomolecules, and subsequent creation of micropatterns, more complex designs were called for. To fabricate such patterns, the printing step would require the use of more than one stamp. The difficulty of this approach is the alignment between the second stamp and the first pattern avoiding any damage to the pattern.

The first one required solely the rotation of the stage holder in its vertical axis. The first pattern was intended to create crossing parallel lines at an $\measuredangle = 60°$. Although perfectly well transferred from the stamp, Figure 2.26A-C shows, the displacement between the patterned protein lines is 5° off. This unwanted displacement is due to a misalignment between sample and stamp. Still, a very close approximation with an error of ~8% was obtained

Interlocking features offer opportunities to study elements in proximity. For that same reason, the first truly multiplexed pattern was fabricated. As presented in Figure 2.26D, an initial protein was patterned at random location which was defined as $(x_0,\ y_0) = (0,\ 0)\ \mu m$. The next intended position $(x_1,\ y_1)$ was defined with the coordinates $(10,\ 10)\ \mu m$ and subsequently patterned, obtaining the position presented in Figure 2.26E. After analyzing the location of both patterning processes with a similar approach as the one discussed in Section 2.5.1.3 with a relation of 7.03 $pixel\ \mu m^{-1}$, the deviation of the second pattern from the initial zero-position was calculated at $2.06 \pm 0.25\ \mu m$ and $0.25 \pm 0.07\ \mu m$ on the $x-$ and $y-$ axes, respectively.

The last column on Figure 2.26 shows the sequential printing of two inks to obtain the closest distance between patterns without overlapping. As previously discussed, a first stamp was used to pattern the sample. Afterwards, the second inked stamp was aligned, and the patterning process was concluded. In this approach, the space between patterns was $<1\ \mu m$. It can be noted that some of the spots on the patterns are not as defined as others, this is due to the time it takes to align and print consecutively. It has been reported that solely after $\sim 1\ min$ in a dry state, the efficiency of the transfer greatly decreases, hence, the pattern is transferred incompletely.[34]

Bou Chakra *et al.*[44], using their customized PDMS stamps, were capable of sequentially patterning a substrate, yet the deviation observed when patterning with two stamps was $>10\ \mu m$. This same value was reached in another publication.[47] A better precision was obtained by Trinkle and Lee[43]. In their work, two antibody patterns

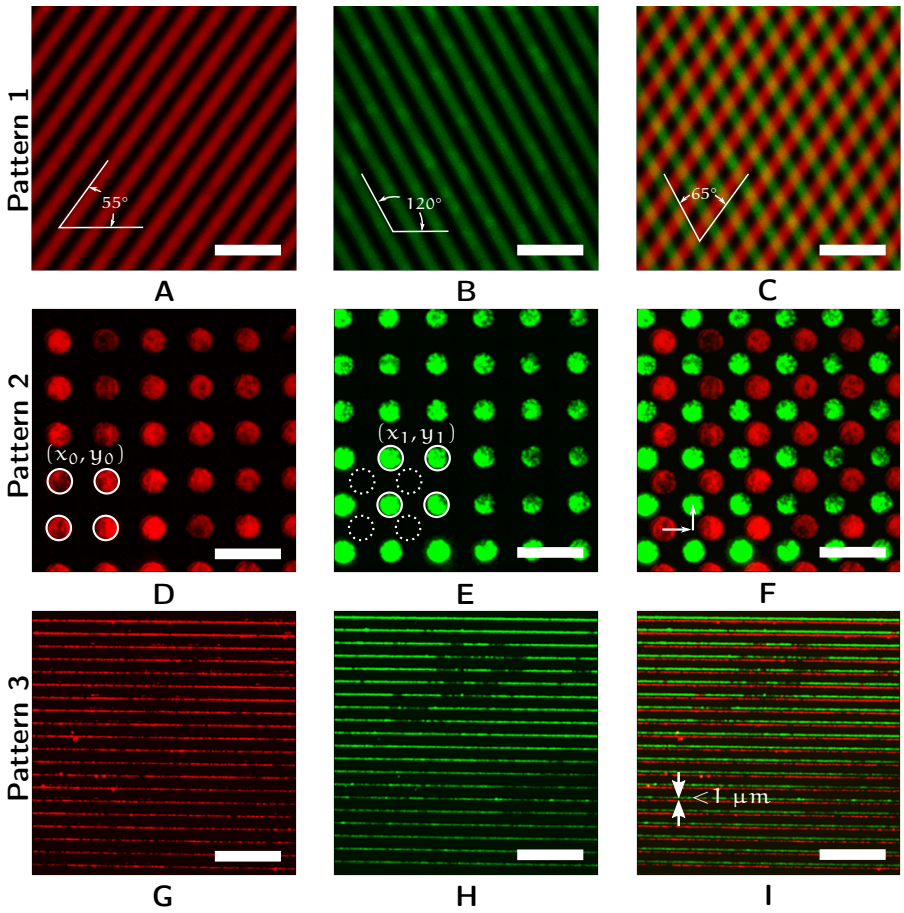

Figure 2.26: **Printing multi-proteins spots to create increasingly complex patterns.** Lines of WGA labeled with TxR (A) and lines of PHA labeled with AF_{488} (B) printed on an epoxy-modified SiOx substrate. (C) Merged image of the crossed patterns having a displacement of 65°. A first pattern of spots of SAV labeled with TxR (D) and a subsequent pattern of spots of NAV labeled with OG_{488} (E) printed on an epoxy-modified SiOx substrate. (F) Merged image of the obtained fluorescent patterns. The complex pattern was fabricated by displacing the second printing process by 7 µm on the x− axis and 5 µm o the y− axis from the first printing process. (G) Lines of WGA conjugated with TxR (H) and lines of PHA labeled with AF_{488} printed on an epoxy-modified SiOx substrate. Both patterns remain parallel throughout the substrate, indicating a correct alignment. (I) Merged image of the parallel patterns. Scale bars = 25 µm.

were transferred using different stamps, and obtained a deviation of 5 µm between patterns. The best alignment was obtained by Takulapalli *et al.*[41] when the stamp was rotated using its integrated Moiré fringes. They were able to pattern 16 lines of nanopillars of 500 nm with a stamp with a tolerance of 500 nm. None of the other mentioned patterning tools include the ability to create multiplex patterns. [42, 45, 46]

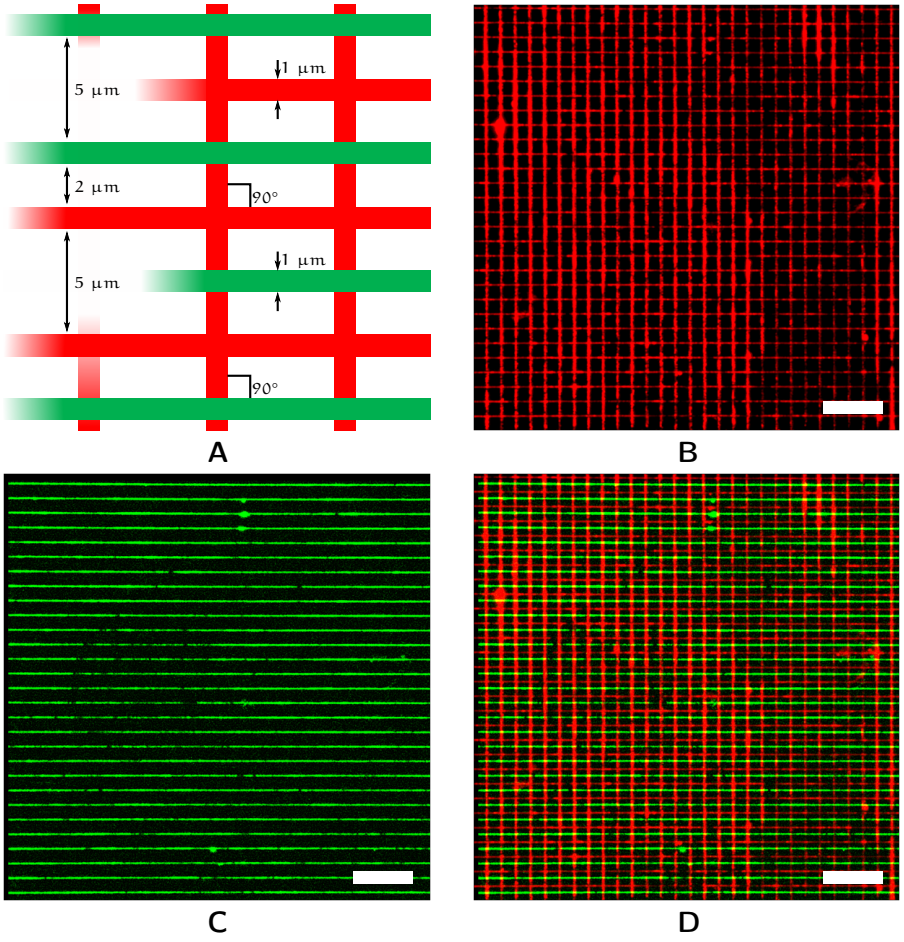

Figure 2.27: **Complex multiplexed embedded pattern.** (A) Design and parameters of the stamping process. (B) Two consecutive patterns of WGA labeled with TxR printed at 90° of each other, and a third printing of lines of PHA labeled with AF_{488} (B) all printed on an epoxy-modified SiOx substrate. (C) Merged image of the aligned patterns. Scale bar = 20 µm.

Figure 2.27 presents the most complicated printed pattern. It consists on interlocked parallel running lines of two different proteins. The initial stamp was used twice, first at a random location, and a second position, at an $\measuredangle = 90°$ from the first one. This pattern a collection of crossing lines at the exact angle. The next pattern was transferred using a stamp with the same features as the previous one. The important achievement was the actual localization of the last pattern. Figure 2.27A shows the design of the pattern, with the consecutive images showing the different fluorescent emissions of each conjugated protein. The alignment of the intermediate PHA-AF_{488} lines was an intended symmetrical distance between the previously printed lines with a separation of 2 µm on both sides. The image analysis with a relation of 15 $pixels\ \mu m^{-1}$, obtained an average of 1.77 ± 0.04 µm for the distance on top of the line, and 2.41 ± 0.12 µm on the bot-

tom. Also, as suspected, the line was not completely parallel towards the first pattern. The second line had a slight misalignment of $<0.1°$ throughout the sample.

2.6 CONCLUSIONS

This Chapter described the characteristics and general approaches to solve some patterning issues associated with Microcontact printing (μCP). Traditionally, this patterning technique has been performed manually, and the success, or failure, to obtain a correct pattern, falls solely on the ability of the researcher. Here an automatized μCP tool has been described and its functions characterized in the hope of improving and standardizing this patterning technique.

Initially, thiols of different length and terminal groups were patterned on gold substrates. Their property to mask the gold substrate in the patterned areas during etching was advantageous to create permanent gold features that were later characterized. The information obtained from these features helped understand the dynamics involved during the patterning process. Using the automated μCP tool, the entire printing process was tuned by controlling the printing pressure and printing dwell time. A model that relates the force during the printing process, and the mechanical properties of the polymeric stamp with the final feature size was developed. Afterwards, the rate at which the surface is covered by the transported ink was also studied. Later, using the submicrometer aligning capabilities of the μCP tool, complex features were fabricated without the need of new polymeric stamps or additional printing processes.

Subsequently, biomolecules were directly transfered to functionalized substrates to create bioactive surfaces with interesting biological functions. Complex and multiplexed biomolecular patterns were fabricated using the completely customized μCP tool.

2.7 REFERENCES

[1] Qin, D; Xia, Y; and Whitesides, GM. 'Soft lithography for micro- and nanoscale patterning.' *Nature protocols*, 5 (3) (2010) 491–502. URL http://www.ncbi.nlm.nih.gov/pubmed/20203666

[2] Fodor, S; Read, J; Pirrung, M; Struyer, L; Lu, A; and Solas, D. 'Light-directed, spatially addressable parallel chemical synthesis'. *Science*, 251 (February) (1991) 767–773. URL http://www.ncbi.nlm.nih.gov/pubmed/1990438

[3] Pease, AC; Solas, D; Sullivan, EJ; Cronin, MT; Holmes, CP; and Fodor, SP. 'Light-generated oligonucleotide arrays for rapid DNA sequence analysis.' *Proceedings of the National Academy of Sciences of the United States of America*, 91 (11) (1994) 5022–6. URL http://www.pubmedcentral.nih.gov/articlerender.fcgi?artid=43922&tool=pmcentrez&rendertype=abstract

[4] Delamarche, E. 'Microcontact Printing of Proteins'. In AR Fersht, editor, 'Nanobiotechnology', pages 1–24. Wiley-VCH Verlag GmbH & Co. KGaA, Weinheim, Germany (2008). URL http://doi.wiley.com/10.1002/9783527610754

[5] Kumar, A and Whitesides, GM. 'Features of gold having micrometer to centimeter dimensions can be formed through a combination of stamping with an elastomeric stamp and an alkanethiol "ink" followed by chemical etching'. *Applied Physics Letters*, 63 (14) (1993) 2002. URL http://link.aip.org/link/APPLAB/v63/i14/p2002/s1&Agg=doi

[6] Kaufmann, T and Ravoo, BJ. 'Stamps, inks and substrates: polymers in microcontact printing'. *Polymer Chemistry*, 1 (4) (2010) 371. URL http://xlink.rsc.org/?DOI=b9py00281b

[7] Lisensky, G and Campbell, D. 'Replication and compression of surface structures with polydimethylsiloxane elastomer'. *Journal of Chemical Education*, 75 (4) (1999) 537–541. URL http://pubs.acs.org/doi/abs/10.1021/ed076p537

[8] Johnston, ID; McCluskey, DK; Tan, CKL; and Tracey, MC. 'Mechanical characterization of bulk Sylgard 184 for microfluidics and microengineering'. *Journal of Micromechanics and Microengineering*, 24 (3) (2014) 035017. URL http://stacks.iop.org/0960-1317/24/i=3/a=035017?key=crossref.cf83b17be3210f20943ae0e9169fc9b8

[9] Lee, JN; Park, C; and Whitesides, GM. 'Solvent compatibility of poly(dimethylsiloxane)-based microfluidic devices.' *Analytical chemistry*, 75 (23) (2003) 6544–54. URL http://www.ncbi.nlm.nih.gov/pubmed/14640726

[10] Berthier, E; Young, EWK; and Beebe, D. 'Engineers are from PDMS-land, Biologists are from Polystyrenia.' *Lab on a chip*, 12 (7) (2012) 1224–37. URL http://www.ncbi.nlm.nih.gov/pubmed/22318426

[11] Alom Ruiz, S and Chen, CS. 'Microcontact printing: A tool to pattern'. *Soft Matter*, 3 (2) (2007) 168. URL http://xlink.rsc.org/?DOI=b613349e

[12] Delamarche, E; Schmid, H; Bietsch, A; Larsen, N; Rothuizen, H; Michel, B; and Biebuyck, H. 'Transport mechanisms of alkanethiols during microcontact printing on gold'. *The journal of physical chemistry. B*, 102 (18) (1998) 3324–3334. URL http://pubs.acs.org/doi/abs/10.1021/jp980556x

[13] Jang, MJ and Nam, Y. 'Geometric effect of cell adhesive polygonal micropatterns on neuritogenesis and axon guidance.' *Journal of neural engineering*, 9 (4) (2012) 046019. URL http://www.ncbi.nlm.nih.gov/pubmed/22814204

[14] Morton, K and Fountain, E. 'Meeting of the Minds - Art of Science Competition' (2006). URL http://www.princeton.edu/artofscience/gallery2006/view.php%3Fid=31.html

[15] Paretkar, D; Kamperman, M; Schneider, AS; Martina, D; Creton, C; and Arzt, E. 'Bioinspired pressure actuated adhesive system'. *Materials Science and Engineering: C*, 31 (6) (2011) 1152–1159. URL http://linkinghub.elsevier.com/retrieve/pii/S0928493110002419

[16] Petrzelka, JE and Hardt, DE. 'Static load-displacement behavior of PDMS microfeatures for soft lithography'. *Journal of Micromechanics and Microengineering*, 22 (7) (2012) 075015. URL http://stacks.iop.org/0960-1317/22/i=7/a=075015?key=crossref.2aa6298d3364ce6415d59f1a6bcfd459

[17] Elhadj, S; Rioux, RM; Dickey, MD; DeYoreo, JJ; and Whitesides, GM. 'Subnanometer replica molding of molecular steps on ionic crystals.' *Nano letters*, 10 (10) (2010) 4140–5. URL http://www.pubmedcentral.nih.gov/articlerender.fcgi?artid=2956021&tool=pmcentrez&rendertype=abstract

[18] Liao, X; Braunschweig, AB; Zheng, Z; and Mirkin, Ca. 'Force- and time-dependent feature size and shape control in molecular printing via polymer-pen lithography.' *Small*, 6 (10) (2010) 1082–6. URL http://www.ncbi.nlm.nih.gov/pubmed/19859944

[19] Bergmair, I; Mühlberger, M; Lausecker, E; Hingerl, K; and Schöftner, R. 'Diffusion of thiols during microcontact printing with

rigid stamps'. *Microelectronic Engineering*, 87 (5-8) (2010) 848–850. URL http://linkinghub.elsevier.com/retrieve/pii/S0167931709009010

[20] Xia, Y and Whitesides, G. 'Extending microcontact printing as a microlithographic technique'. *Langmuir*, 7463 (18) (1997) 2059–2067. URL http://pubs.acs.org/doi/abs/10.1021/la960936e

[21] Bessueille, F; Pla-Roca, M; and Mills, C. 'Submerged Microcontact Printing: An Unconventional Printing Technique of Thiols Using High Aspect Ratio, Elastomeric Stamps'. *Langmuir*, 21 (10) (2005) 12060–12063. URL http://pubs.acs.org/doi/abs/10.1021/la0513095

[22] Geissler, M and Bernard, A. 'Microcontact-printing chemical patterns with flat stamps'. *Journal of the American Chemical Society*, 122 (26) (2000) 6303–6304. URL http://pubs.acs.org/doi/pdf/10.1021/ja000476i

[23] Ricoult, SG; Pla-Roca, M; Safavieh, R; Lopez-Ayon, GM; Grütter, P; Kennedy, TE; and Juncker, D. 'Large dynamic range digital nanodot gradients of biomolecules made by low-cost nanocontact printing for cell haptotaxis.' *Small*, 9 (19) (2013) 3308–13. URL http://www.ncbi.nlm.nih.gov/pubmed/23606620

[24] Tien, J; Xia, Y; and Whitesides, G. 'Microcontact printing of SAMs'. In 'Thin Films', volume 24, pages 227–250. Academic Press (1998). URL http://scholar.google.com/scholar?hl=en&btnG=Search&q=intitle:Microcontact+Printing+of+SAMs#4

[25] Love, JC; Estroff, LA; Kriebel, JK; Nuzzo, RG; and Whitesides, GM. 'Self-assembled monolayers of thiolates on metals as a form of nanotechnology.' *Chemical reviews*, 105 (4) (2005) 1103–69. URL http://www.ncbi.nlm.nih.gov/pubmed/15826011

[26] Wolfe, DB; Love, JC; Paul, KE; Chabinyc, ML; and Whitesides, GM. 'Fabrication of palladium-based microelectronic devices by microcontact printing'. *Applied Physics Letters*, 80 (12) (2002) 2222. URL http://scitation.aip.org/content/aip/journal/apl/80/12/10.1063/1.1463719

[27] Vericat, C; Vela, ME; Benitez, G; Carro, P; and Salvarezza, RC. 'Self-assembled monolayers of thiols and dithiols on gold: new challenges for a well-known system.' *Chemical Society reviews*, 39 (5) (2010) 1805–34. URL http://www.ncbi.nlm.nih.gov/pubmed/20419220

[28] Ulman, A. 'Self-assembled monolayers of alkyltrichiorosilanes: Building blocks for future organic materials'. *Advanced Materials*,

2 (12). URL http://onlinelibrary.wiley.com/doi/10.1002/adma.19900021203/abstract

[29] Wang, M; Liechti, KM; Wang, Q; and White, JM. 'Self-assembled silane monolayers: fabrication with nanoscale uniformity.' *Langmuir*, 21 (5) (2005) 1848–57. URL http://www.ncbi.nlm.nih.gov/pubmed/15723481

[30] James, C; Davis, R; and Kam, L. 'Patterned protein layers on solid substrates by thin stamp microcontact printing'. *Langmuir*, 14 (4) (1998) 741–744. URL http://pubs.acs.org/doi/abs/10.1021/la9710482

[31] Schmalenberg, K; Buettner, H; and Uhrich, K. 'Microcontact printing of proteins on oxygen plasma-activated poly(methyl methacrylate)'. *Biomaterials*, 25 (10) (2004) 1851–1857. URL http://linkinghub.elsevier.com/retrieve/pii/S0142961203006847

[32] Rozkiewicz, DI; Kraan, Y; Werten, MWT; de Wolf, Fa; Subramaniam, V; Ravoo, BJ; and Reinhoudt, DN. 'Covalent microcontact printing of proteins for cell patterning.' *Chemistry*, 12 (24) (2006) 6290–7. URL http://www.ncbi.nlm.nih.gov/pubmed/16741908

[33] Renault, JP; Bernard, A; Juncker, D; Michel, B; Bosshard, HR; and Delamarche, E. 'Fabricating microarrays of functional proteins using affinity contact printing.' *Angewandte Chemie*, 41 (13) (2002) 2320–3. URL http://www.ncbi.nlm.nih.gov/pubmed/12203579

[34] Bernard, A; Renault, JP; Michel, B; Bosshard, HR; and Delamarche, E. 'Microcontact Printing of Proteins'. *Advanced Materials*, 12 (14) (2000) 1067–1070. URL http://doi.wiley.com/10.1002/1521-4095%28200007%2912%3A14%3C1067%3A%3AAID-ADMA1067%3E3.3.CO%3B2-D

[35] Nichkova, M; Dosev, D; Perron, R; Gee, SJ; Hammock, BD; and Kennedy, IM. 'Eu3+-doped Gd2O3 nanoparticles as reporters for optical detection and visualization of antibodies patterned by microcontact printing.' *Analytical and bioanalytical chemistry*, 384 (3) (2006) 631–7. URL http://www.ncbi.nlm.nih.gov/pubmed/16416096

[36] Inerowicz, H; Howell, S; Regnier, F; and Reifenberger, R. 'Multiprotein immunoassay arrays fabricated by microcontact printing'. *Langmuir*, 18 (13) (2002) 5263–5268. URL http://pubs.acs.org/doi/abs/10.1021/la0157216

[37] LaGraff, JR and Chu-LaGraff, Q. 'Scanning force microscopy and fluorescence microscopy of microcontact printed antibodies and antibody fragments.' *Langmuir*, 22 (10) (2006) 4685–93. URL http://www.ncbi.nlm.nih.gov/pubmed/16649783

[38] Renault, J; Bernard, A; Bietsch, A; Michel, B; Bosshard, HR; and Delamarche, E. 'Fabricating arrays of single protein molecules on glass using microcontact printing'. *The journal of physical chemistry. B*, 107 (3) (2003) 703–711. URL http://pubs.acs.org/doi/abs/10.1021/jp0263424

[39] Xu, C; Taylor, P; Ersoz, M; Fletcher, PDI; and Paunov, VN. 'Microcontact printing of DNA-surfactant arrays on solid substrates'. *Journal of Materials Chemistry*, 13 (12) (2003) 3044. URL http://xlink.rsc.org/?DOI=b307788h

[40] Thibault, C; Le Berre, V; Casimirius, S; Trévisiol, E; François, J; and Vieu, C. 'Direct microcontact printing of oligonucleotides for biochip applications.' *Journal of nanobiotechnology*, 3 (2005) 7. URL http://www.pubmedcentral.nih.gov/articlerender.fcgi?artid=1184096&tool=pmcentrez&rendertype=abstract

[41] Takulapalli, BR; Morrison, ME; Gu, J; and Zhang, P. 'A nanocontact printing system for sub-100 nm aligned patterning.' *Nanotechnology*, 22 (28) (2011) 285302. URL http://www.ncbi.nlm.nih.gov/pubmed/21636882

[42] Choonee, K and Syms, RRA. 'Hydraulically actuated micro-contact printing engines'. *Journal of Micromechanics and Microengineering*, 21 (8) (2011) 085013. URL http://stacks.iop.org/0960-1317/21/i=8/a=085013?key=crossref.b8b8883bef74a4de7638936933acbeff

[43] Trinkle, CA and Lee, LP. 'High-precision microcontact printing of interchangeable stamps using an integrated kinematic coupling.' *Lab on a chip*, 11 (3) (2011) 455–9. URL http://www.ncbi.nlm.nih.gov/pubmed/21116585

[44] Bou Chakra, E; Hannes, B; Dilosquer, G; Mansfield, CD; and Cabrera, M. 'A new instrument for automated microcontact printing with stamp load adjustment.' *The Review of scientific instruments*, 79 (6) (2008) 064102. URL http://www.ncbi.nlm.nih.gov/pubmed/18601419

[45] Elloumi-Hannachi, I; Maeda, M; Yamato, M; and Okano, T. 'Portable microcontact printing device for cell culture.' *Biomaterials*, 31 (34) (2010) 8974–9. URL http://www.ncbi.nlm.nih.gov/pubmed/20817249

[46] Cau, JC; Ludovic, L; Marie, N; Adriana, L; and Vincent, P. 'Magnetic field assisted microcontact printing: A new concept of fully automated and calibrated process'. *Microelectronic Engineering*, 110 (2013) 207–214. URL http://linkinghub.elsevier.com/retrieve/pii/S0167931713003961

[47] McNulty, JD; Klann, T; Sha, J; Salick, M; Knight, GT; Turng, LS; and Ashton, RS. 'High-precision robotic microcontact printing (R-μCP) utilizing a vision guided selectively compliant articulated robotic arm.' *Lab on a chip*, 14 (11) (2014) 1923–30. URL http://www.ncbi.nlm.nih.gov/pubmed/24759945

[48] Group, E. 'EVG 6200 Infinity Automated Micro Contact Printing Systems' (2011). URL http://www.azonano.com/article.aspx?ArticleID=2767

[49] Gesellschaft für Silizium-Mikrosysteme mbH. 'GeSim MicroContactPrinter' (2013). URL http://www.gesim.de/en/contact-printers/instruments/

[50] Kim, TH; Cho, KS; Lee, EK; Lee, SJ; Chae, J; Kim, JW; Kim, DH; Kwon, JY; Amaratunga, G; Lee, SY; Choi, BL; Kuk, Y; Kim, JM; and Kim, K. 'Full-colour quantum dot displays fabricated by transfer printing'. *Nature photonics*, 5 (February) (2011) 176–182. URL http://dx.doi.org/10.1038/nphoton.2011.12

[51] Horcas, I; Fernández, R; Gómez-Rodríguez, JM; Colchero, J; Gómez-Herrero, J; and Baro, AM. 'WSXM: a software for scanning probe microscopy and a tool for nanotechnology.' *The Review of scientific instruments*, 78 (1) (2007) 013705. URL http://www.ncbi.nlm.nih.gov/pubmed/17503926

[52] Eichelsdoerfer, DJ; Liao, X; Cabezas, MD; Morris, W; Radha, B; Brown, Ka; Giam, LR; Braunschweig, AB; and Mirkin, Ca. 'Large-area molecular patterning with polymer pen lithography.' *Nature protocols*, 8 (12) (2013) 2548–60. URL http://www.ncbi.nlm.nih.gov/pubmed/24263094

[53] Prats-Alfonso, E; García-Martín, F; Bayo, N; Cruz, LJ; Pla-Roca, M; Samitier, J; Errachid, A; and Albericio, F. 'Facile solid-phase synthesis of biotinylated alkyl thiols'. *Tetrahedron*, 62 (29) (2006) 6876–6881. URL http://linkinghub.elsevier.com/retrieve/pii/S0040402006007204

[54] Holmberg, A; Blomstergren, A; Nord, O; Lukacs, M; Lundeberg, J; and Uhlén, M. 'The biotin-streptavidin interaction can be reversibly broken using water at elevated temperatures.' *Electrophoresis*, 26 (3) (2005) 501–10. URL http://www.ncbi.nlm.nih.gov/pubmed/15690449

[55] Perl, A; Reinhoudt, DN; and Huskens, J. 'Microcontact Printing: Limitations and Achievements'. *Advanced Materials*, 21 (22) (2009) 2257–2268. URL http://doi.wiley.com/10.1002/adma.200801864

[56] Chen, T; Jordan, R; and Zauscher, S. 'Dynamic microcontact printing for patterning polymer-brush microstructures.' *Small*, 7 (15) (2011) 2148–52. URL http://www.ncbi.nlm.nih.gov/pubmed/21598381

[57] Offenhäusser, A; Böcker-Meffert, S; Decker, T; Helpenstein, R; Gasteier, P; Groll, J; Möller, M; Reska, A; Schäfer, S; Schulte, P; and Vogt-Eisele, A. 'Microcontact printing of proteins for neuronal cell guidance'. *Soft Matter*, 3 (3) (2007) 290. URL http://xlink.rsc.org/?DOI=b607615g

[58] Nam, Y; Branch, DW; and Wheeler, BC. 'Epoxy-silane linking of biomolecules is simple and effective for patterning neuronal cultures.' *Biosensors & bioelectronics*, 22 (5) (2006) 589–97. URL http://www.ncbi.nlm.nih.gov/pubmed/16531038

[59] Sharon, N and Lis, H. 'History of lectins: from hemagglutinins to biological recognition molecules.' *Glycobiology*, 14 (11) (2004) 53R–62R. URL http://www.ncbi.nlm.nih.gov/pubmed/15229195

[60] Carter, D and Ho, J. 'Structure of serum albumin'. In 'Advances in protein chemistry', volume 45, pages 153–203. Academic Press, Inc. (1994). URL http://ntrs.nasa.gov/search.jsp?R=19970005608

[61] Porter, M; Bright, T; Allara, D; and Chidsey, C. 'Spontaneously Organized Molecular Assemblies. 4. Structural characterization of n-alkyl thiol monolayers on gold by optical ellipsometry, infrared spectroscopy, and electrochemistry'. *Journal of the American Chemical Society*, 109 (12) (1987) 3559–3568. URL http://pubs.acs.org/doi/abs/10.1021/ja00246a011

[62] Techane, S; Baer, DR; and Castner, DG. 'Simulation and modeling of self-assembled monolayers of carboxylic acid thiols on flat and nanoparticle gold surfaces.' *Analytical chemistry*, 83 (17) (2011) 6704–12. URL http://www.pubmedcentral.nih.gov/articlerender.fcgi?artid=3165144&tool=pmcentrez&rendertype=abstract

[63] Caballero, D; Pla-Roca, M; Bessueille, F; Mills, Ca; Samitier, J; and Errachid, A. 'Atomic Force Microscopy Characterization of a Microcontact Printed, Self-Assembled Thiol Monolayer for Use in Biosensors'. *Analytical Letters*, 39 (8) (2006) 1721–1734. URL http://www.tandfonline.com/doi/abs/10.1080/00032710600714014

[64] Barreiros dos Santos, M; Agusil, JP; Prieto-Simón, B; Sporer, C; Teixeira, V; and Samitier, J. 'Highly sensitive detection of pathogen Escherichia coli O157:H7 by electrochemical

impedance spectroscopy.' *Biosensors & bioelectronics*, 45 (2013) 174–80. URL http://www.ncbi.nlm.nih.gov/pubmed/23500360

[65] Ebrahimi, R and Najafizadeh, A. 'A new method for evaluation of friction in bulk metal forming'. *Journal of Materials Processing Technology*, 152 (2) (2004) 136–143. URL http://linkinghub.elsevier.com/retrieve/pii/S0924013604004492

[66] Sharpe, RBA; Burdinski, D; Huskens, J; Zandvliet, HJW; Reinhoudt, DN; and Poelsema, B. 'Spreading of 16-mercaptohexadecanoic acid in microcontact printing.' *Langmuir*, 20 (20) (2004) 8646–51. URL http://www.ncbi.nlm.nih.gov/pubmed/15379487

[67] Barreiros dos Santos, M; Azevedo, S; Agusil, JP; Prieto-Simón, B; Sporer, C; Torrents, E; Juárez, A; Teixeira, V; and Samitier, J. 'Label-free ITO-based immunosensor for the detection of very low concentrations of pathogenic bacteria'. *Bioelectrochemistry*, 101 (2015) 146–152. URL http://linkinghub.elsevier.com/retrieve/pii/S1567539414001558

[68] González, L; Otero, J; Agusil, JP; Samitier, J; Adan, J; Mitjans, F; and Puig-Vidal, M. 'Micropattern of antibodies imaged by shear force microscopy: comparison between classical and jumping modes.' *Ultramicroscopy*, 136 (2014) 176–84. URL http://www.ncbi.nlm.nih.gov/pubmed/24184681

[69] Mahmud, G; Campbell, CJ; Bishop, KJM; Komarova, YA; Chaga, O; Soh, S; Huda, S; Kandere-Grzybowska, K; and Grzybowski, Ba. 'Directing cell motions on micropatterned ratchets'. *Nature Physics*, 5 (8) (2009) 606–612. URL http://www.nature.com/doifinder/10.1038/nphys1306

[70] Lange, SA; Benes, V; Kern, DP; Hörber, JKH; and Bernard, A. 'Microcontact printing of DNA molecules.' *Analytical chemistry*, 76 (6) (2004) 1641–7. URL http://www.ncbi.nlm.nih.gov/pubmed/21978556

3

FABRICATION OF SUSPENDED PLANAR MULTIPLEXED MICROARRAYS

This Chapter presents the use of the patterning on specialized substrates to fabricate arrays over small areas. Here, several microstructured silicon oxide substrate formed by anchored microparticles were patterned with proteins and small molecules using a technique called Polymer Pen Lithography together with the upgraded version of the Microcontact Printing Tool. The anchored microparticles were later liberated to obtain suspended planar microarrays.

3.1 BACKGROUND

The biological functions in all living systems are controlled by proteins. With no exception, the biological functions in humans is governed by a proteome that exceeds 100,000 different proteins[1], assembled from approximately 293,000 distinct peptides.[2] Proteomics, is the study of the structure and function of proteins. Enzyme-linked immunosorbent assay (ELISA) and immuno- (Western) Blots have been traditionally the most widely used methods to detect and analyze proteins in samples. Both techniques rely on the interaction of the target proteins with antibodies. In Western Blots, the proteins in the sample are separated based on their molecular weight and charge by electrophoresis using a gel matrix. Immediately afterwards, they are transferred to a membrane and probed with an enzyme-linked antibody complementary to the intended protein. When the enzyme is exposed to its substrate, a colourimetric reaction takes place producing a change in colour proportional to the amount of protein. On the other hand, ELISAs use fixed antigens to the walls of a well plate. Afterwards, the wells are inundated with a solution with the specific antibody. Either the initial antibody, or a secondary antibody, specific to the first one, is conjugated with an enzyme. When the substrate of the enzyme is added, a visible reaction is observed. A direct relationship between the change and concentration of analyte can be defined.

Other more complex, high-throughput screening tools have been developed to accelerate the processing of proteins: mass spectrometry and genomic modification. Mass spectrometry is a tool to detect the mass to charge ratio of a sample. Proteins are purified, denatured, digested, and the peptides separated by liquid chromatography. Afterwards, the separated product is ionized by electrospraying and analyzed with a mass analyzer (mass spectrometer). The characteristics of the protein can be correlated with the change of the ionized state and the measured mass.[3, 4]

Alternatively, direct genetic modification requires a known DNA strand with the desired sequence of a selected protein. Yeast or microbes can be modified to express the chosen protein. Naturally occurring fluorescent proteins are assembled by the biological mechanisms present on the microbes and characterized with traditional fluorescence microscopy.[5]

While highly specific and sensitive, all of the previous methods can only manipulate a single protein per assay, and the shear number of existing proteins represent an immense challenge to understand their unique biological role. Protein microarrays present the best alternative to run multiple proteomic studies in parallel.

3.2 PROTEIN MICROARRAYS

Planar protein arrays are a collection of spotted and fixed proteins on a solid substrate.[6–8] Each spot is composed by the sequestration of proteins covering a defined area. The first reported protein array, developed by Chang[9], consisted on an antibody matrix with spots from 0.25 mm to 1 mm, manually positioned over a glass substrate with a micropipette. In the work, mononuclear cells were bound on the spotted areas on 1 cm^2 substrates. The first high-throughput method was developed by Schena *et al.*[10] to study gene expression, localization of transcription factor binding sites, and detection of sequence mismatch on planar DNA microarrays. The microarrays were patterned with a high-speed robotic printer. This technology paved the road to create the actual, multiplexed, and miniaturized planar protein arrays. Planar protein microarrays have been used as drug and disease screening tools, as well as the analysis of the biochemical pathway and interaction of proteins. Studies on vaccine-, enzyme/substrate- and immuno-profiling have all been conducted using planar protein microarrays.[11]

Figure 3.1 presents the basic procedure to work with planar protein microarrays. Initially, the spotted proteins are covalently bound to a solid substrate. Although the spots are oriented on both x− and y− axes, their binding position and orientation in the spot is random. An immunoassay with fluorescent antibodies helps identify the spotted proteins. An array scanner or fluorescence microscopy is used to characterize the immunoassay.

Since then, an enormous amount of scientific research has been focused on the development of improved planar protein microarrays. This technology has been proven to detect low-abundance proteins in complex environments with improved sensitivity and specificity with low sample consumption. Still the main advantage is the multiplex detection on a single platform.[11, 12]

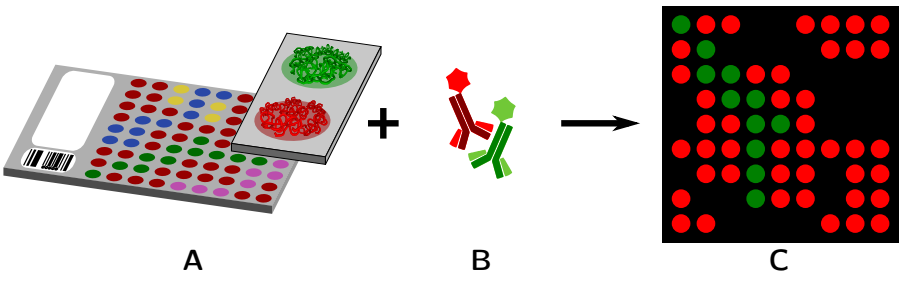

Figure 3.1: **Planar arrays.** (A) Traditional planar arrays consist of many spots of biomolecules immobilized on a substrate, usually at the cm^2 range. When exposed to a fluorescent complementary probe (B), the spots where the probe was captured can be characterized with fluorescence microscope (C).

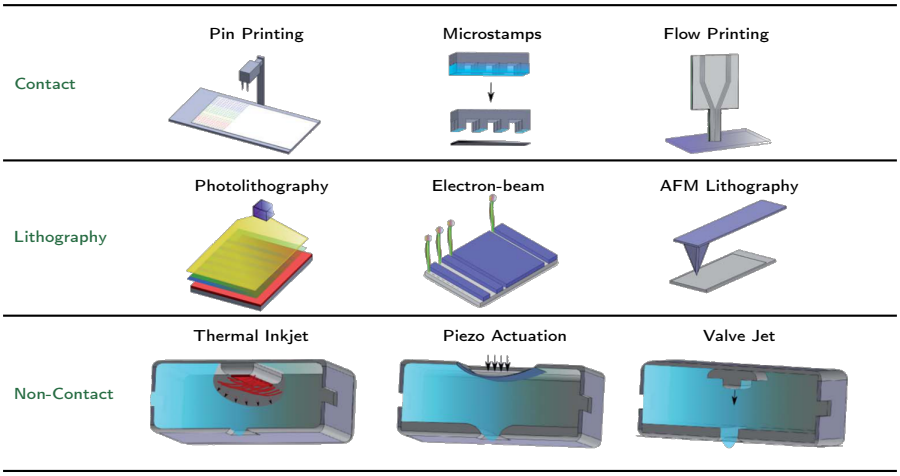

Figure 3.2: **Fabrication of planar microarrays.** Contact, litographic, and non-lithographic fabrication technologies. Adapted from [11].

Several microarray fabrication methods are presented in Figure 3.2. Each method has advantages and drawbacks and should be chosen for the final application of the microarray. Fabrication by contact is produced when the biomolecules is positioned on the desired location by direct placement. The most widely used technology is pin printing. This technique uses solid, split or quill pins to transfer the protein solution onto a solid surface, and its continued fame is primarily due to the repercussion of the creation of the first DNA array.[10] This technique is relatively fast and cheap, still, the size of the pin and an inherently dry atmosphere limits the resolution and morphology of the printed spots. Fabrication by contact using microstamps has been described previously in Chapter 2. Flow-printing uses a specialized three-dimensional microfluidic printing head which is placed directly into the substrate and delivers the protein solution at a constant flow. Each spot is created by an independent microfluidic circuit controlling the direction and force of the flow. This technology creates defined spots without exposure to air. The spots are rinsed after the printing reaction with the same printing head still on the same position, hence, preventing the removal of unbound molecules to the rest of the substrate when washing the substrate. Although promising, this technology is rather slow compared to other microarray fabrication technologies, limiting throughput.[13]

Lithographic methods to fabricate protein microarrays have been traditionally separated into three categories: Photolithography, electron beam, and AFM-based lithographies. In photolithography, an undeveloped photoresist is first spin-coated on the desired substrate, which is then be exposed to UV light through a photomask. The micropattern is obtained after developing the photoresist. Generally,

proteins are covalently bound to the protruding photoresist, thus, defining the biomolecular spots. Although a high-throughput fabrication technique, the resolution of the spots is limited to the diffraction of the shinning light, and can only create microarrays of a single protein. Alternatively, electron-beam lithography uses a defined stream of electrons to change the chemical properties of the photoresist. Having a smaller wavelength than light, this beam can create structures down to the nanoscale. Unfortunately, as with UV photolithography, the final biological coating is limited to a single protein. Additionally, this is a rather expensive fabrication technique requiring clean-room facilities.[14] AFM-based lithography uses the scanning probe to remove material form the surface or to transfer adsorbed molecules towards the substrate. Nanografting uses the AFM tip to scrape away areas of a protein-resistant SAM which are later replaced with protein-adherent molecules. The proteins adsorb or bind to the new SAM. The morphology of the array is controlled by the exposed areas created initially. Protein patterns as small as 40×40 nm have been reported with this technique.[15] Piner *et al.*[16] developed Dip-pen nanolithography (DPN), which uses an AFM tip to deposit adsorbed molecules onto a substrate. Initially, the tips are dipped in an ink and later positioned on the desired location. A water meniscus is formed in the tip-substrate interface which guides the diffusion of the adsorbed molecules towards the substrate. Their initial studies transporting thiols from the tip, gave way to the first protein array fabricated by Wilson *et al.*[17]. Spots of few tens of nm have been since presented.[15] Both nanografting and dip-pen nanolithography present unparalleled miniaturization of protein arrays, yet the small overall area and low fabrication speed limit the applications of either technique for high-throughput studies.

The non-contact fabrication of protein arrays represents the last microarray technology presented in Figure 3.2. As inferred from the name, in these fabrication methods, no contact occurs between the printing tool and substrate to deposit the molecules. The overall idea is to transport the ink solution from a nozzle to the substrate via jet ejection. Three different ejection methods have been widely used to transport the solution to the substrate: Thermal ejection, piezo-actuation, and valve-ejection. In thermal ejection, a heated gas bubble is created inside the ink reservoir, prompting an increase of internal pressure. After reaching a critical point, the bubble collapses, pushing the ink out the nozzle in the form of small drops. Generally, spots from 100 µm to 1 mm are obtained with this ejection system.[18] The piezo-actuation ejection systems use a piezoelectric component located behind a diaphragm fixed on the ink reservoir. The piezo is excited, creating a abrupt volumetric change, which induces a sudden pressure variation, causing the ink to exit in the form of droplets. Spots from 50 µm to 500 µm have been reported.[19]

Although not entirely designed to pattern biomolecules, in valve-ejection, a valve located on the ink reservoir is opened and closed consecutively while the entire set-up is under continuous high pressure, ejecting a stream of droplets.[11] Either system is intended to create homogeneous patterns on various substrates. High-throughput and low cross-contamination are the greatest advantages any of these systems offer. While obstruction of the nozzle and the inherently "large" spots limit their application at the micro- and nanoscale.

3.2.2 *Suspended protein arrays*

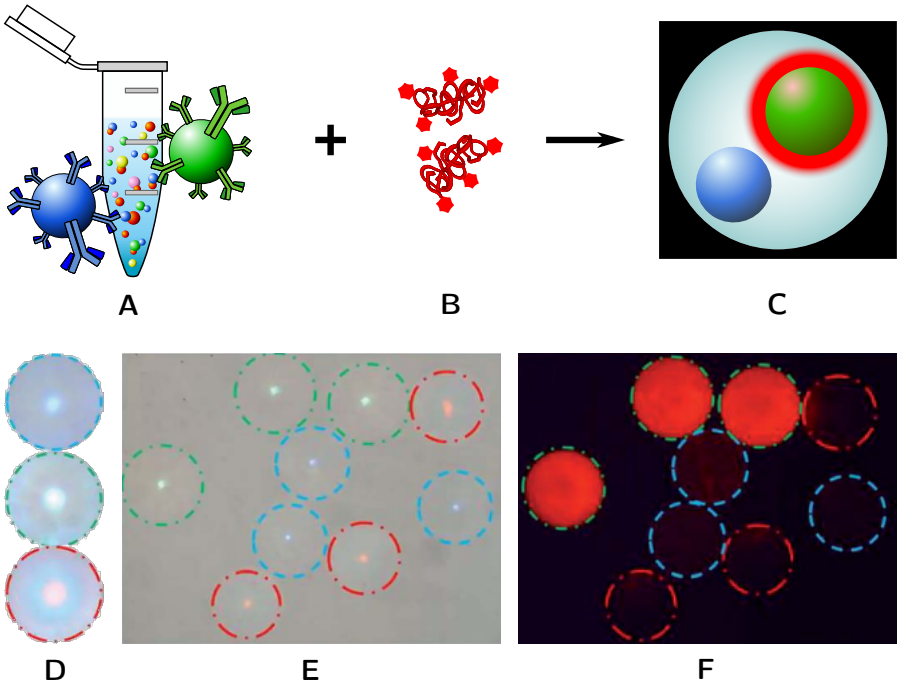

Figure 3.3: **Suspended arrays.** (A) Suspended arrays are composed of a dispersion of several microparticles independently functionalized with an individual probe. When exposed with an analyte (B), only the complementary probes will capture the suspended analyte (C). (D-E) Bright field and (F) fluorescence images of silicon microspheres decorated with complementary (green spheres), single-mismatched (red spheres), and non-complementary (blue spheres) DNA strands, later hybridized with a fluorescent-labeled strand. Adapted from [20]

Another class of high density arrays are suspended arrays, which consist on a collection of independently-modified structures dispersed in a medium.[21] Each structure, typically micrometer-sized polymeric microspheres, is decorated with an unique covalently bound protein analogous to a single spot on a planar array. Figure 3.3 represents the assemble to obtain the complete collection of functionalized microspheres.[22] Each receptor on the surface of the sphere is

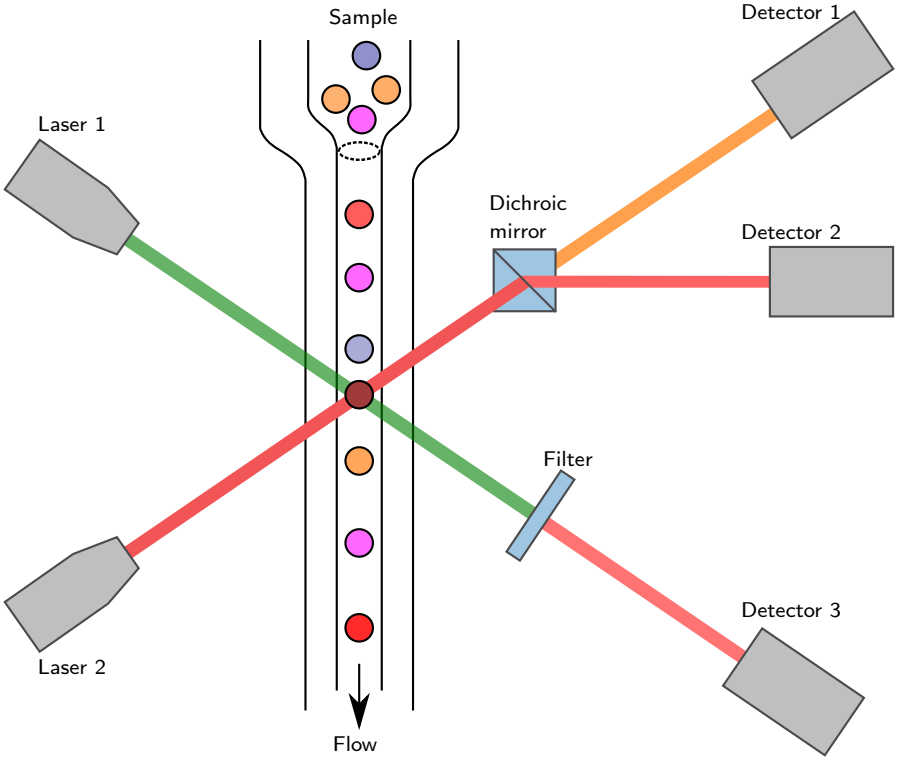

Figure 3.4: **Schematic diagram of flow cytometry.** Hydrodynamically focused microspheres pass through two different laser beams. The initial laser excites the microsphere and the fluorescence is detected at two wavelengths which identifies the encoding dye. The second laser excites the fluorescence of the bound analyte.

unique, thus, the population of same microparticles allows a repeated result form each evaluation. Biomolecular analyses with nucleic acids, proteins, enzymes, or other complex molecules have been applied with microsphere arrays for research and clinical applications.[20, 21]

This type of arrays present significant advantages over planar arrays. First, every array element in each planar array is fabricated individually, as described previously. The main limitation is the number of arrays that can be fabricated in parallel. In contrary, the elements on suspended arrays are prepared in bulk. The complete suspension of microspheres may contain millions of particles per milliliter, accounting for many assays.[21] Secondly, the slow diffusion of molecules to target sites on planar arrays limit some of its applications. The radial diffusion of analytes in suspended arrays provide more flexibility for the detection and shorter reaction times.[20] An important characteristic of these modified microspheres is that they are analyzed using flow cytometry, allowing highly multiplexed analysis of heterogeneous samples, exemplified in Figure 3.4, accounting for a fast screening method but limited in the final applications.[22, 23] The main limitation of these arrays is the inherent individuality. Each microparticle is modified with a single biomolecule, thus, can

only record an independent assay, following this path, a collection of different microparticles have to be used to track all the variables in a single study. This can prove difficult in small volume or low-analyte samples.

Multiplexed microparticles could overcome the isotropy of traditional suspended arrays. Different approaches have been recently followed to fabricate microparticles, leading to an astounding variety of shapes, patterns, and chemical compositions.[24–26]

The vast anisotropies on these microparticles differ greatly with the traditionally used microspheres. Apart from the obvious grouping of microparticles by their physical properties, i. e. *inter alia*, shape, roughness, size, and aspect ratio, these particles can be described by their functionalization capabilities, more specifically, the creation of multiplexed bioactive microparticles.

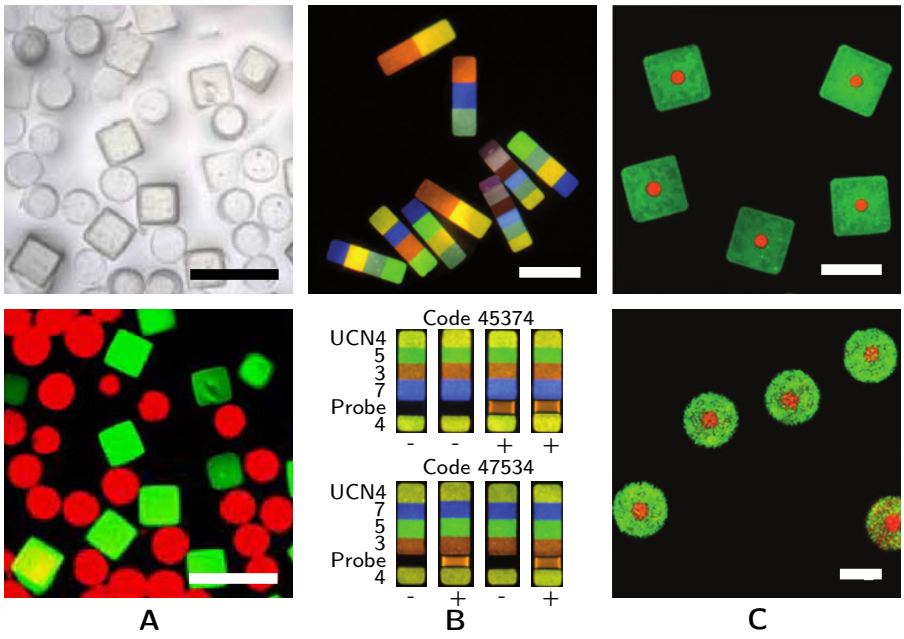

Figure 3.5: **Microparticles with integrated functionality.** (A) Various enzyme-functionalized hydrogel microparticles.[27] (B) Luminescence images of encoded microparticles and RNA multiplexed bioassay.[28] (C) Square non-biodegradable and circular biodegradable microparticles fabricated by the layer-by-layer dipping method.[29] Scales bars = 500 µm in (A), 200 µm in (B) and 10 µm in (C).

Two approaches can be followed to create bioactive microparticles. The first one, is the direct embedding of biomolecules during the fabrication process. This approach is limited as most fabrication methods require harsh and non biological-compatible steps, including ultra high vacuum, high temperatures and the exposure to both, aqueous and vapour etching environments. Few publications present biocompatible fabrication methods. Lee *et al.*[27] developed hydro-

gel microparticles fabricated by photopatterning entrapping different enzymes within the three-dimensional polymeric matrix. With this technique, particles from 50 to 300 μm with a thickness of 47 μm were obtained. The reactivity of the enzymes was tested with the fluorescence emission when exposed to their substrates (Figure 3.5A). A similar approach was followed by Lee *et al.*[28]. In their work, Ribonucleic acid (RNA) target strands were incorporated on encoded polymer microparticles. Stop-flow lithography was used to photopolymerize co-flowing laminar streams of photocurable monomers under a photomask, obtaining particles of ~250 × 70 × 36 μm (Figure 3.5B). To obtain different colour codes, each monomer stream was mixed with spectrally distinct upconversion nanocrystals, which emit different wavelengths when excited with the same light. Zhang *et al.*[29] used layer-by-layer assembly to coat a PDMS stamp with protruding features with an initial thermoplastic dot, and various subsequent films of polyelectrolytes which could contain DNA, chitosan or PLL, creating biodegradable and non-biodegradable microparticles. To release the particles, the complete assemble was deprinted from the stamp against a polyvinyl alcohol film on a glass slide, that was later dissolved in water. Features from 2 to 20 μm in length and a thickness of 12.8 nm are described (Figure 3.5C). So far, any of the presented microparticles could be used to track a single biomolecular analyte, limiting their function as multiplexed suspended arrays. The requirement to have defined patterned areas motivates the development of post-fabrication microparticle functionalization.

The second approach consists on the modification of the fabricated microparticles. The functionality of the microparticles can be, thus, tailored to the increase their applications. The chemistry on the surfaces plays the central role on the desired decoration. Single modifications can be readily obtained by isotropic coating, that it, the entire coverage of the exposed surface of the microparticle. Silanes on silicon-based microparticles, and thiols on gold microparticles are favoured to create a bioactive shell surrounding each particle. When two bioactive entities are desired on each microparticle, a further fabrication step, such as coating half the microparticle with a reactive shell, or successive orthogonal chemistries are required.[24]

Figure 3.6A presents bifunctional microparticles known as Janus microparticles. This type of microparticles intends to create biologically or chemically differentiated hemispheres.[30] First, silica particles with a diameter of 4.7 μm were spread to coat a glass slide. Later, the exposed half was coated with gold by thermal evaporation and after sonication, the microparticles were ready to functionalize. Evidently, up to this step, no biomolecule would remain intact if exposed to the functionalization method. Two different proteins were independently bound via thiol or silane linkers on the gold and silicon hemispheres, respectively. It is worth noting, that the binding

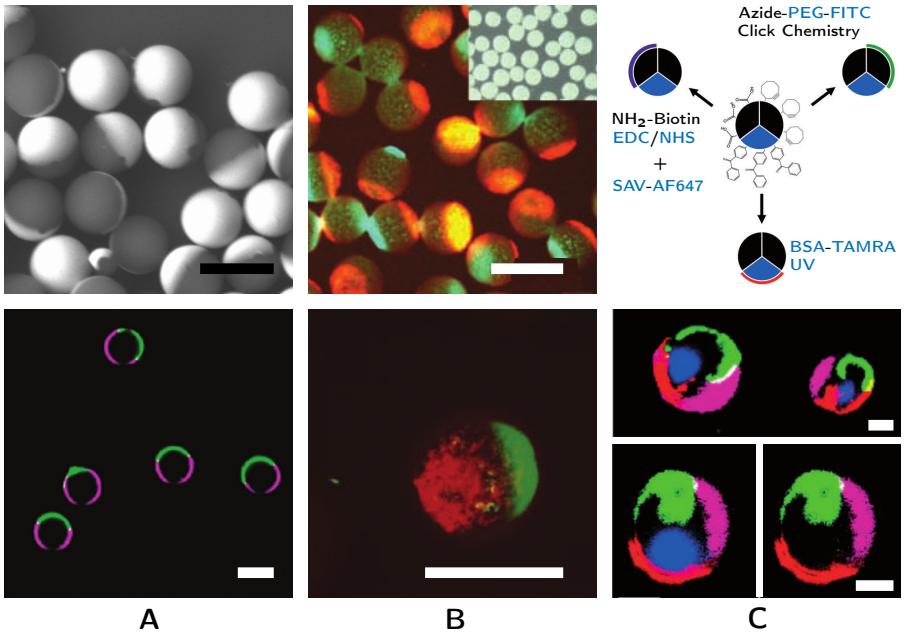

Figure 3.6: **Functionalized microparticles.** (A) SEM and fluorescent images of gold-coated silica microparticles. Two different antibodies, independently tagged with AF_{488} and AF_{647} were probed on the gold ans silica surfaces, respectively.[30] (B) Top: Fluorescent image of Janus polymer microparticles fabricated by sandwich-printing red an blue dyes. Bottom: same polymer microparticles with two printed carbohydrates.[31] (C) Top: Selective modification by orthogonal chemistries of the three different functional patches on the microparticles fabricated by electrohydrodynamic co-jetting. Bottom: Confocal microscopy images of the surface modifications.[32] Scales bars = 5 μm in (A), 200 μm in (B) and 5 μm in (C).

of the proteins was produced in a sequential manner, so that the hemispheres were independently coated. Another modification mechanism to create Janus microparticles was developed by Kaufmann *et al.*[31]. In their work, sandwich μCP was used to coat the top and bottom portions of epoxy-functionalized polymeric spheres. A microparticle monolayer was assembled over a flat PDMS stamp loaded with an amine ink. A second flat stamp loaded with a different amine ink was placed over the microparticle monolayer and left to react. Afterwards, the microparticles were derivatized with protein-binding carbohydrates, among others. Figure 3.6B shows the Janus polymeric particles conjugated with rhodamine ethylenediamine (red) and dansylcadaverine (blue) dyes. The same procedure was used to fabricate Janus particles with the amino-β-galactoside and amino-α-mannoside carbohydrate inks on the opposing poles, which are selective to peanut agglutinin and concanavalin A, respectively. The carbohydrate affinity allowed the selective conjugation without protein interference. Interestingly, both, the dye and the carbohydrate Janus microparticles

required a reaction temperature of 120 °C, extremely high for any biomolecule, hence, limiting the biofunctionalization to subsequent chemical steps.

Rahmani *et al.*[32] recently published the development of microparticles with three independent and chemically orthogonal regions. The work is based on the creation of polymeric microparticles with multiple surface moieties combining electrohydrodynamic co-jetting and customized polymer chemistry. Each region consist on anchoring sites from functionalized polylactide polymers with different derivatives adequate for orthogonal surface modification without interference. The first region was developed for subsequent photo-immobilization, the second region to obtain covalent bonds under the copper-free click reaction, and last one was designed to work with the 1-Ethyl-3-(3-dimethylaminopropyl)carbodiimide (EDC) N-Hydroxysuccinimide (NHS) reaction. As presented in Figure 3.6C, each region was functionalized following and independent chemistry without affecting the remaining others. BSA-TAMRA was immobilized using UV photo-immobilization and is represented in red. Azide-PEG-FITC, presented in green, was bound using Cu-free click reaction on the cyclooctyne-modified polymer. The last region false-coloured in purple, used SAV-Alexa Fluor® 647 (AF647) to probe an initial coating layer of amine-PEG-biotin, bound to the carboxylic acid-modified polymer region. The confocal microscopy image clearly shows the divided microparticles.

Although an incredible advance in the development of multiplexed particles, a multi-protein microparticle would be impossible to build following orthogonal chemistry, as the repeating amino and carboxyl moieties on every protein would limit a selective binding. A miniaturized planar array could overcome the intrinsic disadvantages previously discussed. This system could provide a multiplexed platform on each microparticle for parallel studies with the freedom of movement of suspended arrays. Unfortunately, non biological-compatible fabrication methods, or the inherently interfering functionalization strategies, limit the development of such tools. These motivations were integrated to develop a new family of arrays: suspended, planar, and multiplexed protein microarrays.

3.2.3 *Suspended planar microarrays*

The miniaturization of sensing platforms has provided several approaches to study various physical and chemical properties in small-volume samples. These platforms can simultaneously detect multiple biomolecules, accelerate the identification of analytes, and reduce sample volumes.[26] The smallest units of life, cells, offer the final frontier to study systems in constricted and well-defined volumes, which would present discoveries to enlighten of their highly orga-

nized, internal functions. Traditional planar arrays enables the parallel study of proteins from cell extracts, providing a single portrait of the average proteomic interaction, not counting cell-to-cell variation. A first approach to understand the variation between cells was developed by Gandor *et al.*[33]. There, a protein array was fabricated directly inside a cell by membrane receptors that transfered an antibody surface patten from the substrate into a complementary bait protein arrangement formed by proteins in the cell membrane. Arrabito *et al.*[34] produced a similar approach to track the expression of proteins directly into the cell. Instead of creating external pattens to translate the information towards the cell, suspended planar microarrays could deliver the pattern directly into the cell, helping in the study and understanding of the individual intracellular biophysical parameters and proteome.

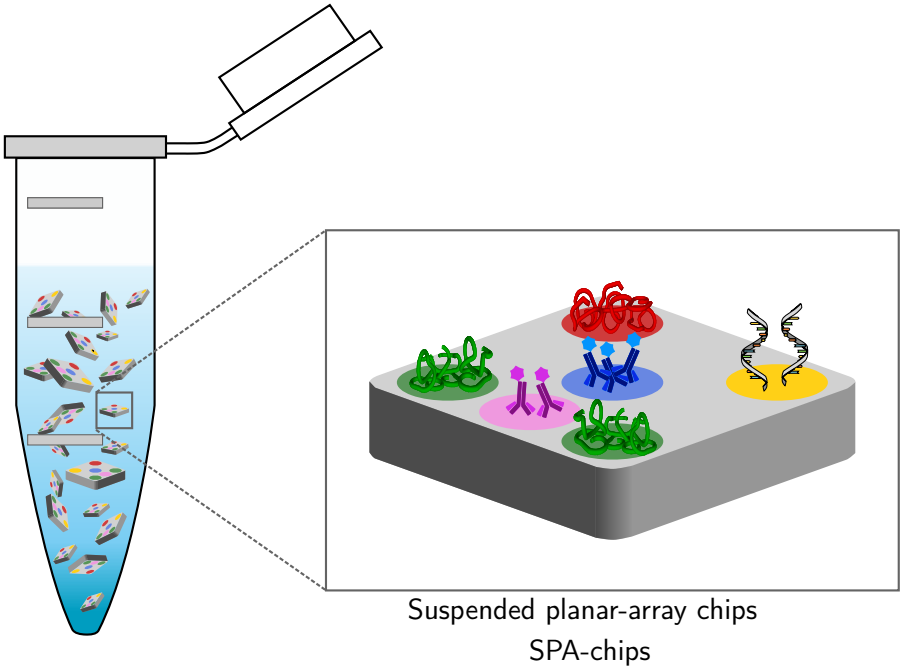

Figure 3.7: **Suspended planar-array chips.** Schematic showing the concept of suspended multifunctionalized microparticles which combine the planar and suspended array strategies to create planar arrays at the microscale.

Several other biophysical parameters that affect the cell function have been studied using nanoparticles. Vetrone *et al.*[35] measured the internal temperature of the cell using intracellular nanothermometers, Fercher *et al.*[36] measured the cell oxygenation concentration with O_2 sensing nanoparticles in the cytoplasm. Guo *et al.*[37] measured the cellular pH with sensing nanoparticles. Nanoparticles, contrarily to microparticles, can access the cell easily, and navigate almost freely once inside, making this approach interesting for some applications. Still, the fate and final distribution of the intracellular nanoparticles

is poorly understood, creating complex obstacles for further sensing applications.[38]

On the other hand, microparticles, have been internalized in cells as a initial step for the future development of intracelluar chips.[39] Following a similar path, micromachined particles have been proven useful as barcodes to tag and track cells during complete cell cultures.[40, 41] Also, intracellular silicon microparticles were developed to deliver drugs with positively or negatively charged surfaces,[42] and even measure pressure changes in living cells.[43] Combining the final applications of cell tagging, and direct internalization of miniaturized protein microarrays, a complex, multiplexed system as the one depicted in Figure 3.7 can be designed.

3.2.3.1 *Technology implemented for the fabrication of suspended planar microarrays*

A functionalization strategy in collaboration with the Centre Nacional de Microelectrònica (http://www.imb-cnm.csic.es/), and the Laboratory of Organic Chemistry, at the Faculty of Pharmacy from the University of Barcelona, both in Barcelona, Spain, was developed to fabricate miniaturized and multiplexed protein microarrays. The main goal was to develop a parallel patterning method to directly position the desired biomolecules on microparticles. To facilitate the patterning and manipulation of the microparticles, a micromachined substrate with anchored microparticles was envisioned and developed on silicon, using well-established technology for microelectromechanical applications.[39, 43]

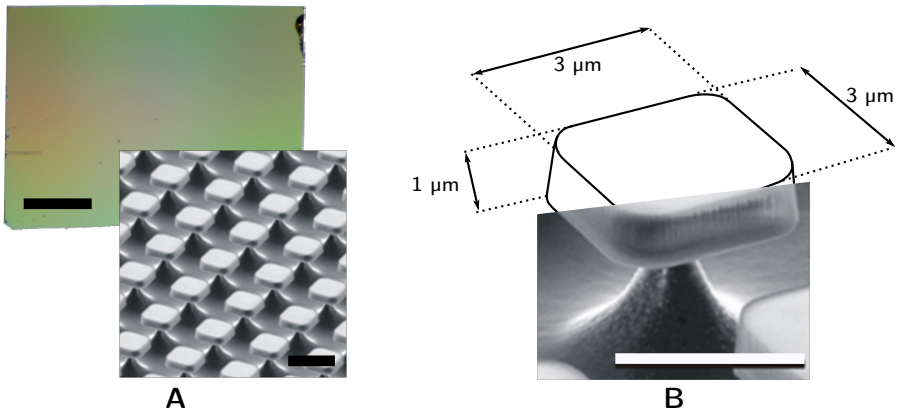

Figure 3.8: **Anchored microparticles at different scales.** (A) Digital photography and SEM image of an entire substrate before functionalization. (B) Dimensions of an individual anchored microparticle present on the substrate. Scale bars = 250 µm and 5 µm in (A) and 5 µm in (B).

The substrate is presented in Figure 3.8 at different magnifications. An initial portion of an entire micromachined silicon wafer with an

area of ~1.33 cm^2 can be seen in Figure 3.8A together with a SEM image of several anchored microparticles distributed evenly through the $x-$ and $y-$ axes. Figure 3.8B shows the SEM image of an anchored microparticle measuring $3 \times 3 \times 1$ μm, and a pitch of 3 μm on both planar axes. The anchoring element was designed to break when a lateral load is applied on the anchored microparticle, yet resist vertical loads.

The consecutive steps to pattern and liberate the microparticles are represented in Figure 3.9. An initial microarray has to be fabricated on each particle, replicating the same distribution along all the other particles. The subsequent step would require the liberation of the anchored microparticles breaking the anchoring element. This process should maintain a suitable environment to protect the conformation and functionality of the derivatized biomolecules. Finally, the liberation matrix should be able to be removed, allowing the resuspension of the microparticles on any other medium.

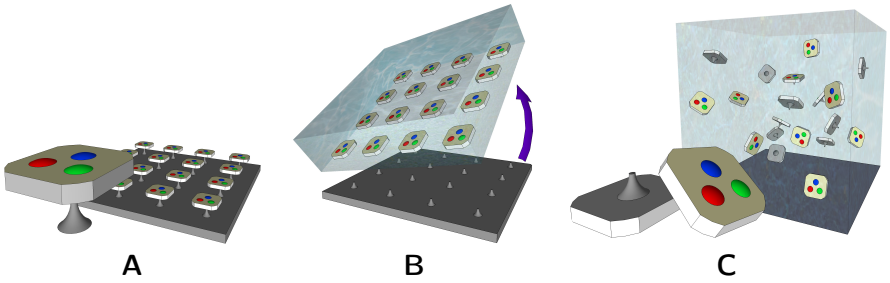

Figure 3.9: **Strategy to fabricate suspended planar arrays.** (A) Parallel patterning of anchored microparticles. (B) Liberation of particles without damaging the printed biomolecules. (C) Resuspension of planar arrays in the desired solution.

Direct biomolecule placement presents the best choice to create the parallel microarrays. The best alternative to covalently bind proteins would be using molecular glues similar to the ones presented in Section 2.4.3.1. The main limitation of this approach is the actual positioning of repeated patterns on top of every microparticle. An initial technique to print the individual, submicrometer spots on the multiplexed array over every independent microparticle is DPN.[16] As described previously, this patterning technique uses a probe similar to an AFM tip to transport adsorbed molecules on its surface to a substrate using a water meniscus formed between the tip and sample. The size of the spot is controlled by the contact time and the humidity, increasing if any of the variables increase. Submicrometer structures have been formed using organic molecules and biomolecules on various substrates.[44] However, the sequential printing mechanism would not be able to cope with the distribution and density of $\sim 2.78 \times 10^6$ anchored microparticles per cm^2, therefore, consuming immense amounts of time.[16, 34] Further on, the 55,000-pen 2D

DPN cantilever array developed by Salaita *et al.*[45] would require >50 printing repetitions to pattern a single cm^2. Similarly, μCP would be able to pattern the microparticles. Nevertheless, the desired spot dimension on the microparticle surface are at the very limit of traditional μCP.

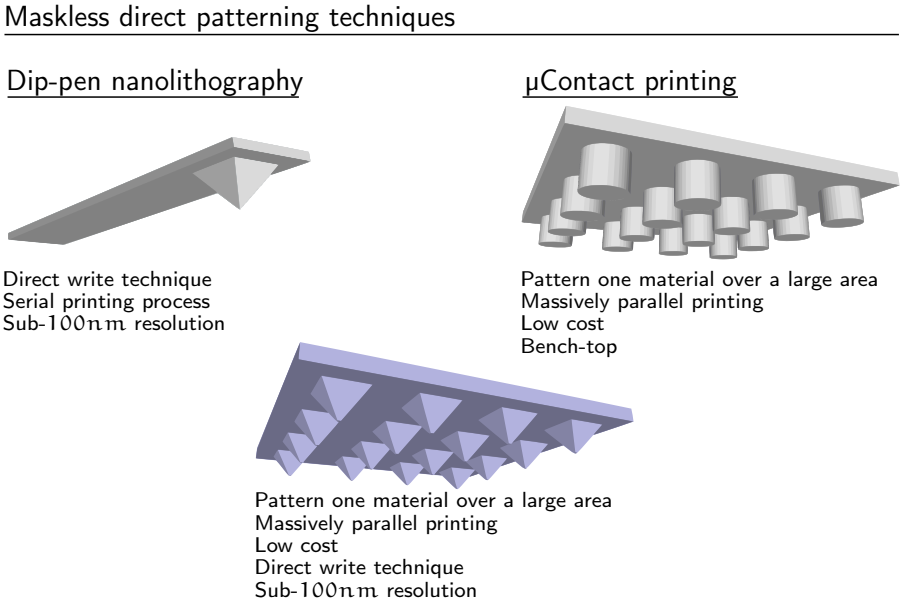

Figure 3.10: **Direct patterning techniques.** Main characteristics of μCP and DPN, and their contribution on PPL.

Fortunately, Huo *et al.*[46] developed a direct patterning technique which merges the characteristics of μCP and DPN presented in Figure 3.10. Their development was defined as Polymer Pen Lithography.

3.2.4 *Principles of Polymer Pen Lithography*

Polymer pen lithography (PPL) is a high-throughput contact lithography method that uses elastomeric tips to transfer inks to a surface. This technique incorporates the large-area printing capabilities of μCP with the sub-micrometer feature size control of DPN.[46] Figure 3.11 presents the entire process to obtain a pattern with PPL. The apexes of the elastomeric pyramids on the replicated stamp function as tips delivering the adsorbed ink to the substrate. As with μCP, the geometry and distribution of the pyramidal features on the stamp are defined by the master. The small area of the polymer tips is greatly affected by the vertical load, thus, nano- and micrometric structures can be easily obtained just by varying the printing pressure.

PPL has been extensively used to pattern array onto flat surfaces with thiols[46–48], different biomolecules such as proteins[49] and biotinylated antigens[50], complex polymer brushes[51], and sub-10 nm

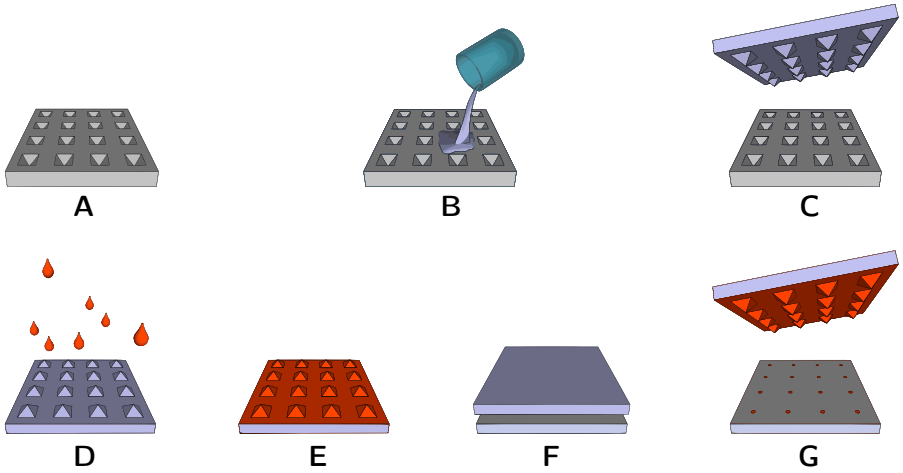

Figure 3.11: **Sequential steps in PPL.** (A) A microfabricated master with inverted pyramidal feature is covered by uncured PDMS (B). (C) Once solidified, the stamp is peeled from the master, and inked with an ink solution (D). The excess of the ink is removed from the stamp (E), and it is brought in contact with the appropriate substrate (F). (G) The printed features correspond to the size and deformation of the tips on each pyramidal feature. The stamp can be inked again and used to print more substrates (D-G).

nanoparticles[52]. Additionally, several stamp modifications have produced hard silicon and gold coated tips. The hard tips were developed to pattern with a higher resolution and for nanoindentation studies.[53] On the other case, after coating the elastomeric pyramids with gold, the stamps where later pressed against a PMMA surface to create an opening at the apex of each pyramidal feature. Subsequently, light was shinned through the stamp reacting with a flat substrate previously coated with a photoresist, creating features only where the light was shone.[54]

Traditional PPL was selected for the fabrication of the miniaturized protein microarrays on the anchored microparticles. To accomplish this, an elastomeric stamp with pyramidal pens was fabricated bearing the same distribution as the features on the substrate. Contrarily as in every publication, where the complete final features were initially created with a starting pivotal spot at a random position on the substrate, the fabrication of suspended planar arrays required perfect initial alignment on both, $x-$ and $y-$ axes. Additionally, PPL requires a more complex leveling procedure for the polymer pens to touch the substrate simultaneously. It is important to mention the upgrade of the μCP tool initially presented on Section 2.3.2 on both, the mechanical and sensing mechanism, to develop this work.

3.3 UPGRADING THE MICROCONTACT PRINTING TOOL

As with any prototype, the μCP tool had features which were not necessarily useful or practical, or lacked some others for some new application. Another reason may be the overcoming of simple problems leading to more complex ones requiring a more thorough system. In any case, the printing system went through an entire overhaul and received several updates. Figure 3.12 presents an schematic illustration of the updated version of the μCP tool. Special attention was placed on the new optical monitoring system. A completely new Charge-coupled device (CCD) camera was fixed on top of an automatic filter wheel with red, green, blue, magenta, and cyan optical filters. The wheel was mounted onto a zoom control with a range from 0.5× to 4.5× where light diverted from a dichroic mirror cube passed. Light form a new fiber optics port was beamed towards the sample and brought back to the camera through a 10× objective and the dichroic mirror. The entire optical system can be regulated to obtain images with zooms from 5× up to 45×. A new `focus` actuator was integrated on the arm holding the optical monitoring system. This actuator raised and lowered the entire head to set the camera to the desired focus plane. The position of the field of view along the substrate was still controlled by two microscrews fixed on the base of the arm holding the print head.

To obtain a finer control on the displacement of the print head, a piezoelectric actuator identified as `z-piezo` was fixed opposing the movement of the $z-$ actuator. The opposite actuation increased the total displacement by 20 μm and granted a step resolution of 20 nm.

The last modification was required to obtain a completely parallel alignment between stamp an substrate. For this reason the substrate holder was fitted with two goniometers to translate the substrate angularly on the $x-$ and $y-$ directions. The dynamic alignment between the stamp and substrate is shown in Figure 3.13 where the two-dimension localization allowed a perfect alignment between sample and stamp. The actuators, piezoelectric, and stages were obtained from Thorlabs, Inc. A digital photograph is shown in Figure A.10.

3.3.1 *Integration of new software functions*

The upgraded prototype allowed the implementation of new resources to tackle patterning procedures. Evidently, as shown in Figure 3.14, all the new actuators `Tilt X`, `Tilt Y`, $z-$`piezo`, and `Focus` received an individual state in the program. Yet the two most interesting upgrades were defined first by the implementation of a complete subroutine to create multiple prints on a single substrate following a programmed map. This upgrade opened the opportunities to create

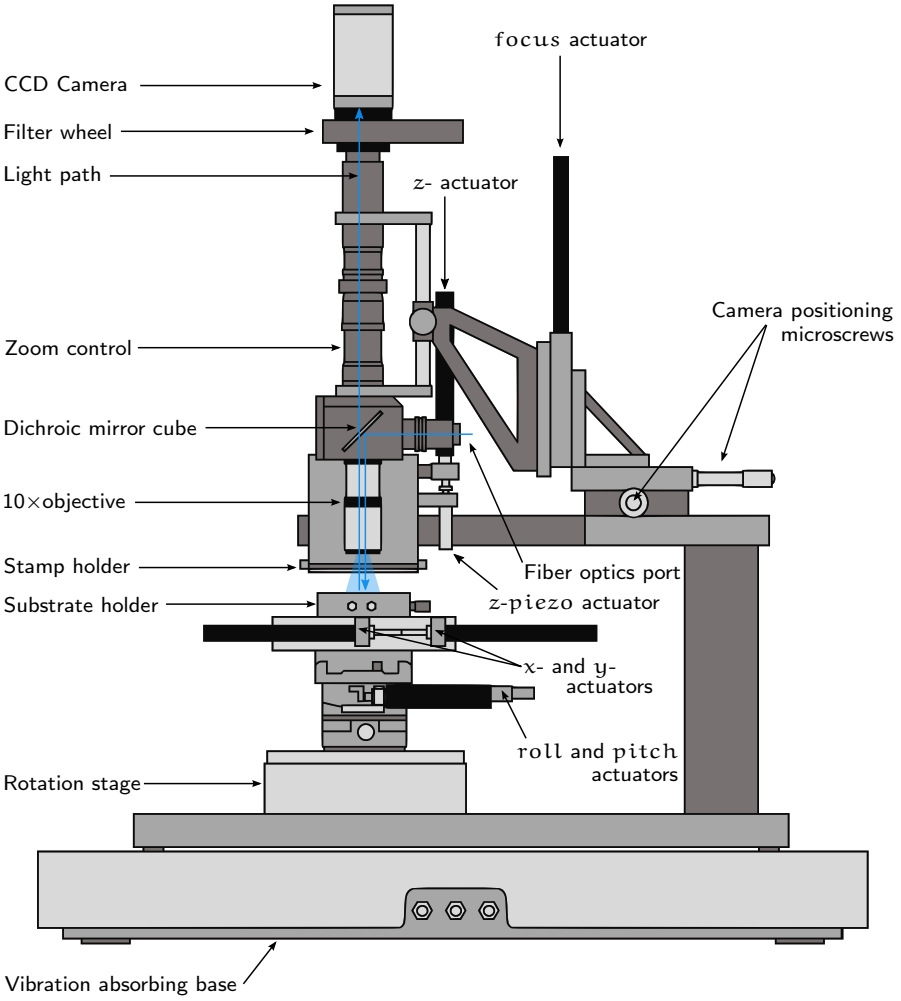

Figure 3.12: **Schematic of the upgraded μCP Tool.** New optical sensing mechanisms for fluorescence microscopy and new actuators to align the substrate and print at the nanoscale were included with the upgrade.

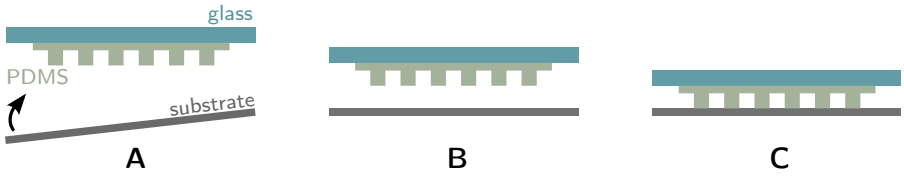

Figure 3.13: **Parallel alignment between the stamp and the substrate.** The x— and y— goniometers are used to tip and tilt the substrate (A) until both, the substrate and stamp are parallel. The z— actuator approaches the stamp towards the substrate (B), until the stamp contacts the substrate (C), transferring the pattern. The system is similar to the one used in [55].

multiplexed arrays. The second program, included the implementation of a subroutine to machine flat polymeric substrates following a

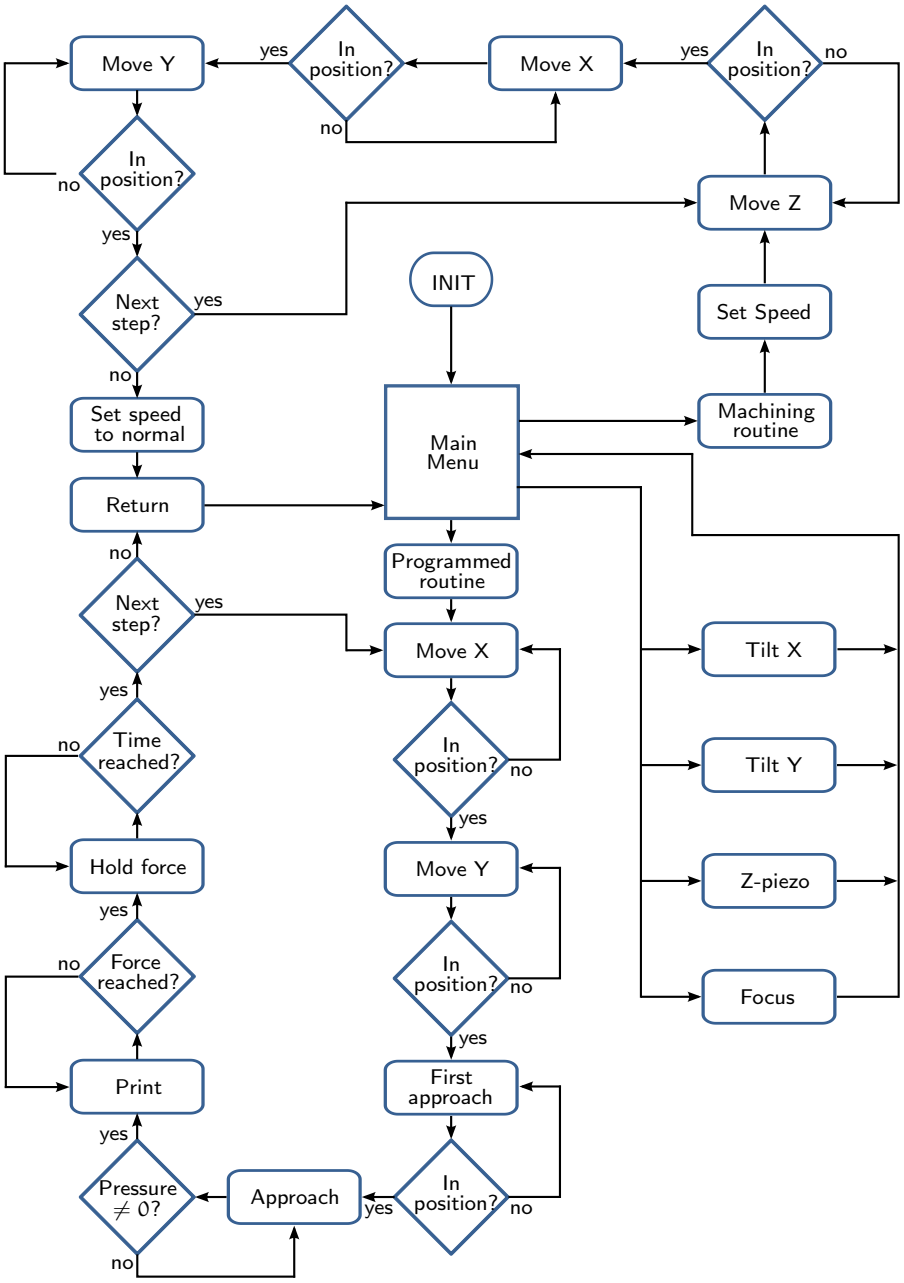

Figure 3.14: **Simplified state machine of the improved µCP Tool.** The updated state-machine includes the same routines presented in Figure 2.12 with several additions: x— and y— goniometers, focus— actuator, a complete cycle for multiple prints following a programmed subroutine, and another subroutine to machine flat substrates.

programmed path. Each state on the state-machine read the current position of the actuator before advancing to the next state.

3.4 EXPERIMENTAL PROCEDURES FOR THE FABRICATION OF SUSPENDED PLANAR ARRAYS

The purpose of this research was to create patterns on a complex substrate with the upgraded printing tool. The strengths of the automatized μCP Tool offer the perfect mechanism to create biomolecule and small molecule patterns on the specialized micromachined substrates. The patterns were fabricated following the surface chemistries discussed on Chapter 2 taking into account the new challenges presented on the creation patterns on very constricted areas. The alignment between the PPL elastomeric stamp and the substrate represented the main obstacle to overcome. A standardized protocol presented the perfect opportunity to create in parallel and in bulk, functional, miniaturized microarrays.

3.4.1 *Anchored microparticles: Patterning on constricted areas*

The specialized micromachined substrate described and shown in Figure 3.8 presented several challenges for the creation of patterns on a raised topography. As described previously, the only pathway to create a multiplexed array on each anchored microparticle was direct placement. This method required the fabrication of specialized PDMS stamps, and this inevitably created another complex issue to tackle: the perfect alignment between stamp and substrate. The upgraded μCP tool offered a big advantage to cope with the parallelization between substrate and stamp, and the new monitoring system provided the means to align the stamp and substrate.

3.4.2 *Surface activation of the anchored microparticles*

As described in Section 2.4.3.1, the primary amine groups present in proteins and antibodies serve as a target location to create covalent bonds. Following a similar activation method, an epoxy-terminated SAM was used to bind the biomolecules to the surface of the anchored microparticles. To produce the active layer, the entire substrate was plasma-activated for 30 s and immediately afterwards, it was printed with a flat PDMS stamp previously inked with a 2% GOPDMS ethanolic solution. After curing for 1 h at 75°C and rinsed with absolute ethanol, the substrate was ready to be patterned.

3.4.3 *Patterning anchored microparticles*

Two proposals were established with different PDMS stamps. First, with the use of protruding lines. This proposal assured the patterning of every anchored microparticle with at least a portion of the

PDMS stamp. The second and last approach required individual spots replicated on every anchored microparticle.

3.4.4 *Fabrication of PDMS stamps*

An initial approach to create a multi-protein array on each anchored microparticle consisted on two sequential printings with a stamp with protruding lines. The parallel lines guaranteed the patternening of every anchored microparticle. A first PDMS stamp with parallel lines and pitch of 2.5 µm was fabricated as described in Section 2.4.1.

The second stamp, with lines of 1 µm and pitch of 5 µm was replicated form the master used to fabricate the stamps to obtain the PHA-AF488 patterns described in Table 2.2 and the WGA-TxR and PHA-OG488 patterns indicated in Table 2.3.

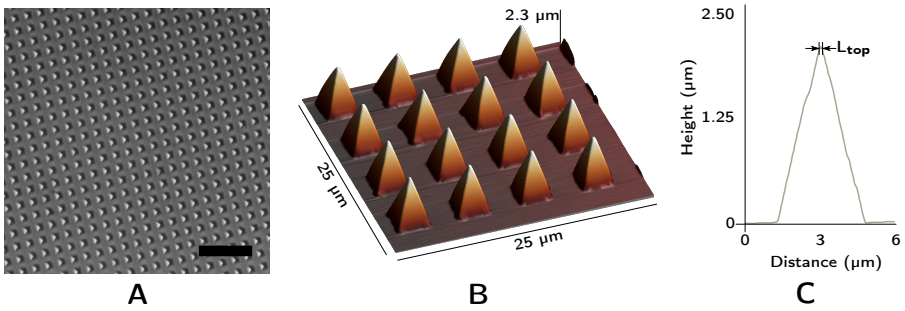

Figure 3.15: **Microscopy images of the PPL stamps.** (A) Optical and (B) AFM images of the PDMS stamp. Each tip from the pyramidal features had an average edge length of $L_{top} = 212 \pm 23$ nm. Scale bar = 25 µm.

The third PDMS stamp was fabricated to create individual spots on every anchored microparticle. Figure 3.15 shows the pyramidal features on the PPL stamp. The optical microscopy image presents the distribution and scale of the replicated microstructures, while the AFM topographical representation helped measure the tip edge length, L_{top}, calculating an average of 212 ± 23 nm. The pyramidal-shaped master was fabricated from a SiOx wafer following a protocol similar to the one used by Eichelsdoerfer *et al.*[55]. Briefly, the wafer is spin-coated with a positive photoresist and exposed to UV light through a photomask with the exact feature distribution as the one used to fabricate the microparticles. After developing, the wafer is submerged in HF to etch the thermal oxide layer. Immediately afterwards, the etched wafer is submerged in a potassium hydroxide (KOH) solution for the anisotropic etching of the <100> plane. This is a self-terminating process as the <111> on the exposed SiOx plane is not etched. The <111> plane forms the internal faces of each inverted pyramid. A subsequent PFOTCS coating created a non-adherent layer

over all the substrate. A fabricated stamp with three different patterning regions is shown in Figure 3.16.

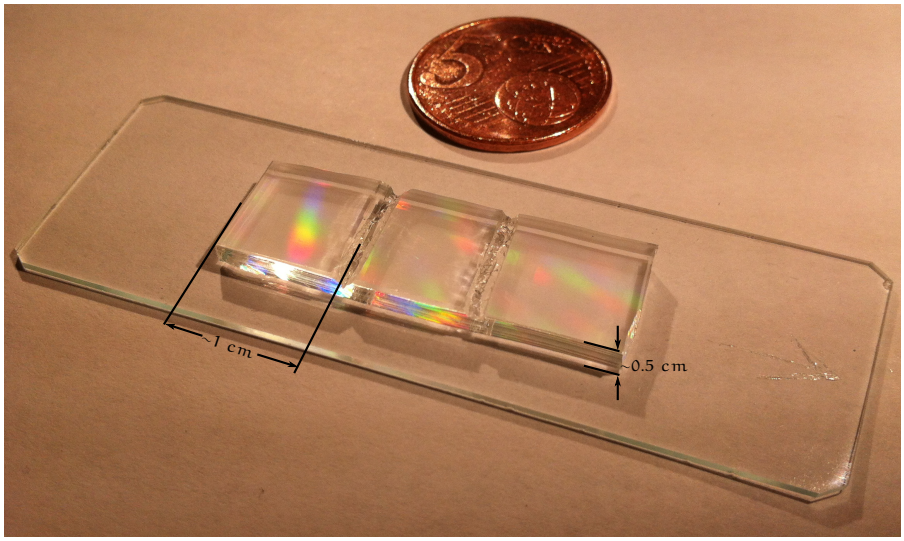

Figure 3.16: **PDMS stamp for PPL.** Digital photography of a PDMS stamp with three different patterning regions.

3.4.4.1 *Patterning using stamps with lines*

The first stamp was used to print successive patterns of WGA-TxR and WGA-OG_{488} on the anchored particles substrate at different crossing angles. The 2.5 μm contact area assured the patterning of most of the microparticle surface, and the shape of the printed feature depended on the distribution of this area. Both inks where individually patterned from a 40 $\mu g\ ml^{-1}$ PBS protein solution after a 15 min incubation time and for 5 min.

Two approaches were followed with the second stamp. The first approach consisted on the creation of parallel-running features along the substrate. To accomplish this, the PDMS stamp was loaded on the μCP tool and aligned to match the distribution of the anchored microparticles. The intended printing position would allow the subsequent patterning. Afterwards, the stamp was inked with a 40 $\mu g\ ml^{-1}$ PBS solution of WGA-TxR during 15 min, then rinsed with Milli-Q water and dried under a flow of N_2. The printing process was produced at a force of 0.5 N during 5 min. After the initial patterning, the PDMS stamp was washed by sonication for 15 min and subsequently rinsed with absolute ethanol, dried, and inked with a 40 $\mu g\ ml^{-1}$ PBS solution of WGA-OG_{488} during 15 min. The stamp was loaded and aligned on the μCP tool and the substrate was printed following the same printing protocol.

3.4.4.2 *Patterning using polymer pens*

Increasing the number of potential spots on every anchored microparticle required the use of smaller features to transfer the ink. The pyramidal stamp with sharp tips allowed the creation of submicrometric biomolecule spots. Liao *et al.*[47] developed Equation 3.1 which calculates the overall spot size using the inverted pyramids correlating the printing force, F, the initial tip edge length, L_{top}, and the number of polymer pens, N:

$$L_{edge} = L_{top} + \frac{\nu}{NEL_{top}}F \tag{3.1}$$

where the mechanical properties of the material, in this case PDMS, were ν, the Poisson's number and the Young's modulus, E.

To calculate the size of the printed spots, every micromachined chip was initially measured to approximate the number of anchored microparticles. When the PPL stamp is perfectly aligned, the number of polymer pens, N, is exactly the same as the number of anchored microparticles to pattern. The $L_{top} = 212 \pm 23$ nm from the profile from Figure 3.15, and using a printing force of $F = 480 \pm 2$ mN a $L_{edge} = 742 \pm 62$ nm was calculated with Equation 3.1. To print, first, the stamp was loaded on the μCP tool and the $x-$ and $y-$ goniometers were used to place the substrate parallel to the stamp. Afterwards, the stamp was aligned on the $x-$ and $y-$ directions on the flat Cartesian plane over the substrate.

An important characteristic of PDMS stamps is the immediate shrinkage after peeling from the master. Stamps can shrink from a ratio of 1.06 to 1.94% depending on the curing temperature.[56] As discussed previously, any defect on the stamp is translated to the printed features. As a result, some areas of the micromachined substrate were not patterned. The inherent misalignment produced by the shrinkage of the PDMS stamp required the implementation of a new stamp-fabrication technology to correct. A translation protocol was later designed to deposit the selected ink onto each anchored microparticle. Figure 3.17 shows the patterning process to transfer ink at least once to each anchored microparticles with the PDMS pens. After aligning the stamp, both planar and radially, the stamp was inked and rinsed as in previous experiments, and brought into contact with the substrate. After printing for 5 min, the stamp was raised 100 μm from the substrate and positioned on the second absolute coordinate. The same was done for each step until four patterning process were completed.

It is interesting to note, that the ink on the polymer pens over the unpatterned areas remained absorbed on the surface of the stamp, therefore, the patterning on the next coordinate was produced without the need of a subsequent inking step. The translation distance

between printings of 3 μm on both axes was chosen as it is half the distance between neighboring anchored microparticles.

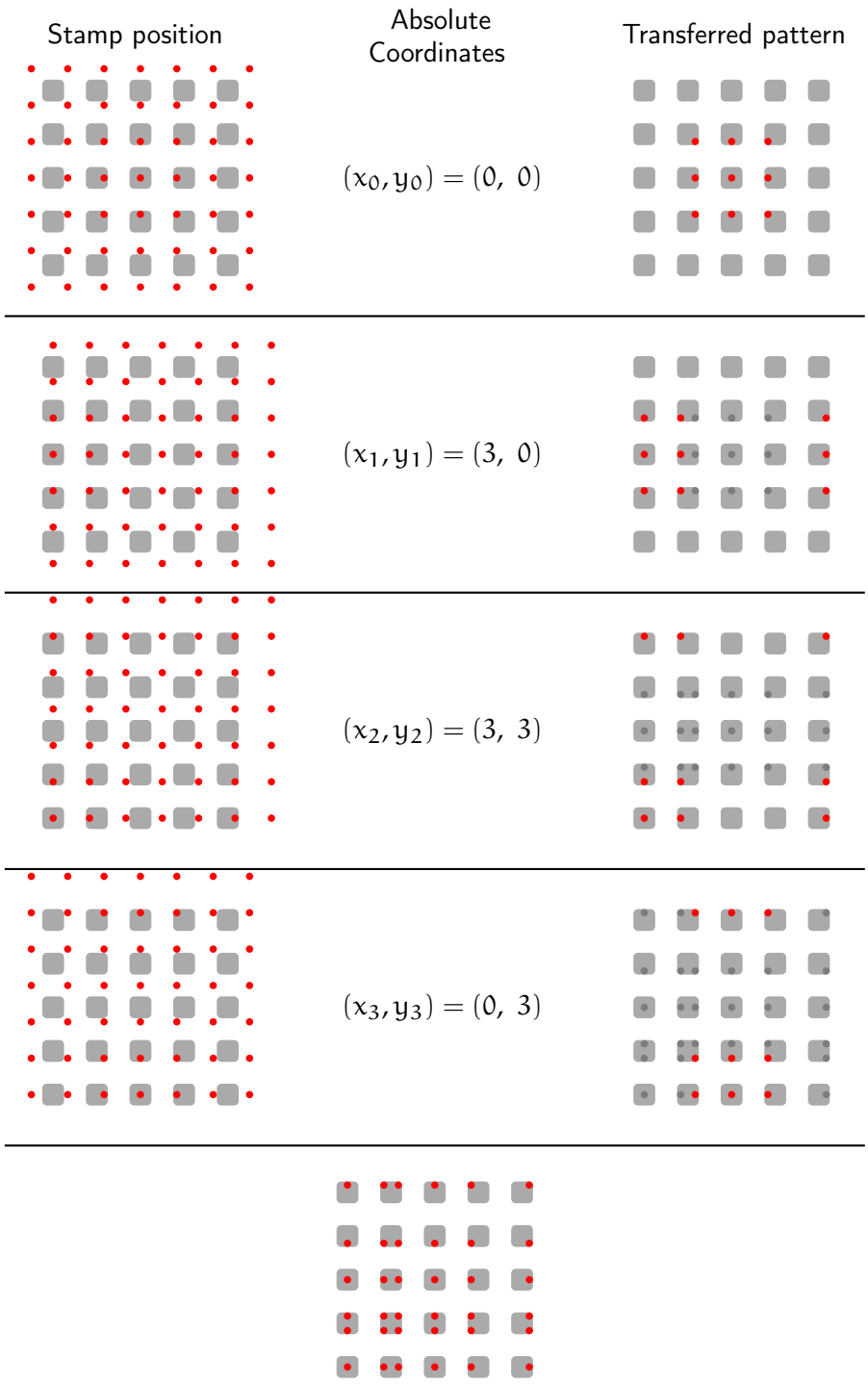

Figure 3.17: **Patterning with a shrunken stamp.** The ink will transfer only where the polymer pens contact the anchored microparticles. Subsequent printings on the absolute coordinates can pattern at least once every anchored microparticle resulting on an array of complex patterns.

Initially, a 40 µg ml^{-1} WGA-TxR solution in PBS was used as the ink. One to four spots were replicated on individual anchored microparticles. Later experiments with two inks proved successful in the creation of multiplex microparticles with a variety of different spot arrangement on their surfaces.

To create a multiplexed pattern, the stamp was incubated with WGA-TxR and WGA-OG488, each from a 40 µg ml^{-1} PBS solution over an individual patterning area from the stamp shown in Figure 3.16. After a 15 min incubation step, and subsequent Milli-Q rinsing, the substrate was patterned. Fluorescence microscopy was used to characterize the all the resulting patterns.

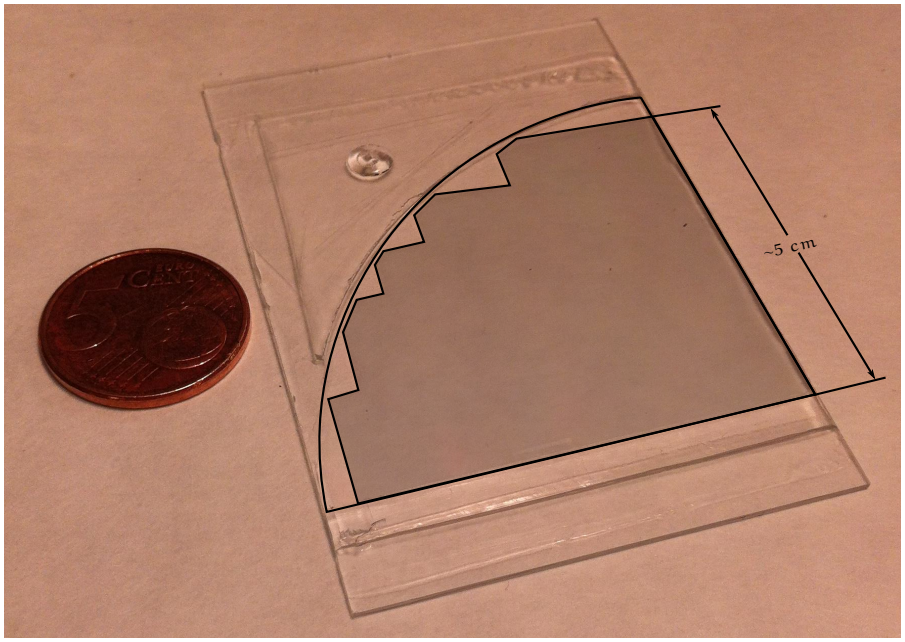

Figure 3.18: **Updated PDMS stamp for PPL.** Digital photography of a PDMS stamp with a larger patterning area (shaded area) and a glass backbone. The stamp had a thickness of ~100 µm.

To prevent the shrinkage, new stamps with a rigid backbone were fabricated. The result is shown in Figure 3.18. One fourth of a micromachined wafer with the inverted pyramids was used to replicate a pattern. First, 75 × 50 mm microscope glass slides from Corning Inc. (Corning, NY, USA) were sonicated for 15 min in a 1 M NaOH solution and subsequently rinsed with Milli-Q and sonicated in a 1 M HCl solution for another 15 min. Finally, a stream of N_2 was used to dry the glass. These activation steps create reactive hydroxyl groups on the surface of the glass. A 10:1 w/w PDMS mixture was poured over the immobilized wafer and the activated glass slide was placed over the mixture preventing the entrapment of air bubbles. The stamp was cured at room temperature for 24 h and later at 75 °C for 2 h. Lastly, the new stamp was carefully separated from the master. The average thickness of the patterned area measured ~100 µm

3.4.4.3 *Alignment between polymer pens and substrate*

The glass backbone created a rigid foundation and prevented the shrinkage of the stamp. The result created a distribution of polymer pens matching that of the anchored microparticles. This allowed the parallel printing and a spot distribution equal on every anchored microparticle. An interesting phenomena can be seen when the loaded stamp on the μCP tool is moved closer to the substrate: Moiré patterns. These interference patterns are created by a misalignment of the substrate and stamp. Figure 3.19A shows the Moiré patterns obtained from various decreasing degrees of rotation between substrate and stamp from a macroscopic point of view. The microscopic image obtained with the optical controller from μCP tool shows the patterns at a microscale. A vast difference between the misalignment of ~4° and ~2° between substrate and stamp is observed in Figure 3.19B and C. The substrate was rotated until the Moiré patterns disappeared on the image. The border of the substrate on a perfectly aligned stamp is shown in Figure 3.19D.

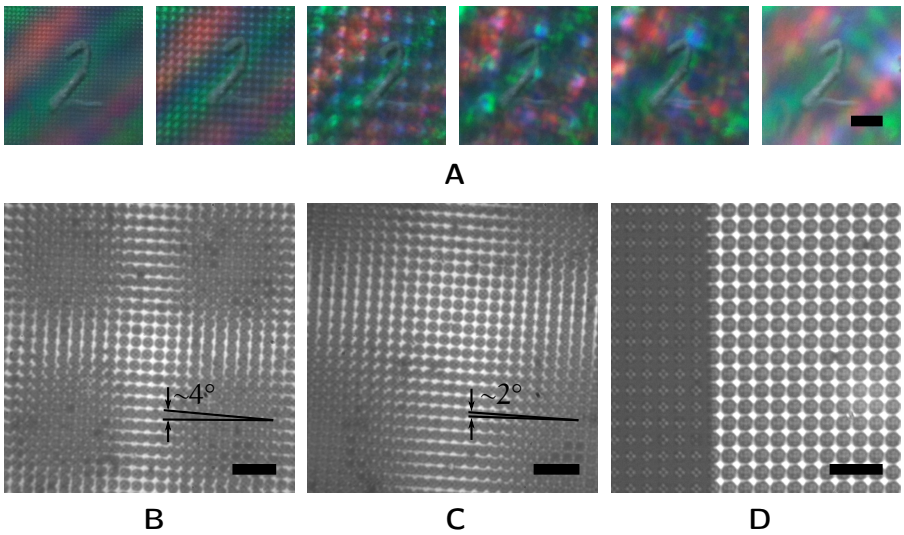

Figure 3.19: **Moiré patterns during the approach of the stamp towards the substrate.** (A) Digital photography of a PDMS stamp on top of a anchored microparticle substrate. The fringes increase until they disappear, when reaching a perfect alignment. (B-C) Microscopic images of the fringes at different rotation angles. (D) Perfect alignment between substrate and stamp. The image shows the edge of the substrate. Scale bars = 250 μm in (A) and 20 μm in (B-D).

Every printing step required the alignment of the substrate with the inked stamp. To prevent the transfer of adsorbed in onto the surface of the anchored microparticles, the stamp was lowered until the features of the pyramids could be observed on the same field of view as the anchored microparticles. Figure 3.20A presents the position of the PPL stamp on the same field of view as the substrate. Notice that the

dark spot on each anchored microparticles is the tip of the polymer pen. This spot disappears when the pyramid contacts the anchored microparticle (Figure 3.20B).

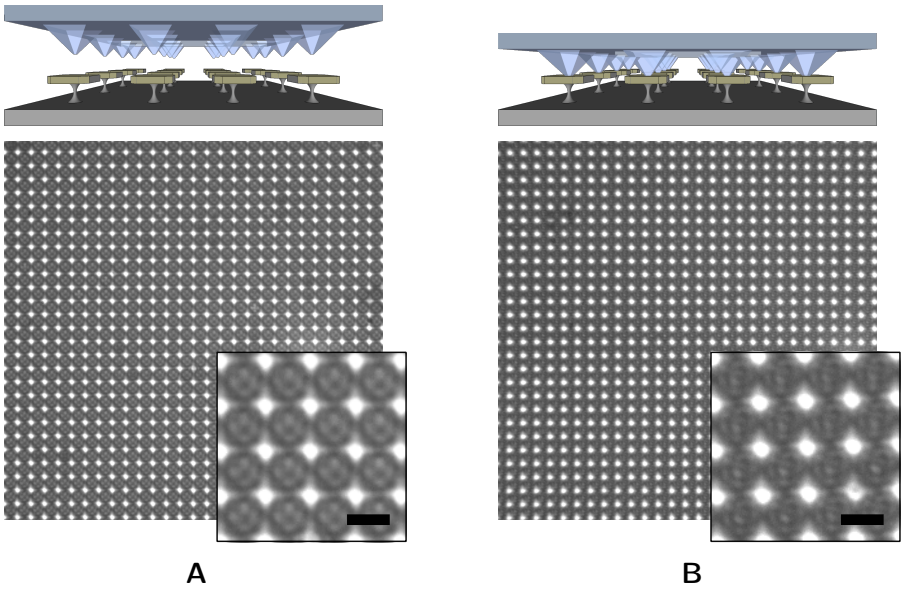

Figure 3.20: **Alignment and printing with a PPL stamp.** Microscopic images of the approach (A), and contact (B) of the stamp with the substrate. The lack of Moiré patterns represent a perfect alignment. Scale bars = 5 μm.

To print more than one ink, the aligning step was repeated the same number as that of inks to pattern. To avoid printing over a previously patterned area, the stamp was translated by less than 1 μm at any direction. Having established a printing protocol, different (bio)molecules were patterned onto the anchored microparticles.

3.4.5 *Printing patterns onto anchored microparticles*

Initially, proteins and biomolecules were printed on the anchored microparticles. Subsequently, to increase the scope of the technique, fluorophore arrays were later fabricated.

3.4.5.1 *Multiplexed biomolecule array*

Various biomolecules were patterned on each microparticle, as represented in Figure 3.21. Each biomolecule had a fluorescent probe to later characterize with fluorescence microscopy. WGA-TxR, WGA-OG_{488} and Aminomethyl coumarin acetate (AMCA) rabbit anti-goat IgG (H+L) from Vector Laboratories, Inc. (Burlingame, CA, USA) were used. Each biomolecule was suspended at a final concentration of 40 μg mL^{-1} in a 30 mM (Na_2HPO_4) solution. Three independent PDMS stamps were inked with one solution and incubated for 15 min, then rinsed with Milli-Q water, and blown dry with H_2. Immediately

afterwards, the stamp was loaded to the μCP tool and the patterning process proceeded as previously described.

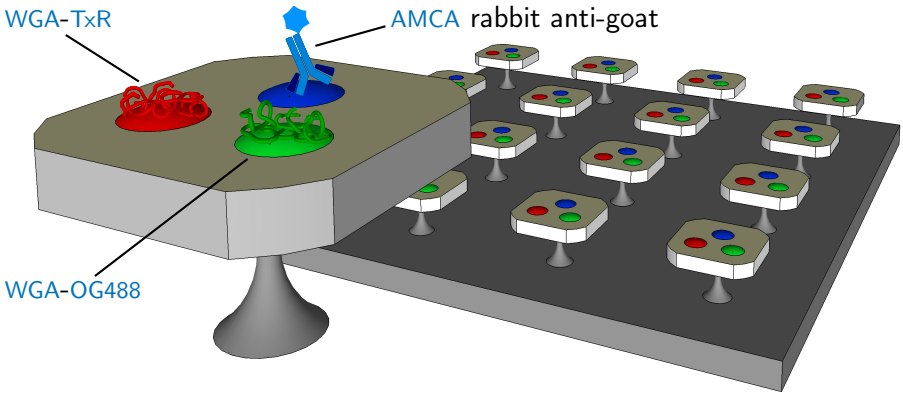

Figure 3.21: **Final concept of an microprotein array printed on a microparticle.** Two proteins, WGA-TxR and WGA-OG488, and an antibody, AMCA rabbit anti goat, created the microarray on each microparticle.

3.4.5.2 *Multiplexed fluorophore array*

As an added functionality, the patterning protocol was extended to create pH sensing microarrays. A sensing microarray was designed to include pH dependent fluorescent probes. A schematic of the pattern is shown in Figure 3.22 presenting the three fluorescent probes: Oregon Green® 488 (OG488), Alexa Fluor® 647 (AF647), pHrodo™ Red (pHrodo). The molecular formulas of each probe are shown in Figure 3.23, and as it can be noted, all of them contained a reactive N-Hydroxysuccinimide (NHS)-ester group. The emission of each probe was carefully selected to create a narrow maximum peak, hence, preventing the overlapping of any of the other two peaks from immobilized probes. OG488 has a maximum emission at 524 nm, while pHrodo at 590 nm, and AF647 at 665 nm.

The second important characteristic is that each fluorescent probe reacts differently to the ambient pH. OG488 increases its emission as the value of pH increases. The opposite occurs with pHrodo, which decreases its emission at high pH values. The emission ratio between these probes allow the calculation of the ambient pH. The last probe, AF647 was used as a control, as its emission remains constant at pH values ranging form 2 to 10. These microparticles could perform sensing studies in systems with very limited sample volume or in constricted environments.

The NHS-ester group was targeted to bind the probes to the anchored microparticles. As represented in Figure 3.24, it reacts with primary amines yielding stable amide bonds. To create the amine-modified surface, the substrate was initially plasma-activated and immediately afterwards, printed with a flat PDMS stamp previously

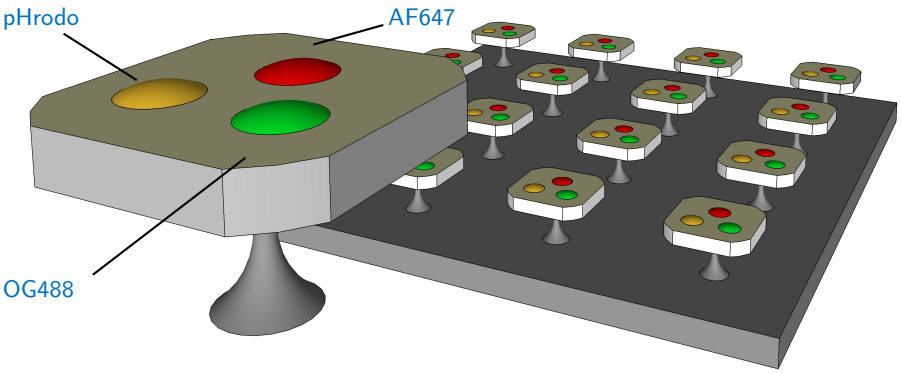

Figure 3.22: **Fluorescent probes array on the anchored microparticles.** NHS-conjugated pHrodo, OG488, and AF647 were printed directly onto the anchored microparticles to create a 3-variable system to measure pH.

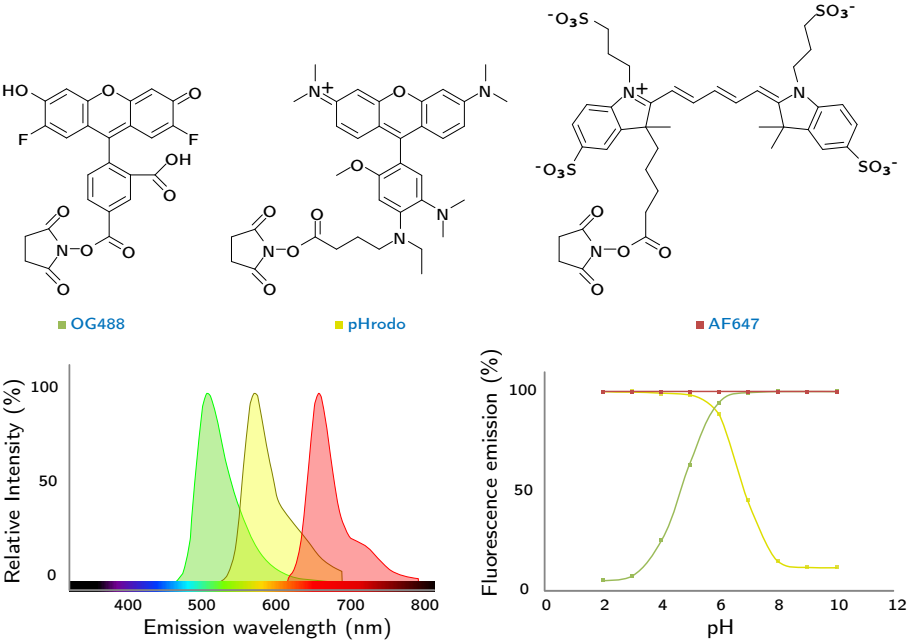

Figure 3.23: **pH dependent fluorescent probes.** Three NHS-conjugated pH dependent probes were chosen: pHrodo[57], OG488[58], and AF647[59]. The emission bands are narrow and sufficiently separated to measure each spot individually. The emission of OG488 increases with higher pH, while pHrodo decreases. The AF647 maintains the maximum emission at a wide range of pH values from 2 to 10.

inked with a 2% ethanolic (3-Aminopropyl)triethoxysilane (APTES) solution purchased from Sigma-Aldrich (St. Louis, MO, USA). After curing for 1 h at 75 °C and rinsed with absolute ethanol, the substrate was ready to be patterned.

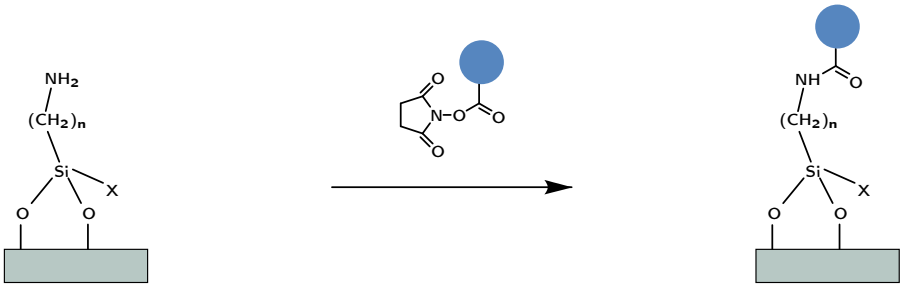

Figure 3.24: **Reaction of amine groups.** An amine-silane SAM is reactive towards NHS moieties.

Three new PDMS stamps were fabricated to pattern each individual probe. The dessicated probes were obtained from Life Technologies (Carlsbad, CA, USA) and resuspended in anhydrous Dimethyl sulfoxide (DMSO) from Sigma-Aldrich (St. Louis, MO, USA) to obtain a concentration of 100 µM. Acetonitrile from Panreac (Barcelona, Spain) was later used to aliquot the inks to a final concentration of 10 µM. Before patterning, each stamp was plasma-activated during 30 s and 5 µL of the ink solution was subsequently placed over the stamp. After drying with N_2, the stamps were ready to be loaded onto the µCP tool and used to print.

After printing, the substrates were subjected to a new washing protocol to remove the excess of ink and to prevent the unspecific absorption of unbound probes. First, the entire substrate was placed at 4°C during 20 min. Immediately afterwards, and preventing the condensation of ambient humidity, the substrate was immersed in a cooled 2% v/v solution of 2-(1-hydroxy)-ethoxy-eth-1-yl methanesulfonate (EG2OMS) from ProChimia Surfaces sp. z o.o. (Sopot, Poland) in water, and left to react for 30 min. The substrate was subsequently rinsed with Milli-Q water, dried under a stream of N_2, and characterized with fluorescence microscopy.

3.4.6 *Liberation of multiplexed microparticles*

The intended microarrays required the liberation of the patterned microparticles. To achieve this, an initial protocol based on cryofracture was established. This type of fracture is based on a procedure to prepare cells for successive SEM imaging in which the sample is rapidly frozen and later broken with a sharp blow. For a quick freeze, a small volume of PBS-Tween 20 was placed on top of the chip with the anchored microparticles and immediately afterwards, submerged in liquid N_2. An initial theory rooted on the idea that the fast freezing of the sample would create various mechanical stresses on the different materials of each microparticle was tested. These stresses would transmit throughout the sample breaking the anchor on each anchored particle. It is important to mention that based on some reports, the

structure and functionality of the patterned biomolecules should not be damaged by the fast freezing.[60]

Although the cryofracture method proved somewhat feasible, as some particles were liberated from the substrate, the main issue with this method was the liberation of all the microparticles with a single sharp blow. Thus, consecutive freeze-blow cycles had to be performed to liberate the maximum amount of microparticles. The main drawback was that the patterned biomolecules where eroded after several cycles.

To characterize the liberated microparticles, the frozen buffer suspension was left to thaw and subsequently centrifuged at 8000 rpm for 60 s to concentrate the microparticles. The collection required the elimination of most of the suspension buffer and the resuspension of the microparticles in liquid Fluoromount™ aqueous mounting medium from Sigma-Aldrich (St. Louis, MO, USA). This medium solidifies at room temperature locking the microparticles on site, allowing the characterization with fluorescence microscopy, eliminating artifacts produced by Brownian motion.

The solidified Fluoromount™ envelops the patterned biomolecules preventing any conformational change, and can be dissolved in any aqueous solution. The entrapping mechanism used to characterize the microparticles was extrapolated to create a new liberation step. First, a small drop of the mounting medium was placed on the patterned microparticles and is left to solidify. Afterwards, the thin membrane was peeled from the substrate. All the microparticles are entrapped and liberated with this method, in a single step and protecting the micropatterns. The membrane can be then dissolved in Milli-Q water and deposited on a microscope slide to be characterized.

3.4.7 *Protein recognition after microparticle liberation*

The intended approach to create the suspended planar protein microarrays required the conformation and functionality of the anchored biomolecules to remain intact. An antibody binding assay was developed to probe the proteins on each microparticle to test their functionality. After peeling the solidified Fluoromount™, the membrane was dissolved in a 10 µM PBS solution of primary goat anti-WGA antibody from Vector Laboratories, Inc. (Burlingame, CA, USA) and left to react for 1 h. Afterwards, the suspension was centrifuged at 8000 rpm for 60 s and the collection at the bottom was dispersed in a 1 µM AMCA rabbit anti-goat IgG (H+L) antibody PBS solution and left to react for 1 h. After three different resuspensions in Milli-Q water, centrifugation, and collection, the microparticles were characterized using fluorescence microscopy.

3.5 RESULTS, EVALUATION, AND INFLUENCE OF THE DIFFERENT EXPERIMENTAL PARAMETERS

The creation of suspended planar arrays may produce interesting approaches to study (bio)molecular interactions in small volumes. The main limitations to create functional arrays on such small areas are contemplated in two main groups: the fabrication methods and the orthogonality if subsequently functionalized. The complexity of the design fell on the limited technology to fabricate such arrays in constricted areas. Patterning, blocking, and liberation protocols were developed to translate the printing of the anchored microparticles to their liberation and final characterization using an antibody assay.

3.5.1 *Patterning with Microcontact printing*

The direct placement of biomolecules onto the micromachined substrate was initially produced with μCP. This method helped transfer the pattern dictated by the protruding traits of a PDMS stamp. Lines were chosen to pattern parallel features throughout the anchored microparticles, guaranteeing a complete surface coverage. Figure 3.25A and B presents the fluorescent microscopy image of two individually labeled WGA proteins transferred to the substrate.

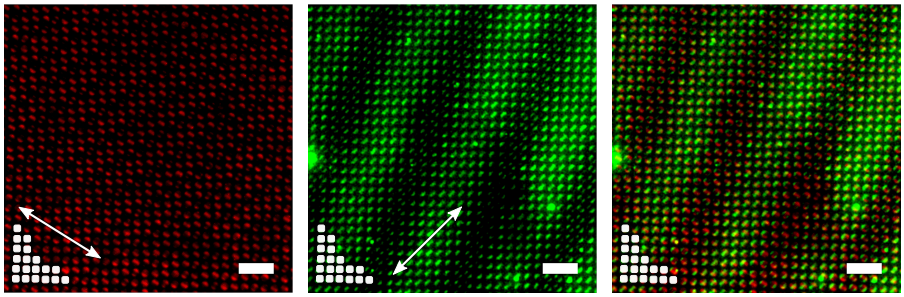

Figure 3.25: **Printing directly into the anchored microparticles.** An initial PDMS stamp with 2.5 μm lines was used to print (A) WGA-TxR and (B) WGA-OG488 on a functionalized substrate. To cover the maximum surface area, each pattern was printed at a different angle. (C) The merged image from both emission channels. The white squares represent the position of the anchored microparticles and the scale bars = 20 μm

The printing angle was different between patterning processes, obtaining complex designs on every anchored microparticle. This modification strategy was able to functionalize each microparticle with two biomolecular inks. As it can be observed in Figure 3.25C, each anchored microparticle had a portion of its surface patterned with each ink. However, the degree of coverage varied on each anchored microparticle. This variance, lead to the fabrication of a new PDMS

stamp with narrower lines and a separation between lines matching that of the anchored microparticles.

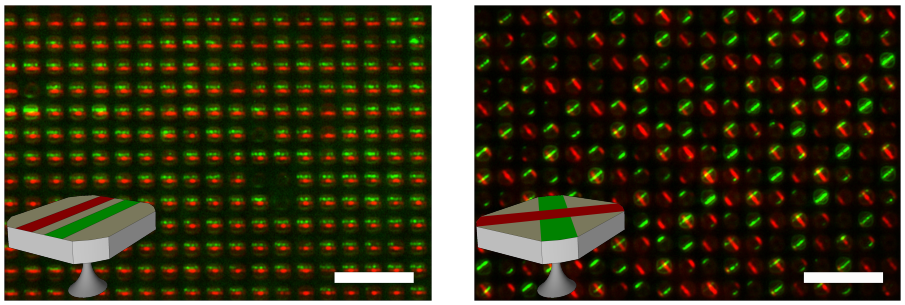

Figure 3.26: **Different patterns can printed on the anchored microparticles.** (A) 1 µm WGA-TxR and WGA-OG488 lines run parallel on top of the anchored microparticles. (B) A similar approach was followed to create crossed patterns on the substrate. Scale bars = 20 µm.

The initial approach to print with the new PDMS stamp replicated the same pattern over every anchored microparticle. Figure 3.26A shows that the amount of coverage of each ink was almost equal on each feature and the distribution of both inks is replicated on all the substrate. Using the same PDMS stamp, various features were obtained when each ink was patterned at $\measuredangle = \pm 45°$ from the anchored microparticle. This created the crossing pattern shown in Figure 3.26B. It is worth mentioning that the distribution of the lines of the stamp matched that of the anchored microparticles, thus, the patterns at a different angle varied significantly from that of the parallel features. To obtain perfect crossing features, the separation between the middle of the 1 µm lines should be 4.243 µm. After subtracting the width of the line, the separation between features arrives to 3.243 µm. Future experiments could arrive to the creation of such designs.

DWL presented in Section A.1.2 was used to fabricate the master with lines by repeating a 100 µm by 100 µm design to cover the entire 1 cm by 1 cm area. Unfortunately, the repeated stitching of the pieces forming the pattern is not accurate. This small inaccuracy is translated to the stamp and eventually to the substrate. Figure 3.27A shows the results of the inaccurate seam of the master translated to a WGA-TxR pattern via a PDMS stamp. It is worth noting that the stamp was not aligned to the substrate, causing some areas to remain unpatterned. The blue lines in Figure 3.27B represent the expected pattern from a seamless area of the stamp. The red lines represent the displacement of the pattern form the stitching area, following the gap between patterning areas.

Pushing the limits of patterning techniques, thus, creating complex and smaller features, required the use of novel printing methods. As described previously, Polymer pen lithography (PPL) offers a plau-

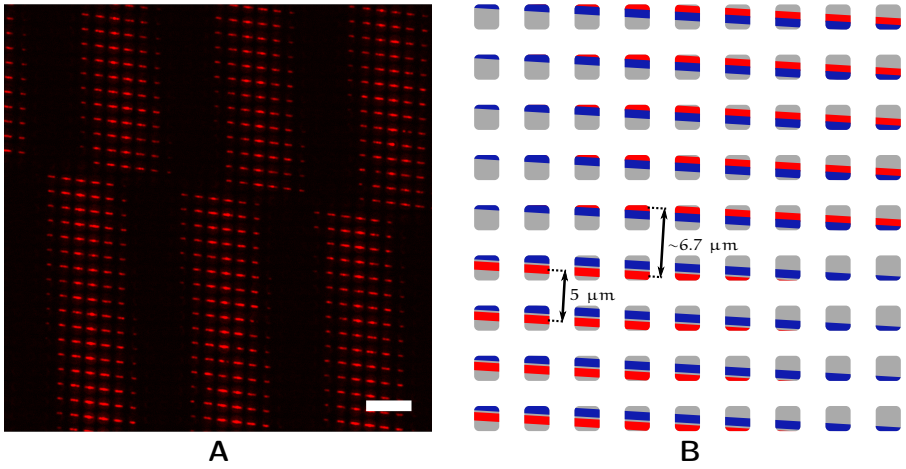

Figure 3.27: **Contraction and fabrication defects of the µCP stamp alter the patterning.** (A) A stamp with 1 µm lines was used to print the anchored microparticles. Any fabrication defect is translated to the substrate. (B) A schematic view of the intended pattern in blue, and the obtained pattern in red due to defects. Scale bar = 20 µm.

sible method to create more complex designs on the anchored microparticles.

3.5.2 *Patterning with Polymer pen lithography*

Polymer pen lithography (PPL) uses a stamp with inverted pyramids to create small spots on the surface of a substrate. This small spots would allow the creation of multiplexed pattens on every anchored microparticle. The initial step to work with PPL requires the fabrication of the specialized PDMS stamps. The first PDMS replica was fabricated from the micromachined master obtaining thick slab and was later separated into different inking areas. Each printing procedure required the loading and inking of the PDMS stamp using the µCP tool.

3.5.2.1 *Direct patterning of proteins*

This approach followed the same steps used to pattern using µCP. The interesting fact encountered while printing is presented in Figure 3.28A , where it shows the WGA-TxR spots transferred to the anchored microparticles. As it can be observed, the contraction of the stamp altered the final pattern. This phenomena is depicted in Figure 3.28B. There, a perfectly aligned stamp without contraction would create the pattern represented with blue spots, while the red spots represent the actual pattern due to the contraction, as PDMS contracts after demoulding.[56]

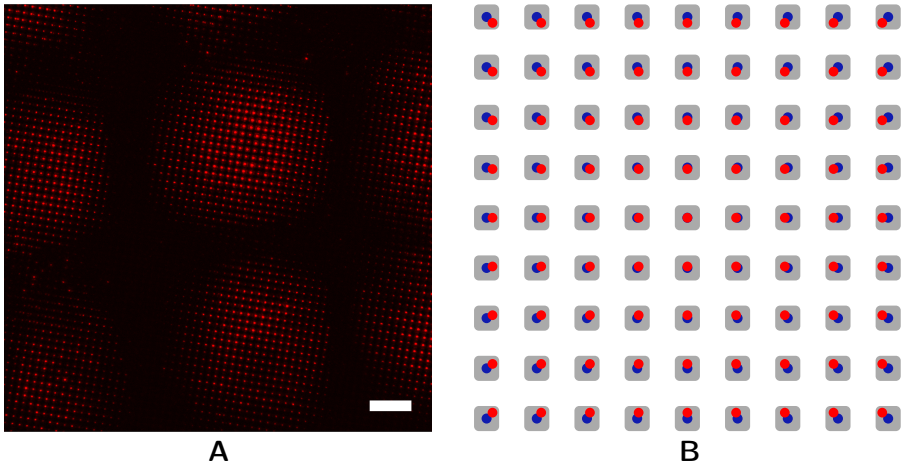

Figure 3.28: **Contraction and fabrication defects of the PPL stamp alter the patterning.** (A) Printing with a contracted PPL stamp. The pyramidal features are no longer aligned with the anchored microparticles. Patterning will occur only on the zones where the stamp contacts the substrate. (B) A schematic of the intended pattern represented with blue spots and the obtained pattern in red. Scale bar = 20 µm.

To pattern a whole substrate using a shrunken stamp, multiple printings where required and the protocol followed the distribution previously stated in Figure 3.17. This multiprinting mechanism created complex patterns on neighboring anchored microparticles and the single or multiple spots were repeated throughout the substrate. Figure 3.29A shows the results from the multiprinting procedure, highlighting the different areas with the various distribution of spots. One, two, and four spots were transferred to the anchored microparticles.

To create more complex patterns, the PPL stamp was inked with two different protein inks, each labeled with an individual fluorophore. The stamp was aligned so that the patterns were interlocked between labeled proteins. The WGA-TxR was initially patterned following the four defined absolute coordinates. A second inked zone from the PPL stamp was loaded with WGA-OG488 and the µCP was used to align the pattern to create the multiplexed color codes presented in Figure 3.29B. There, the zoomed-out areas of a substrate show the complex design in which the patterned areas are complementary and no overlapping occurs.

An interesting advantage of this multiprinting method is that the correct position between the PPL stamp and the substrate is tolerant to a slight misalignment, making it easier to load and position before printing. Although the protocol creates complex and multiplexed patterns, it significantly increases the difficulty to print more than two inks. The complexity lies on arriving with the desired ink to the com-

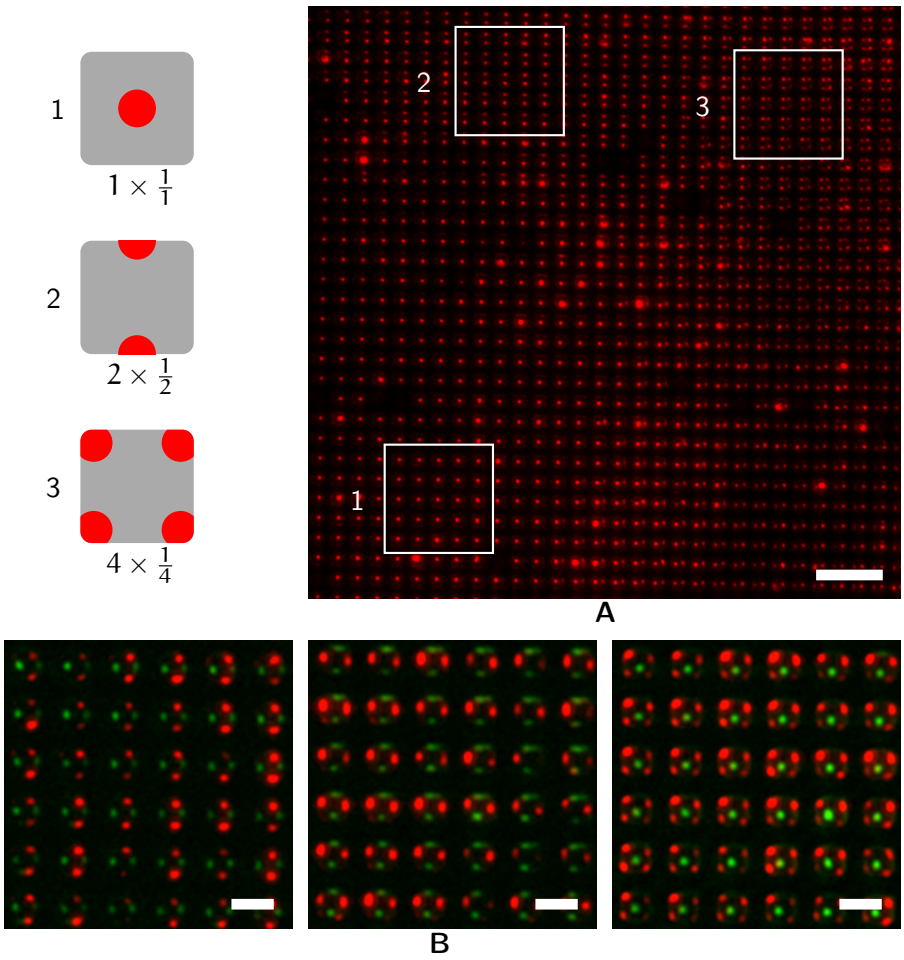

Figure 3.29: **Multipatterns fabricated with a contracted PDMS pyramidal stamp.** (A) Consecutive printing cycles with a PDMS with no support backbone. The translation of the stamp allowed to create different patterns on top of the anchored microparticles. Each schematic recounts the number of spots per microparticle. The fluorescence microscopy image presents the areas described by the schematics. (B) Multiplexed protein patterns with two different inks in complementary positions. Scale bars = 20 µm in (A) and 5 µm in (B).

plementary position on the substrate. Coupled with the complexity of adding more inks, the microparticles end up with several spot distribution along the substrate. If a design that repeats itself is required, a shrunken stamp would make it impossible.

A solution to create multiprotein arrays with repeating spot position along the substrate, requires the use of a stamp that maintains its feature distribution after demoulding, matching that of the anchored microparticles. As mentioned before, a stamp with a glass understructure corrected the distortion of the polymer and helped create parallel patterns with more inks.

The PDMS stamp with the glass backbone maintained the pyramidal feature distribution exactly as that of the master, which is trans-

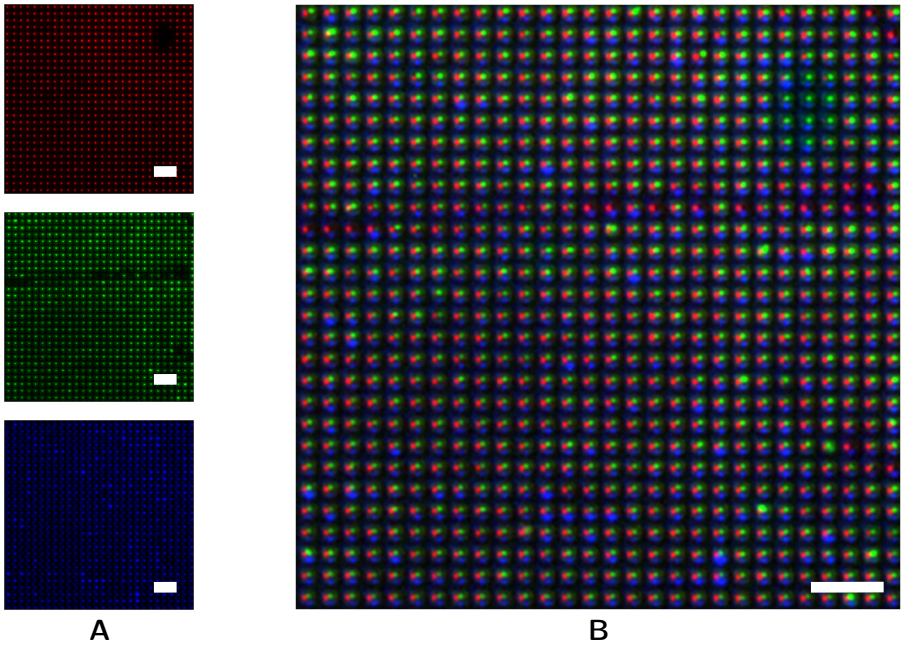

Figure 3.30: **Multiplexed protein microarrays.** Massively functionalization of anchored microparticles with three different proteins. (A) Each protein had an specific emission to prevent overlapping. (B) Merged image of the three emission channels showing the distribution of the spots on every anchored microparticle. Scale bars = 20 μm.

lated to the position of the anchored microparticles on the substrate. The multiplexed biomolecular array is presented in Figure 3.30. The three independent fluorophore emissions form the two WGAs and the anti-goat IgG are show in Figure 3.30A. A larger view of the merged emission channels is presented in Figure 3.30B. It is interesting to mention, that the distribution of the spots prevents the overlapping of the fluorescent signal. These results help formulate the term array-of-arrays, in which every anchored microparticle has an individual protein array forming part of a wider array of microparticles.

Future experiments with a finer control on the x– and y– positioning could create more complex patterns by increasing the number of spots printed on the surface of the anchored microparticles. The same occurs if sharper or harder polymer pens are used, allowing an increase of bound molecules on the microparticles. Extending the range of functionality, DNA could also be patterned on these substrates following the principles presented in Section 2.5.2, being the PPL stamp fabricated with the same material as the stamps used to pattern with μCP.

3.5.2.2 *Feature size and morphology*

Based on several printing experiments, the spot size and overall fluorescence emission values were studied. It is imperative to maintain values that fall into a similar range to secure an even distribution of the printed spots. These parameters are important to correlate the particles between samples. Figure 3.31 summarizes the edge length (A) and emission mean value (B) of the spots patterned via PPL. An average of $L_{print} = 890 \pm 136$ nm was obtained from different samples accounting to 2352 individual spots. This value was obtained by analyzing the fluorescence emission of the spots at their FWHM with a relationship of 5.9 $pixels\ \mu m^{-1}$ used to define the size of the printed features. The measured value is comparable to the one obtained with Equation 3.1, where a $L_{edge} = 742 \pm 62$ nm was calculated.

On the other hand, a mean gray value of 188 ± 9 a.u. was measured delimiting the area of the spots at the FWHM. This value is obtained averaging the values of each pixel inside the delimiting area, referred to as Region of interest (ROI).

An interesting finding is that both, the L_{print} and the mean gray value have a Gaussian distribution, and both values correlate to create a compact heat map presented in Figure 3.31C. This helps conclude that the spots maintain a similar size and fluorescence emission between printing processes, guaranteeing an even distribution throughout samples.

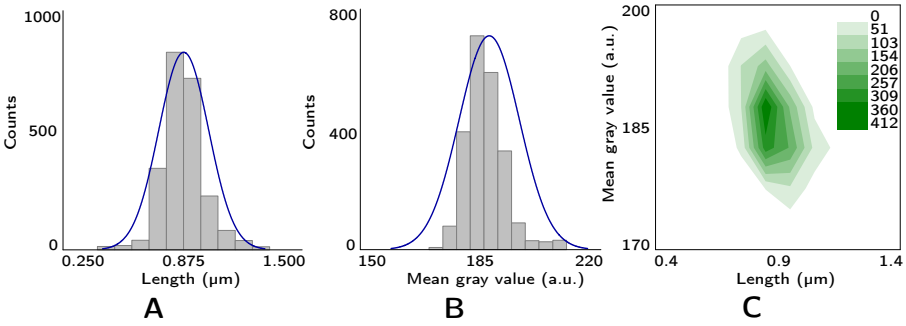

Figure 3.31: **Feature edge length and emission mean value of the printed spots.** (A) The histogram shows the number of counts versus edge length of the printed protein spots. (B) Histogram presenting the number of counts versus the mean emission value of each spot. (C) Heat map correlating the edge length and emission of each spot. $n = 2352$ in all three charts.

The technology developed to fabricate microarrays on the anchored microparticles can serve as a foundation to explore the patterning of other inks to tackle new obstacles and to develop new applications based on specialized materials.

3.5.2.3 *Direct patterning of fluorophores*

Fluorescent probes have been used to track the presence of heavy metals, the degree of hypoxia, and pH inside cells.[61] All the results relied on a solution of the fluorophore and its interaction with the environment. Although functional, diffusion, containment, and image processing issues, limited the application of these probes. Immobilizing the probes on a solid yet movable medium prevents the interference from the inherent limitations. Similar to the suspended array described Section 3.2.2, fluorescent microspheres have been used to track cellular mechanisms and the relationship of cells with the surrounding medium.[62]. Yet, a limited number of publications have shown the versatility to print fluorophores directly onto the substrate. Basabe-Desmonts *et al.*[63] demonstrated the sensing of various ions with a reactive μCPed fluorophore SAM. In their results, the emission intensity varied when the fluorophores were exposed to Co^{+2}, Ca^{+2}, Cu^{+2}, and Pb^{+2}, obtaining a label-free detection system.

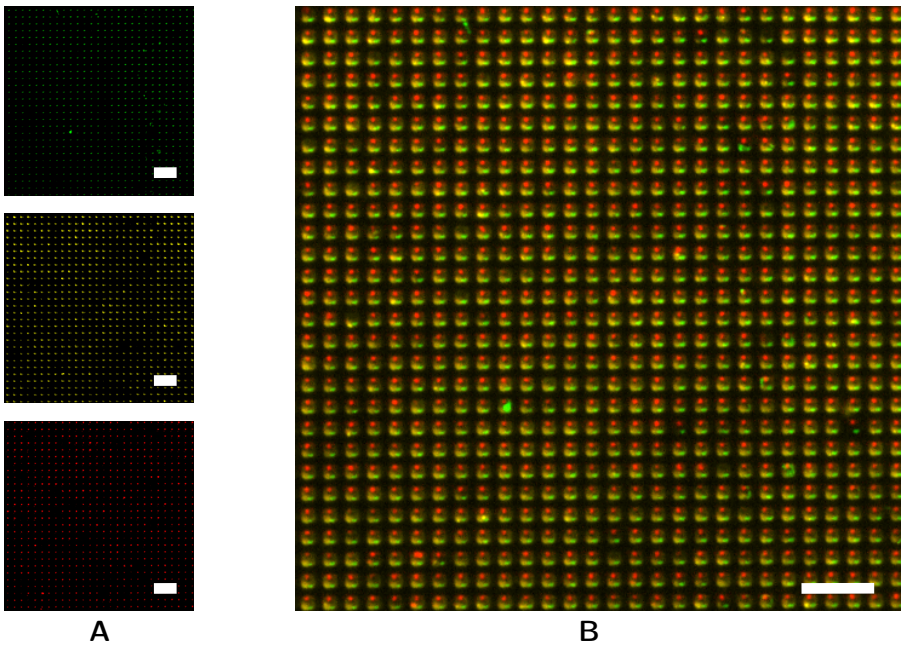

Figure 3.32: **Multiplexed fluorophore microarrays.** Anchored microparticles printed with three consecutive fluorophores. (A) The independent emission allowed to inspect the individual patterning. (B) Merged image of the three flourophore spots. Scale bars = 20 μm.

Multiplexed functionalization, that is, an increased amount of immobilized molecules, is inexistent on fluorescent probes. Therefore, the direct placement of reactive fluorophores could increase the scope of the printed microparticles. To continue with the developed patterning protocol, three pH-dependent fluorophores where patterned on the anchored microparticles. Figure 3.32A show the three inde-

pendent emission channels of OG488, pHrodo, and AF647, which were covalently bound to an active APTES SAM. As with the biomolecular inks, the direct placement of fluorophores proved successful, and Figure 3.32B shows an enlarged view of the patterned anchored microparticles. The three probe system allows to measure a wide range of pH values $(4-10)$ calculating the emission ratio of two of the probes coupled with a non-fluctuating probe as reference.

Experiments concerning the characterization of small volumes with pH fluctuation could be studied with movable sensing platforms. This approach provides the mobility of fluorescent-labeled microparticles, with the multiple probes on solution-based systems.

3.5.3 *Liberation of multiplexed microparticles*

The next step to fabricate the suspended planar arrays required the liberation of the patterned microparticles. The anchoring element had to be broken, while maintaining the shape and size of the microparticle, and most importantly, the pattern should remain intact.

Several methods were proposed to brake the anchoring element. Initially, a sharp scalpel was used to scratch the patterned substrate hoping it would sever the anchor while releasing the undamaged microparticles. Figure 3.33A shows and optical microscopy image of suspended microparticles after their release with the scratching method. Most of the microparticles were liberated intact and with ease, but an alarming amount of debris was produced. This tiny pieces were suspended portions of the broken anchors as well as fractured microparticles. As the scratching showed many drawbacks, patterned substrates were not subjected to this method.

Alternatively, liberation by sonication was tested. Several protein purification protocols require the protein solution to be sonicated for varying amounts of time. These protocols assure the proteins remain intact as the total energy translated to the protein is lower than that required to unfold or break them.[64] Some reports challenge these claims by the creation of protein aggregates.[65] Still, these aggregates require several proteins to come together. Proteins bound to a solid substrate, prevent such results. The pressure generated by the sound waves severed the anchors under the microparticles, liberating them. Patterned microparticles liberated by sonication are shown in Figure 3.33B. The image shows some protein retained on the surface of the microparticles, but in average, after calculating the mean fluorescence emission, the amount is lower than before the sonicating process.

Another proposed method was liberating the anchored microparticles by the creation of intimate contacts with a low-adhesive surface. Using physical interactions, the microparticles would adhere to the surface with sufficient strength to hold them in place. A subsequent

swift movement would brake the anchors. The physical attraction between substrate and microparticle albeit strong, should be breakable to achieve separation. Two approaches were followed. The first one used a glass slide as transferring substrate. A patterned chip was pressed against a slide and slightly rotated to sever the anchors. The liberated microparticles are shown in Figure 3.33C. The second approach used a fluorosilane-modified PDMS slab as transferring substrate. Again, the microparticles were liberated. To image the microparticles, 5 µL of Milli-Q was placed on top of the transferred microparticles and a micropipette was used to separate them from the substrate. For both cases, fouling of the transferring substrate occurred and loss of fluorescence was observed. In the case of the PDMS slab, most of the microparticles remained adhered to the substrate, as evidenced on Figure 3.33D.

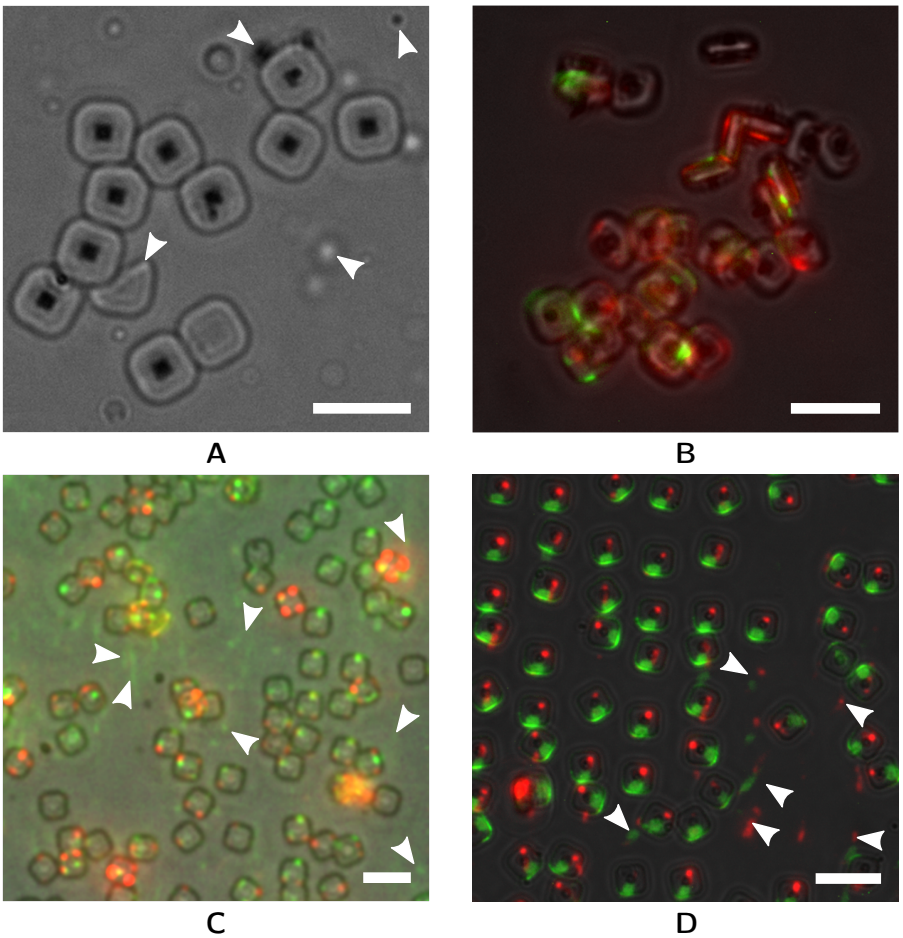

Figure 3.33: **Different liberation methods.** (A) Scratching the substrate with a sharp scalpel. The arrows point to broken microparticles and debris resulting form this liberation method. (B) Liberation by sonication of the patterned substrate. The bound biomolecules were displaced from their patterning area. (C) Intimate contact with a glass slide. The arrows point to fouling on the slide. (D) Conformal contact with a flat PDMS stamp. The arrows show to fouling sites on the stamp. Scale bars = 5 µm.

3.5.3.1 *Liberation under freeze-blow cycles using liquid N_2*

The previous liberation mechanisms where not entire successful, as protein loss or damage to the microparticles occurred. An initial attempt was to create a big temperature difference so the stresses felt across the anchor would be sufficient to separate it from the substrate. Liquid N_2 offers an accessible solution to generate such temperature shocks. Unfortunately, this method did not proved sufficient to liberate all the microparticles.

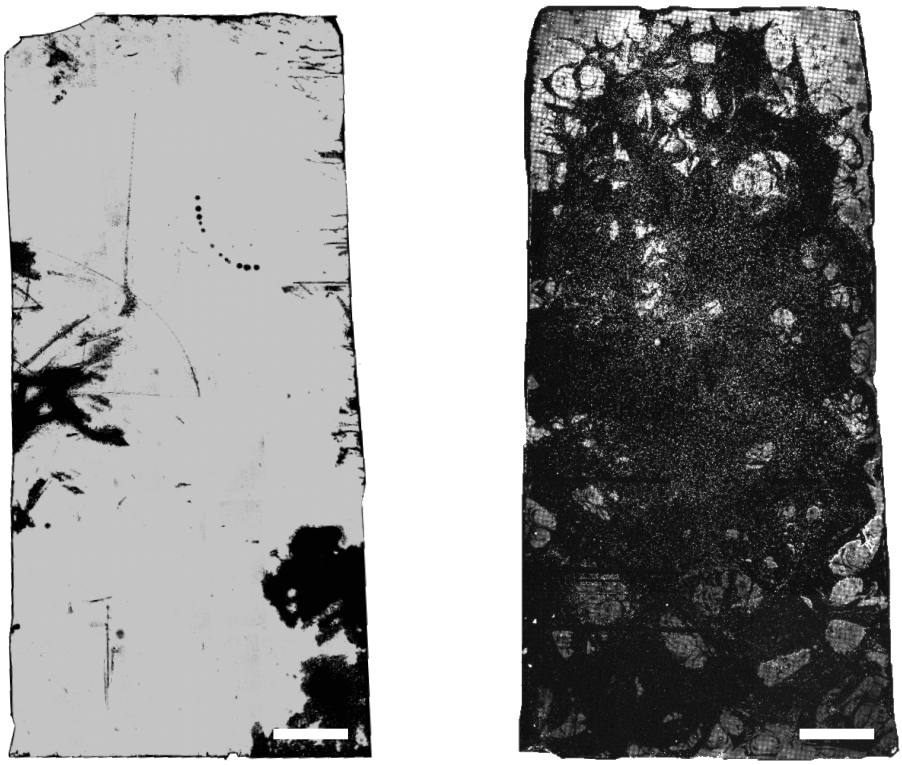

Figure 3.34: **Substrate before and after cryofracture.** (A) Montage of microscopic images of a substrate where all the surfaces of the microparticles are covered with BSA-AF555. The dark zones show areas without microparticles, mostly damaged during handling. (B) Montage of microscopic images of a chip after three consecutive freeze-blow cycles. The dark areas correspond to microparticle-free zones. Scale bars = 100 µm.

The next approach required the creation of a solid matrix around the microparticles that would entrap them, and the lift-off of such matrix would carry the microparticles. The first attempt was to create a solid enclosure with a frozen aqueous medium that would separate when a mechanical force (i. e. a blow) was applied, carrying the microparticles with it. Thawing the recovered solid piece of medium would allow the collection of the microparticles via centrifugation or filtration. With every freeze-blow cycle, some microparticles were lib-

erated. In Figure 3.34A an AF555 functionalized chip was subjected to three freeze-blow cycles to liberate the anchored microparticles. The dark areas show parts of the chip without functionalization, that is because no anchored microparticles existed or where removed during handling. Another resulting chip after three cycles can be seen in Figure 3.34B. It is interesting to note the patterns created by the dynamics of the changing temperature in the liquid medium where the N_2 boiled. These areas remained due to entrapped gas between the ice and the substrate. Even after several cycles, ~26% of the microparticles remained on the substrate.

3.5.3.2 *Liberation using Fluoromount™*

The best liberation strategy followed a simple discovery obtained during the characterization of various samples. First, to fix the microparticles for microscopic imaging Fluoromount™ was used. This mounting medium solidifies after some time, locking the microparticles on site and preventing any movement which would be recorded on the microscope. After manipulating the samples, it was observed that the solidified medium created a robust matrix that was easily peeled, carrying the entrapped microparticles. And finally, the matrix was dissolved in any aqueous solution.

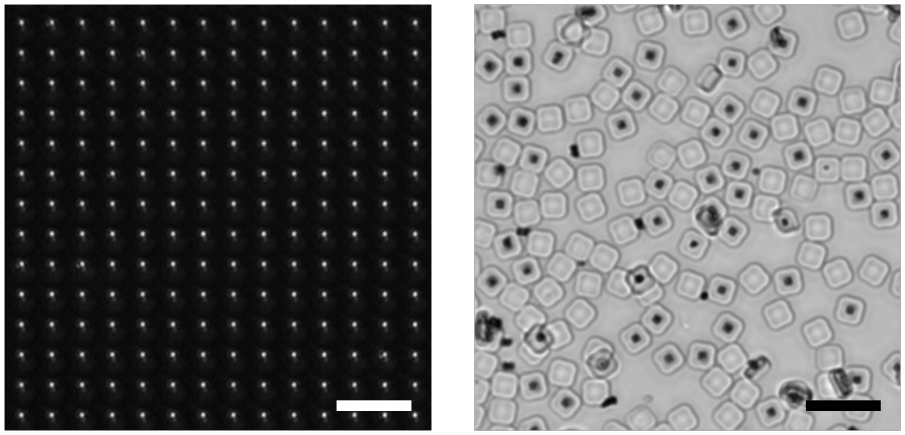

Figure 3.35: **Substrate and microparticles after the liberation step.** (A) microscopic image of the remaining anchors on the substrate. (B) Liberated microparticles. Scale bars = 15 µm in (A) and 10 µm in (B).

A drop of Fluoromount™ was directly placed on the substrate and left to solidify. 100% of the entrapped microparticles were liberated with this method, leaving only the bottom half of the anchoring elements as shown in Figure 3.35A. After the membrane was dissolved, the microparticles were collected in a clean, debris-free dispersion. Figure 3.35B shows the large amount of liberated microparticles obtained using this method. It is worth mentioning that Shah *et al.*[66] used a similar method with the solidification of Polyvinyl

alcohol (PVA) to manipulate and modify a monolayer of polymeric microparticles.

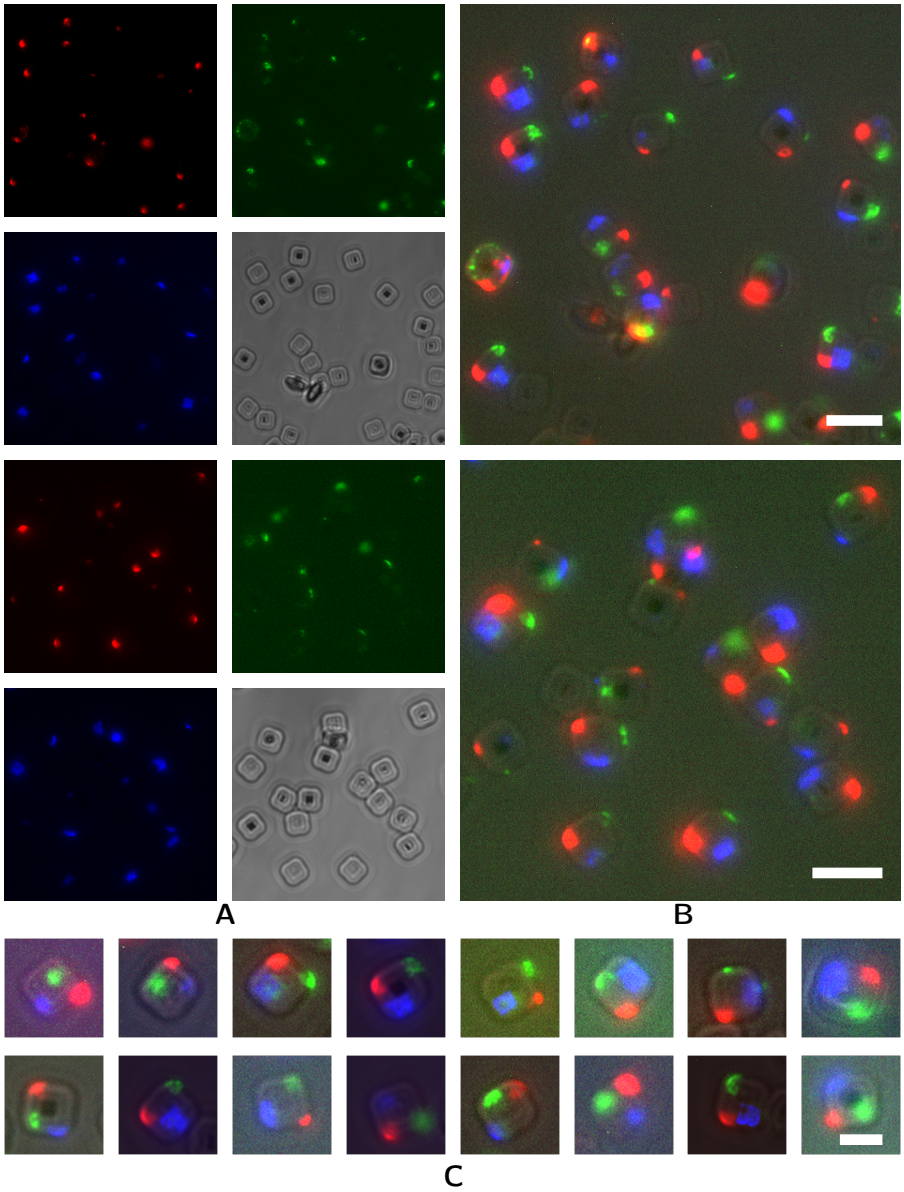

Figure 3.36: **Liberated multiplexed microparticles.** (A) Four channel emission microscopic images of liberated microparticles. (B) Merged images of the emission channels. (C) Collection of microparticles with the three protein on each one. The false-coloured images represent WGA-TxR in red, WGA-OG488 in green, and the AMCA rabbit anti-goat in blue. Scale bars = 5 µm in (B) and 3 µm in (C).

The interesting application of this method is the encircling of the anchored microparticles by the matrix. The subsequent liberation does not erode or modify the position of the patterned biomolecules. Several experiments were repeated and confirmed the application of the liberation method obtaining outstanding results as the ones shown

in Figure 3.36. Figure 3.36A shows the fluorescent emission channels of the WGA-TxR, WGA-OG488, and AMCA anti goat, as well as the particles under white light. An zoomed view of a sample is presented in Figure 3.36B. The enlarged microparticles in Figure 3.36C present the three biomolecules forming the microarray on their surface.

3.5.4 *Recognition of patterned proteins with an antibody sandwich assay*

If an individual multiplexed microparticle is selected, it is well sustained to refer to it as the smallest planar multiprotein microarray ever fabricated. After this affirmation, it is required that the functionality of the grafted proteins remained intact so the system can actually function as traditional protein microarrays.

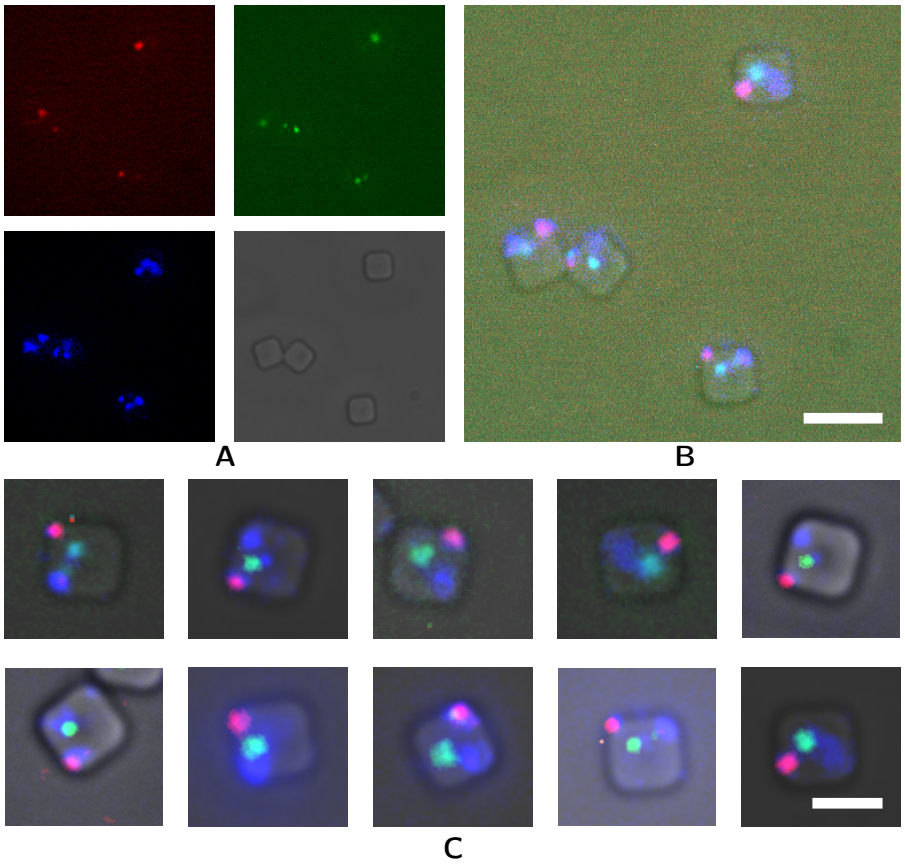

Figure 3.37: **Antibody binding assay of multiplexed microparticles.** (A) Four channel emission of the liberated microparticles. (B) Merged image. (C) Collection of microparticles with the three spots. The change in colour compared from Figure 3.36 represent the sum of red and blue, and green and blue, obtaining magenta and cyan, respectively. Scale bars = 10 µm in (B) and 3 µm in (C).

An antibody binding assay was used to verify the recognition between a specialized antibody and the patterned protein. The fluorescence of the antibody assay is shown in Figure 3.37. It can be observed

that the number of imaged microparticles is lower than that presented on Figure 3.36. This is due to the manipulation of the sample during the different steps of the antibody assay.

In this assay, the sum of the fluorescence emissions is the evidence that the antibodies grafted the immobilized proteins. The false colouring of the WGA-TxR with the AMCA labeled antibody resulted in a magenta emission. While in the case of the WGA-OG488, the false colouring is represented in cyan. The enlarged view of the microparticles in Figure 3.37C help identify the assay.

With such a small printed spot, the characterization with fluorescence microscopy my pose complecations as it can be assumed that with large spot size, the total amount of grafted molecules is greater, resulting in a higher spot signal. However, the signal density, i. e. the signal per spot area, starts to decrease with larger spots as the probing molecule becomes the limiting factor. The capture-probe conjugation is also distributed over a larger area, hence, a lower maximum signal is obtained. On the same path, decreasing the spot size will decrease the total spot signal, yet the signal density will increase. As presented in Figure 3.38, a maximum signal density is maintained below a certain spot size. Therefore, higher signal intensities can be obtained with small spots.[7] The patterned submicrometric spots maintain a constant signal density which guarantees a correct signal-to-noise ratio.

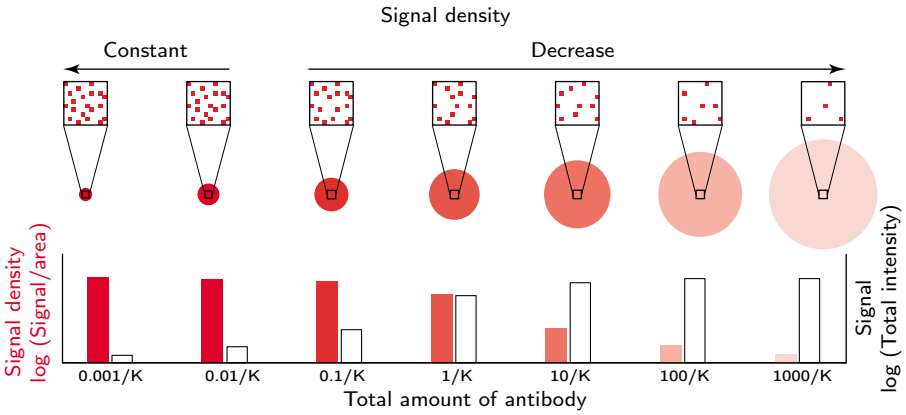

Figure 3.38: **Signal density on immobilized spots.** Signal density at different concentration of probed molecules. Total signal (total intensity) increases with growing spot size, yet signal density (signal/area) increases with decreasing spot size, reaching a constant level when the spotted molecules concentration is <0.1/K (K = association constant). Adapted from [7].

Seen that the grafted proteins are the limiting factor for the detection, the amount of probing antibody would maintain a constant signal density. This helps to obtain a similar detection signal independently of the size of the spot.

3.6 CONCLUSIONS

This Chapter described the creation of suspended planar multiprotein microarrays using several fabrication techniques. The main challenge was to create a multiprotein array on a constricted area with a technique that would deliver the proteins without damage. The constricted area corresponded to an individual anchored microparticles from a micromachined substrate. The surface of every microparticle was chemically functionalized to covalently bind the desired biomolecules. To transfer the protein on such surfaces, the Polymer pen lithography (PPL) technique was adopted and applied with the upgraded μCP tool.

Several liberation methods were studied to break the patterned anchored microparticles from the substrate. The most successful method was found to be a solidified matrix encircling the microparticles that was later peeled from the substrate carrying the microparticles with it. This membrane was later dissolved in any aqueous medium and the microparticles were collected.

An antibody binding assay was used to test the integrity of the bound proteins. The selective affinity of the antibodies to the grafted proteins proved the patterning and liberation methods to be biocompatible. Future applications could expand the number of patterned proteins as well as different microparticle shapes. Other proteins, antibodies, and various complex biomolecules as DNA, could expand the application for this technology.

3.7 REFERENCES

[1] Pandey, A and Mann, M. 'Proteomics to study genes and genomes'. *Nature*, 405 (June) (2000) 837–46. URL http://www.nature.com/nature/journal/v405/n6788/abs/405837a0.html

[2] Kim, MS; Pinto, SM; Getnet, D; Nirujogi, RS; Manda, SS; Chaerkady, R; Madugundu, AK; Kelkar, DS; Isserlin, R; Jain, S; Thomas, JK; Muthusamy, B; Leal-Rojas, P; Kumar, P; Sahasrabuddhe, NA; Balakrishnan, L; Advani, J; George, B; Renuse, S; Selvan, LDN; Patil, AH; Nanjappa, V; Radhakrishnan, A; Prasad, S; Subbannayya, T; Raju, R; Kumar, M; Sreenivasamurthy, SK; Marimuthu, A; Sathe, GJ; Chavan, S; Datta, KK; Subbannayya, Y; Sahu, A; Yelamanchi, SD; Jayaram, S; Rajagopalan, P; Sharma, J; Murthy, KR; Syed, N; Goel, R; Khan, AA; Ahmad, S; Dey, G; Mudgal, K; Chatterjee, A; Huang, TC; Zhong, J; Wu, X; Shaw, PG; Freed, D; Zahari, MS; Mukherjee, KK; Shankar, S; Mahadevan, A; Lam, H; Mitchell, CJ; Shankar, SK; Satishchandra, P; Schroeder, JT; Sirdeshmukh, R; Maitra, A; Leach, SD; Drake, CG; Halushka, MK; Prasad, TSK; Hruban, RH; Kerr, CL; Bader, GD; Iacobuzio-Donahue, CA; Gowda, H; and Pandey, A. 'A draft map of the human proteome.' *Nature*, 509 (7502) (2014) 575–81. URL http://www.ncbi.nlm.nih.gov/pubmed/24870542

[3] Ho, Y; Gruhler, A; Heilbut, A; Bader, GD; Moore, L; Adams, Sl; Millar, A; Taylor, P; Bennett, K; Boutilier, K; Yang, L; Wolting, C; Donaldson, I; Schandorff, S; Shewnarane, J; Vo, M; Taggart, J; Goudreault, M; Muskat, B; Alfarano, C; Dewar, D; Lin, Z; Michalickova, K; Willems, AR; Sassi, H; Nielsen, PA; Rasmussen, KJ; Andersen, JR; Johansen, LE; Matthiesen, J; Hendrickson, RC; Gleeson, F; Pawson, T; Moran, MF; Durocher, D; Mann, M; Hogue, CWV; Figeys, D; and Tyers, M. 'Systematic identification of protein complexes in Saccharomyces cerevisiae by mass spectrometry'. *Nature*, 415 (January) (2002) 2–5. URL http://www.nature.com/nature/journal/v415/n6868/abs/415180a.html

[4] Aebersold, R and Mann, M. 'Mass spectrometry-based proteomics.' *Nature*, 422 (6928) (2003) 198–207. URL http://www.ncbi.nlm.nih.gov/pubmed/12634793

[5] Ghaemmaghami, S; Huh, WK; Bower, K; Howson, RW; Belle, A; Dephoure, N; O'Shea, EK; and Weissman, JS. 'Global analysis of protein expression in yeast.' *Nature*, 425 (6959) (2003) 737–41. URL http://www.ncbi.nlm.nih.gov/pubmed/14562106

[6] Hall, DA; Ptacek, J; and Snyder, M. 'Protein microarray technology.' *Mechanisms of ageing and development*, 128 (1) (2007) 161–7. URL http://www.pubmedcentral.nih.gov/articlerender.fcgi?artid=1828913&tool=pmcentrez&rendertype=abstract

[7] Templin, MF; Stoll, D; Schrenk, M; Traub, PC; Vöhringer, CF; and Joos, TO. 'Protein microarray technology'. *TRENDS in Biotechnology*, 20 (4) (2002) 815–22. URL http://www.ncbi.nlm.nih.gov/pubmed/12546969

[8] Sun, H; Chen, GYJ; and Yao, SQ. 'Recent advances in microarray technologies for proteomics.' *Chemistry & biology*, 20 (5) (2013) 685–99. URL http://www.ncbi.nlm.nih.gov/pubmed/23706635

[9] Chang, TW. 'Binding of cells to matrixes of distinct antibodies coated on solid surface.' *Journal of immunological methods*, 65 (1-2) (1983) 217–23. URL http://www.ncbi.nlm.nih.gov/pubmed/6606681

[10] Schena, M; Shalon, D; Davis, RW; and Brown, PO. 'Quantitative monitoring of gene expression patterns with a complementary DNA microarray.' *Science*, 270 (5235) (1995) 467–70. URL http://www.ncbi.nlm.nih.gov/pubmed/7569999

[11] Romanov, V; Davidoff, SN; Miles, AR; Grainger, DW; Gale, BK; and Brooks, BD. 'A critical comparison of protein microarray fabrication technologies.' *The Analyst*, 139 (6) (2014) 1303–26. URL http://www.ncbi.nlm.nih.gov/pubmed/24479125

[12] Chandra, H; Reddy, PJ; and Srivastava, S. 'Protein microarrays and novel detection platforms.' *Expert review of proteomics*, 8 (1) (2011) 61–79. URL http://www.ncbi.nlm.nih.gov/pubmed/21329428

[13] Natarajan, S; Katsamba, PS; Miles, A; Eckman, J; Papalia, Ga; Rich, RL; Gale, BK; and Myszka, DG. 'Continuous-flow microfluidic printing of proteins for array-based applications including surface plasmon resonance imaging.' *Analytical biochemistry*, 373 (1) (2008) 141–6. URL http://www.ncbi.nlm.nih.gov/pubmed/17868635

[14] Kolodziej, C and Maynard, H. 'Electron-beam lithography for patterning biomolecules at the micron and nanometer scale'. *Chemistry of materials*, 24 (5) (2012) 774–780. URL http://pubs.acs.org/doi/abs/10.1021/cm202669f

[15] Christman, KL; Enriquez-Rios, VD; and Maynard, HD. 'Nanopatterning proteins and peptides'. *Soft Matter*, 2 (11) (2006) 928. URL http://xlink.rsc.org/?DOI=b611000b

[16] Piner, RD; Zhu, J; Xu, F; Hong, S; and Mirkin, CA. '"Dip-Pen" Nanolithography'. *Science*, 283 (29) (1999) 661–663. URL http://www.sciencemag.org/cgi/doi/10.1126/science.283.5402.661

[17] Wilson, DL; Martin, R; Hong, S; Cronin-Golomb, M; Mirkin, CA; and Kaplan, DL. 'Surface organization

and nanopatterning of collagen by dip-pen nanolithography.' *Proceedings of the National Academy of Sciences of the United States of America*, 98 (24) (2001) 13660–4. URL http://www.pubmedcentral.nih.gov/articlerender.fcgi?artid=61097&tool=pmcentrez&rendertype=abstract

[18] Zheng, Q; Lu, J; Chen, H; Huang, L; Cai, J; and Xu, Z. 'Application of inkjet printing technique for biological material delivery and antimicrobial assays.' *Analytical biochemistry*, 410 (2) (2011) 171–6. URL http://www.ncbi.nlm.nih.gov/pubmed/20971057

[19] Fujita, S; Onuki-Nagasaki, R; Fukuda, J; Enomoto, J; Yamaguchi, S; and Miyake, M. 'Development of super-dense transfected cell microarrays generated by piezoelectric inkjet printing.' *Lab on a chip*, 13 (1) (2013) 77–80. URL http://www.ncbi.nlm.nih.gov/pubmed/23165644

[20] Yang, Z; Chen, B; Pei, X; and Shangguan, F. 'Multiplex analysis of tumor multidrug-resistance genes expression with photonic suspension array.' *The Analyst*, 137 (14) (2012) 3343–8. URL http://www.ncbi.nlm.nih.gov/pubmed/22683740

[21] Nolan, JP and Sklar, LA. 'Suspension array technology: evolution of the flat-array paradigm.' *TRENDS in Biotechnology*, 20 (1) (2002) 9–12. URL http://www.ncbi.nlm.nih.gov/pubmed/11742671

[22] LaFratta, CN and Walt, DR. 'Very high density sensing arrays.' *Chemical reviews*, 108 (2) (2008) 614–37. URL http://www.ncbi.nlm.nih.gov/pubmed/18229955

[23] Jun, BH; Kang, H; Lee, YS; and Jeong, DH. 'Fluorescence-based multiplex protein detection using optically encoded microbeads.' *Molecules*, 17 (3) (2012) 2474–90. URL http://www.ncbi.nlm.nih.gov/pubmed/22382526

[24] Glotzer, SC and Solomon, MJ. 'Anisotropy of building blocks and their assembly into complex structures.' *Nature materials*, 6 (8) (2007) 557–62. URL http://www.ncbi.nlm.nih.gov/pubmed/17667968

[25] Kim, SK and Lee, SB. 'Highly encoded one-dimensional nanostructures for rapid sensing'. *Journal of Materials Chemistry*, 19 (10) (2009) 1381. URL http://xlink.rsc.org/?DOI=b814408g

[26] Cederquist, KB; Dean, SL; and Keating, CD. 'Encoded anisotropic particles for multiplexed bioanalysis.' *Wiley interdisciplinary reviews. Nanomedicine and nanobiotechnology*, 2 (6) (2010) 578–600. URL http://www.ncbi.nlm.nih.gov/pubmed/20890960

[27] Lee, W; Choi, D; Kim, JH; and Koh, WG. 'Suspension arrays of hydrogel microparticles prepared by photopatterning for multiplexed protein-based bioassays.' *Biomedical microdevices*, 10 (6) (2008) 813–22. URL http://www.ncbi.nlm.nih.gov/pubmed/18561028

[28] Lee, J; Bisso, PW; Srinivas, RL; Kim, JJ; Swiston, AJ; and Doyle, PS. 'Universal process-inert encoding architecture for polymer microparticles'. *Nature materials*, 13 (5) (2014) 524–9. URL http://www.nature.com/nmat/journal/v13/n5/full/nmat3938.html

[29] Zhang, P; Liu, Y; Xia, J; Wang, Z; Kirkland, B; and Guan, J. 'Top-down fabrication of polyelectrolyte-thermoplastic hybrid microparticles for unidirectional drug delivery to single cells.' *Advanced healthcare materials*, 2 (4) (2013) 540–5. URL http://www.ncbi.nlm.nih.gov/pubmed/23184769

[30] Tang, JL; Schoenwald, K; Potter, D; White, D; and Sulchek, T. 'Bifunctional Janus microparticles with spatially segregated proteins.' *Langmuir*, 28 (26) (2012) 10033–9. URL http://www.pubmedcentral.nih.gov/articlerender.fcgi?artid=3428262&tool=pmcentrez&rendertype=abstract

[31] Kaufmann, T; Gokmen, MT; Wendeln, C; Schneiders, M; Rinnen, S; Arlinghaus, HF; Bon, SAF; Du Prez, FE; and Ravoo, BJ. '"Sandwich" microcontact printing as a mild route towards monodisperse Janus particles with tailored bifunctionality.' *Advanced materials*, 23 (1) (2011) 79–83. URL http://www.ncbi.nlm.nih.gov/pubmed/21069890

[32] Rahmani, S; Saha, S; Durmaz, H; Donini, A; Misra, AC; Yoon, J; and Lahann, J. 'Chemically Orthogonal Three-Patch Microparticles'. *Angewandte Chemie*, 126 (9) (2014) 2364–2370. URL http://doi.wiley.com/10.1002/ange.201310727

[33] Gandor, S; Reisewitz, S; Venkatachalapathy, M; Arrabito, G; Reibner, M; Schröder, H; Ruf, K; Niemeyer, CM; Bastiaens, PIH; and Dehmelt, L. 'A protein-interaction array inside a living cell.' *Angewandte Chemie*, 52 (18) (2013) 4790–4. URL http://www.pubmedcentral.nih.gov/articlerender.fcgi?artid=3652028&tool=pmcentrez&rendertype=abstract

[34] Arrabito, G; Reisewitz, S; Dehmelt, L; Bastiaens, PI; Pignataro, B; Schroeder, H; and Niemeyer, CM. 'Biochips for cell biology by combined dip-pen nanolithography and DNA-directed protein immobilization.' *Small*, 9 (24) (2013) 4243–9. URL http://www.ncbi.nlm.nih.gov/pubmed/23881817

[35] Vetrone, F; Naccache, R; Zamarrón, A; Juarranz de la Fuente, A; Sanz-Rodríguez, F; Martinez Maestro, L; Martín Rodriguez, E;

Jaque, D; García Solé, J; and Capobianco, Ja. 'Temperature sensing using fluorescent nanothermometers.' *ACS nano*, 4 (6) (2010) 3254–8. URL http://www.ncbi.nlm.nih.gov/pubmed/24881520

[36] Fercher, A; Borisov, SM; Zhdanov, AV; Klimant, I; and Papkovsky, DB. 'Intracellular O2 sensing probe based on cell-penetrating phosphorescent nanoparticles.' *ACS nano*, 5 (7) (2011) 5499–508. URL http://www.ncbi.nlm.nih.gov/pubmed/21671589

[37] Guo, J; Xiong, S; Wu, X; Shen, J; and Chu, PK. 'In situ probing of intracellular pH by fluorescence from inorganic nanoparticles.' *Biomaterials*, 34 (36) (2013) 9183–9. URL http://www.ncbi.nlm.nih.gov/pubmed/24008041

[38] Tantra, R and Knight, A. 'Cellular uptake and intracellular fate of engineered nanoparticles: A review on the application of imaging techniques.' *Nanotoxicology*, 5 (September) (2010) 381–392. URL http://www.ncbi.nlm.nih.gov/pubmed/20846020

[39] Gómez-Martínez, R; Vázquez, P; Duch, M; Muriano, A; Pinacho, D; Sanvicens, N; Sánchez-Baeza, F; Boya, P; de la Rosa, EJ; Esteve, J; Suárez, T; and Plaza, JA. 'Intracellular silicon chips in living cells.' *Small*, 6 (4) (2010) 499–502. URL http://www.ncbi.nlm.nih.gov/pubmed/20025079

[40] Fernandez-Rosas, E; Gómez, R; Ibañez, E; Barrios, L; Duch, M; Esteve, J; Nogués, C; and Plaza, JA. 'Intracellular polysilicon barcodes for cell tracking.' *Small*, 5 (21) (2009) 2433–9. URL http://www.ncbi.nlm.nih.gov/pubmed/19670393

[41] Penon, O; Novo, S; Durán, S; Ibañez, E; Nogués, C; Samitier, J; Duch, M; Plaza, JA; and Pérez-García, L. 'Efficient biofunctionalization of polysilicon barcodes for adhesion to the zona pellucida of mouse embryos.' *Bioconjugate chemistry*, 23 (12) (2012) 2392–402. URL http://www.ncbi.nlm.nih.gov/pubmed/23185984

[42] Serda, RE; Gu, J; Bhavane, RC; Liu, X; Chiappini, C; Decuzzi, P; and Ferrari, M. 'The association of silicon microparticles with endothelial cells in drug delivery to the vasculature.' *Biomaterials*, 30 (13) (2009) 2440–8. URL http://www.ncbi.nlm.nih.gov/pubmed/19215978

[43] Gómez-Martínez, R; Hernández-Pinto, AM; Duch, M; Vázquez, P; Zinoviev, K; de la Rosa, EJ; Esteve, J; Suárez, T; and Plaza, JA. 'Silicon chips detect intracellular pressure changes in living cells'. *Nature nanotechnology*, 8 (June) (2013) 517–521. URL http://www.nature.com/doifinder/10.1038/nnano.2013.118

[44] Oberhansl, S; Hirtz, M; Lagunas, A; Eritja, R; Martinez, E; Fuchs, H; and Samitier, J. 'Facile modification of silica substrates provides a platform for direct-writing surface click chemistry.' *Small*,

8 (4) (2012) 541–5. URL http://www.ncbi.nlm.nih.gov/pubmed/22258752

[45] Salaita, K; Wang, Y; Fragala, J; Vega, RA; Liu, C; and Mirkin, CA. 'Massively parallel dip-pen nanolithography with 55 000-pen two-dimensional arrays.' *Angewandte Chemie*, 45 (43) (2006) 7220–3. URL http://www.ncbi.nlm.nih.gov/pubmed/17001599

[46] Huo, F; Zheng, Z; Zheng, G; Giam, LR; Zhang, H; and Mirkin, CA. 'Polymer pen lithography.' *Science*, 321 (5896) (2008) 1658–60. URL http://www.ncbi.nlm.nih.gov/pubmed/18703709

[47] Liao, X; Braunschweig, AB; Zheng, Z; and Mirkin, CA. 'Force- and time-dependent feature size and shape control in molecular printing via polymer-pen lithography.' *Small*, 6 (10) (2010) 1082–6. URL http://www.ncbi.nlm.nih.gov/pubmed/19859944

[48] Liao, X; Braunschweig, AB; and Mirkin, CA. '"Force-feedback" leveling of massively parallel arrays in polymer pen lithography.' *Nano letters*, 10 (4) (2010) 1335–40. URL http://www.ncbi.nlm.nih.gov/pubmed/20184292

[49] Zheng, Z; Daniel, WL; Giam, LR; Huo, F; Senesi, AJ; Zheng, G; and Mirkin, CA. 'Multiplexed protein arrays enabled by polymer pen lithography: addressing the inking challenge.' *Angewandte Chemie*, 48 (41) (2009) 7626–9. URL http://www.pubmedcentral.nih.gov/articlerender.fcgi?artid=3523346&tool=pmcentrez&rendertype=abstract

[50] Brinkmann, F; Hirtz, M; Greiner, AM; Weschenfelder, M; Waterkotte, B; Bastmeyer, M; and Fuchs, H. 'Interdigitated Multicolored Bioink Micropatterns by Multiplexed Polymer Pen Lithography.' *Small*, pages 1–10. URL http://www.ncbi.nlm.nih.gov/pubmed/23554307

[51] Xie, Z; Chen, C; Zhou, X; Gao, T; Liu, D; Miao, Q; and Zheng, Z. 'Massively Parallel Patterning of Complex 2D and 3D Functional Polymer Brushes by Polymer Pen Lithography.' *ACS applied materials & interfaces*, 6 (15) (2014) 11955–64. URL http://www.ncbi.nlm.nih.gov/pubmed/24417672

[52] Wu, J; Zan, X; Li, S; Liu, Y; Cui, C; Zou, B; Zhang, W; Xu, H; Duan, H; Tian, D; Huang, W; and Huo, F. 'In situ synthesis of large-area single sub-10 nm nanoparticle arrays by polymer pen lithography.' *Nanoscale*, 6 (2) (2014) 749–52. URL http://www.ncbi.nlm.nih.gov/pubmed/24309996

[53] Shim, W; Braunschweig, AB; Liao, X; Chai, J; Lim, JK; Zheng, G; and Mirkin, CA. 'Hard-tip, soft-spring lithography.' *Nature*, 469 (7331) (2011) 516–20. URL http://www.ncbi.nlm.nih.gov/pubmed/21270890

[54] Huo, F; Zheng, G; Liao, X; Giam, LR; Chai, J; Chen, X; Shim, W; and Mirkin, CA. 'Beam pen lithography.' *Nature nanotechnology*, 5 (9) (2010) 637–40. URL http://www.ncbi.nlm.nih.gov/pubmed/20676088

[55] Eichelsdoerfer, DJ; Liao, X; Cabezas, MD; Morris, W; Radha, B; Brown, KA; Giam, LR; Braunschweig, AB; and Mirkin, CA. 'Large-area molecular patterning with polymer pen lithography.' *Nature protocols*, 8 (12) (2013) 2548–60. URL http://www.ncbi.nlm.nih.gov/pubmed/24263094

[56] Lee, SW and Lee, SS. 'Shrinkage ratio of PDMS and its alignment method for the wafer level process'. *Microsystem Technologies*, 14 (2) (2007) 205–208. URL http://link.springer.com/10.1007/s00542-007-0417-y

[57] Ogawa, M; Kosaka, N; Regino, CAS; Mitsunaga, M; Choyke, PL; and Kobayashi, H. 'High sensitivity detection of cancer in vivo using a dual-controlled activation fluorescent imaging probe based on H-dimer formation and pH activation.' *Molecular bioSystems*, 6 (5) (2010) 888–93. URL http://www.pubmedcentral.nih.gov/articlerender.fcgi?artid=3464101&tool=pmcentrez&rendertype=abstract

[58] Han, J and Burgess, K. 'Fluorescent indicators for intracellular pH.' *Chemical reviews*, 110 (5) (2010) 2709–28. URL http://www.ncbi.nlm.nih.gov/pubmed/21530914

[59] ATDBio Ltd. 'Alexa® dyes' (2014). URL http://www.atdbio.com/content/34/Alexa-dyes

[60] Deng, J; Davies, DR; Wisedchaisri, G; Wu, M; Hol, WGJ; and Mehlin, C. 'An improved protocol for rapid freezing of protein samples for long-term storage'. *Acta Crystallographica Section D Biological Crystallography*, 60 (1) (2003) 203–204. URL http://scripts.iucr.org/cgi-bin/paper?S0907444903024491

[61] Qian, X; Xiao, Y; Xu, Y; Guo, X; Qian, J; and Zhu, W. '"Alive" dyes as fluorescent sensors: fluorophore, mechanism, receptor and images in living cells.' *Chemical communications*, 46 (35) (2010) 6418–36. URL http://www.ncbi.nlm.nih.gov/pubmed/20589288

[62] Steinberg, BE; Scott, CC; and Grinstein, S. 'High-throughput assays of phagocytosis, phagosome maturation, and bacterial invasion.' *American journal of physiology. Cell physiology*, 292 (2) (2007) C945–52. URL http://www.ncbi.nlm.nih.gov/pubmed/17020932

[63] Basabe-Desmonts, L; Beld, J; Zimmerman, RS; Hernando, J; Mela, P; García Parajó, MF; van Hulst, NF; van den Berg, A;

Reinhoudt, DN; and Crego-Calama, M. 'A simple approach to sensor discovery and fabrication on self-assembled monolayers on glass.' *Journal of the American Chemical Society*, 126 (23) (2004) 7293–9. URL http://www.ncbi.nlm.nih.gov/pubmed/15186166

[64] Mason, TJ and Peters, D. *Practical Sonochemistry: Uses and Applications of Ultrasound*. Horwood Publishing, second edition (2011). URL http://scholar.google.com/scholar?hl=en&btnG=Search&q=intitle:Practical+sonochemistry,+1991#2

[65] Stathopulos, PB; Scholz, GA; Hwang, YM; Rumfeldt, JAO; Lepock, JR; and Meiering, EM. 'Sonication of proteins causes formation of aggregates that resemble amyloid.' *Protein science: a publication of the Protein Society*, 13 (11) (2004) 3017–27. URL http://www.pubmedcentral.nih.gov/articlerender.fcgi?artid=2286572&tool=pmcentrez&rendertype=abstract

[66] Shah, AA; Schultz, B; Kohlstedt, KL; Glotzer, SC; and Solomon, MJ. 'Synthesis, assembly, and image analysis of spheroidal patchy particles.' *Langmuir*, 29 (15) (2013) 4688–96. URL http://www.ncbi.nlm.nih.gov/pubmed/23510525

4

CONTACT REPLICATION OF DNA MICROARRAYS FROM DNA MASTERS

Current DNA arrays are fabricated either by transporting the complete chain to the desired spot or assembling the chain base by base. Both methods offer inherent advantages and disadvantages. This Chapter presents a new method to fabricate DNA arrays by direct placement by dehybridization and enzymatic extension combining the advantages of both fabrication methods.

4.1 BACKGROUND

Several analytical tools have been used in genomic studies, yet DNA microarrays provide the best alternative to study and characterize gene expression, genotyping, single nucleotide polymorphisms, and mutations.[1] DNA arrays consist on ten to up to hundreds of thousands spots of DNA probes immobilized on a surface. The vast number of individual DNA spots on a microarray allows the parallel and simultaneous analysis of large number of genes or multiple regions of a genome, opening a broad path for high-throughput applications.

DNA microarray technology is based on a combination of research fields. Firstly, mechanics, microfabrication, and microfluidics are used to fabricate the substrates and place the capture probe on the desired position forming discreet bioactive areas. Secondly, chemistry, biochemistry, and enzymology are necessary to fix and understand the behaviour of the DNA, including the probe and target preparation. Thirdly, optics and bioinformatics are required to acquire and interpret the data.[2] The working principle of DNA arrays is based on the highly specific interaction between the grafted probe with a complementary strand. The specific attraction between both strands form a selective and unique recognition event. This event is referred to as hybridization. The first high-throughput array was developed in 1995 by Schena *et al.*[3]. In their work, 45 different probes were spotted on a glass slide and was later used to analyze the gene expression of a wild type and a mutated specimen overexpressing a single transcription factor of the small flowering plant *Arabidopsis thaliana*, paving the road for future genetic studies with denser DNA microarrays. Target strands are typically modified to include fluorescent dyes or anchoring sites for future labeling. After hybridization, the target-probe recognition can be detected, and at a certain extent, the hybridization efficiency, yet the length or sequence of the captured strand remains unknown.[2]

According to Dufva[4], microarray technology can be described as the improvement of dot blot technique, where the DNA is immobilized on a membrane and probed with radioactive targets. Three defining factors helped coin this conclusion. Firstly, the miniaturization of the spots, as this improves the sensitivity of the system by responding quickly to slight changes. This also reduces the amount of reagents. Secondly, the use of fluorescent instead of radioactively-labeled targets, allowing co-hybridization studies by mixing various strands with different fluorophores. Finally, the use of a rigid substrate instead of membranes which are complicated and far more delicate to handle. The characteristics surrounding the hybridization of target sequences to the immobilized probes form a powerful tool that has been exploited to develop at extraordinary paces new molecular assays.

Complex organisms are composed of trillions of cells, where most of those contain DNA, storing all the instructions for cellular function. As shown in Figure 4.1, DNA is composed of nucleotides, each formed by three components: a nitrogenous base, a deoxyribose sugar, and a phosphate group. The four nitrogenous bases are paired into two categories: the purines (Adenine and Guanine), with two fused rings, and pyrimidines (Cytosine and Thymine).[5]

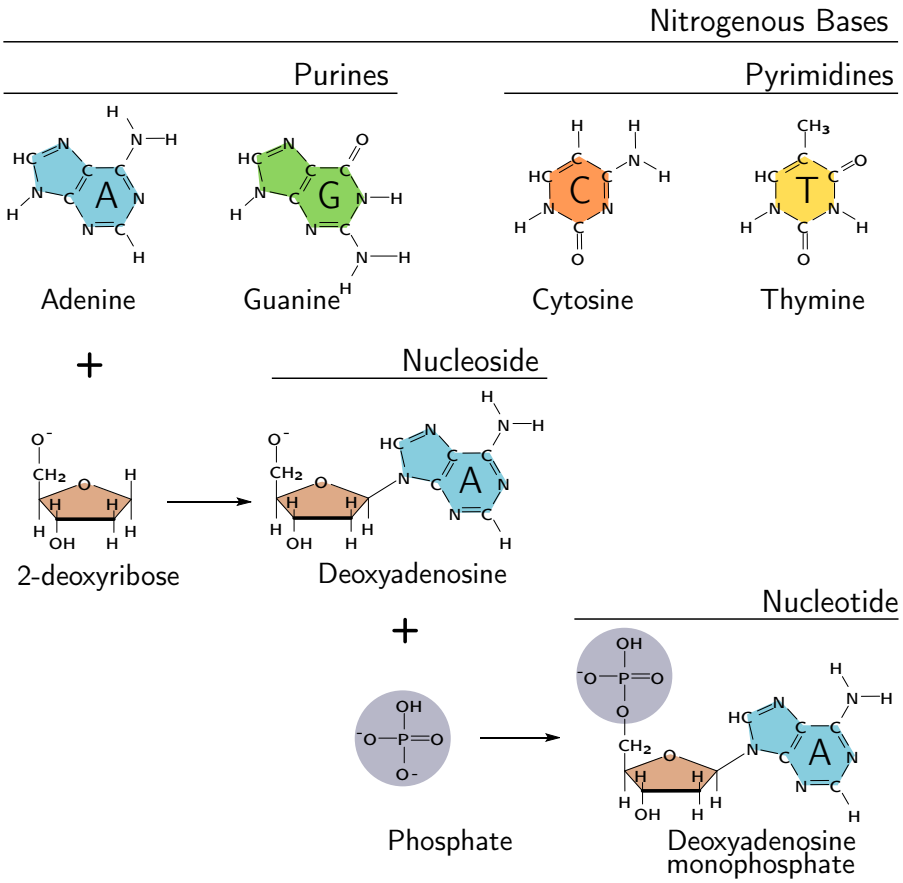

Figure 4.1: **From bases to nucleotides.** The chemical structure of a nucleotide is made up of three different components: a nitrogen-containing base, a pentose, and a phosphate group.

Several studies where centered in the understanding of the components and form of the DNA molecule during the first half of the last century. Chargaff[6] developed a chromatography method to separate and identify minute amounts of organic materials. With this, a mayor milestone was reached when he realized that the amount of nucleotides varied among different species, forming complex nucleotide combinations. Then, he noted that the DNA from any organism maintains approximated amounts of Adenine and Thymine (A = T), and the total Guanine is similar to that of Cytosine (G = C). He concluded

that the total amount of purines (A + G) is nearly equal to the amount of pyrimidines (C + T), resulting in the term "Chargaff's rule."

Although DNA was discovered several years before Chargaff, the description of the double-helix, polynecleotide structure of DNA was formulated by Watson and Crick[7]. Their conclusions were actually sustained on the Chargaff's rule and important X-ray chromatography work by Rosalind Franklin and Maurice Wilkins. Figure 4.2 shows the three-dimensional structure of DNA where the complementary bases fit perfectly, and are held together by hydrogen bonds, following the Chargaff's rule. Another interesting feature is that the DNA double helix is anti-parallel, meaning that a 5′ end ($-PO_4^-$) of a single strand is always paired with the 3′ end ($-OH$) of its complementary strand, and vice versa.[5]

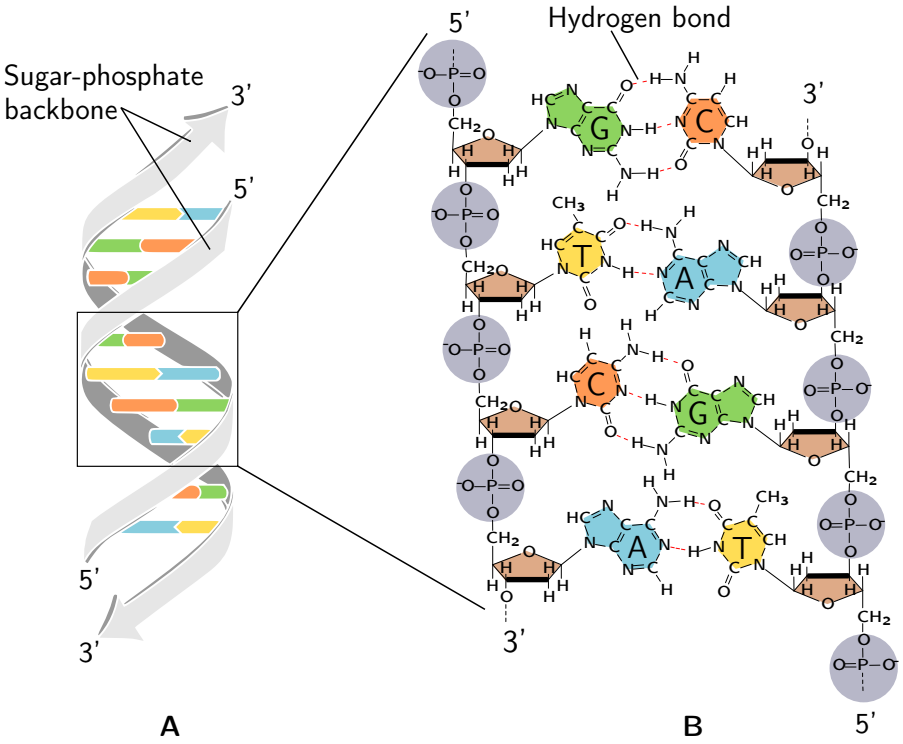

Figure 4.2: **Double-helical structure of DNA.** (A) The double helix coil of DNA formed by the intercalation of complementary strands. (B) Hydrogen bonds pair the complementary nitrogenous bases.

With all the combined work to develop the genetic structure, researchers continue to understand the genome. The complete genetic information is encoded by the order in which the four bases are arranged throughout the DNA. The genome of every organisms is divided into shorter regions called genes. The expression of genes, that is, obtaining a copied instruction from that gene, encodes the information to synthesize the proteins that are responsible for the structure and the function of every cell, and consequently, the entire organism.

4.2.0.1 *Polymerase chain reaction: replicating information*

In all organisms, the genetic information is translated by the replication of DNA, creating the foundation of biological inheritance. In this process, the DNA double helix unwinds and each strand serves as a template to synthesize two new strands. Immediately afterwards, a short RNA strand called primer, hybridizes at a specific location on the exposed Single-stranded DNA (ssDNA) chain. An enzyme, called DNA polymerase starts to assemble the new DNA by inserting complementary nucleotides on the 3' end of the hybridized primer.

The DNA replication can be performed outside a cell providing the DNA polymerase harvested from cells and natural or artificial template DNA and primers. Mullis *et al.*[8] developed the amplification method described in Figure 4.3, known as Polymerase chain reaction (PCR). This method uses thermal cycling to separate and multiply the DNA strands. A complete replication cycle involves three steps: (1) **Denaturation**, this step takes place at high temperatures (~94 °C) and its function is to separate a DNA molecule into its two complementary strands. (2) **Annealing**, here the primers bind to the complementary site of the previously separated DNA, this step occurs at ~56 °C. In the last step, (3) **Extension**, the DNA polymerase assembles the complementary strand with neighbouring free oligonucleotides at a temperature of ~65 – 72 °C. The result is two exact copies of the initial DNA strand. Repeating the cycle produce two copies for each initial strand, therefore, the accumulating products are cloned exponentially. Standardized protocols use 25 to 35 PCR cycles.

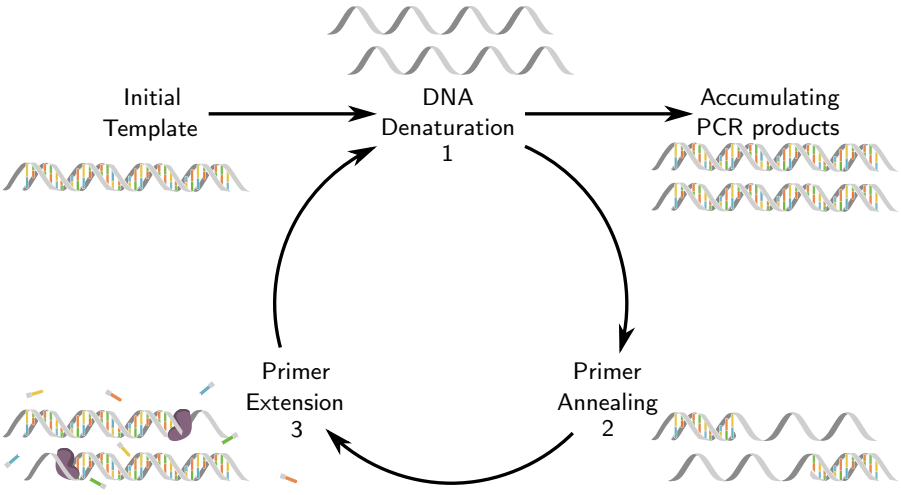

Figure 4.3: **Polymerase chain reaction (PCR): cloning DNA strands.** A complete replication cycle involves three steps: (1) **Denaturation**, (2) **Annealing**, and (3) **Extension**.

The work of Mullis *et al.*[8] was accomplished using the Klenow fragment of the DNA Polymerase I from *E. coli*. As expected, the DNA polymerase, as any enzyme, is highly sensitive to high temperatures.

In their work, new polymerase had to be added after the DNA was melted. Just after the isolation of the DNA polymerase from the thermophile *Thermus aquaticus* by Chien *et al.*[9] known as *Taq* polymerase, the standardized PCR was developed.[10] This improvement helps maintain the same volume of reaction, limiting any artifacts that may occur by diluting the total amount of reagents. Closed-circuit mechanisms were later developed to facilitate and accelerate the complete reaction.

4.2.1 *Immobilization of DNA*

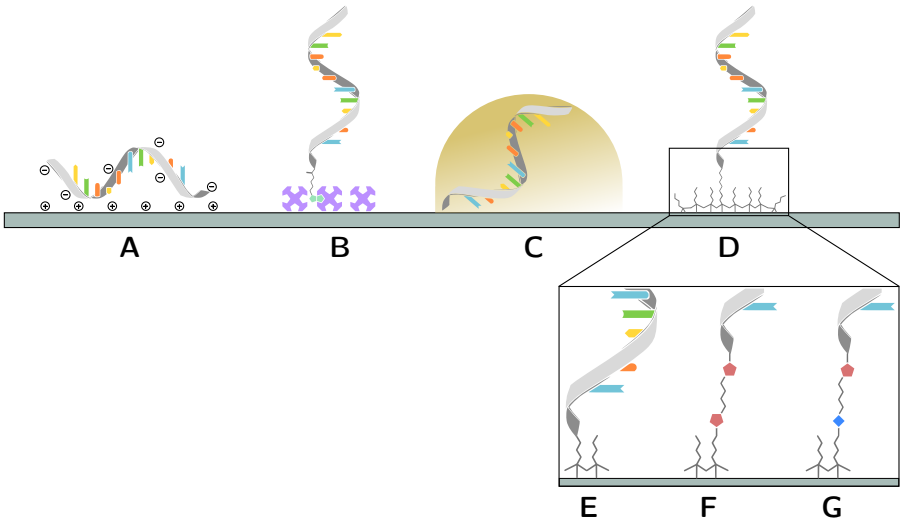

Figure 4.4: **Different DNA immobilization strategies.** (A) Electrostatic interactions. (B) Biotin-Avidin. (C) Entrapment during a polymerization process. (D) Different covalent binding-strategies: (E) Direct immobilization of modified strands with a zero-length cross-linker. Attachment using either homobifunctional, (F), or heterobifunctional, (G), linking molecules.

Intracellular machineries replicate, interpret, and store genetic information based on the rules of molecular recognition. Base pairing offers the capacity to recognize complementary sequences of every nucleic acid strand. This recognition can be resolved in parallel studies, and, at a certain extent, from complex mixtures.[11]

The best approach to create parallel studies is based on the immobilization of DNA strands on various substrates. The fixed strands work as a biosensor to detect target DNA. Fixing the strands also provided miniaturized test sites at localized areas, creating a physical coordinate system where the result of the hybridization can be easily read.[12]

Figure 4.4 presents the four basic strategies that have been followed to immobilize DNA onto different substrates. The first method takes

into account the negatively charged backbone of any DNA strand, due to the $-O^-$ present in each phosphate group, as seen in Figure 4.2B. When using substrates with a positively charged surface, e. g. Poly(ethyleneimine) (PEI), the electrostatic interactions between the negative backbone are strong enough to fix the strand.[13]

The second immobilization strategy is based on the strong, non-covalent bond between biotin and avidin conjugates, previously described in Section 2.4. A biotin-modified DNA strand is fixed to any avidin-derivatized substrate. Several publications used this immobilization to fix DNA onto glass and other polymers.[14–16]

Alternatively, DNA can be fixed on conductive surfaces and used as electrochemical biosensors. Physisorption has been a straightforward method to derivatize conductors with DNA. It is important to take into account that the change of the surface charge can either fix (if the net charge is positive) or repel (if the charge is negative) the strands. Thiol-modified DNA strands can be readily adsorbed on any gold surface forming a robust, *quasi*-covalent bond.[17, 18] Unfortunately, thiols are easily stripped from the substrate if a pulse of 1.4 V is applied on the substrate for as little as 30 s.[19]

To solve some of the immobilization issues, DNA strands have been entrapped on conductive polymers during their polymerization to create derivatized conductive surfaces.[20] The 3D matrix generated after the polymerization process, offers extended area where the strands can bind. Also, simple electrostatic interactions help fix the DNA strands. This kind of materials has been used not only for their conductive properties, but for their high stability and simple synthesis.

Covalent bonds offer the strongest link between two neighbouring molecules. It comes as no surprise that the most stable DNA immobilization protocols form a covalent bond. Modified probes can be readily immobilized to derivatized substrates. Figure 4.4E shows the immobilization of a modified probe using a zero-length cross-linker. These reactive species add an active moiety to the substrate without chain elongations. Direct probe immobilization to a silane SAM, is an example of this kind of strategy. A complete explanation of this chemistry is discussed in Section 2.2.3.1. A representation of DNA immobilization using homobifuctional cross-linkers is shown in Figure 4.4F. This linkers are double sided with the same reactive group. One end is fixed to the substrate, the other to the modified strand. Finally, heterobifunctional cross-linkers consist on a chain with two different reactive groups providing an oriented coupling. It is important to mention that homobifunctional cross-linkers may be less efficient than the zero-length or heterobifunctional cross-linkers as the reactivity is not directed. Activated groups on the surface of the substrate may be joined with a single cross-linker, limiting the free reactive sites. If the probes are modified in solution, the same can happen between two free strands.[1, 21]

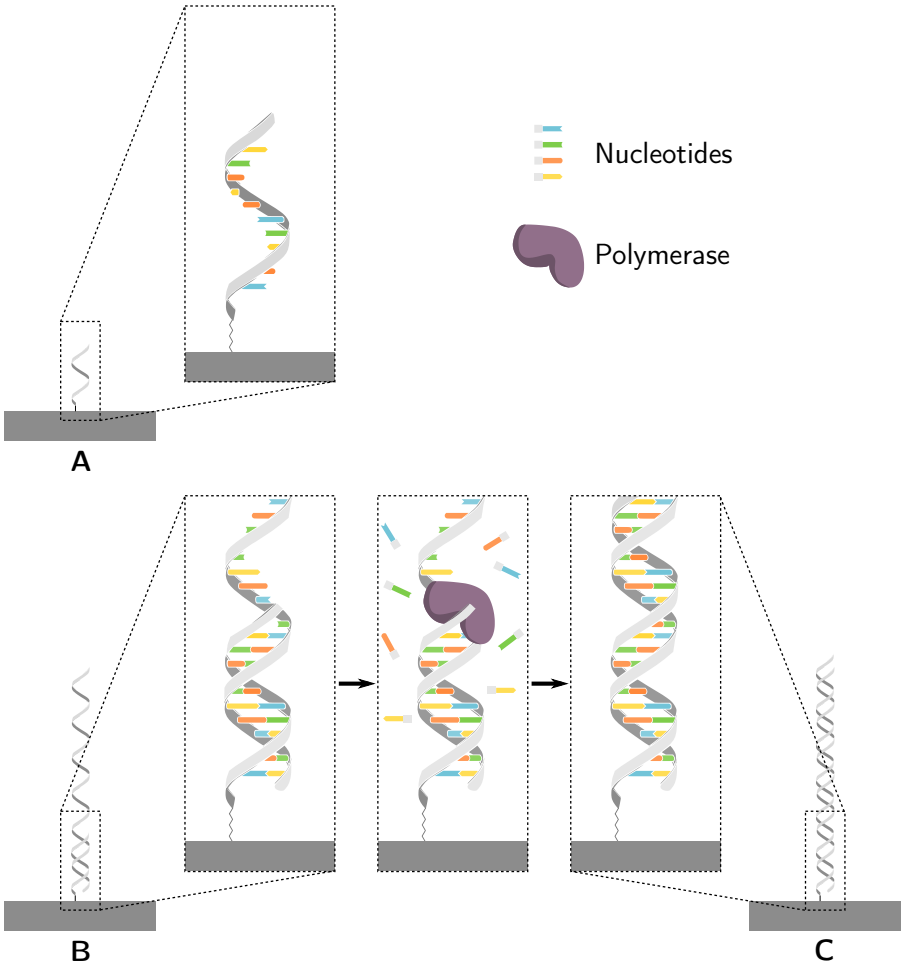

Figure 4.5: **Consecutive steps involved on Solid-Phase PCR.** (A) An initial forward primer is immobilized on a solid substrate. (B) The primer is complementary to the end of a template DNA strand. The polymerase starts assembling the complementary strand with free nucleotides present on the medium. (C) The extension finish when the polymerase reaches the end of the strand.

As described in Section 4.2.0.1, the PCR replicates the information condensed in a DNA strand. It can be concluded that PCR can be a tool to characterize, directly or indirectly, the sequence of such strand. Yet, the complex nature and variability of the genetic information in a chosen biological sample, hinders the isolation and identification of individual traits. This is even more challenging if the DNA sample is present in a solution, as the movement and unknown relative position complicates its separation and identification. Restricting the movement of these biomolecules provides a simple solution and facilitates their characterization by PCR.

An initial approach to identify the presence of genetic material, developed by fixing the product of a PCR was investigated by Kohsaka

and Carson[22]. In their work, they used to principles of PCR with a fixed primer and followed the steps shown in Figure 4.5. They called this replication technique Solid-phase polymerase chain reaction (SP-PCR).

The motivation of their work was the amplification and identification of the Human Immunodeficiency Virus type 1 (HIV-1) on infected lymphoblasts. The first step was the covalent immobilization of amino-modified forward primers to the surface of polycarbonate wells. Subsequently, the DNA template and reverse primers were added to each well and PCR was performed. The result of this step is the creation of a double stranded DNA chain bound to the surface of each well. Then, each well was subjected to a wash with a 0.1 N NaOH solution to dehybridize the DNA and was later exposed to a digoxigenin-labeled strand with the complementary sequence of a section of the newly synthesized strand. Finally, a peroxidase conjugated anti-digoxigenin antibody was grafted to the complementary target. Optical density was used to characterize the binding of the antibody. The antibody would give a positive result only if the initial strand was extended.

4.2.2 *Fabrication of DNA arrays*

Either hybridization events, or the extension of bound primers have been traditionally used to study the contents and availability of a specific genetic sequence in a sample. When the number of test sites are increased, that is, several discreet spots of immobilized strands, the sample analysis can produce more complex results. This allocation of various DNA spots on a solid substrate at selected coordinates, originated the DNA array technology. As mentioned before, Schena *et al.*[3] immobilized 45 probes to study the expression of a transcription factor. Modified complementary targets, labeled with fluorophores, were hybridized to the printed spots. The affinity between capture probe and target was analyzed with fluorescence microscopy. The fluorescence emission was directly proportional to the amount of hybridized target strand.

Each individual spot on a DNA array contains a predefined nucleotide sequence, and two strategies have been traditionally followed to fabricate this encoded spots. The first approach is to deposit on the predefined area of the substrate the complete DNA strand with the desired sequence, represented in Figure 4.6A. This strategy is referred to as *ex situ* fabrication. Artificial primers and PCR products can be transported to the substrate to form the spot.

Alternately, the *in situ* strategy builds the DNA strand from scratch by a nucleotide-by-nucleotide chemical assembly. This method uses de-protection steps to allow the reaction of chemical moieties. As presented in Figure 4.6B, a defined area of the substrate, derivatized

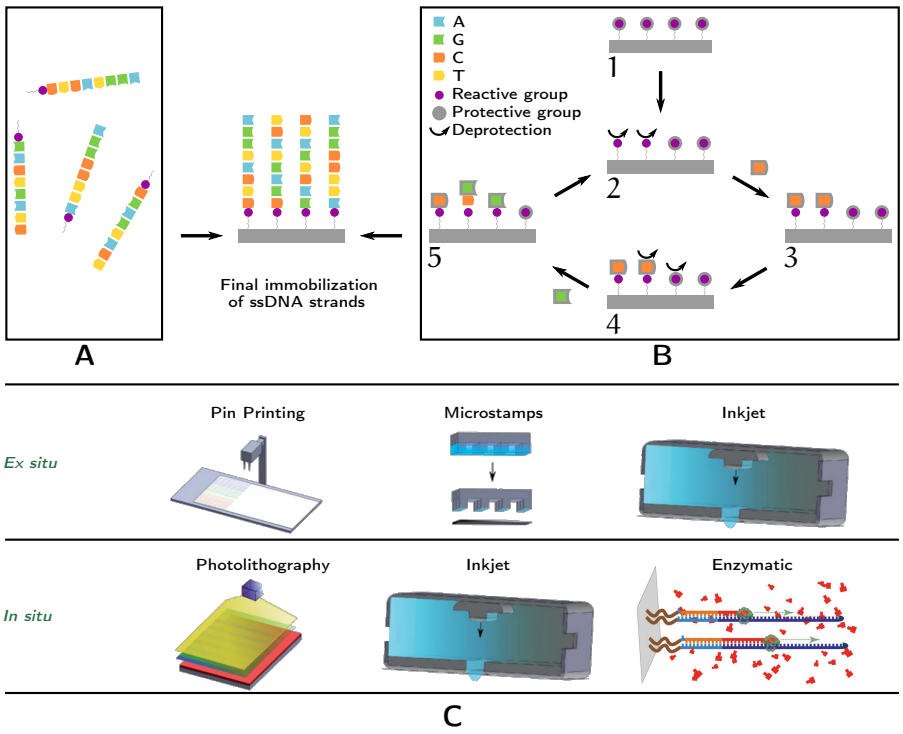

Figure 4.6: **Fabrication of DNA arrays.** Two main strategies are followed to fabricate DNA arrays. The bottom-up approach known as *in situ* fabrication while the top down is called *ex situ* fabrication. (A) The *ex situ* approach uses a physical mechanism to transports a complete DNA to the substrate for it to bind. (B) The *in situ* generation requires a substrate coated with a reactive group protected with a cleavable protective moiety, (1). In the initial cycle, the protective groups at a defined area are removed by irradiation or by a liquid reagent, (2). Then, the first nucleotide with the same protective group is added and binds to the reactive group, now without protective moieties, (3). A second de-protection cycle is produced, (4), leaving active areas for a second nucleotide, (5), to bind to the active areas. These cycles are repeated until the length of the complete DNA chain is obtained. (C) Several technological approaches have been developed to accomplish both types of fabrications. Adapted from [23] and [24].

with a protected reactive group, is exposed to a de-protection method to cleave the protective group. The now de-protected moiety is exposed to the first oligonucleotide, which is in turn protected with the same group as the substrate. The oligonucleotide binds to the exposed group increasing the DNA strand by an single step. After washing any unreacted oligonucleotide, a second de-protection protocol is followed on the desired zone, cleaving the exposed groups. The substrate is subsequently flooded with the next protected oligonucleotide, increasing the sequence of the exposed area or strand by one unit. The de-protection, flooding, and washing cycles are repeated until the desired length is achieved.

Figure 4.6C presents a collection of fabrication methods to create DNA arrays following the *ex situ* and *in situ* strategies.

Using the *ex situ* strategy, robotic printers with specialized hollow pins have been used to collect and transport complete strands from a container to the desired location on a substrate. Capillary forces play a major role when the tip of the pin is initially submerged on the solution, carrying with it the free strands. Then, the robotic printer positions and moves the pin towards the substrate. The DNA is finally transferred when the pin contacts the surface. This technology allows to create DNA spots with a diameter raging from 50 to 200 µm.[4]

Pin printing is the most widely used fabrication method to create DNA arrays for basic research and diagnostic. Huber *et al.*[25]worked on the detection of single nucleotide polymorphisms using SP-PCR after spotting the forward primer on polyethyleneimine-coated glass slides. Fluorescence microscopy was used to track the differences between the wild-type and the mutated codons of the human *p*53 gene. Similarly, Mitterer *et al.* [26] used amine-modified primers from twenty three different bacterial strains which were spotted on derivatized glass slides and were later differentiated by the solid-phase extension of their individual DNA templates. Again, fluorescent microscopy was used to characterize the amount of extended DNA per spot. Khodakov *et al.*[27] extended primers grafted on polyacrylamide spots to simultaneous identify and quantify HIV-1 and hepatitis B and C viruses (HBV and HCV) in plasma samples. Sun *et al.*[28] developed a microarray-based SP-PCR approach to detect the subtypes H5, and H7 of the influenza virus type A, by spotting and grafting the primers by UV cross-linking over unmodified glass. The same group then used this technology integrating in on a portable Lab-on-a-chip device.[29] Finally, Hoffmann *et al.*[30] developed an universal protocol with the linker 1,4-phenylenediisothiocyanate (PDITC) to graft primers to amino-functionalized PDMS, polypropylene (PP), cyclic olefin polymer (COP), or cyclic olefin copolymer (COC), as well as glass. They later investigated the performance of the spotted primers with SP-PCR

Another *ex situ* method is the direct placement of adsorbed DNA strands from a stamp, as thoroughly explained in Section 2.5.2. Finally, inkjet printers eject tiny drops of DNA carrying solution from a compartment. The printing head is first placed on the defined position and a subsequent stream of drops is ejected towards the substrate. The accumulation of liquid on the substrate defines the size of the printed spot. Spots from 50 to 100 µm are regularly fabricated with this method.[31, 32] The same principle was followed by Goldmann and Gonzalez[33] when they transferred DNA with a standard Hewlett Packard DJ 550C desktop printer over nitrocellulose or nylon membranes. Later, to test the transfer, the emission of radioactive-labeled complementary strands was read after the hybridization with

the printed probes. It is worth noting, that in any *ex situ* protocol, the modified DNA strands have to react with the derivatized substrate after printing, to guarantee a robust bond.

Contrarily to *ex situ*, *in situ* fabrication strategies require to deprotect a selected zone from the substrate. Photolithography was borrowed from the microelectronics industry and has been used to synthesize the strands by allowing UV light to cross on the designated areas of a photomask, cleaving the exposed protective moieties. Fodor *et al.*[34] developed Light-directed chemical synthesis to create arrays of 1024 peptides by assembling the sequential chains by deprotecting the individual building blocks. The same technique was later applied by Pease *et al.*[35] to create the first light-generated oligonucleotide arrays. It is important to point out that this technique requires four different chromium photomask for every added base, and each array takes one hour per nucleotide, thus a 25 bp probe would require 100 masks and over a day to synthesize.

Nuwaysir *et al.*[36] used a digital light processor mounted on a maskless photolithographic instrument to fabricate DNA microarrays, synthesized *in situ*, containing up to 195 000 features. A digital light processor is formed by a collection of micrometric mirrors positioned in a matrix over a chip. These mirrors can be repositioned to reflect light to a desired position. Using traditional photolabile chemistry, the micromirrors reflected UV light to deprotect and grow the DNA on site. Strands up to 90 bp were synthesized. This technology reduces dramatically the costs of fabricating super dense DNA arrays as it does not requires the implementation of expensive chromium photomasks. Maskless photolithography is used to obtain features from 2.25 to 50 µm.[37]

Whether applying traditional or maskless photolithography, after each de-protection step, the entire substrate has to be flooded with a solution bearing the next oligonucleotide. Alternatively, the subsequent oligonucleotide can be delivered to the position using an inkjet printer instead of flooding the entire chip with the solution.[38] Blanchard *et al.*[39] developed an system with four inkjet pumps to deliver small droplets of each of the nucleotides. The sequential synthesis started by the activation of the substrate and delivery of the first nucleotide to every spot. Subsequently, the entire substrate was washed to remove all the unreacted nucleotides and rinsed with an acid wash to deprotect the end of the probe. Immediately afterwards, all the oligo spots received the next nucleotide. The washing-deprotecting-spotting cycles continued until the final length was reached. A substrate with 10 bp probes required 10 cycles. Automatized systems have been developed to increase the throughput being able to synthesize 9 800-feature oligonucleotide arrays with strands up to 40 bp.[40]

A final *in situ* approach is to use the polymerase enzyme to assemble the complementary RNA strand from a DNA strand. In this

protocol, a ssDNA template is synthesized using photolithography on a activated substrate, where RNA is subsequently assembled with the complementary bases. The DNA is later digested with DNAase I, leaving single-stranded RNAs.[24]

4.2.2.1 *Alternative fabrication methods*

The constant need to improve the fabrication of DNA arrays has expanded on many roads, and different approaches have been followed to construct these analytical tools. The description of the following fabrication methods is more diverse to fit into the previously mentioned protocols. Special interest is shown in those methods which were followed to develop DNA by contact replication.

The first approach to build DNA arrays by using PCR was developed by Mitra and Church.[41] In their work, PCR was performed on a thin polyacrylamide film loaded with template DNA and was later thermally amplified. The accumulated products remained near the templates forming PCR colonies or 'polonies'. The 236 bp cloned template formed randomly distributed polonies throughout the matrix. When using Acrydite™-modified primers, the products were covalently bound to the polyacrylamide matrix. If two polyacrylamide membranes are placed against each other, with the template DNA sandwiched between them, the accumulated products were transferred to both membranes, creating a mirror copy of each other.

Kim *et al.*[42] spotted and UV-cross-linked three initial probes from 268 to 467 bp onto a nylon membrane. After washing, the membrane was later submerged to a solution with the complementary targets to the immobilized probes. After hybridization, a second membrane was placed in contact with the initial membrane. The setup was heated and the hybridized complex was melted, hence, the probes were transported to the second membrane. The transfer was characterized with fluorescence microscopy after the hybridization of complementary, fluorescent-labeled strands.

A similar approach was followed to cross-link thiol-modified oligos and epoxy-functionalized substrates in a single-step just requiring the light to be shined through a photomask over functionalized SiOx[43], or SU-8 resin[44] both first covered with the modified strand, creating a thioether bond.

Combining an inkjet printer with uncured PDMS, Heyries *et al.*[45] fabricated an array of 20 bp strands in a single step. First, they printed vinyl-modified oligos on a Teflon substrate with an inkjet arrayer. Immediately afterwards, liquid PDMS was poured covering the spots. The vinyl groups facing the PDMS formed a bond with the polymer matrix, binding the DNA. Chemiluminiscent labeling of biotinylated complementary strands helped characterize the functionality of the attached probes.

Several contact replication methods have been described to fabricate DNA arrays the transport of either hybridized or extended strands from a DNA master.[14–16, 46–49] An initial method is represented in Figure 4.7. First, ssDNAs are printed and strongly bound to a flat surface. This derivatized substrate is referred to as 'master'. Then, the master is exposed to a solution with the complementary strands of the bound probes and left to hybridize. These last strands are labeled with a biotin on their 5′-end. Subsequently, a SAV-modified flat stamp is placed in contact with the hybridized probes. After allowing the biotin to bind to the SAV, the flat stamp, now referred to as 'replica', is mechanically separated from the master.[14, 16]

Instead of transferring hybridized strands, Kim and Crooks[15] used a short biotinylated target and a RNA sequence that were hybridized on 28 bp amino-modified DNA probes previously spotted on epoxy-modified glass slides using a micropipette or microarrayer. The small biotinylated target hybridized to the exposed end of the grafter probe, while the RNA hybridized to the rest of the chain. Then, the short probe and the RNA were linked to form a complete complementary strand. Finally, a SAV-modified PDMS stamps was brought into conformal contact and later mechanically separated transferring the replica.

Alternately, the contact replication can be achieved by the transferring a polymerase extension product.[50, 51] Briefly, a biotinylated primer was hybridized onto spotted amino-modified DNA probes over epoxy-modified glass slides. The set up was exposed to a polymerase reaction mixture with free oligonucleotides to extend the primer and obtain various strands of 23 bp. The strands were separated using a SAV modified PDMS slab, as discussed previously. The force required to break the biotin-SAV bond is ~100 pN [52], and the force to separate a DNA strand is ~2 pN bp^{-1}[53, 54]. Therefore, this fabrication technique is limited to strands < 50 bp.

A similar approach was followed by Yu *et al.*[46] to fabricate DNA arrays on aldehyde-functionalized PMMA using amine-modified complementary strands initially hybridized on a printed DNA array. Other similar protocols were defined to transfer thiol-modified strands onto various gold substrates. The transfer relied on the strong bond between the thiol moiety and the surface.[47–49]

Finally, Yu and Stellacci[55] used Acrydite™-modified primers hybridized on previously patterned DNA and fabricated the complementary array by pouring uncured PDMS onto the hybridized strands. The strands were covalently bound to the PDMS during polymerization. After curing the set-up, the stamp was peeled with the newly fabricated array.

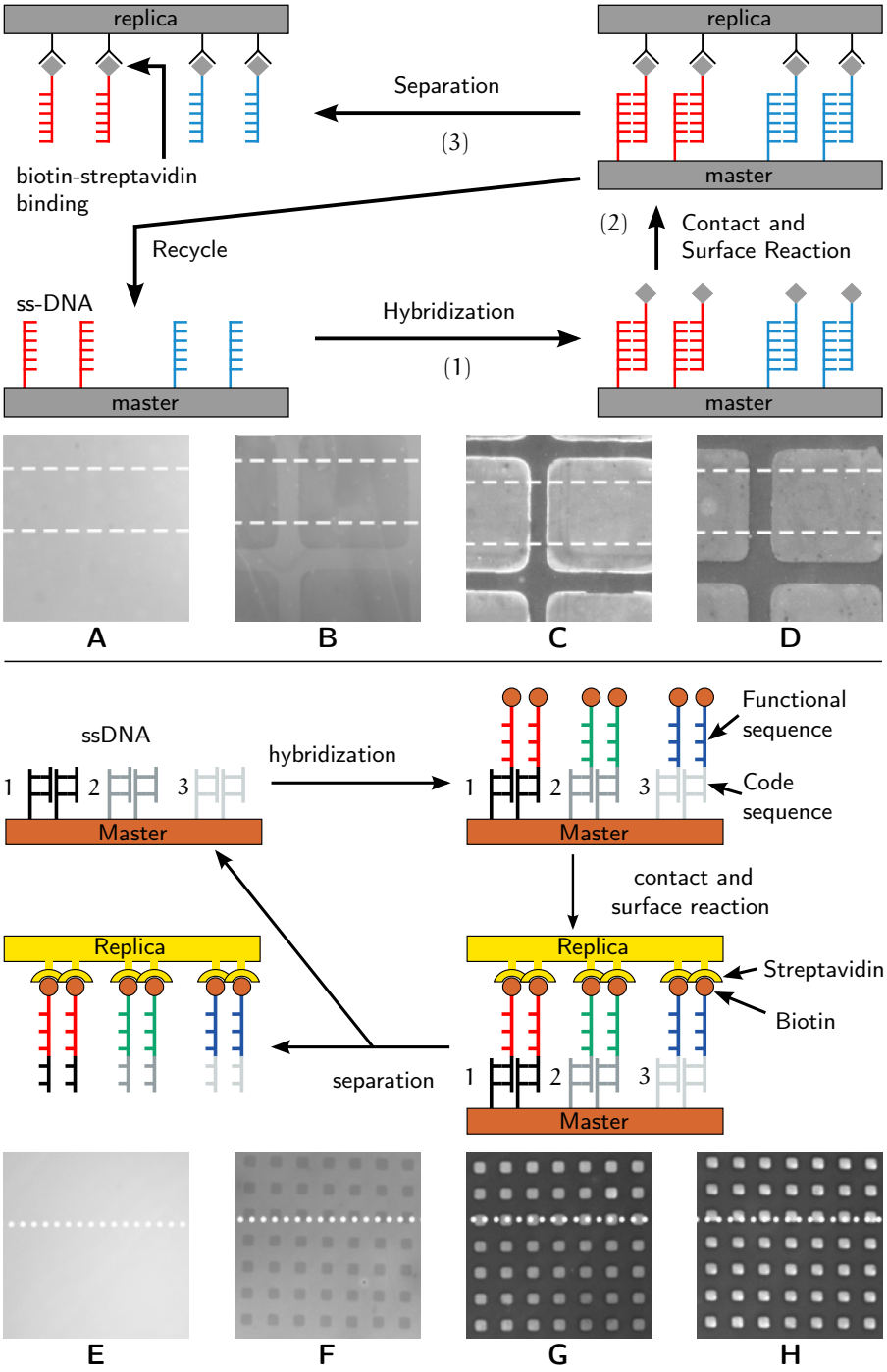

Figure 4.7: **Contact replication of DNA strands.** Two initial replication methods are described. The method on top requires a DNA strand complementary to the whole sequence to transfer[14], while the bottom method is produced with an immobilized fraction complementary to the sequence to transfer.[16] For each transferring method, (A) and (E) show fluorescent image of hybridized DNA on a previous DNA-coated master. (B) and (F) present the residual fluorescence after contact and surface reaction with a PDMS stamp. First, (C) and (G), and third, (D) and (H), replicas from the master.

Affinity Contact printing (αCP) was used by Chen and Yang[13] to fabricate a DNA array on a positively charged substrate, as represented on Figure 4.8. Initially, DNA probes were covalently bound to a functionalized stamp. Then, the stamp was exposed to the complementary strand and was left to hybridize. The stamp was later brought in contact to a PEI-coated glass slide. The positive charges on the surface of the stamp were strong enough to fix the complementary target strand on the contact region.

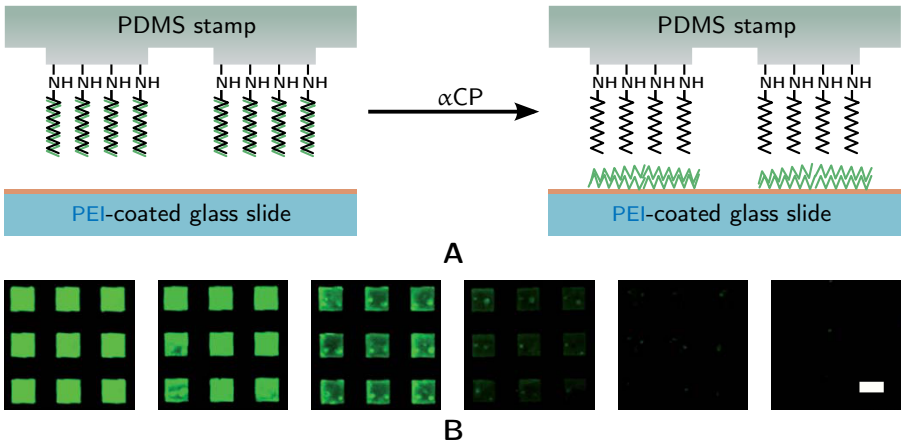

Figure 4.8: **αCP and hybridization of printed DNA strands.** (A) Transfer of DNA targets from DNA probes immobilized on a PDMS stamp. (B) Fluorescence image of printed DNA and subsequently hybridized with 40 $\mu g\ mL^{-1}$, 4 $\mu g\ mL^{-1}$, 400 $ng\ mL^{-1}$, 40 $ng\ mL^{-1}$, 4 $ng\ mL^{-1}$, or 400 $pg\ mL^{-1}$ DNA targets.[13] Scale bar = 200 μm.

4.3 EXPERIMENTAL PROCEDURES FOR THE REPLICATION OF DNA ARRAYS

All the contact printing techniques transfer either a hybridized probe or a PCR extension product, thus, obtaining an array of just complementary strands. To clone the entire information condensed on the original array, it is required a second hybridization or extension. Unfortunately, no publication so far has been found to describe this approach. For such reasons, the purpose of this Chapter is to situate and expand the limits of current DNA array fabrication strategies, and establishes a new proposal to clone master arrays using both, hybridization and extension of DNA.

4.3.1 *Immobilization of DNA strands onto various substrates*

The foundational step to create a DNA master array requires the selective immobilization of the probes. A first approach was based on the strong thiol-gold bond using modified strands. To localize the strands on various spots, first, a PDMS stamp with circular holes with a diameter of 10 μm was inked with a 2 mM Triethylene glycol mono-11-mercaptoundecyl ether (PEG_3-thiol) ethanolic solution, loaded into the μCP tool, and was later used to pattern a clean, gold substrate. Immediately afterwards, a drop of a 0.5:4.5 μM 5SH-3:6-Mercapto-1-hexanol (MCH) solution in Milli-Q was placed on the previously patterned substrate. The short MCH thiol competes with the modified oligos to bind to the exposed gold. This competition forces the ssDNA to remain upwards away from the substrate, making it more accessible for the complementary target strands to hybridize. After 1 h, the substrate was washed with Milli-Q water.

A second approach using direct placement via μCP was followed to create discreet DNA spots. This approach was adapted from the protocol previously discussed in Section 2.5.2. Briefly, a PDMS stamp with protruding features was inked with a 5 μM DNA probe solution in a 30 mM sodium phosphate dibasic (Na_2HPO_4) buffer for 2 min. Afterwards, the inked stamp was loaded into the μCP tool and brought into contact with the substrate. This approach was used to fabricate DNA arrays on gold and epoxy-functionalized glass and PDMS.

To test the efficiency and range of other microarray fabrication techniques, the Nano-plotter™ inkjet from GeSiM mbH (Großerkmannsdorf, Germany) and the SpotBot© 2 contact microarrayer from Arrayit Corp. (Sunnyvale, CA, USA) were used to create DNA arrays on both, epoxy-functionalized glass and PDMS. When using either the inkjet or contact arrayer the concentration of the probe was standardized to 5 μM suspended on the phosphate buffer. To prevent the contamination between probes, both, the inkjet and contact arrayer pins, were

thoroughly washed by sonication using the SpotBot® Wash Buffer (1×) from Arrayit Corp.

4.3.2 *Contact replication of hybridized DNA*

The contact replication method to clone master DNA microarrays is represented in Figure 4.9, and follows some of the fabrication steps from several publications.[14–16, 46–49] The important feature of this replication method is the complete transferring of genetic information between steps, obtaining a true and exact copy.

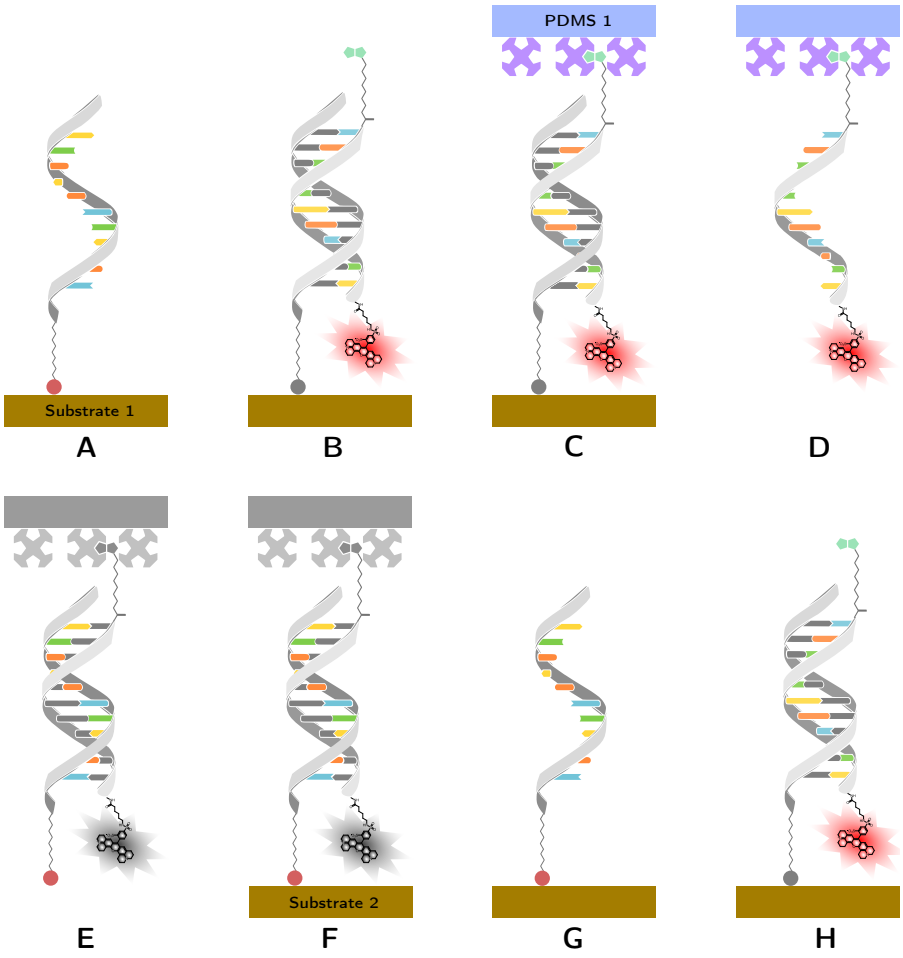

Figure 4.9: **Contact replication of hybridized DNA strands.** (A) First, the master array is immobilized on a substrate. (B) Then, the complementary strand is hybridized onto the printed probe. (C) A modified flat stamp is pressed against the DNA SAM, and is mechanically peeled afterwards, (D). (E) The probe on the stamp is re-hybridized and subsequently pressed against a new substrate, (F). (G) The flat stamp is removed, leaving the dehybridized strand bound to the substrate. (H) A final hybridization with the fluorescent probe is used to characterize the transfer of the initial probe.

Three key elements were defined to develop the replication process:

1. Fabrication of the DNA master array: The master array required the collection of individual DNA spots strongly bound to a substrate. The bond was required to be stable enough to withstand the mechanical separation of the hybridized strand, yet remain unaltered with the immobilization chemistry.

2. Derivatization of replicating stamp: A flexible material was required to fabricate the transporting element between master and replica. Conformal contact was also an imperative feature needed to accomplish this step. As with the substrate, this material required a strong mechanical stability and minimal chemical interference with the probes.

3. Direct transfer of hybridized strands: The final step involves the intimate contact between the replicating stamp and the new substrate. As it can be deduced, this material requires to form a strong bond between the strands, yet eliminate any interference during the printing mechanism.

4.3.2.1 *Fabrication of the DNA master array*

The replication steps start with the immobilization of the 5SH-3 capture probes on gold using either the positive or negative μCP approaches. All the gold substrates were initially rinsed with acetone from Panreac (Barcelona, Spain), blown dry with N_2 and carefully scrubbed with a concentrated Tween 20 solution in Milli-Q water. Subsequently, the substrates were rinsed with Milli-Q water and blown dry with N_2. Afterwards, the 5BT-3TR complementary strand was added to the hybridization buffer consisting of an aqueous solution of 10 mM TRIS, 1 mM EDTA, and 1 M sodium chloride (NaCl) to a final concentration of 2.5 μM and placed on top of the patterned substrate. The 2 h hybridization time was constant throughout the work. To prevent any interference with salt crystals from the dried buffer, the substrate was briefly rinsed with Milli-Q water and blown dry.

4.3.2.2 *Derivatization of replicating stamp*

The most suitable material to fabricate the intermediate transferring element was found to be PDMS. The elastomeric material creates conformal contact when pressed against a substrate. Standardized chemical protocols have been previously discussed to endow specific properties to the surface of this material.

First, a flat PDMS stamp was fabricated by pouring a 1:10 (w/w) mixture of uncured prepolymer over a clean SiOx wafer. After the PDMS was thermally cured, its surface was plasma-activated for 30 s and subsequently immersed in a 2% v/v GOPDMS ethanolic solution

during 1 h. After the reaction time, the stamp was rinsed with absolute ethanol, dried with a stream of N_2, and cured for 30 min at 120 °C. As discussed in Section 2.4.3.1, this functionalization step adds free epoxy- moieties on the surface of the stamp. Afterwards, the stamps was again rinsed with absolute ethanol, dried with N_2, and submerged in a 1 mM ethanolic solution of EZ-Link Amine-PEG3-Biotin from Thermo Fisher Scientific, Inc. (Rockford, IL, USA) and was left to react overnight. The amine group in the EZ-Link forms a secondary amine bond with the epoxy ring directing a free biotin outwards the stamp. Finally, after rinsing the stamp with absolute ethanol and dried, a drop of 1 µg mL^{-1} NAV solution from Invitrogen (Eugene, OR, USA) in PBS was placed on top of the stamp. After reacting for 1 h, the NAV-modified stamp was rinsed with Milli-Q water.

4.3.2.3 *Direct transfer of hybridized strands*

The hybridized target provided a free biotin group protruding from each strand. When the NAV-modified stamp was brought into conformal contact with the biotin groups, a strong binding event fixed the strand to the stamp. As previously discussed, the force needed to separate the 21 bp from the double strand was lower to that needed to break the NAV-biotin bond. A controlled, mechanical separation provided the adequate method to separate the strands. The new array was at this point formed by single complementary strands. To expand the already published results, the complementary array was hybridized with the original 5SH-3 strand following the same hybridization protocol, and rinsed with Milli-Q water afterwards. The new double-stranded DNA array was brought into conformal contact with a new, clean gold substrate. The thiol group forms an spontaneous bond with the surface of the substrate and is strong enough to withstand the mechanical separation of the PDMS stamp. One last hybridization event with the complementary 5BT-3TR strand was required to characterize the correct transferring using fluorescence microscopy.

4.3.2.4 *Calculation of the hybridization efficiency*

As the replication of DNA master arrays requires the true and exact copy of the immobilized strands, an important parameter to take into account is the efficiency in which the complementary targets hybridize to the immobilized strands. Three independent experiments were established to characterize firstly, the hybridization efficiency, secondly, the repeatability of hybridizing events, and lastly, the effect of non-complementary strands when interacting with the immobilized probe.

Surface plasmon resonance (SPR) was used to analyze the amount of bound DNA probes and their interaction with target strands. All the experiments were conducted using a SPR RT2005 instrument from Resonant-Technologies GmbH (Framersheim, Germany). Every the SPRchip™ gold substrates from GWC Technologies (Madison, WI, USA) were throughly washed as previously discussed, index-matched to the prism, fitted into the custom made flow cell, described in Section A.1.6, and connected to peristaltic pump from Ismatec - IDEX Health & Science GmbH (Wertheim, Germany).

An initial experiment was performed to characterize the amount of hybridized molecules. A continuous flow of hybridization buffer was first injected to the flow cell until the SPR signal was stable. Immediately afterwards, a 0.5:4.5 µM 5SH-3:MCH solution in the same hybridization buffer was injected and incubated under continuous flow during 1 h. After injecting the same buffer to remove any unbound molecules, the complementary strand, 5BT-3TR, suspended in the same buffer at a final concentration of 1 µM, was recirculated and incubated for 1 h. After rinsing with the buffer, a 1% *v*/*w* NAV solution was injected during 30 min and rinsed afterwards.

The second experiment followed a similar approach, yet in this case, after the incubation of the chip with the 5SH-3:MCH mixture, a 10 mM NaOH solution was injected for 180 s and rinsed with the hybridization buffer before the 5BT-3TR solution was recirculated for 1 h. The NaOH intermediate step increases the pH, thus, increasing the number of negatively-charged hydroxide ions which break the hydrogen bonds between the strands. Four independent denaturation, hybridization, and rinsing cycles were produced to characterize the efficiency of multiple hybridization events.

The last experiment was performed to characterize the amount of non-complementary target probe immobilized onto the bound strand. The protocol followed the previous experiments with the difference of adding a solution of the 5OG-3 strand instead of the complementary 5BT-3TR strand. The initial 5SH-3:MCH solution was recirculated for 1 h, followed by 180 s of the NaOH solution, then the hybridization buffer, and finally exposed to the non-complementary strand during 30 min. After rinsing with the buffer, the complementary strand was injected and left to hybridize during 1 h. To regenerate the surface of the chip, a final NaOH was performed. Regenerating the surface provides an insight of the amount of material that was bound to the surface. In this case, the amount should match that of the immobilized initial DNA SAM before the hybridization.

On every experiment, the time-dependent reflectivity variations were acquired at a fixed angle, and all the mass-deposition measurements were performed after rinsing the substrate to remove unbound molecules. This also guarantees the same diffraction index when performing the experiment.

4.3.3 *In situ amplification and contact replication of a DNA arrays*

The basis to transfer the complete genetic information encoded on DNA by contact replication has been limited to short hybridized or extended strands. The *in situ* fabrication allows the transferring of longer chains.

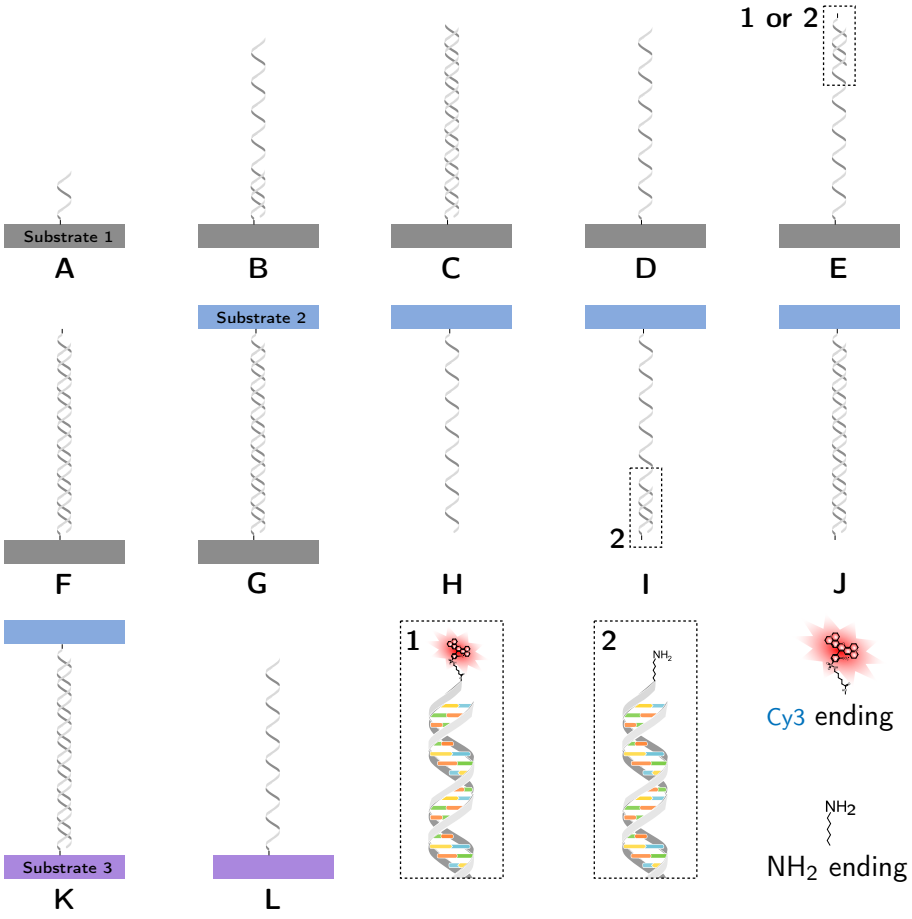

Figure 4.10: **Steps involved on the contact replication of DNA arrays.** (A) The forward primer is immobilized on an epoxy-functionalized PDMS substrate. (B) Following the steps on the SP-PCR, a ssDNA template hybridizes to the anchored primer, (B), followed by the extension to create double stranded DNA, (C). The DNA strand is melted, (D), and a reverse primer (1 or 2) hybridizes to the end of the strand, (E), and the DNA is extended for a second time, (F). The amine-modified reverse primer reacts to a second epoxy-functionalized PDMS substrate when placed in contact, (G). The PDMS-DNA-PDMS sandwich is heated to melt the complementary strands, (H). After separating the PDMS substrates, a second amine-modified forward primer is hybridized to the free strand, (I). The DNA is extended for a third time, (J), and a third epoxy-modified PDMS substrate is placed in contact with the amine-modified terminated DNA strands, (K). A final melting step is used to separate the extended strands, (L).

The complete protocol to replicate long DNA strands synthesized *in situ* is presented Figure 4.10. A small PDMS slab was plasma activated during 30 s and submerged into a 2% v/v GOPDMS ethanolic solution for 30 min. After rinsing with absolute ethanol, the slab was cured at 75 °C for 1 h, rinsed again with ethanol and blown dry with N_2. Covalent silane modifications were favored instead of biotin-NAV interactions due to the denaturation and thus inactivation of avidin compounds when exposed to high temperatures.[56]

4.3.3.1 *Fabrication of the DNA master array*

µContact, inkjet, or pin printing were used to immobilize the amine-modified strands on the epoxy-functionalized stamp. The final strand concentration was standardized at 5 µM in a 30 mM sodium phosphate dibasic (Na_2HPO_4) buffer. To prevent evaporation during the pin printing protocol, either 10% glycerol or 10% DMSO was added to the spotting solution. To initially characterize the pin printer, a 40 µg mL^{-1} BSA-AF555 solution in the phosphate buffer was patterned over epoxy-modified glass slides and PDMS.

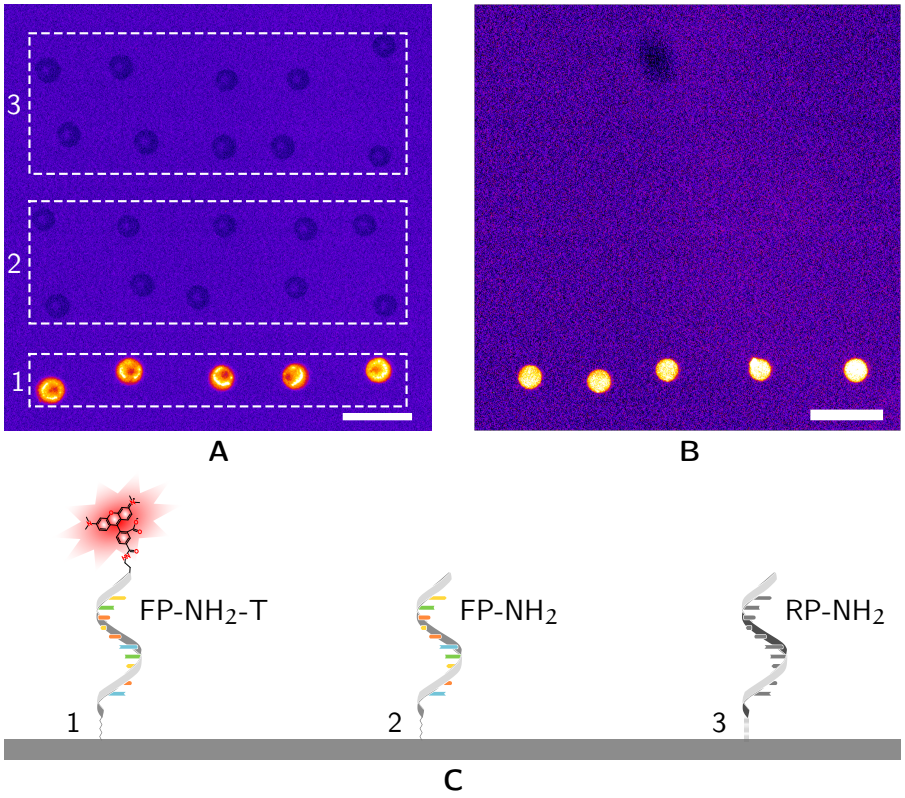

Figure 4.11: **Immobilization of primers.** Fluorescent microscopic images showing the position of recently printed, (A), and washed, (B), substrates with the DNA strands represented on (C): FP-NH_2-T, FP-NH_2, and RP-NH_2, over epoxy-functionalized PDMS. Scale bars = 100 µm

The final spot distribution is summarized in Figure 4.11 where three DNA strands were immobilized. The row of printed FP-NH_2-T spots served as an array position indicator. It also functioned to characterize the loss of grafted probes due to thermal cycling. The second strand, FP-NH_2, allowed the extension of DNA in two printed rows, while the third non-complementary strand, RP-NH_2, served as a control to guarantee the directed extension of DNA in the last two printed rows.

After printing, the substrates were left to reach for 1 hr and subsequently washed and blocked by submerging during 1 h into either a 2% w/v BSA solution in PBS, Super G Blocking Buffer from Grace Bio-Labs, Inc. (Bend, OR, USA), or a 2% v/v solution of Ethylamine from Sigma-Aldrich (St. Louis, MO, USA) in Milli-Q water. The substrates were ready after rinsing with Milli-Q water and blowing dry with N_2. To initially characterize the correct immobilization and blocking protocols, the printed substrate was exposed to the complementary 5OG-3 strand suspended in the hybridization buffer which binds to the FP-NH_2 strand. Fluorescence microscopy was used to characterize the hybridization.

The DNA extension mechanism is shown in Figure 4.10B-F and was used in both, regular and solid-phase PCRs. The patterned PDMS slab was inserted into a thin-walled PCR tube placed on ice and 25 µL of the PCR mixture summarized in Table 4.1 were added.

Table 4.1: PCR protocol standardized throughout the chapter.

COMPONENT	QUANTITY
PCR Master Mix (2×)	12.5 µL
Forward Primer	0.5 µM in regular PCR 0.125 µM in SP-PCR[30]
Reverse Primer	0.5 µM
Template DNA	10 ng
Nuclease-free water	up to 25 µL

Both, the PCR Master Mix (2×) and Nuclease-free water were purchased from Thermo Fisher Scientific, Inc. (Rockford, IL, USA). The followed PCR thermal cycling conditions are outlined in Table 4.2. All the experiments were carried in a PTC-200 Thermal Cycler from MJ Research, Inc. (Waltham, MA, USA).

After the thermal cycles, the PDMS slabs were extensively washed with three different washing buffers of decreased stringency. The initial solution was formulated with a 5× Saline-sodium citrate (SSC) solution with 0.1% SDS. The next washing solution consisted of a 2× SSC, and the last wash was done with a 0.1× SSC solution. Each washing step required the sample to be shaken for 5 min in the solution. Finally, each sample was rinsed with Milli-Q water. These

Table 4.2: PCR thermal cycling conditions.

STEP	TEMPERATURE (°C)	TIME (min)	CYCLES
Taq Activation	95	5:00	1
Denaturation	94	0:20	35
Annealing	56	0:45	
Extension	72	1:00	
Final Extension	72	3:00	1

steps guarantee just long, perfectly-matched DNA strands bound to the PDMS slab. The RP-Cy3 reverse primer was used to characterize the anchored synthesis using fluorescence microscopy. Unfortunately, this reverse primer could not be replicated to the second substrate as depicted in Figure 4.10G. To successfully replicate the strand, one must endow the DNA with active areas. To accomplish this, the RP-NH_2 reverse primer was used.

The free amine groups present on the extended strands were targeted with a second, epoxy-functionalized PDMS slab. When in placed together, the conformal contact assured a close encounter between the epoxy moieties and the amines. The contact was produced at controlled humidity ranging from $33 - 38\%$ by placing the sample and injecting argon into a portable Atmosbag glove bag from Sigma-Aldrich (St. Louis, MO, USA). According to Yu and Stellacci[55], high humidity allows the condensation of water around the immobilized strands, limiting the exposure of the reactive moieties. On the contrary, low humidity exposes more of the intermediate regions of the bound DNA, which might be damaged during the replication process. To separate the PDMS slabs with the anchored DNA on both surfaces, the complete set up was incubated at 95 °C for 30 min, dehybridating the DNA. The extended strand was then bound to the second substrate as shown in Figure 4.10H.

The replicated array was immediately submerged during 1 h into the blocking solution to deactivate any free epoxy groups and subsequently rinsed with Milli-Q water. Afterwards, a second extension protocol was used to synthesize the complementary strand from the newly fabricated array. The substrate was submerged into the PCR solution without the reverse primer, adding more water to reach the 25 µL. The thermal cycling was also altered to direct the PCR towards the bound strands with no denaturation steps, consisting on 5 consecutive annealing and extension cycles. The FP-NH_2 primer was used to add the reactive moiety to the strand. After the three-step washing protocol, the new array was introduced into the glove bag along a new epoxy-modified PDMS substrate. After stabilizing the humidity at the mentioned range, the array was replicated. The PDMS slabs were separated after thermal incubation, and subsequently blocked. As represented in Figure 4.10L, this replication protocol obtained a

clone of the initial long bound DNA strands on a new substrate. The master arrays were lastly hybridized with the RP-Cy3 primer after replication.

4.3.4 *Characterization methods*

Two methods were used to characterize the fabrication and replication of all DNA arrays. The first method was fluorescence microscopy, while DNA gel electrophoresis was the second.

4.3.4.1 *Fluorescence analysis*

Apart form localizing the printed spots, fluorescence microscopy provided the tools to perform a thorough pixel analysis to understand and perfect the steps taken to replicate the arrays.

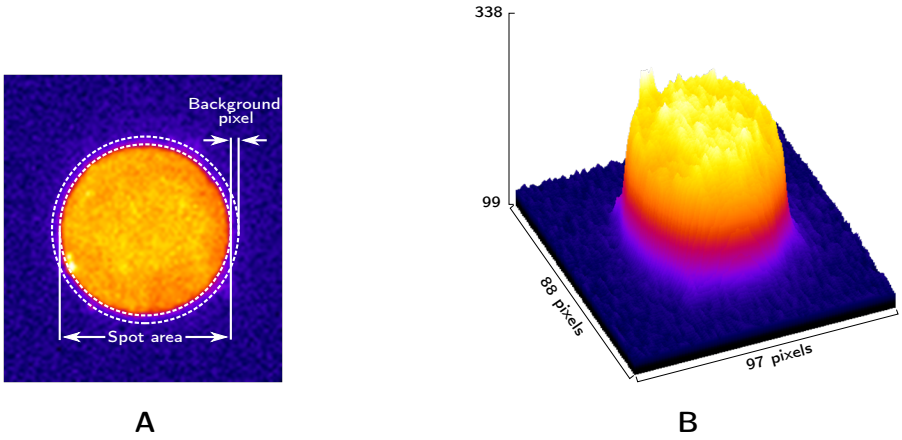

Figure 4.12: **Pixel intensity analysis.** (A) Background subtracted intensity (B.S.I) values are calculated from the pixel analysis of a printed spot. (B) 3D representation of the same spot.

Figure 4.12 shows the parameters taken into account to study the intensity of a printed spot. The background-subtracted intensity is obtained by eliminating the background intensity corresponding to the pixels surrounding the printed spot. This value is removed from the mean fluorescence emission for each printed spot, and is directly proportional to the amount of grafter fluorescent molecules. To eliminate difference between samples sue to varied spot size, the final intensity was dependent to the spot area, that is, the number of pixel inside the ROI. Equation 4.1 presents the final parameters to calculate the final Background-subtracted intensity (BSI).

$$BSI = \frac{\sum_{i=1}^{n} Sp_i}{Sn} - \frac{\sum_{i=1}^{n} Bp_i}{Bn} \tag{4.1}$$

Where Sp_i is the intensity value of the pixel inside the spot, Sn represents the number of pixels, which determines the spot area. The background parameters are defined by Bp_i and Bn, representing the background pixel and area, respectively. The Image Studio™ image analysis software from LI-COR Biosciences (Lincoln, NE, USA) was used to define the ROIs and analyze the pixel intensity for both, spot and background pixels. Intensity profiles and stack images were analyzed with ImageJ.

4.3.4.2 *DNA gel electrophoresis*

Gel electrophoresis was used to characterize the suspended strands as described in Section A.1.7. Initially, PCR products were characterized from the regular TB-ropB strand replication process, as presented in Figure 4.13.

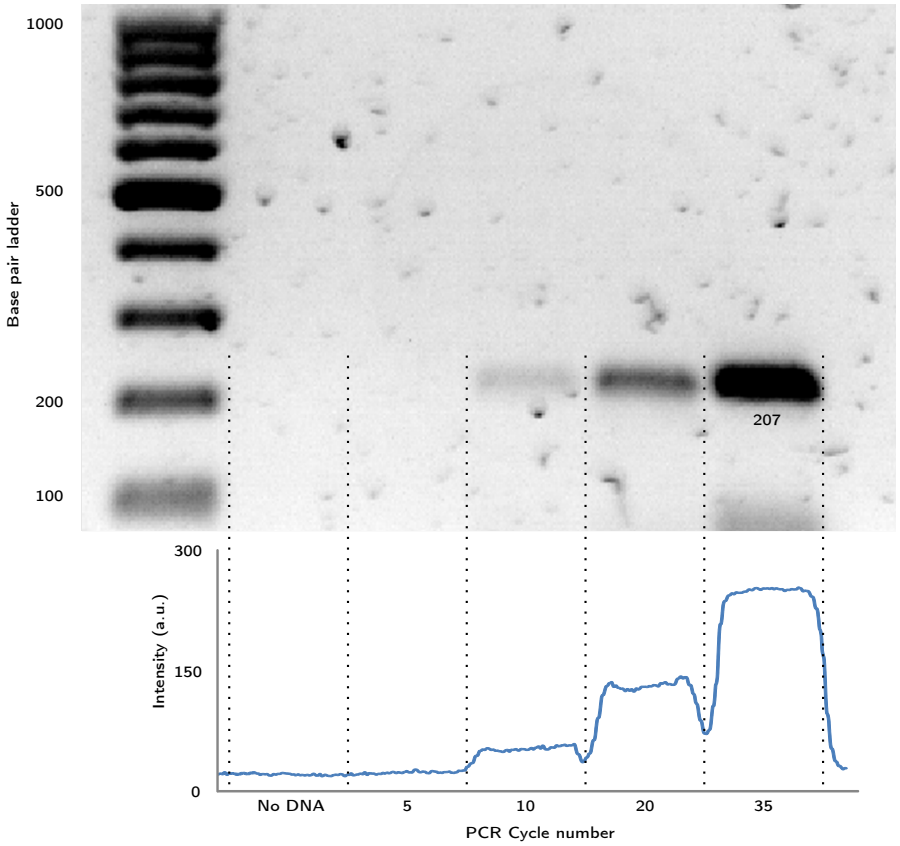

Figure 4.13: **Multiplication of DNA strands.** DNA gel electrophoresis of the 207bp TB-ropB strand after 5, 10, 20, and 35 PCR cycles.

A second method was developed and based on the extraction of the grafted information from the DNA arrays. As Figure 4.14 shows, the implementation of this protocol is focused in duplicating the bound DNA and transferring the encoded information to a liquid medium.

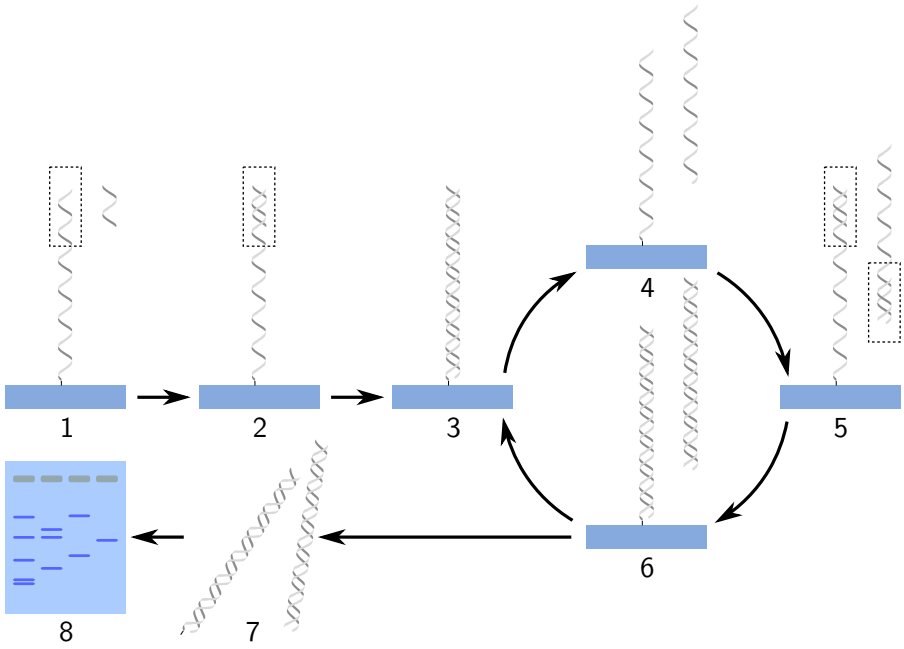

Figure 4.14: **Extraction of the information from solid substrate to a liquid medium.** (1) The bound ssDNA was introduced into the PCR solution. (2) A primer binds to the exposed end of the bound strand. (3) The primer is extended to reach the end of the strand. (4) After denaturation, the original ssDNA remains fixed on the substrate, while the complementary strand is released to the liquid medium. (5) Both, the fixed and liberated ssDNAs are hybridized with their corresponding primer, and extended, (6). (7) The cycle is repeated to obtain an exponential number of suspended DNA. (8) The accumulated PCR products are analyzed by gel electrophoresis.

To extract the information from solid substrate to a liquid medium, the DNA array was introduced into the PCR solution containing free oligonucleotides, DNA polymerase, and the FP1 and RP1 primers. No template DNA was added, as the immobilized strand was the backbone to replicate. First, the characterization of the intermediate transfer substrate (Figure 4.10H), required the binding of the FP1 primer to the strand, while the RP1 primer binded to the exposed end of the final replicated array (Figure 4.10L). Both primers were extended, and after denaturation, the original ssDNA remained bound to the substrate, while the complementary strand was released to the liquid medium. In the next step, both RP1 and FP1 primers binded to the immobilized and free strands, respectively, and both chains were extended. The melting-annealing-extension cycle was repeated resulting in the accumulation of an exponential amount of DNA. This product was pipetted from the reaction tube and analyzed by gel electrophoresis. It is important to note that the entire extraction of information relied on the presence of immobilized strands from the beginning. The lack of strands would hinder the copy of information.

4.4 RESULTS, EVALUATION, AND INFLUENCE OF THE DIFFERENT EXPERIMENTAL PARAMETERS

The fabrication of DNA arrays via contact replication provides a high-throughput mechanism to create master arrays. The dehybridization and *in situ* synthesis replication processes expands this fabrication method by providing an alternative not just to transfer spatial information but chemical information coded on the DNA sequence. Contact replication also permits the parallel transfer of the information.

4.4.1 *Contact replication of hybridized DNA*

The initial approach to replicate the a DNA master array was based on the fabrication of an intermediate array to store both, spatial distribution and chemical information. The storing mechanism was based on complementary strands maintaining a fixed location. The sequence provided an unique combination preventing the loss of information. The 5SH-3 master array presented in Figure 4.15A is visible on the fluorescence microscopy images as a result of the hybridized 5BT-3TR complementary strand.

The intermediate complementary DNA array is obtained from the mechanical separation of the previously hybridized strands. A strong bond is spontaneously formed by the biotin-modified 5BT-3TR strand and the NAV-functionalized flat PDMS stamp. The fluorescence microscopy image from the separated strands is shown in Figure 4.15B where the spatial distribution mirrors that of the master array. The subsequent exposition to the 5SH-3 strand, localizes the encoded information on the patterned spots. The thiol moiety adds a reactive site to anchor the strand on a new substrate.

The conformal contact between the intermediate array and a new gold substrate fixes the hybridized strands on a chosen location. The spatial distribution is now an exact replica of that of the initial master array. The encoded information is also maintained throughout the patterning process. Figure 4.15C presents the fluorescence emission of a second hybridization event between the newly replicated, immobilized array and the 5BT-3TR strand.

The fluorescent emission is related to the amount of hybridized target molecules. The image analysis of individual spots provided an insight on the amount of hybridized strands. Under each microscope image in Figure 4.15, an intensity profile is presented to describe the change between replication stemps. The histograms present the fluorescence intensity Gaussian distribution from the first, intermediate, and last replication steps. The average intensity values correspond to 685.59 ± 34.28, 596.08 ± 14.78, and 523.87 ± 14.95 a.u. It is evident the loss of intensity between the master and intermediate replica.

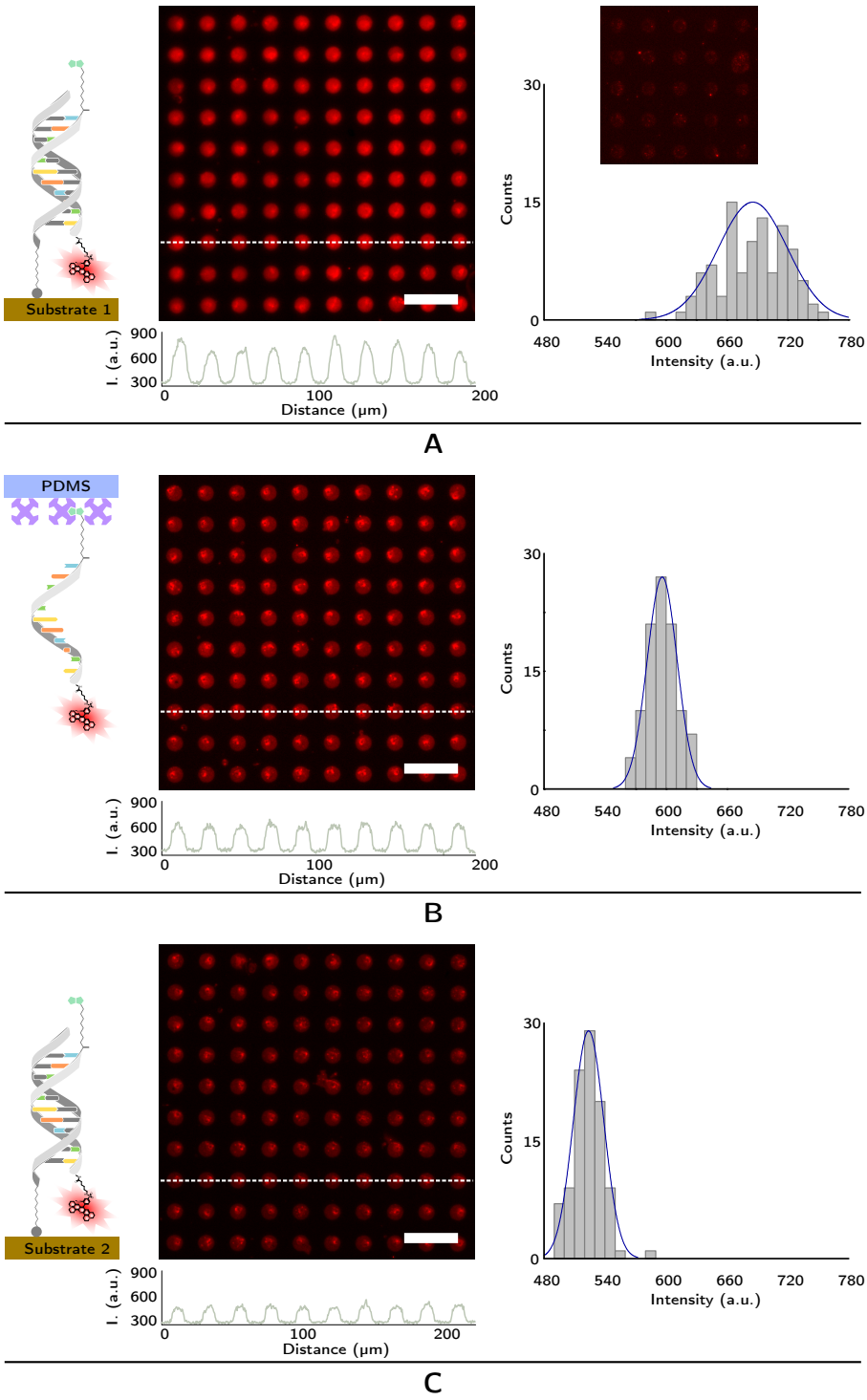

Figure 4.15: **Contact replication of hybridized DNA strands.** Fluorescence microscopy images of the fabricated and replicated DNA arrays. (A) The initial 5SH-3 array on gold and subsequently hybridized with 5BT-3TR. (B) Shows the previously hybridized strand transferred to the NAV-functionalized PDMS by contact replication. The new array was later hybridized with 5SH-3 and brought into contact with a new gold substrate. (C) Shows the transferred array finally hybridized with 5BT-3TR. The intensity values form a Gaussian distribution on the histogram corresponding to each step ($n = 100$). Scale bars = 50 µm.

The inset in Figure 4.15A shows the remaining fluorescence from the master array. This left over DNA contributes to the loss of fluorescence intensity between the intermediate and last replication steps. The efficiency between replication steps can be calculated with the amount of transferred fluorescent-labeled DNA, achieving ~87% between the master and intermediate array and a total ~76% from the master to the new substrate. The transfer between the intermediate and the last array also obtained an efficiency of ~87%.

Multiple replicas can be obtained using a single intermediate stamp with the remaining bound DNA. The intermediate stamp was rehybridized and loaded into the μCP Tool. The patterns in Figure 4.16 were fabricated after two and three consecutive patterning processes. As expected, the fluorescence drops between the first and second, and between the second and third replications steps.

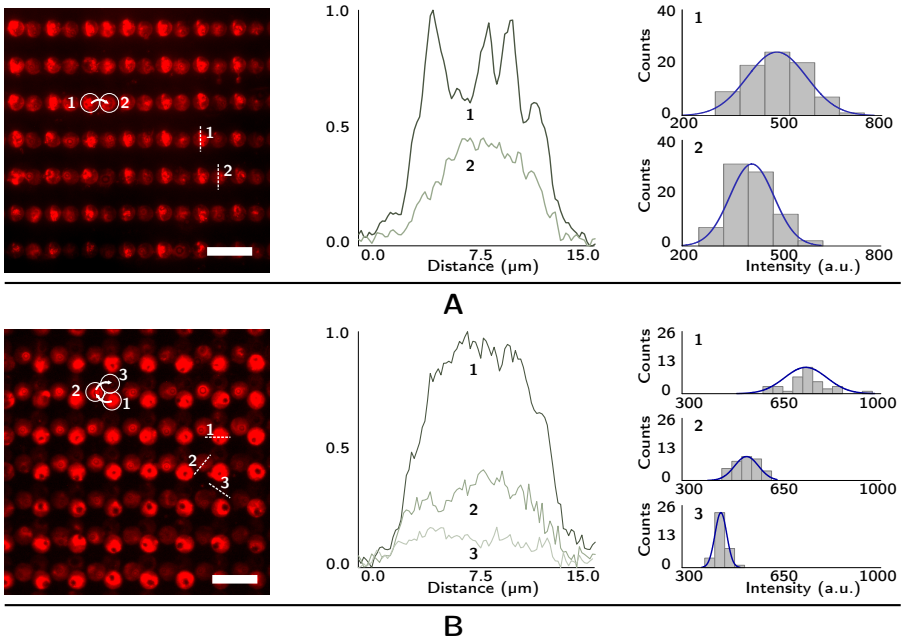

Figure 4.16: **Multiple contact replication of hybridized DNA strands.** Fluorescence microscopy images of two ,(A), and three, (B), consecutive patterning procedures with a single intermediate replication process. The profiles cross the dashed lines presented on each microscopy image, together with the trajectory of the patterning process. The histograms present the mean intensity from each replication step. ($n = 36$ and $n = 80$). Scale bars = 50 μm.

Previous publications[14–16, 46–49], present the contact replication as a fabrication technique to create complementary DNA arrays from an initial array. The work presented here expands this fabrication technique to clone the information and distribution present on the master array. This proof-of-concept could be expanded to fabricate DNA arrays with various strands and geometries. Still, it is important to

mention that this replication technique is limited to strands no longer of 50 bp. Nevertheless, a single time-consuming fabrication method would be needed to fabricate the initial master array, all the consecutive copies could be fabricated from the stored information in the intermediate stamp. This technique could also be used to hybridize the intermediate layer with strands modified with different reactive groups and create master arrays on other substrates.

4.4.2 *Hybridization efficiency of grafted DNA strands*

The amount of transferred DNA is dictated by the quantity of hybridized complementary strands on the initial array. The efficiency of the hybridization mechanism on solid substrates relies on several parameters including buffer stringency, SAM thickness, and the length of the spacer chains fixing the strands to the substrate.[57–59]

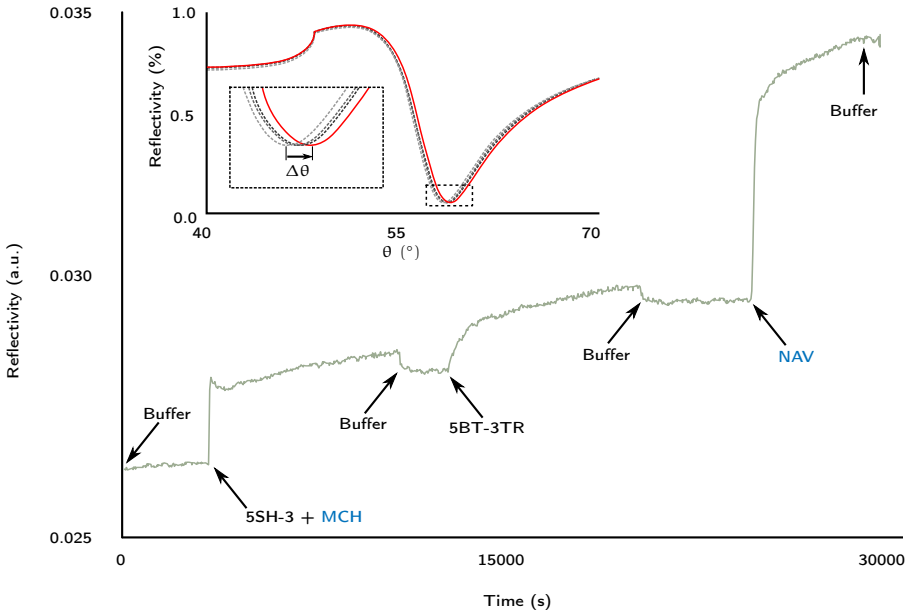

Figure 4.17: **Characterization of the hybridization of grafted strands.** SPR time-dependent sensogram with the hybridization of 5BT-3TR on a 5SH-3 SAM. NAV was used to ascertain the hybridization of the biotin-labelled strand. The inset presents the plasmon spectra showing the shift of the resonance angle from the buffer baseline to the washing step after the NAV immobilization.

Figure 4.17 SPR presents the time-dependent sensogram from the initial immobilization protocol. The curve follows the increment of deposited mass onto the gold substrate. An initial hybridization buffer injection set the base for the consecutive measurements. Then the subsequent 5SH-3:MCH injection increased the deposited mass. After a quick buffer wash, the complementary 5BT-3TR strand was injected. As displayed on the curve, the hybridization procedure in-

creased the mass anchored to the substrate, confirming a positive recognition event. The final NAV injection assured the presence of biotin binding groups from the complementary strand. Several publications have confirmed a relationship between the angle shift from the plasmon spectra and the amount of deposited mass, obtaining the ratio of 100 ng cm^{-2} = 122 m°.[60–62] The inset in Figure 4.17 present the angle shift starting at the baseline up to the NAV incubation.

Table 4.3: Amount of immobilized molecules after hybridization.

STEP	ADSORPTION		
	(ng cm^{-2})	(pmol cm^{-2})	(molecules cm^{-2})
Baseline	0.00	0.00	0.00
5SH-3	146.15	22.03	1.33×10^{13}
5BT-3TR	54.26	7.02	4.23×10^{12}
NAV	197.30	3.29	1.98×10^{12}

The ssDNA surface density has been shown to be between the values of 2.0×10^{12} and 3.8×10^{13} molecules cm^{-2}[58, 63, 64], and the calculated probe density from the values summarized in Table 4.3 are within the mentioned range. The probe and target surface densities were calculated with the molecular weight, M_w, from the 5SH-3 strand (M_w = 6634.2 g mol^{-1}) and 5BT-3TR (M_w = 7733.2 g mol^{-1}) along the Avogadro's number. The coverage of the first probe was calculated assuming each ssDNA strand had a diameter of 1.1 nm, hence, each strand would cover a circular surface area of 0.95 nm^2.[64] The maximum surface coverage by hexagonal packing would then be 9.07×10^{13} molecules cm^{-2}. This calculation is based on the packed density defined as the ratio of total area occupied by circles to area for an infinite hexagonal packing, $\rho = \frac{\pi}{2\sqrt{3}}$. The calculated coverage was 14.63%.

In this first experiment the hybridization efficiency was calculated at 32%, being lower than that previously published data. Future experiments were modified to include a NaOH wash to align and increase the receptivity of the bound strands, hence, improving the hybridization efficiency. With the subsequent addition of NAV bearing a M_w = 60 kDa a ratio of ~2 hybridized strands per NAV was calculated. This tetrameric protein has four active binding sites forming interactions with several individual biotin-bearing strands.

To guarantee multiple replication procedures, each master array should be able to replicate at least three times. This is necessary to produce three identical arrays for three subsequent individual experiments. The curve in Figure 4.18 follows a similar patter as the curve from the single hybridization. The DNA SAM immobilization is evident with the increase on reflectivity. To improve the hybridization, the SAM is incubated for 180 s with the NaOH solution and rinsed with the hybridization buffer. The complementary strand was

injected and left to react, the reflectivity increased due to the hybridization event. After a quick dehybridization with the NaOH and subsequent wash with the buffer, the angle shift was measured arriving to the initial SAM value, ascertaining a complete dehybridization. The same procedure was repeated three more times, measuring the angle shifts to calculate the adsorption and desorption of the complementary strand. The values are summarized on Table 4.4. Positive values represent an mass increase, while removal is represented with negative values.

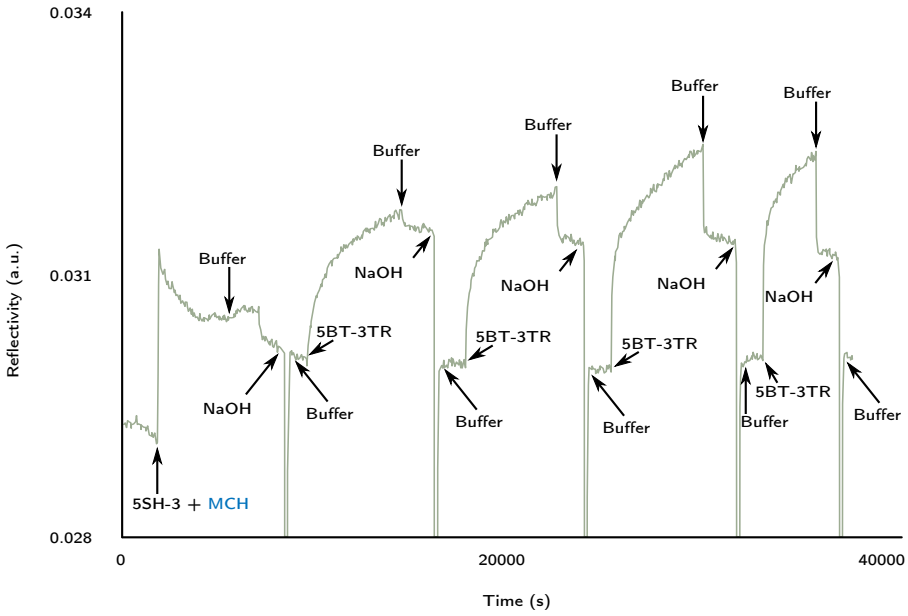

Figure 4.18: **Characterization of multiple hybridization and dehybridization events.** SPR time-dependent sensogram with various hybridization events of 5BT-3TR on an immobilized 5SH-3 SAM.

The initial 5SH-3 surface coverage was calculated at 9.52% while the efficiency from the four hybridization events correspond to 62, 60, 63, and 49%, respectively.

The highly selective dehybridization was calculated with the adsorption/desorption ratio from the obtained data. It is also evident the increase on hybridization efficiency with the initial NaOH wash. With the reflectivity values after dehybridization returning to the those of the 5SH-3 SAM, it can be concluded that the erosion of this layer is limited.

In the last SPR characterization, a non-complementary strand was incubated and left to hybridize to the previously immobilized 5SH-3 probe. The different sequences might interplay by weak electrostatic interactions. The reflectivity increment seen in Figure 4.19 after the injection of the strands is a result of these weak interactions. Still, the lack of perfect-match permits an easy strand removal. A subsequent buffer wash removed most of the non-complementary strand.

Table 4.4: Multiple hybridization dynamics on the immobilized strand.

STEP	ADSORPTION		
	($ng\ cm^{-2}$)	($pmol\ cm^{-2}$)	($molecules\ cm^{-2}$)
Baselin	0.00	0.00	0.00
5SH-3	95.08	14.33	8.63×10^{12}
1^{st} 5BT-3TR	68.28	8.83	5.32×10^{12}
1^{st} NaOH	−61.98	−9.34	-5.63×10^{12}
2^{nd} 5BT-3TR	66.48	8.60	5.18×10^{12}
2^{nd} NaOH	−59.43	−8.96	-5.39×10^{12}
3^{th} 5BT-3TR	69.92	9.04	5.44×10^{12}
3^{th} NaOH	−56.15	−8.46	-5.10×10^{12}
4^{th} 5BT-3TR	54.02	6.98	4.21×10^{12}
4^{th} NaOH	−47.13	−7.10	-4.28×10^{12}

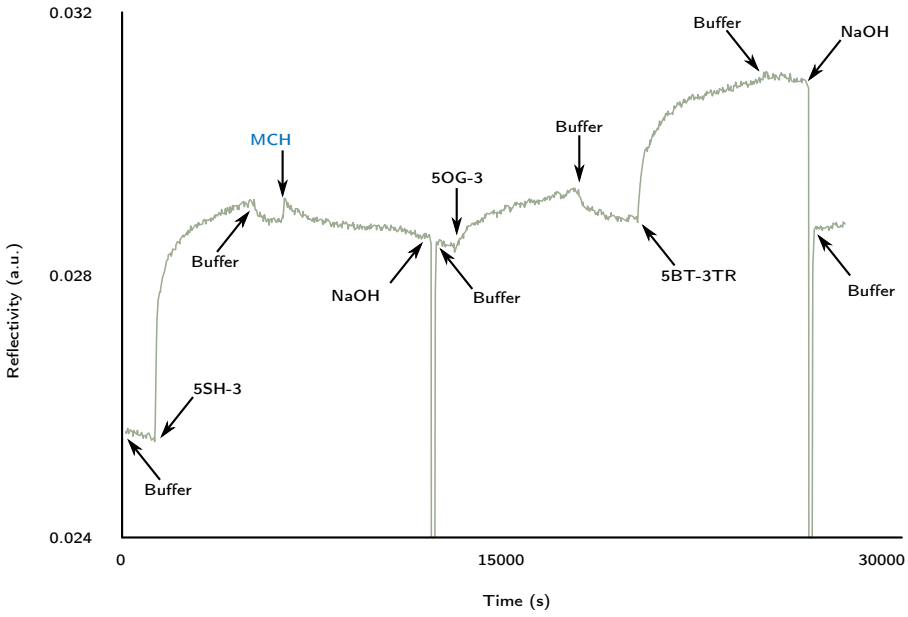

Figure 4.19: **Characterization of hybridization of non-complementary strands.** A 5SH-3 SAM was exposed to a non-complementary 5OG-3 strand. Afterwards, the complementary strand, 5BT-3TR, was added to test the hybridization of the SAM.

The complete values extracted form the experiment are summarized in Table 4.5. A 12.16% surface coverage was obtained with the 5SH-3 SAM, and with this, the calculated hybridization efficiency reached 67.09%. Incorporating the weight of the non-complementary strand, 5OG-3, at $M_w = 6967.2\ g\ mol^{-1}$, the non-specific adsorption was calculated at 11.18%. These results could pave the way to develop contact replicated arrays with different DNA strands. The localization

of the intended position and chemical information could therefore, be dramatically increased.

Table 4.5: Interaction between the immobilized strand and non-complementary target.

STEP	ADSORPTION		
	($ng\ cm^{-2}$)	($pmol\ cm^{-2}$)	($molecules\ cm^{-2}$)
Baseline	0.00	0.00	0.00
5SH-3	121.48	18.31	1.10×10^{13}
5OG-3	14.18	2.04	1.23×10^{12}
5BT-3TR	94.75	12.25	7.38×10^{12}
NaOH	−99.02	−12.80	-7.71×10^{12}

After analyzing the SPR results, the hybridization efficiency reached on average >60% and presented a strategy to reuse the master arrays to create multiple contact replications.

4.4.3 *In situ amplification and contact replication of a DNA arrays*

The DNA extension based on SP-PCR requires thermal cycling to denature and synthesize the strands. A high thermal stability is required to guarantee a robust replicating platform. μCP was the initial approach to graft the primers to fabricate the master array following the protocols presented in Section 2.4.3. An initial μCPed FP-NH_2-T array on functionalized glass was submerged in PCR buffer and placed inside a the thermal cycler for 35 cycles.

Figure 4.20 shows the array before and after the thermal cycling. It is evident the primer erosion, yet some strands remain on the substrate. This great loss would, therefore, hinder the creation of a master array, and limit the replication protocol thereof. A second unintended finding was caused by the substrate manipulation. Large, functionalized glass slides required a specialized PDMS gasket to retain the PCR buffer while the set up was inside the thermal cycler. To improve the manipulation, PDMS was used for further experiments.

The small spot size on super dense arrays via μCP is translated to few immobilized DNA strands. Therefore, even a small primer loss would dramatically alter the replication of arrays. To tackle this problem, a PDMS stamp with larger features was used to pattern a second version of the array. The bigger spots would contain more immobilized DNA and would pave the way to replicate the features by contact. A PDMS stamp with 200 μm-diameter posts was inked and subsequently used to print.

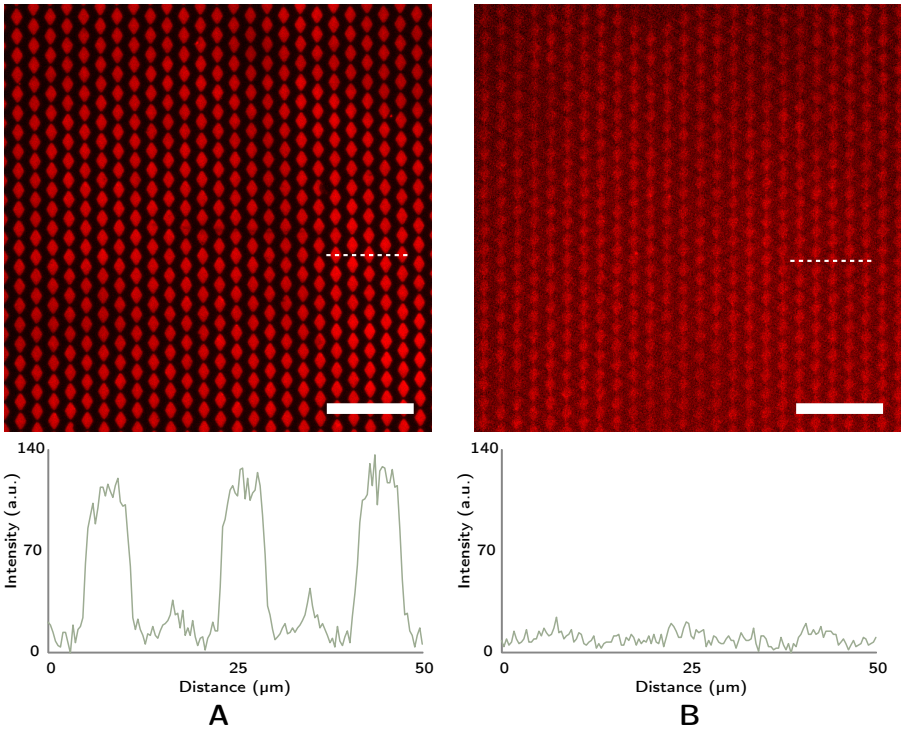

Figure 4.20: **Thermal damage of µCPed primers.** Fluorescence emission before, (A), and after, (B), 35 PCR cycles of µCPed FP-NH_2-T on epoxy-functionalized glass. The profiles follow the dashed line on each image show the loss of grafted primer. Scale bars = 50 µm.

4.4.3.1 *Patterning primers with the Nano-plotter™ and pin printer*

Figure 4.21A presents the fluorescence emission µCPed FP-NH_2-T over spoxy-functionalized PDMS. Unfortunately, the pattern presented huge irregularities, limiting the reproducibility. In bigger features, the hydrophobic nature of PDMS plays a mayor role when the buffer is being dried, concentrating the suspended probes on the last areas it covers before evaporation. Future experiments could be contemplated using dynamic inking to coat the PDMS stamp.[65]

To try to improve the repeatability, an alternative patterning method was followed: inkjet printing. This approach uses nanoliter-sized drops ejected from a specialized nozzle towards the substrate. The accumulation of drops over the surface spread, increasing the spot size. A computerized direction system allows the delivering of drops onto the desired spot. The epoxy-functionalized PDMS substrate was loaded into the printer, and a 5×5-feature array was printed. The final array is shown in Figure 4.21B. As with µCP, the final spots were irregular on both, size and fluorescent emission. These drawbacks greatly limit the reproducibility, and an alternative method had to be explored.

After evaluating the behaviour of the two previous patterning methods, pin printing was used to pattern both, epoxy-functionalized glass

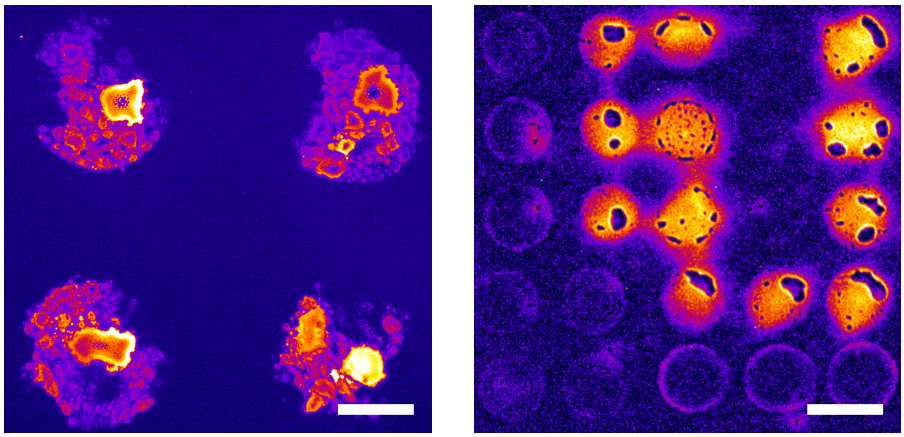

A B

Figure 4.21: **Fabrication of DNA arrays.** The FP-NH_2-T strand immobilized onto epoxy-functionalized PDMS with μCP, (A), using a PDMS stamp with circular posts with a diameter of 200 μm, and using an inkjet, (B). Scale bars = 100 μm.

and PDMS. The interesting feature when pin printing is the spot size due to the spread of the solution, leaving a footprint at the location where the pin contacted the substrate. The behaviour of the aqueous BSA-AF_{555} solution after being patterned over a hydrophilic glass substrate is shown in Figure 4.22.

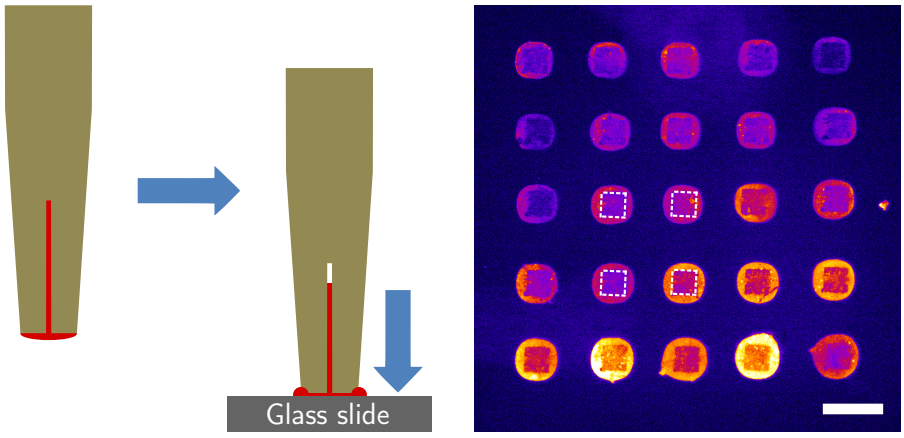

A B

Figure 4.22: **Printing on hydrophilic substrates.** (A) Behaviour of an aqueous solution when patterning with a pin printer onto a hydrophilic substrate. (B) BSA-AF_{555} printed on a glass slide. The dashed lines represent the printing pin absolute position. Scale bar = 100 μm

The dashed squares indicate the point of contact in a 5 × 5-feature array. For most spots, this point is centered, describing a homogeneous radial spread over the hydrophilic substrate. To understand the spreading behaviour the schematic in Figure 4.22A represents the aqueous flow at the moment the pin contacts the substrate.

Contrarily, when pin printing over hydrophobic substrates, the aqueous solution spreads towards a random position after the pin contacts the substrate. Figure 4.23 presents the outlined points of contact and final spot distribution of an aqueous FP-NH_2-T strand solution. Although when using the hydrophobic substrate may increase the printing complexity, the versatility of a soft substrate eclipses such drawbacks.

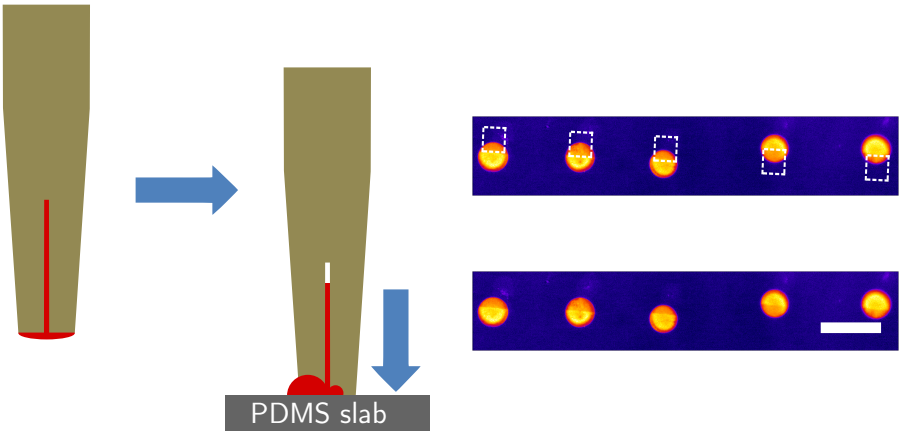

Figure 4.23: **Printing on hydrophobic substrates.** (A) Behaviour of an aqueous solution when patterning with a pin printer onto a hydrophobic substrate. (B) The FP-NH_2-T strand printed on a epoxy-functionalized PDMS slab. The lines present the location where pin contacted the substrate. Scale bar = 100 µm

To prevent the quick water evaporation from the spotted features, solvents with high boiling points were added to the spotting solution. The addition to the mixture of 10% glycerol or 10% DMSO permitted the creation of secondary amine bond between the modified strands and the epoxy-derivatized substrate. Both solvents also maintained an even solute distribution inside each drop, allowing the creation of a more homogeneous spot. Five different rows were printed over the substrate with the solvents at the final distribution shown in Figure 4.24A. After printing, the substrate were left to react and subsequently washed and blocked. As presented in Figure 4.24B, the addition of glycerol hindered the binding reaction, while in the case of just spotting buffer, the spots proved extremely irregular. Hence, the subsequent experiments were continued with the exclusive addition of DMSO.

The first characterization was produced with the hybridization of complementary strands onto the pin printed spots. The two-channel fluorescent images in Figure 4.25 show the emission from the printed FP-NH_2-T and hybridized 5OG-3 strands. It is evident some irregularities on the spot morphology and the comet tails produced after the substrate was blocked with the BSA solution. The curves in Figure 4.25D present the averaged profile values from the printed and

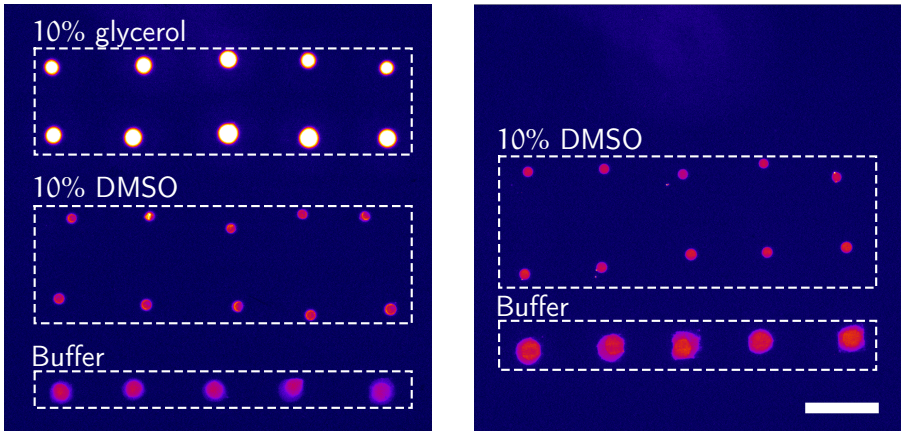

Figure 4.24: **Different carrying solutions.** (A) Fluorescent microscopic image showing the printed FP-NH_2-T spots using various printing solutions onto functionalized PDMS. (B) Printed substrate after washing. Scale bar = 100 µm

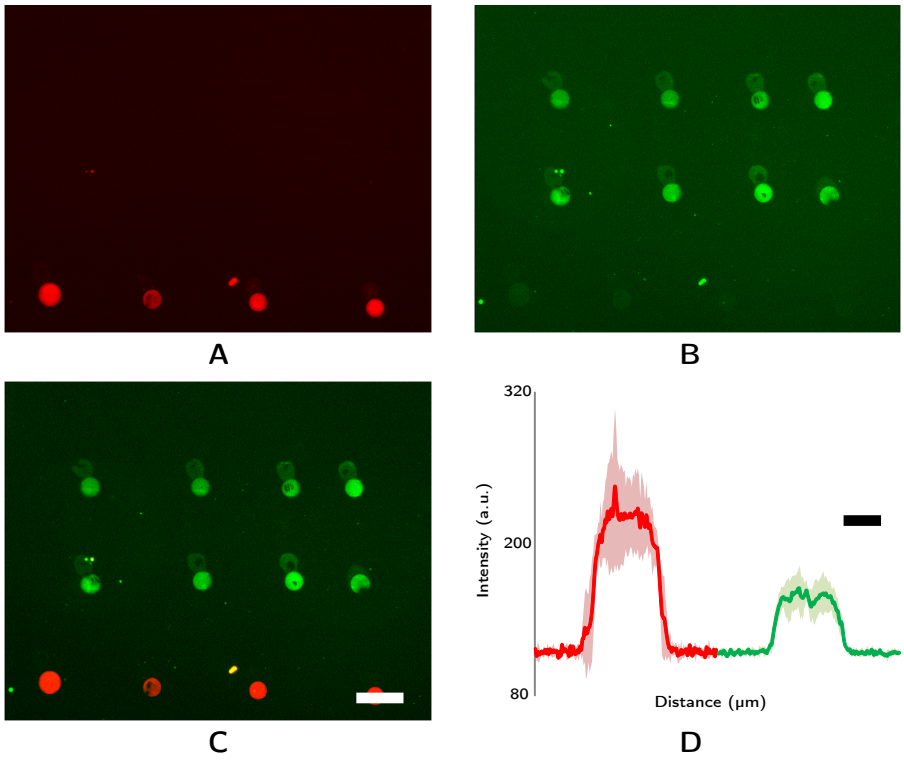

Figure 4.25: **Hybridization assay.** (A) Fluorescence emission of patterned FP-NH_2-T. (B) Emission of hybridized 5OG-3 strands to previously patterned FP-NH_2. (C) Merged image with both emissions. (D) Graph presenting the averages and standard deviations from all printed spots. Scale bar = 100 µm in (A-C) and 20 µm in (D).

hybridized spots. The error represents the pixel-by-pixel standard deviation. The hybridization on the non-fluorescent probes confirm the

correct immobilization and washing strategies, a consequence of the availability of bound strands to interact between the complementary strand in solution.

4.4.3.2 *Amplification of grafted primers via SP-PCR*

Primer extension is governed by the replication of information present on a template. The amplification of grafted primers allow to translate the information from a liquid medium towards a solid substrate. Consequently, the localized primers spots also create a defined distribution where the information is stored. The first step on the amplification procedure was to understand the interactions between the blocking agents and bound primers during the SP-PCR cycles. To study this relevant step, the pin printed spots were washed with three different washing buffers prior the extension. The fluorescent emissions from extended primers are registered in Figure 4.26. Image analysis provided the best insight to choose the best blocking protocol. Spot morphology, low background signal, and homogeneous intensity distribution were taken into account to choose the most adequate washing and blocking buffer. After analysis, subsequent printed arrays were blocked with the Super G Blocking buffer.

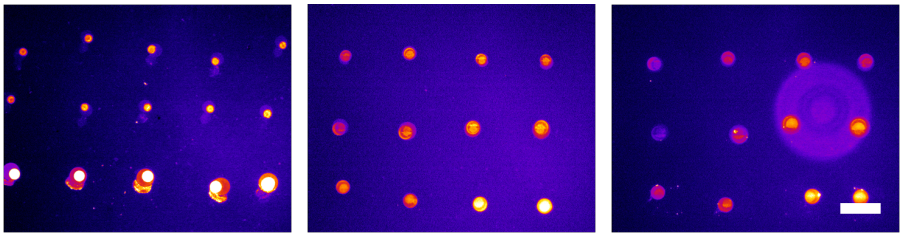

Figure 4.26: **Washing with various blocking solutions.** Three different patterned substrates were washed independently with a 2% *w*/*v* BSA solution in PBS, (A), with Super G Blocking buffer, (B), or a 2% *v*/*v* Ethylamine solution in Milli-Q water, (C). Scale bar = 100 µm

As with the µCPed arrays, several pin printed FP-NH_2-T features were subjected to various PCR cycles to characterize their thermal stability. A collection of fluorescent emission intensities from single spots from independent arrays after 0, 10, 15, 20, 25, 30, or 35 cycles is presented in Figure 4.27. All the spot intensities from the array were averaged to characterize the primer loss after the cycles. These calculated values are plotted on the curve under the microscopy images. The remaining fluorescence emission was calculated at >66% from that before any thermal cycle. An interesting finding is an initial loss of grafted primer without any more loss on subsequent cycles. This stability was found to remain constant throughout the thermal cycles, establishing a foundation for fluorescence calibration.

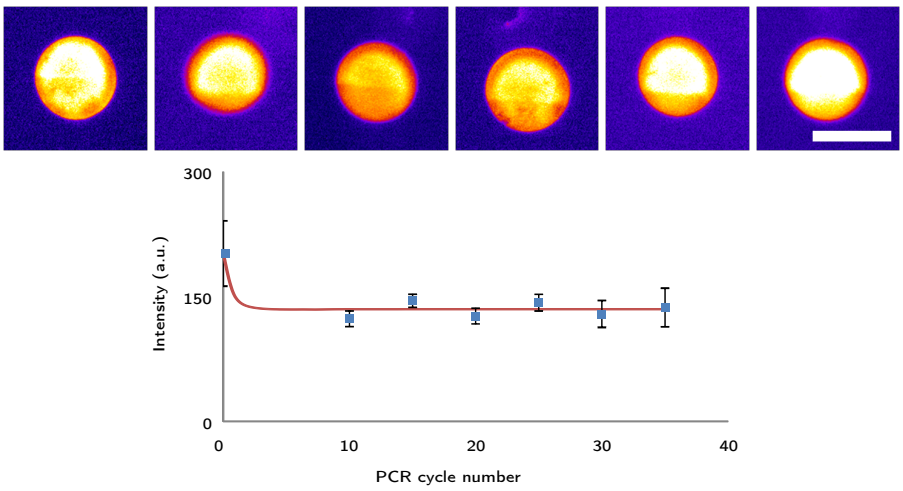

Figure 4.27: **Fluorescence emission of control spots.** Printed FP-NH_2-T spots after 0, 10, 15, 20, 25, 30, or 35 SP-PCR cycles. The graph shows a constant fluorescence emission after an initial loss throughout the subsequent cycles. Scale bar = 50 µm.

As previously discussed, the DNA replication process synthesize exponentially the chosen sequence until the availability of free primers or nucleotides is restricted. Therefore, the amount of grafted DNA grows following a similar pattern. All the arrays in Figure 4.28 were fabricated from the same batch and extended for the number of cycles indicated on each array. The fluorescence emission is a direct correlation on the amount of the RP-Cy3 primer from the extended DNA. There, the fluorescent spots arranged in a line on every array where used as control, following the calibration protocol discussed on Figure 4.27.

The next step was to characterize the fluorescence emission using the control spots as a reference for the absolute intensity. It is important to create a similar comparative pattern through samples to achieve the best analysis. Two approaches were followed to understand the DNA extension. In the initial approach the intensity profile was acquired for every printed and extended spots. The intensity was normalized to the highest control value. The results are presented under each single extended spot in Figure 4.29. The curves present the mean value as well as a pixel-by-pixel standard deviation taken from the analysis of all the spots present on the array. The second analysis approach used the Equation 4.1 to calculate the mean emission and was later normalized against the control spots. The resulting curve is plotted under the independent profile curves in Figure 4.29.

The parameters that described the previous PCR product curve were arranged with a theoretical fitting based on the sigmoid model explained in Figure 4.30.

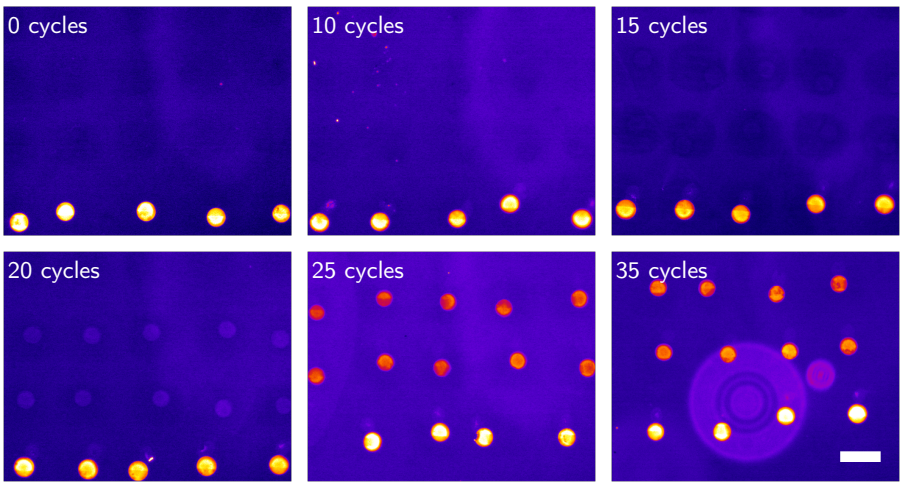

Figure 4.28: **Fluorescence emission of grafted primers after SP-PCR.** Fluorescence microscopy images showing the increase of the emission of the extended DNA strands after the indicated SP-PCR cycles. Scale bar = 100 µm.

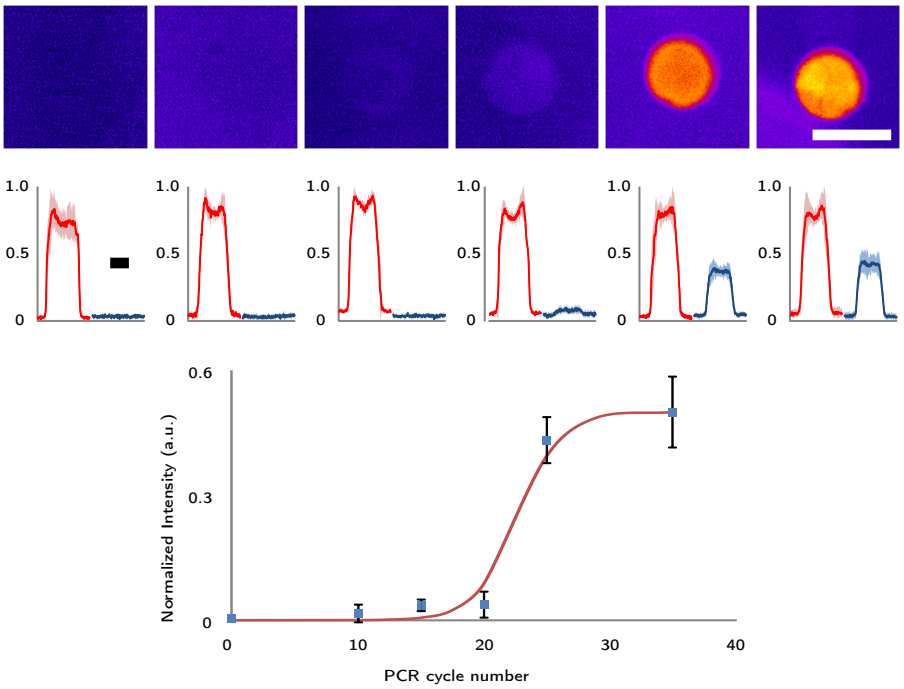

Figure 4.29: **SP-PCR of grafted primers.** Fluorescence emission of the printed FP-NH_2 forward primer spots after 0, 10, 15, 20, 25, and 35 SP-PCR cycles using the RP-Cy3 reverse primer. The graphs underneath the spots represent the averaged normalized emission of the spots (blue line) against the emission of the control spots (red lines). The curve at the bottom summarizes the data to demonstrate the exponential increase of the emission between the 20 and 30 cycles, reaching a plateau after 35 cycles. Scale bar = 50 µm on the images and 20 µm on the graphs.

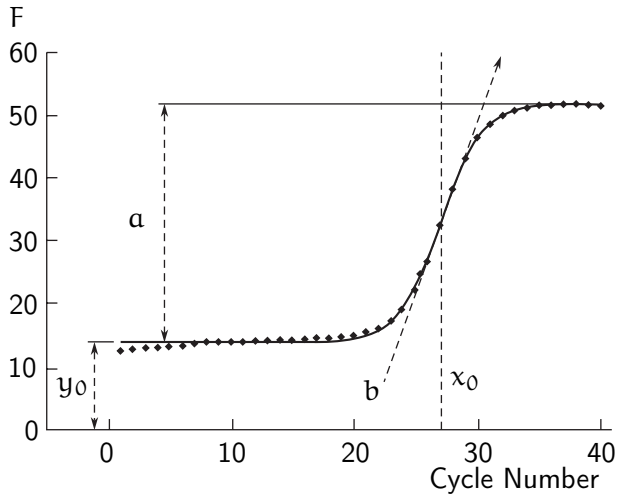

Figure 4.30: **Parameters describing the PCR product curve.** The sigmoid model describes the PCR curve based on the fluorescent baseline, y_0, difference between maximum emission and baseline, a, the derivative maximum, x_0, and the slope, b. Adapted from [66].

The fluorescent analysis approach helped understand the behaviour and reach of the first step of this replication technique. The final replication protocol required the use of NH_2-modified primers to create strong, covalent bonds between the intermediate and final replicated arrays.

4.4.3.3 *First contact replication of amplified DNA*

The previous fluorescent results paved the path to follow with the next replication processes. The next step required the creation of the intermediate replicated array. This was produced with the conformal contact between the epoxy-functionalized PDMS and the previously extended DNA. The process is similar to that presented by Kim and Crooks[50, 51]. Their work concluded with the creation of the complementary DNA array. In this work, the chemical information is stored on the intermediate copy, for a later replication.

To verify the presence of stored information, the fixed DNA was used as template and the sequence was translated into suspended complementary copies. These copies were later characterized with gel electrophoresis. Figure 4.31 presents the stained gel with two bands produced by the presence of the 207 bp strand. This image demonstrates the existence of bound DNA on the intermediate stamp. Fedurco *et al.*[67] used a similar approach to characterize the extension of DNA on their substrate. In their work, the replicated DNA was cleaved at a known sequence and later processed with gel electrophoresis. The bands confirmed the existence of synthesized DNA.

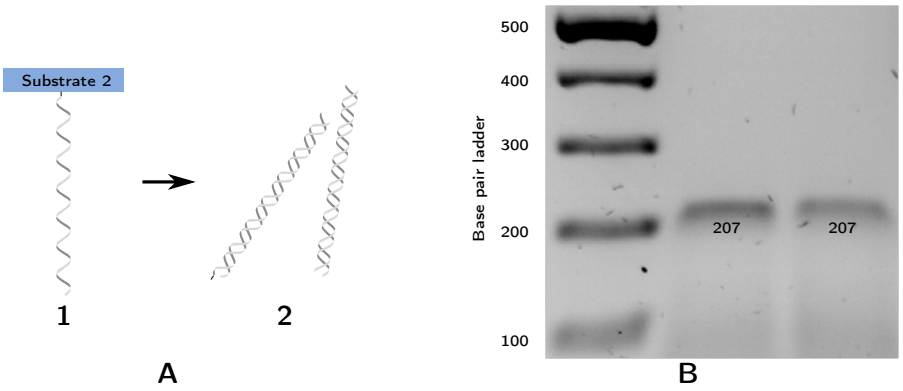

Figure 4.31: **DNA information from the intermediate replication step.** (A) The ssDNA on the substrate, (1), from the intermediate replication step (Figure 4.10H) after extracting the complementary strand, (2), as described on Figure 4.14. (B) Stained gel of the extracted DNA from two different substrates.

4.4.3.4 *Second contact replication of amplified DNA*

The final replication step, to create a cloned array from the printed master, required the conformal contact between the intermediate substrate and a new PDMS slab. To confirm the presence of bound DNA, the last replicated array was subjected to the same DNA extracting procedure. The 207 bp bands seen in Figure 4.32 corroborate the replication of the intermediate layer.

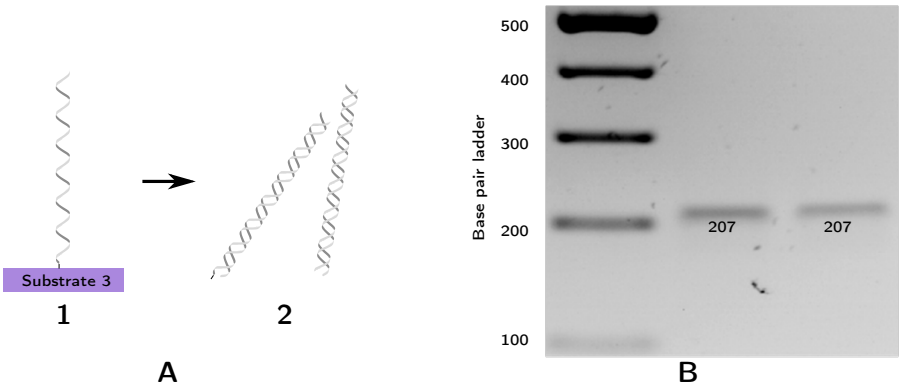

Figure 4.32: **DNA information from the last replication step.** (A) The ssDNA on the substrate, (1), from the last replication step (Figure 4.10L) after extracting the complementary strand, (2), as described on Figure 4.14. (B) Stained gel of the extracted DNA from two different substrates.

The last verification step is represented in Figure 4.33. The master arrays were re-hybridized after the replication step with the RP-Cy3 primer, complementary to the end of the extended DNA. If either the initial extension or the subsequent replication process were unsuccessful, this primer would not be able to hybridize. Thus, the

actual hybridization confirms the extension and final transfer of the extended DNA.

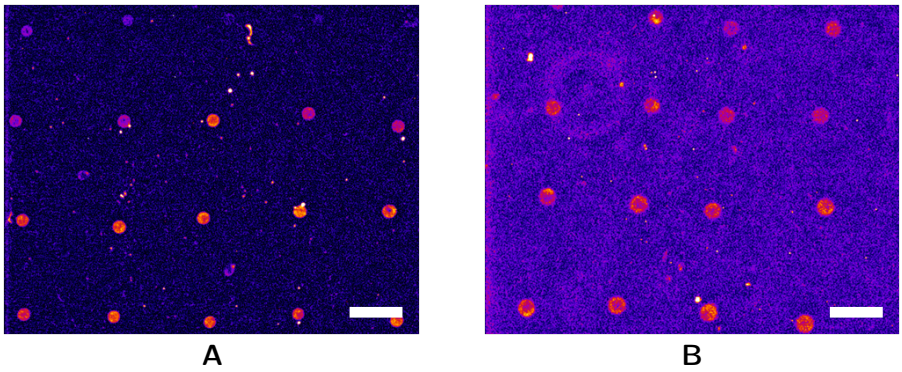

Figure 4.33: **Rehybridization of master arrays.** Two different DNA master arrays hybridized with RP-Cy3 after transferring the extended DNA molecule to the second epoxy-functionalized PDMS substrate. Scale bars = 100 µm.

4.5 CONCLUSIONS

This Chapter described two DNA microarray fabrication techniques based on contact replication. The proposed protocols where based on the transferring of chemical as well as spatial registration over several substrates. The encoded sequence unique to each DNA strand was maintained throughout the replication process as it could be confirmed with hybridization events.

The initial contact replication approach fabricated new arrays with a transfer efficiency ~76% calculated with the fluorescent emission between master and replica. This approach used direct hybridization and mechanical transfer to transport the bound molecules to the new substrate. A robust bond between intermediate and final arrays was achieved using a biotin-NAV bond. The efficiency value is consistent with the hybridization efficiencies calculated used mass deposition on a gold substrate and subsequent analysis with SPR.

To transfer longer DNA chains, a new replication method based on localized DNA extension was later developed. This approach permitted the creation of spatially localized strands, synthesized *in situ* and later transferred to new substrates. This replication method explored contact patterning techniques to overcome the inherent limitations of previously discussed fabrication methods.

[1] Heise, C and Bier, FF. 'Immobilization of DNA on Microarrays'. In 'Immobilisation of DNA on Chips II', volume 261, pages 1–25. Springer-Verlag Berlin, Berlin (2006). URL http://link.springer.com/book/10.1007/11544432

[2] Dufva, M. *DNA Microarrays for Biomedical Research: Methods and Protocols*. Humana Press, Hatfield, Hertfordshire, UK (2009). URL http://link.springer.com/content/pdf/10.1007/978-1-59745-538-1.pdf

[3] Schena, M; Shalon, D; Davis, RW; and Brown, PO. 'Quantitative monitoring of gene expression patterns with a complementary DNA microarray.' *Science*, 270 (5235) (1995) 467–70. URL http://www.ncbi.nlm.nih.gov/pubmed/7569999

[4] Dufva, M. 'Fabrication of high quality microarrays.' *Biomolecular engineering*, 22 (5-6) (2005) 173–84. URL http://www.ncbi.nlm.nih.gov/pubmed/16242381

[5] Pray, L. 'Discovery of DNA structure and function: Watson and Crick'. *Nature Education*, 1 (1) (2008) 100. URL http://cajalesygalileos.wordpress.com/author/miguelitoymafalda/page/18/

[6] Chargaff, E. 'Chemical specificity of nucleic acids and mechanism of their enzymatic degradation'. *Experimentia*, VI (6) (1950) 201–209. URL http://www.springerlink.com/index/p562475u36101146.pdf

[7] Watson, J and Crick, F. 'Molecular structure of nucleic acids'. *Nature*, 171 (1953) 737–8. URL http://www.nature.com/physics/looking-back/crick/

[8] Mullis, K; Faloona, F; Scharf, S; Saiki, R; Horn, G; and Erlich, H. 'Specific enzymatic amplification of DNA in vitro: the polymerase chain reaction'. *Cold Spring Harbor Symposia on Quantitative Biology*, 51 (1986) 263–273. URL http://www.labtrade.com.br/blog/wp-content/uploads/2012/04/mullis86.pdf

[9] Chien, A; Edgar, D; and Trela, J. 'Deoxyribonucleic acid polymerase from the extreme thermophile Thermus aquaticus.' *Journal of Bacteriology*, 127 (3) (1976) 1550–1557. URL http://jb.asm.org/content/127/3/1550.short

[10] Saiki, R; Gelfand, D; Stoffel, S; Scharf, S; Higuchi, R; Horn, G; Mullis, K; and Erlich, H. 'Primer-directed enzymatic amplification of DNA with a thermostable DNA polymerase'. *Science*,

239 (4839) (1988) 487–491. URL http://www.sciencemag.org/cgi/doi/10.1126/science.2448875

[11] Lipshutz, RJ; Fodor, SP; Gingeras, TR; and Lockhart, DJ. 'High density synthetic oligonucleotide arrays.' *Nature genetics*, 21 (1 Suppl) (1999) 20–4. URL http://www.ncbi.nlm.nih.gov/pubmed/9915496

[12] Teng, X and Xiao, H. 'Perspectives of DNA microarray and next-generation DNA sequencing technologies.' *Science in China. Series C: Life Sciences*, 52 (1) (2009) 7–16. URL http://www.ncbi.nlm.nih.gov/pubmed/19152079

[13] Chen, CH and Yang, KL. 'Fishing DNA targets in DNA solutions by using affinity microcontact printing.' *The Analyst*, 136 (4) (2011) 733–9. URL http://www.ncbi.nlm.nih.gov/pubmed/21116560

[14] Lin, H; Sun, L; and Crooks, RM. 'Replication of a DNA microarray.' *Journal of the American Chemical Society*, 127 (32) (2005) 11210–1. URL http://www.ncbi.nlm.nih.gov/pubmed/21310028

[15] Kim, J and Crooks, RM. 'Parallel fabrication of RNA microarrays by mechanical transfer from a DNA master.' *Analytical chemistry*, 79 (23) (2007) 8994–9. URL http://www.ncbi.nlm.nih.gov/pubmed/17963362

[16] Lin, H; Kim, J; Sun, L; and Crooks, RM. 'Replication of DNA microarrays from zip code masters.' *Journal of the American Chemical Society*, 128 (10) (2006) 3268–72. URL http://www.ncbi.nlm.nih.gov/pubmed/16522108

[17] Keighley, SD; Li, P; Estrela, P; and Migliorato, P. 'Optimization of DNA immobilization on gold electrodes for label-free detection by electrochemical impedance spectroscopy.' *Biosensors & bioelectronics*, 23 (8) (2008) 1291–7. URL http://www.ncbi.nlm.nih.gov/pubmed/18178423

[18] Carrascosa, LG; Martínez, L; Huttel, Y; Román, E; and Lechuga, LM. 'Understanding the role of thiol and disulfide self-assembled DNA receptor monolayers for biosensing applications.' (2010). URL http://www.ncbi.nlm.nih.gov/pubmed/20358368

[19] Canaria, CA; So, J; Maloney, JR; Yu, CJ; Smith, JO; Roukes, ML; Fraser, SE; and Lansford, R. 'Formation and removal of alkylthiolate self-assembled monolayers on gold in aqueous solutions.' *Lab on a chip*, 6 (2) (2006) 289–95. URL http://www.ncbi.nlm.nih.gov/pubmed/16450040

[20] Velusamy, V; Arshak, K; and Yang, C. 'Comparison Between DNA Immobilization Techniques on a Redox Polymer Matrix'. *American Journal of Analytical Chemistry*, 2 (2011) 392–400. URL http://file.scirp.org/Html/6366.html

[21] Beaucage, S. 'Strategies in the Preparation of DNA Oligonucleotide Arrays for Diagnostic Applications'. *Current Medicinal Chemistry*, 8 (10) (2001) 1213–1244. URL http://www.eurekaselect.com/openurl/content.php?genre=article&issn=0929-8673&volume=8&issue=10&spage=1213

[22] Kohsaka, H and Carson, DA. 'Solid-phase polymerase chain reaction.' *Journal of clinical laboratory analysis*, 8 (6) (1994) 452–5. URL http://www.ncbi.nlm.nih.gov/pubmed/7869187

[23] Romanov, V; Davidoff, SN; Miles, AR; Grainger, DW; Gale, BK; and Brooks, BD. 'A critical comparison of protein microarray fabrication technologies.' *The Analyst*, 139 (6) (2014) 1303–26. URL http://www.ncbi.nlm.nih.gov/pubmed/24479125

[24] Wu, CH; Holden, MT; and Smith, LM. 'Enzymatic Fabrication of High-Density RNA Arrays.' *Angewandte Chemie*, 53 (2014) 1–5. URL http://www.ncbi.nlm.nih.gov/pubmed/25339581

[25] Huber, M; Losert, D; and Hiller, R. 'Detection of single base alterations in genomic DNA by solid phase polymerase chain reaction on oligonucleotide microarrays'. *Analytical Biochemistry*, 299 (1) (2001) 24–30. URL http://www.sciencedirect.com/science/article/pii/S0003269701953552

[26] Mitterer, G; Huber, M; and Leidinger, E. 'Microarray-based identification of bacteria in clinical samples by solid-phase PCR amplification of 23S ribosomal DNA sequences'. *Journal of clinical microbiology*, 42 (3) (2004) 1048–57. URL http://jcm.asm.org/content/42/3/1048.short

[27] Khodakov, D; Zakharova, N; Gryadunov, D; Filatov, F; Zasedatelev, A; and Mikhailovich, V. 'An oligonucleotide microarray for multiplex real-time PCR identification of HIV-1, HBV, and HCV'. *BioTechniques*, 44 (2) (2008) 241–248. URL http://www.biotechniques.com/article/000112628

[28] Sun, Y; Dhumpa, R; Bang, DD; Handberg, K; and Wolff, A. 'DNA microarray-based solid-phase RT-PCR for rapid detection and identification of influenza virus type A and subtypes H5 and H7.' *Diagnostic microbiology and infectious disease*, 69 (4) (2011) 432–9. URL http://www.ncbi.nlm.nih.gov/pubmed/21396541

[29] Sun, Y; Dhumpa, R; Bang, D; Høgberg, J; Handberg, K; and Wolff, A. 'A lab-on-a-chip device for rapid identification of

avian influenza viral RNA by solid-phase PCR'. *Lab on a Chip*, 11 (2011) 1457–1463. URL http://pubs.rsc.org/EN/content/articlehtml/2011/lc/c0lc00528b

[30] Hoffmann, J; Hin, S; Stetten, FV; Zengerle, R; and Roth, G. 'Universal protocol for grafting PCR primers onto various lab-on-a-chip substrates for solid-phase PCR'. *RSC Advances*, 2 (9) (2012) 3885. URL http://xlink.rsc.org/?DOI=c2ra01250b

[31] Okamoto, T; Suzuki, T; and Yamamoto, N. 'Microarray fabrication with covalent attachment of DNA using bubble jet technology.' *Nature biotechnology*, 18 (4) (2000) 438–41. URL http://www.ncbi.nlm.nih.gov/pubmed/10748527

[32] Hughes, TR; Mao, M; Jones, AR; Burchard, J; Marton, MJ; Shannon, KW; Lefkowitz, SM; Ziman, M; Schelter, JM; Meyer, MR; Kobayashi, S; Davis, C; Dai, H; He, YD; Stephaniants, SB; Cavet, G; Walker, WL; West, A; Coffey, E; Shoemaker, DD; Stoughton, R; Blanchard, AP; Friend, SH; and Linsley, PS. 'Expression profiling using microarrays fabricated by an ink-jet oligonucleotide synthesizer.' *Nature biotechnology*, 19 (4) (2001) 342–7. URL http://www.ncbi.nlm.nih.gov/pubmed/11283592

[33] Goldmann, T and Gonzalez, JS. 'DNA-printing: utilization of a standard inkjet printer for the transfer of nucleic acids to solid supports.' *Journal of biochemical and biophysical methods*, 42 (3) (2000) 105–10. URL http://www.ncbi.nlm.nih.gov/pubmed/10737215

[34] Fodor, S; Read, J; Pirrung, M; Struyer, L; Lu, A; and Solas, D. 'Light-directed, spatially addressable parallel chemical synthesis'. *Science*, 251 (1991) 767–773. URL http://www.ncbi.nlm.nih.gov/pubmed/1990438

[35] Pease, AC; Solas, D; Sullivan, EJ; Cronin, MT; Holmes, CP; and Fodor, SP. 'Light-generated oligonucleotide arrays for rapid DNA sequence analysis.' *Proceedings of the National Academy of Sciences of the United States of America*, 91 (11) (1994) 5022–6. URL http://www.pubmedcentral.nih.gov/articlerender.fcgi?artid=43922&tool=pmcentrez&rendertype=abstract

[36] Nuwaysir, EF; Huang, W; Albert, TJ; Singh, J; Nuwaysir, K; Pitas, A; Richmond, T; Gorski, T; Berg, JP; Ballin, J; McCormick, M; Norton, J; Pollock, T; Sumwalt, T; Butcher, L; Porter, D; Molla, M; Hall, C; Blattner, F; Sussman, MR; Wallace, RL; Cerrina, F; and Green, RD. 'Gene expression analysis using oligonucleotide arrays produced by maskless photolithography.' *Genome research*, 12 (11) (2002) 1749–55. URL http://www.pubmedcentral.nih.gov/articlerender.fcgi?artid=187555&tool=pmcentrez&rendertype=abstract

[37] Singh-Gasson, S; Green, RD; Yue, Y; Nelson, C; Blattner, F; Sussman, MR; and Cerrina, F. 'Maskless fabrication of light-directed oligonucleotide microarrays using a digital micromirror array.' *Nature biotechnology*, 17 (10) (1999) 974–8. URL http://www.ncbi.nlm.nih.gov/pubmed/10504697

[38] Moore, S. 'Making chips'. *IEEE spectrum*, 38 (2001) 54–60. URL http://www.eng.ucy.ac.cy/cpitris/courses/ece001/notes/IEEEarticles/MakingChipsToProbeGenes-March2001.pdf

[39] Blanchard, A; Kaiser, R; and Hood, L. 'High-density oligonucleotide arrays'. *Biosensors and Bioelectronics*, 11 (6-7) (1996) 687–690. URL http://linkinghub.elsevier.com/retrieve/pii/0956566396833021

[40] Lausted, C; Dahl, T; Warren, C; King, K; Smith, K; Johnson, M; Saleem, R; Aitchison, J; Hood, L; and Lasky, SR. 'POSaM: a fast, flexible, open-source, inkjet oligonucleotide synthesizer and microarrayer.' *Genome biology*, 5 (8) (2004) R58. URL http://www.pubmedcentral.nih.gov/articlerender.fcgi?artid=507883&tool=pmcentrez&rendertype=abstract

[41] Mitra, RD and Church, GM. 'In situ localized amplification and contact replication of many individual DNA molecules.' *Nucleic acids research*, 27 (24) (1999) e34. URL http://www.pubmedcentral.nih.gov/articlerender.fcgi?artid=148757&tool=pmcentrez&rendertype=abstract

[42] Kim, S; Lim, GS; Lee, SE; Lee, JG; Yun, K; and Park, JK. 'DNA chip replication for a personalized DNA chip.' *Biomolecular engineering*, 23 (2-3) (2006) 129–34. URL http://www.ncbi.nlm.nih.gov/pubmed/16527538

[43] Escorihuela, J; Bañuls, MJ; Puchades, R; and Maquieira, A. 'Development of oligonucleotide microarrays onto Si-based surfaces via thioether linkage mediated by UV irradiation.' *Bioconjugate chemistry*, 23 (10) (2012) 2121–8. URL http://www.ncbi.nlm.nih.gov/pubmed/22992053

[44] Peris, E; Bañuls, MJ; Puchades, R; and Maquieira, A. 'Photoattachment of thiolated DNA probes on SU-8 spin-coated Bluray disk surfaces for biosensing'. *Journal of Materials Chemistry B*, 1 (45) (2013) 6245. URL http://xlink.rsc.org/?DOI=c3tb21026j

[45] Heyries, K; Blum, L; and Marquette, C. 'Direct poly (dimethylsiloxane) surface functionalization with vinyl modified DNA'. *Chemistry of Materials*, 20 (4) (2008) 1251–1253. URL http://pubs.acs.org/doi/abs/10.1021/cm7034745

[46] Yu, AA; Savas, T; Cabrini, S; Difabrizio, E; Smith, HI; and Stellacci, F. 'High resolution printing of DNA feature on poly(methyl methacrylate) substrates using supramolecular nano-stamping.' *Journal of the American Chemical Society*, 127 (48) (2005) 16774–5. URL http://www.ncbi.nlm.nih.gov/pubmed/16316209

[47] Yu, A; Savas, T; and Taylor, G. 'Supramolecular nanostamping: Using DNA as movable type'. *Nano letters*, 5 (6) (2005) 1061–1064. URL http://pubs.acs.org/doi/abs/10.1021/nl050495w

[48] Yu, AA and Stellacci, F. 'Stamping with high information density'. *Journal of Materials Chemistry*, 16 (28) (2006) 2868. URL http://xlink.rsc.org/?DOI=b602552h

[49] Akbulut, O; Jung, JM; Bennett, RD; Hu, Y; Jung, HT; Cohen, RE; Mayes, AM; and Stellacci, F. 'Application of supramolecular nanostamping to the replication of DNA nanoarrays.' *Nano letters*, 7 (11) (2007) 3493–8. URL http://www.ncbi.nlm.nih.gov/pubmed/17941680

[50] Kim, J and Crooks, RM. 'Transfer of surface polymerase reaction products to a secondary platform with conservation of spatial registration.' *Journal of the American Chemical Society*, 128 (37) (2006) 12076–7. URL http://www.ncbi.nlm.nih.gov/pubmed/16967951

[51] Kim, J and Crooks, RM. 'Replication of DNA microarrays prepared by in situ oligonucleotide polymerization and mechanical transfer.' *Analytical chemistry*, 79 (19) (2007) 7267–74. URL http://www.ncbi.nlm.nih.gov/pubmed/17803283

[52] Pincet, F and Husson, J. 'The solution to the streptavidin-biotin paradox: the influence of history on the strength of single molecular bonds.' *Biophysical journal*, 89 (6) (2005) 4374–81. URL http://www.pubmedcentral.nih.gov/articlerender.fcgi?artid=1367001&tool=pmcentrez&rendertype=abstract

[53] Morfill, J; Kühner, F; Blank, K; Lugmaier, RA; Sedlmair, J; and Gaub, HE. 'B-S transition in short oligonucleotides.' *Biophysical journal*, 93 (7) (2007) 2400–9. URL http://www.pubmedcentral.nih.gov/articlerender.fcgi?artid=1965448&tool=pmcentrez&rendertype=abstract

[54] Severin, PMD; Ho, D; and Gaub, HE. 'A high throughput molecular force assay for protein-DNA interactions.' *Lab on a chip*, 11 (5) (2011) 856–62. URL http://www.ncbi.nlm.nih.gov/pubmed/21221429

[55] Yu, AA and Stellacci, F. 'Contact Printing Beyond Surface Roughness: Liquid Supramolecular Nanostamping'. *Advanced materials*, 19 (24) (2007) 4338–4342. URL http://doi.wiley.com/10.1002/adma.200701068

[56] Durance, T and Wong, N. 'Kinetics of thermal inactivation of avidin'. *Food Research International*, 25 (2) (1992) 89–92. URL http://linkinghub.elsevier.com/retrieve/pii/096399699290148X

[57] Steel, AB; Herne, TM; and Tarlov, MJ. 'Electrochemical Quantitation of DNA Immobilized on Gold'. *Analytical Chemistry*, 70 (22) (1998) 4670–4677. URL http://pubs.acs.org/doi/abs/10.1021/ac980037q

[58] Peterson, AW; Heaton, RJ; and Georgiadis, RM. 'The effect of surface probe density on DNA hybridization.' *Nucleic acids research*, 29 (24) (2001) 5163–8. URL http://www.pubmedcentral.nih.gov/articlerender.fcgi?artid=97561&tool=pmcentrez&rendertype=abstract

[59] Peeters, S; Stakenborg, T; Reekmans, G; Laureyn, W; Lagae, L; Van Aerschot, A; and Van Ranst, M. 'Impact of spacers on the hybridization efficiency of mixed self-assembled DNA/alkanethiol films.' *Biosensors & bioelectronics*, 24 (1) (2008) 72–7. URL http://www.ncbi.nlm.nih.gov/pubmed/18440798

[60] Su, X; Wu, YJ; and Knoll, W. 'Comparison of surface plasmon resonance spectroscopy and quartz crystal microbalance techniques for studying DNA assembly and hybridization.' *Biosensors & bioelectronics*, 21 (5) (2005) 719–26. URL http://www.ncbi.nlm.nih.gov/pubmed/16242610

[61] Tang, Q; Su, X; and Loh, KP. 'Surface plasmon resonance spectroscopy study of interfacial binding of thrombin to antithrombin DNA aptamers.' *Journal of colloid and interface science*, 315 (1) (2007) 99–106. URL http://www.ncbi.nlm.nih.gov/pubmed/17689549

[62] Rachkov, A; Patskovsky, S; Soldatkin, A; and Meunier, M. 'Surface plasmon resonance detection of oligonucleotide sequences of the rpoB genes of Mycobacterium tuberculosis.' *Talanta*, 85 (4) (2011) 2094–9. URL http://www.ncbi.nlm.nih.gov/pubmed/21872063

[63] Gong, P; Lee, C; Gamble, L; Castner, D; and Grainger, D. 'Hybridization behavior of mixed DNA/alkylthiol monolayers on gold: Characterization by surface plasmon resonance and 32P radiometric assay'. *Analytical chemistry*, 78 (10) (2006) 3326–3334. URL http://pubs.acs.org/doi/abs/10.1021/ac052138b

[64] Milkani, E; Khaing, AM; Morais, S; Lambert, CR; and McGimpsey, WG. 'SPR-based single nucleotide mismatch biosensor'. *Analytical Methods*, 3 (1) (2011) 122. URL http://xlink.rsc.org/?DOI=c0ay00492h

[65] Fredonnet, J; Foncy, J; Lamarre, S; Cau, JC; Trévisiol, E; Peyrade, JP; François, JM; and Séverac, C. 'Dynamic PDMS inking for DNA patterning by soft lithography'. *Microelectronic Engineering*, 111 (2013) 379–383. URL http://linkinghub.elsevier.com/retrieve/pii/S016793171300347X

[66] Rebrikov, DV and Trofimov, DY. 'Real-time PCR: A review of approaches to data analysis'. *Applied Biochemistry and Microbiology*, 42 (5) (2006) 455–463. URL http://link.springer.com/10.1134/S0003683806050024

[67] Fedurco, M; Romieu, A; Williams, S; Lawrence, I; and Turcatti, G. 'BTA, a novel reagent for DNA attachment on glass and efficient generation of solid-phase amplified DNA colonies.' *Nucleic acids research*, 34 (3) (2006) e22. URL http://www.pubmedcentral.nih.gov/articlerender.fcgi?artid=1363783&tool=pmcentrez&rendertype=abstract

5 GENERAL CONCLUSIONS

Complex (bio)molecular patterns have been developed due to the various advantages presented throughout this work. The main objective of this Thesis was the design, fabrication, and characterization of novel (bio)molecular patterns and the adaptation of automatized methods to improve and expand current state-of-the-art.

Firstly, Chapter 2 described the development and implementation of an automatized Microcontact printing (μCP) Tool to overcome the inherent limitations of manual μCP. Such tool provided unlimited applications to expand the reaches of μCP. The most relevant conclusions form this chapter are:

1. Automatized μCP: The built prototype was successfully characterize and understood to create (bio)molecular patterns over various substrates.

2. Pattern size and morphology at different printing pressures: A mathematical model was developed to describe the printed feature size under any given printing pressure. Subsequently, a two-stage compression modulus was accurately calculated for the PDMS stamps.

3. Pattern size and morphology at different printing dwell times: The spread of ink molecules on the contact point was measured and a linear fit was established, providing the exact dwell time to create correct features.

4. Creation of complex patterns: Various printing steps produced complex patterns with single or multiple stamps. The measured value from the intended position to the actual position had a slight deviation in the order of a few hundred nanometers, paving the road for a broad range of multiplexed (bio)molecular patterns.

In Chapter 3 the automatized μCP Tool was subjected to an upgrade to implement the Polymer pen lithography (PPL) patterning technique. This powerful technique was later used to fabricate protein microarrays on top of anchored SiOx microparticles. The main advances shown in this Chapter are:

1. Adaptation for PPL: The automatized μCP Tool was correctly adapted to used new PPL stamps and characterized throughly to implement this technique on various substrates.

2. PDMS SHRINKING: A three-printing area stamp with a glass backbone was developed to address the shrinking problem inherent to PDMS stamps. This provided a rigid structure and allowed the creation of complex patterns.

3. ALIGNMENT AT THE NANOSCALE: Moiré patterns were used to align the machined substrate and the PPL stamp. This provided the much needed resolution to create nanometer-sized features directly placed on a desired location on the anchored microparticles.

4. NEW LIBERATION PROTOCOL: The anchored microparticles were freed with a novel liberation method which protected the bound molecules, allowing a subsequent antibody assay, detecting the motifs.

Lastly, in Chapter 4 two DNA microarray fabrication methods are described. Both methods replicated a master array obtaining a copy of the initial array on an independent substrate. The first protocol transferred hybridized strands from the master to an intermediate substrate. The second method was based on the direct placement of *in situ* synthesized DNA strands. The most relevant conclusions are:

1. FABRICATION OF DNA MASTER ARRAYS: DNA arrays were fabricated with various contact printing techniques, providing the desired encoded chemical information and spatial distribution.

2. REPLICATION OF DNA ARRAYS: A strong chemical protocol was established to create a robust platform to separate hybridized DNA strands to copy the stored information.

3. DIRECT TRANSFER OF HYBRIDIZED STRANDS: Short DNA chains were successfully transported from a printed master array to an intermediate substrate by means of dehybridization. The subsequent hybridization and contact replication with a third substrate, replicated the master array maintaining a correct spatial distribution. Multiple print were also achieved.

4. *In situ* SYNTHESIS AND SUBSEQUENT TRANSFER OF STRANDS: This replicating technique was expanded with the transfer of newly synthesized long DNA chains. The success of the transfer was characterized with electrophoresis, extracting the information stored on the substrate towards a solution.

6

RESUMEN EN CASTELLANO

Este capítulo es un sumario de todo el trabajo de la Tesis. En la primera parte, se muestra el proceso y fabricación de patrones con la máquina automatizada de microcontacto. Seguidamente, se detalla el proceso para fabricar las micropartículas suspendidas multiplexadas. Finalmente se recopilan los pasos para la replicación por contacto de chips de ADN.

6.1 INTRODUCCIÓN

Un patrón es una colección de unidades formadoras que se repiten predeciblemente en una magnitud definida. Los investigadores han utilizado patrones para garantizar la funcionalidad y repetitividad de sus estudios. Para conseguir eso, los datos obtenidos de los estudios se comparan entre varios resultados, esperando así una correlación. Dos métodos de investigación están basados en patrones: uno requiere un sustrato con unidades repetidas localizadas en un plano cartesiano definido, obteniendo una plataforma de análisis múltiple. El segundo método utiliza localizaciones definidas con diferentes áreas de prueba, creando así una plataforma de multianálisis. La miniaturización de estas pruebas permite reducir el costo, maximizar la eficiencia e incrementar la repetitividad de los ensayos. Los micropatrones consisten en puntos de (bio)moléculas limitados en pequeñas áreas para crear zonas de reacción múltiples. Esta tecnología fue inicialmente utilizada para crear las interacciones del ADN para estudios genómicos. La técnica evolucionó para crear patrones de proteínas y actualmente se utiliza para estudios bioquímicos a gran escala y de muy alto rendimiento. Patrones de una (bio)molécula repetida a través del sustrato son fabricados rutinariamente en muchos laboratorios utilizando técnicas de impresión por contacto, por inyección u otro métodos. El cimiento de estas técnicas es transferir una (bio)molécula de una solución a un sustrato. Esta Tesis pretende expandir los métodos de creación de micropatrones por técnicas de impresión por contacto. Inicialmente se caracterizó una máquina automatizada de impresión por microcontacto para crear patrones y estudiar las variables que afectan al momento de la impresión. Se correlacionaron la presión y el tiempo de impresión para entender la morfología del patrón resultante. Igualmente se caracterizó el posicionamiento micrométrico de los patrones para crear estructuras complejas. Posteriormente, la máquina se modificó para incluir la técnica de impresión con plumas poliméricas. Esta técnica permitió crear micropatrones en superficies minúsculas. Estos micropatrones fueron luego liberados para crear micropartículas que pueden ser personalizadas para aplicaciones diversas. Finalmente, se formuló una nueva técnica de replicación de patrones de ADN desde un patrón inicial, manteniendo la información química y espacial presente en éste.

6.2 PATRONES FABRICADOS CON UNA MÁQUINA AUTOMATIZADA DE MICROCONTACTO

6.2.1 *Introducción*

Una gran meta de la ciencia de los materiales es la creación de patrones miniaturizados sobre diversos sustratos. Cada elemento en el patrón es presenta una zona activa para estudiar diversas interacciones cuando el patrón es expuesto a diferentes ambientes. Estos patrones tienen grandes ventajas al momento de estudiar las reacciones ya que cuentan con puntos múltiples e independientes, utilizando menos reactivos para hacer las pruebas, por lo que generan pocos desechos.

La impresión por contacto fue desarrollada para crear patrones sobre superficies para estudios de microelectrónica. Esta técnica consiste en transportar (bio)moléculas adsorbidas a una base sólida con una geometría definida a un sustrato. Este método de fabricación de patrones desciende del trabajo desarrollado por Kumar y Whitesides[1] en donde un sello de goma fue utilizado para crear patrones en la escala centi- y micrométrica utilizando la adsorción espontánea de tioles sobre oro. Debido a la escala micrométrica, aunado al mecanismo de impresión, se acuñó el nombre de impresión por microcontacto (Microcontact printing (μCP)).

El diseño del sello es primordial para crear patrones fieles al diseño. Regularmente se utilizan gomas o polímeros para fabricarlos ya que presentan propiedades necesarias para crear patrones a la microescala. La relación de aspecto define el tamaño de las estructuras que se pueden diseñar para la posterior fabricación del sello. Si las estructuras son demasiado altas o finas, se daría paso a que éstas se inclinaran o tocaran al momento de aplicar la fuerza de impresión. Por el otro lado, si las estructuras son muy cortas o están demasiado lejos una de la otra, el techo del sello puede colapsar sobre la superficie. En cualquiera de los casos, el diseño del patrón sería modificado, limitando así, la repetitividad de resultados.

La impresión por microcontacto comenzó con la fabricación de patrones de tioles sobre sustratos de oro, y ha sido extendida para trabajar con silanos y varias biomoléculas. Los tioles[2] y los silanos[3] forman capas monomoleculares sobre la superficie en la que son dispuestos. Estas capas pueden cambiar las propiedades del sustrato que cubren para personalizar las necesidades de la aplicación. Por otro lado, las proteínas, anticuerpos y ADN también pueden ser transferidas a un sustrato con un sello, creando así, patrones biomoleculares funcionales.

Esta técnica de impresión ha sido tradicionalmente realizada manualmente, limitando así el éxito o fracaso de la impresión a la habilidad del investigador. Por este motivo, se ha desarrollado una máqui-

na automatizada de microimpresión en colaboración con el Prof. Dr. André Bernard y su grupo en el Institute for Micro and Nanotechnology de la NTB Interstate University of Applied Sciences en Buchs, Suiza (http://institute.ntb.ch).

6.2.1.1 *Máquina automatizada de impresión por microcontacto*

El diseño de la máquina fue cimentado sobre tres parámetros:

1. Sellos: Un sistema que acepte sellos flexibles, inertes, fácilmente moldeables y transparentes, basados en Poly(dimethyl siloxane) (PDMS).

2. Tintas: Un amplio espectro de tintas, desde tioles hidrófobos hasta biomoléculas.

3. Sustratos: Un área de impresión desde 10×10 mm^2 hasta 25×75 mm^2 con sustratos de oro, vidrio, óxido de silicio o polímeros.

Para explotar las funciones de la máquina, se incluyeron sistemas de actuación para posicionar la muestra en el punto exacto con un resolución de < 1 μm, al igual que un actuador para transportar el sello cargado de tinta hacia el sustrato. Cuatro galgas extensiométricas localizadas en las esquinas del sujetador del sello permiten monitorizar la fuerza al momento de imprimir. Finalmente, un sistema óptico formado por una cámara, filtros y zoom permiten registrar y grabar todo el proceso de impresión.

La Figura 6.1 presenta un esquema de la máquina de microcontacto indicando las partes mas importantes de la misma. Los sistemas de acutación y monitorización son controlodos por software dedicado a cada una de las funciones.

6.2.2 *Metodología*

Se fabricaron sellos de PDMS con diversas morfologías para estudiar la repercusión y el cambio de las estructuras influenciados por los diversos parámetros que afectan la impresión por microcontacto.

La máquina automatizada se utilizó para controlar la fuerza y el tiempo de impresión en todos los patrones fabricados. Se utilizaron diversas tintas formadas por tioles, silanos y biomoléculas.

Para crear patrones complejos con un mismo sello, se utilizaron una gran colección de diseños y se trasladaron las coordenadas absolutas a la máquina, que fabricaría el patrón. De la misma manera, se alinearon y utilizaron diversos sellos para crear patrones multiplexados sobre superficies activas.

Las técnicas de microscopía por fuerza atómica (Atomic force microscopy (AFM)) y de fluorescencia fueron utilizadas para caracterizar los resultados de la impresión.

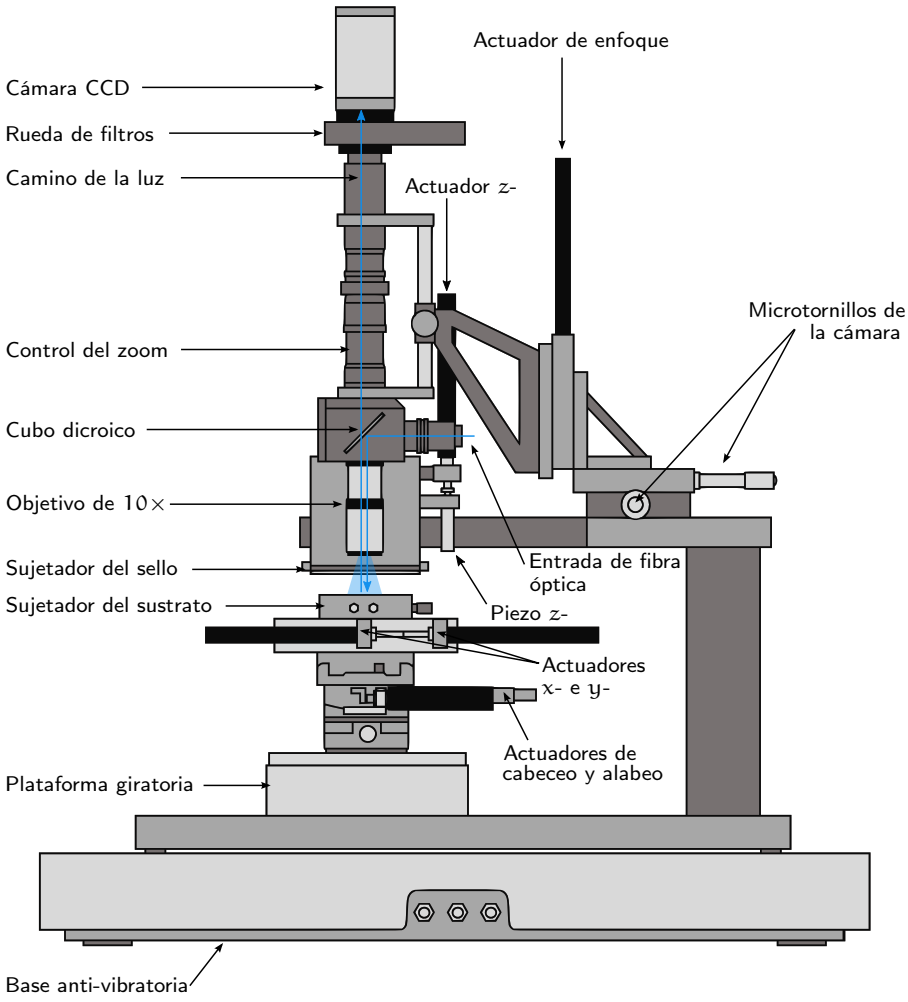

Figura 6.1: **Representación esquemática de la impresora.** Los actuadores posicionan la muestra, manipulan la cámara y controlan la presión durante la impresión. Los sensores en el sujetador del sello proporcionan un ciclo de retroalimentación para monitorizar la presión. Todo el proceso se realiza bajo monitorización óptica a través de una cámara.

6.2.3 *Resultados y Discusión*

El comportamiento del sello de PDMS bajo presión transmite cualquier cambio al patrón.

Primero se calculó el módulo de elasticidad del sello, E, siendo el cociente entre la tensión, σ, y la deformación, ε, ($E = \frac{\sigma}{\varepsilon}$) tomando en cuenta que el PDMS es un material elástico. Para calcular este valor, se siguió una aproximación similar a la de Liao *et al.*[4], en dónde el PDMS tiene un módulo elástico de dos regímenes, uno por debajo de la fuerza de impresión donde $E = E_1$, y por encima cuando $E = E_2$. Los módulos calculados fueron $E = E_1 = 0.500$ MPa y $E = E_2 = 1.851$ MPa, similar a los valores reportados en la bibliografía.[5]

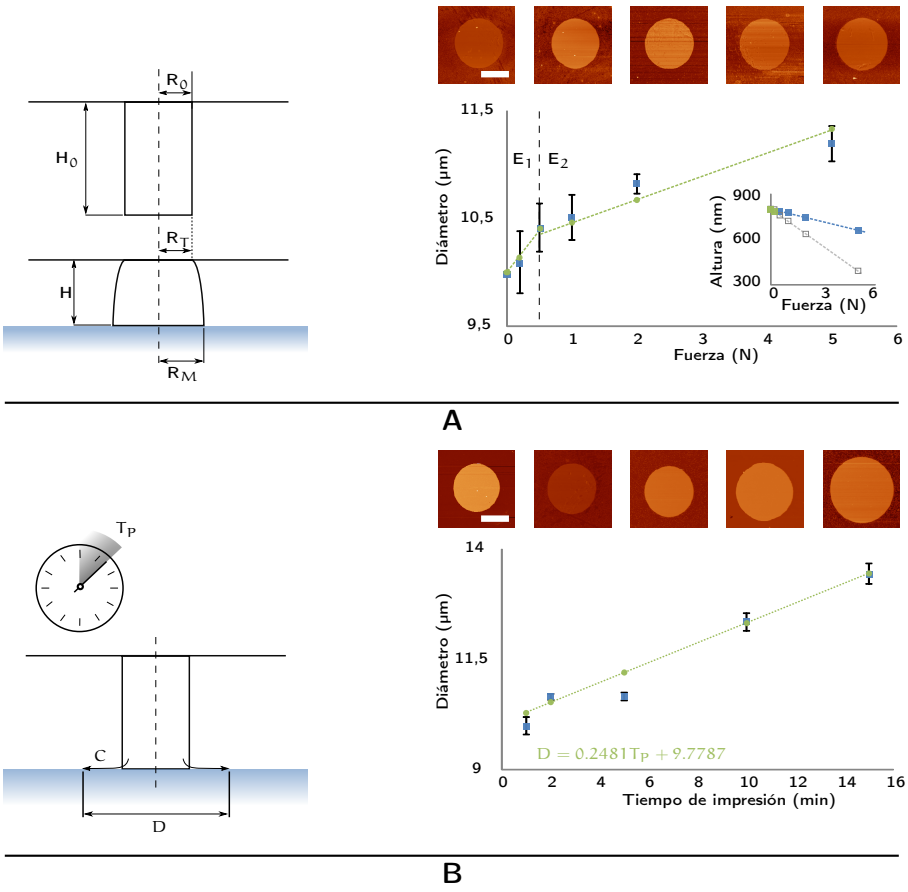

Figura 6.2: **Características del punto impreso bajo diferentes presiones y tiempo de contacto.** (A) La deformación del sello limita el tamaño de los puntos impresos, donde el módulo de elasticidad (E), trabaja en dos regímenes $E = E_1$ y $E = E_2$. Las imágenes muestran un punto impreso a 0.2, 0.5, 1.0, 2.0 o 5.0 N y la gráfica muestra el cambio del diámetro $\pm\sigma$ con la fuerza de impresión ($R^2 > 0.96$). El inserto muestra el δH calculado. (B) El flujo de las moléculas absorbidas migran hacia el sustrato durante la impresión. El diámetro de los puntos impresos a 1, 2, 5, 10 o 15 min siguen la ecuación mostrada en la gráfica ($R^2 > 0.97$). Barras de escala = 5µm

Posteriormente, con los resultados mostrados en Figura 6.2A, se relacionaron la fuerza de impresión, las propiedades mecánicas del material y la geometría del sello para modelar el radio, R_M, de las figuras impresas, utilizando el cambio teorético en la altura del poste, δH, del PDMS y modelado con la Ecuación 6.1:

$$\delta H = \frac{\overrightarrow{F_N} H_0}{E\pi \left(\frac{D}{2}\right)^2} \tag{6.1}$$

en donde el cambio de altura es proporcional a la fuerza en cada poste al momento de imprimir, $\overrightarrow{F_N}$, a la altura original del poste, H_0, y al módulo elástico. Así, lo que se obtiene se muestra en la Ecuación 6.2:

$$R_M = R_0 \sqrt{\frac{1}{2}\left(\frac{3}{1-\frac{\overrightarrow{F}}{NE\pi R_0^2}} - 1\right)} \tag{6.2}$$

donde el radio de la figura impresa, R_M, se correlaciona con la fuerza de impresión, $\overrightarrow{F}$, el número de postes del sello, N, y el radio inicial de cada poste, R_0.

El comportamiento del diámetro también depende del tiempo de impresión. Por lo mismo, se estudió la razón de la cobertura de la tinta con respecto al tiempo de contacto. En Figura 6.2B se muestra la curva obtenida de la relación de tiempo de impresión, T_P, y el diámetro, D, del punto obtenido. La razón de la cobertura fue calculada en $C = 0.08\ \mu m^2\ s^{-1}$.

Los patrones complejos fabricados controlando la posición de impresión se muestran en la Figura 6.3. Cada uno de los pasos que realizaron los actuadores y la posterior impresión se muestran consecutivamente en la imagen. Con este método, se pueden crear patrones complejos utilizando solamente un sello. Es interesante notar que dentro de un mismo sustrato se pueden fabricar una colección de elementos idéntico, es decir, con la misma área superficial y morfología, o se pueden fabricar elementos con diversa morfología y área superficial al manipular de la manera correcta el posicionamiento del sello. Las imágenes mencionadas fueron adquiridas con el AFM y permitieron caracterizar la desviación media de los ejes de los actuadores obteniendo los valores que se encuentran entre los 0.36 y 0.78 μm en el eje x y 0.30 y 0.65 μm en el eje y.

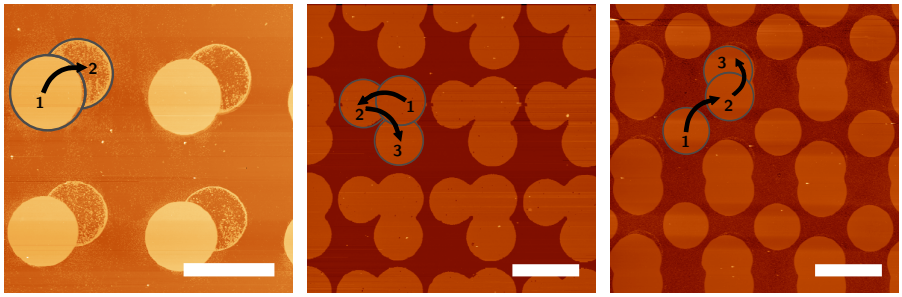

Figura 6.3: **Impresiones múltiples crean patrones complejos.** Puntos fabricados con impresiones consecutivas utilizando un mismo sello de PDMS cargado con una tinta de tioles sobre un sustrato de oro. Las imágenes de AFM muestran la creación de los patrones después del grabado del oro. Barras de escala = 12 μm.

Para extender las aplicaciones de la maquina, un amplio rango de biomoléculas fueron impresas en diversos sustratos. Los patrones ob-

tenidos con proteínas, anticuerpos y ADN se muestran en la Figura 6.4. Las principales aplicaciones de los patrones de proteínas, han sido basadas en la interacción entre éstas y otras proteínas. Los patrones de anticuerpo se han utilizado para desarrollar inmunoensayos para diversas aplicaciones. Finalmente, los patrones de ADN han permitido estudiar el comportamiento de dicha molécula en diversos sustratos y su interacción al momento de conjugarse con su secuencia complementaria.

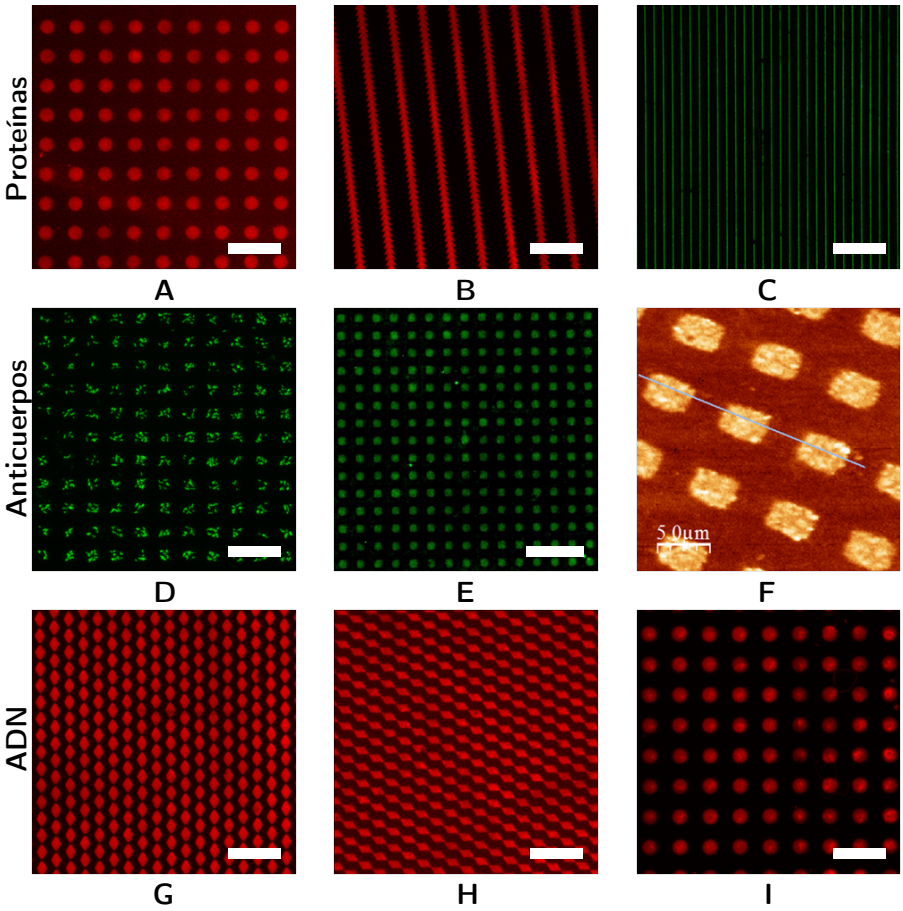

Figura 6.4: **Impresión de diversas biomoléculas.** Proteínas, anticuerpos y ADN impresos sobre varios sustratos. Imágenes de fluorescencia de las proteínas (A) WGA sobre óxido de silicio, (B) BSA sobre vidrio y PHA sobre óxido de silicio. (D) Inmunoensayo de un patrón de anticuerpos de ratón anti-*E. coli* sobre ITO.[6] (E) patrón de anticuerpos de ratón anti-5C3 conjugados con la proteína rhu-S100A4 y el anticuerpo fluorescente secundario. (F) Imagen topográfica de AFM de un patrón de anticuerpos de ratón anti-5C3.[7] Diferentes secuencias de ADN impresas: (G) FP-NH_2-T sobre vidrio, (H) FP-NH_2-T en óxido de silicio, e (I) un patrón de 5SH-3 conjugado con la cadena 5BT-3TR. Barras de escala = 30 µm excepto (F).

Finalmente, se utilizó la máquina para formar patrones biomoleculares complejos sobre diferentes sustratos para llegar al límite de los

diseños que se pueden aplicar utilizando esta técnica. La Figura 6.5 muestra una colección de patrones multiplexados de varias proteínas. Los diseños permiten evaluar la funcionalidad de la máquina así como sus ventajas y límites.

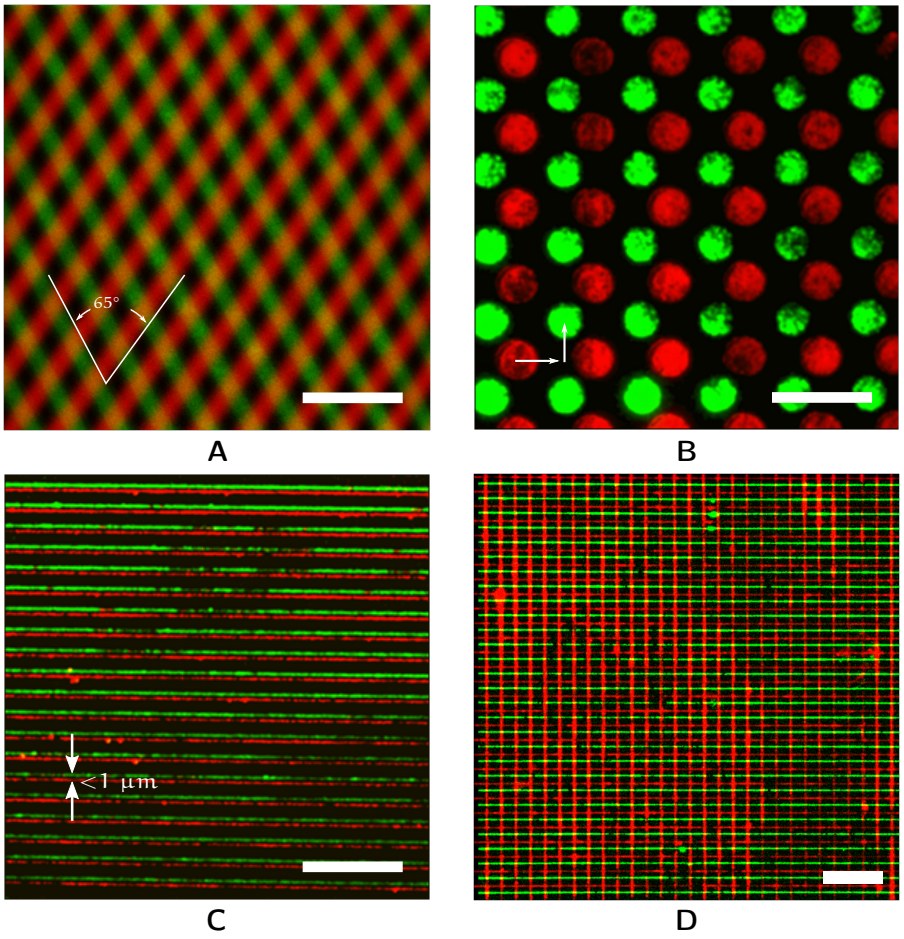

Figura 6.5: **Patrones biomoleculares complejos.** (A) Líneas de WGA en rojo y PHA en verde cruzando a 65° sobre óxido de silicio modificado. (B) Puntos de SAV en rojo y NAV sobre óxido de silicio creando un patón entrelazado al desplazar 7 µm en el eje x y 5 µm en el eje y. (C) Líneas paralelas obtenidas con WGA en rojo y PHA en verde sobre óxido de silicio. (D) Patrón realizado con dos impresiones de WGA a 90° y una tercera impresión con PHA entre las líneas paralelas anteriores. Barras de escala = 20 µm.

6.2.4 *Conclusiones*

En este capítulo se han establecido las principales limitaciones de la técnica de impresión por microcontacto que ha sido principalmente aplicada manualmente. Una herramienta automatizada de impresión ha sido descrita y caracterizada con la aplicación final de estandarizar el protocolo de impresión. Diversos patrones complejos de diferentes

moléculas han sido producidos con la máquina automatizada y han sido posteriormente caracterizados con técnicas de microscopía avanzada.

6.3 FABRICACIÓN DE MICRO*ARRAYS* MULTIPLEXADOS Y SUSPENDIDOS

6.3.1 *Introducción*

Al igual que todos los seres vivos, las funciones biológicas de los humanos están gobernadas por proteínas, formando una colección de más de 100,000 proteínas diferentes[8], ensambladas a partir de más de 293,000 diferentes péptidos.[9] El estudio de dichas proteínas es imperativo para conocer y entender el funcionamiento de nuestro cuerpo.

Los métodos de ensayo basados en la inmunoabsorción ligado a enzimas (Enzyme-linked immunosorbent assay (ELISA)) y electrotransferencia (*Western Blots*) han sido tradicionalmente utilizados para detectar y analizar proteínas en diferentes muestras. Ambos utilizan la interacción de la proteína con su anticuerpo.

Otro tipo de mecanismos de selección (*screening*) de alta densidad han sido desarrollados para acelerar el procesamiento de proteínas. Aquí se incluyen la espectroscopia de masas y la modificación genética. La espectroscopia requiere un tratamiento complejo de la proteína para que sea detectado por el espectrómetro, que relaciona su estado ionizado con la masa detectada. Por otro lado, para estudiar proteínas con modificación genética, es necesario introducir una cadena de ADN conocida a algún organismo para que traduzca la información genética en proteínas.

Todos los métodos anteriores son muy específicos y sensibles, lamentablemente sólo se puede medir una proteína por cada ensayo. Es de esperar, que la gran cantidad de proteínas presentes en los seres vivos presenta un gran reto para entender el papel que interpreta cada proteína. Afortunadamente, existe un método para estudiar la interacción de proteínas en paralelo: *arrays* de proteínas.[10–12]

El procedimiento para trabajar con *arrays* de proteínas sigue el siguiente protocolo: Primero, se crean puntos discretos de proteínas unidos covalentemente a un sustrato sólido. Aunque los puntos están localizados en una coordenada (x, y) definida, la orientación de las proteínas en el punto es aleatorio. Posteriormente se realiza un inmunoensayo con uno o varios anticuerpos que comúnmente están marcados con algún elemento fluorescente. Finalmente, se utiliza un *scanner* o un microscopio de fluorescencia para caracterizar la reacción.

Típicamente, tres métodos se utilizan para fabricar *arrays* de proteínas, por contacto, con litografía o por eyección.[13] Los métodos de fabricación por contacto transfieren una solución o proteínas adsorbidas en el lugar que el elemento impresor toca el sustrato. Los métodos basados en litografía utilizan haces de luz para cambiar la química de la superficie y permitir que la proteína se una a ésta. La

creación de patrones con AFM también entran en esta categoría aún cuando no se use luz. Finalmente, las técnicas por eyección expulsan desde el cabezal de impresión un volumen de líquído en pequeñas gotas hacia el sustrato. Evidentemente, estos métodos de fabricación crean *arrays* primordialmente en superficies planas.

Un método de *arrays* de alta densidad son los *arrays* suspendidos, que consisten en una colección de estructuras modificadas independientemente dispersas en un medio.[14] Típicamente, microesferas recubiertas con una sola proteína forman los elementos de este tipo de *arrays*. Los receptores en la superficie de las esferas son únicos, con lo que una población de las mismas micropartículas permiten obtener resultados repetidos en un mismo experimento. Este sistema tiene algunas ventajas significativas con respecto a los *arrays* planos. Primero, cada elemento en un sistema plano tiene que se fabricado individualmente, limitando la producción en paralelo, en los *arrays* suspendidos, todos los elementos son producidos en masa. Segundo, la difusión lenta de algunas moléculas a su diana en el *array* plano puede llegar a limitar las aplicaciones. La limitación de los *arrays* suspendidos está enfocada a la limitación de moléculas receptoras en su superficie. Consecuentemente, las micropartículas multiplexadas podrían sobrepasar la isotropía de los *arrays* suspendidos tradicionales, sirviendo como base para formar micro*arrays* suspendidos, ejemplificados en la Figura 6.6.

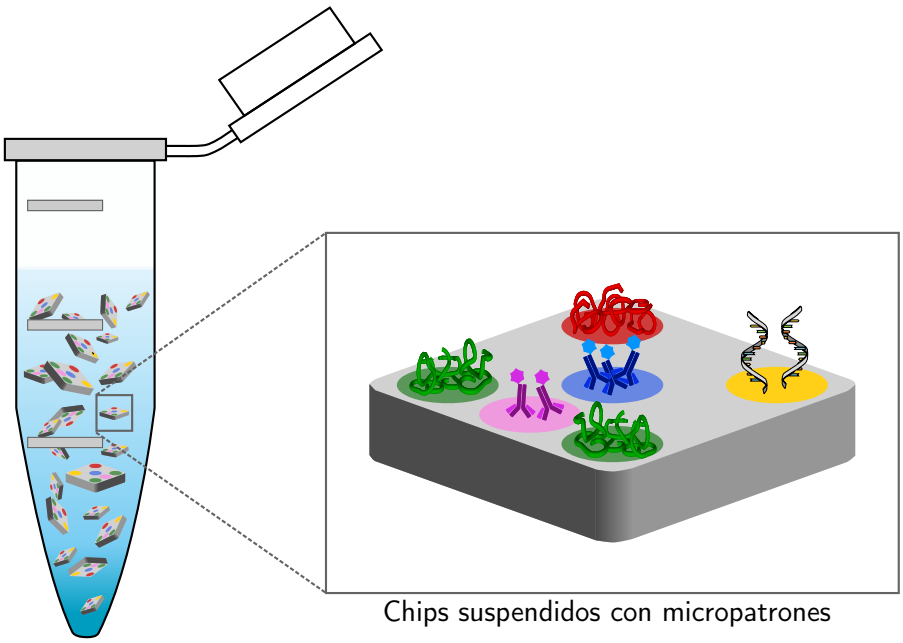

Figura 6.6: **Chips suspendidos con micropatrones.** Esquema mostrando el concepto de las micropartículas multifuncionalizadas y posteriormente suspendidas, generando así, patrones a la escala micrométrica.

6.3.2 *Metodología*

Con la colaboración del Centre Nacional de Microelectrònica (http://www.imb-cnm.csic.es/), y el Laboratorio de Química Orgánica en la facultad de Farmacia de la Universitat de Barcelona, ambos en Barcelona, España, se estableció un protocolo de activación química y de impresión para dotar de un micro*array* a cada una de las partículas dispuestas geométricamente como se muestra en la Figura 6.7A. Las dimensiones de cada micropartícula presentaban un gran reto para la creación de patrones multiplexados y simultáneos sobre todas las superficies. Inicialmente, se utilizaron los sellos utilizados en el capítulo anterior que consistían en líneas paralelas de 2.5 µm y posteriormente de 1 µm.

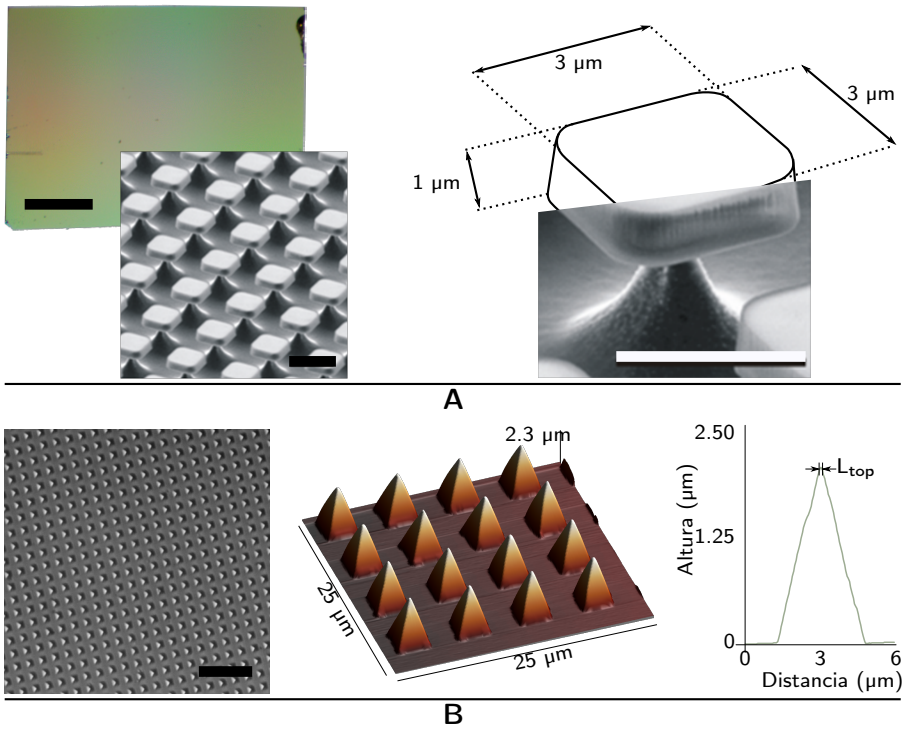

Figura 6.7: **Micropartículas inmovilizadas y sello de PDMS.** (A) Fotografía digital y de SEM del sustrato antes de la impresión, con las dimensiones de las micropartículas. (B) Imágenes de microscopía óptica y de AFM del sello utilizado. El promedio de la punta de cada pirámide es $L_{top} = 212 \pm 23$ nm. Barras de escala = 250 µm y 5 µm en (A) y 25 µm en (B).

Para poder crear micro*arrays* en cada superficie se optó por implementar la técnica de litografía de plumas poliméricas (Polymer pen lithography (PPL)).[15] Esta técnica utiliza un sello de algún polímero fabricado con pirámides invertidas para transportar la tinta a la superficie. Las puntas de las pirámides permite la creación de patrones a la escala nanométrica. En la Figura 6.7B se muestra la caracteriza-

ción óptica y topográfica del sello de PDMS utilizado para fabricar micro*arrays* sobre cada micropartícula inmovilizada. La distribución de las pirámides encaja perfectamente con la de las micropartículas, permitiendo la impresión de todo el sustrato simultáneamente.

Diferentes proteínas y un anticuerpo se imprimieron sobre las micropartículas inmovilizadas previamente funcionalizadas con una monocapa de un silano con grupos epóxidos terminales. Este silano permite la creación de enlaces covalentes entre los grupo amino de las proteínas y anticuerpos.

Un protocolo similar, funcionalizando el sustrato de micropartículas con un silano con grupo amino terminal, se siguió para imprimir fluoróforos modificados con el grupo NHS para formar un enlace covalente.

Posteriormente, se investigó un método para liberar las micropartículas manteniendo la posición y función de los elementos impresos. Se encontró un método para formar una membrana en torno a las micropartículas que serviría como matriz envolvente y que permitiría su ruptura del sustrato al momento de separarla mecánicamente. Esta membrana se disolvía en agua, obteniendo así las partículas suspendidas.

6.3.3 *Resultados y Discusión*

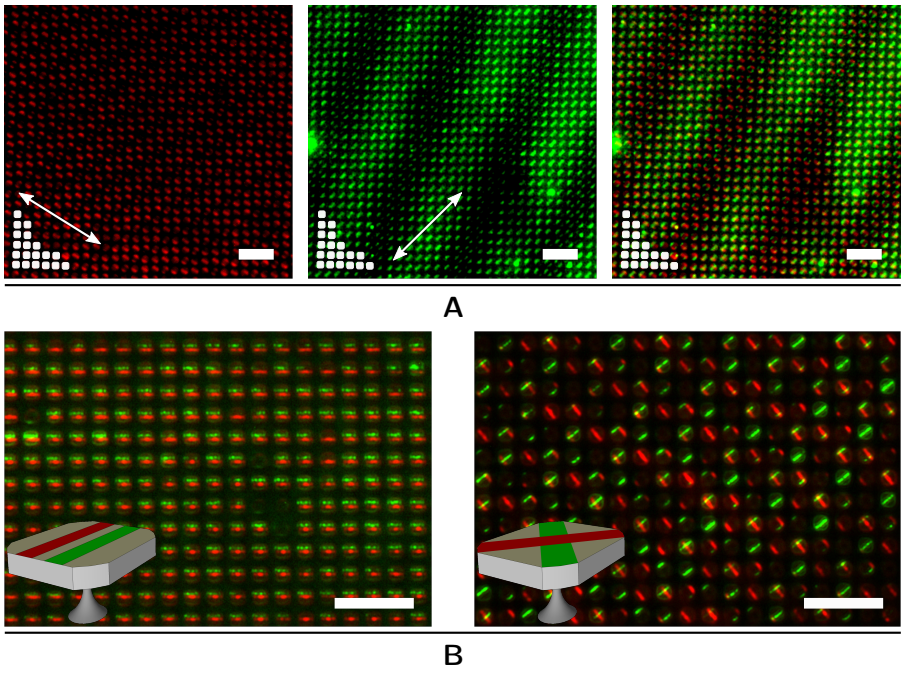

Figura 6.8: **Impresión por microcontacto sobre micropartículas.** (A) Patrones de WGA-TxR y WGA-OG488 creados con líneas de 2.5 µm. (B) Patrones obtenidos con las mismas proteínas utilizando un sello de líneas de 1 µm. Barras de escala = 20 µm.

Para analizar y caracterizar las impresiones se utilizó microscopía de fluorescencia.

La Figura 6.8 muestra los patrones obtenidos con la implementación de la impresión por microcontacto sobre las partículas fijas. Se puede observar que todas las partículas tienen ambas tintas a diferente proporción. El ángulo de impresión producido con el sello de 2.5 µm en la Figura 6.8A varía entre impresiones, limitando la reproducibilidad. Por otro lado, utilizando el sello de 1 µm, como se muestran en la Figura 6.8B, se pueden obtener impresiones más consistentes y con diversas geometrías, incrementando la aplicación de esta técnica.

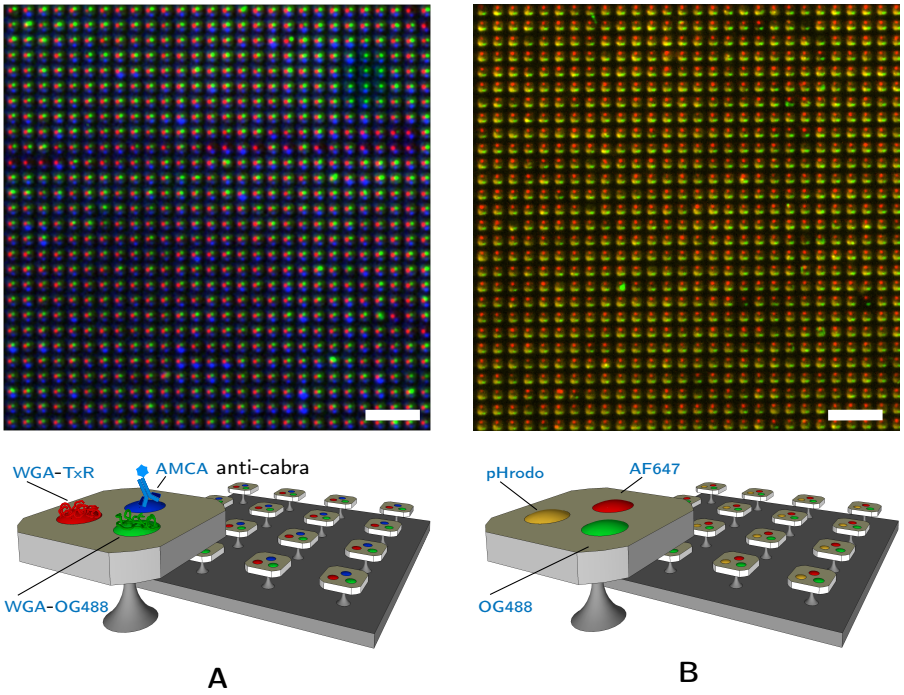

Figura 6.9: **Micro*arrays* de biomoléculas y fluoróforos.** (A) Micropartículas inmovilizadas impresas con las biomoléculas representadas en el esquema. (B) Micropartículas impresas con los puntos de fluoróforos representados en el esquema. Barras de escala = 20 µm.

Para obtener un verdadero sistema multiplexado, se presenta en la Figura 6.10 los patrones obtenidos con la técnica de PPL. Las biomoléculas y los fluoróforos forman un micro*array* sobre cada partícula, el cual se repite sobre el resto de las micropartículas. Es importante mencionar que este sistema permitiría incrementar el número de elementos sobre cada micropartícula al mantener un punto en la escala nanométrica.

Finalmente, se utilizó el sistema de la membrana para romper el anclaje de las micropartículas al sustrato. El resultado de la separación se puede ver en la Figura 6.10A donde se muestra cómo las biomoléculas impresas se mantienen en la posición de impresión.

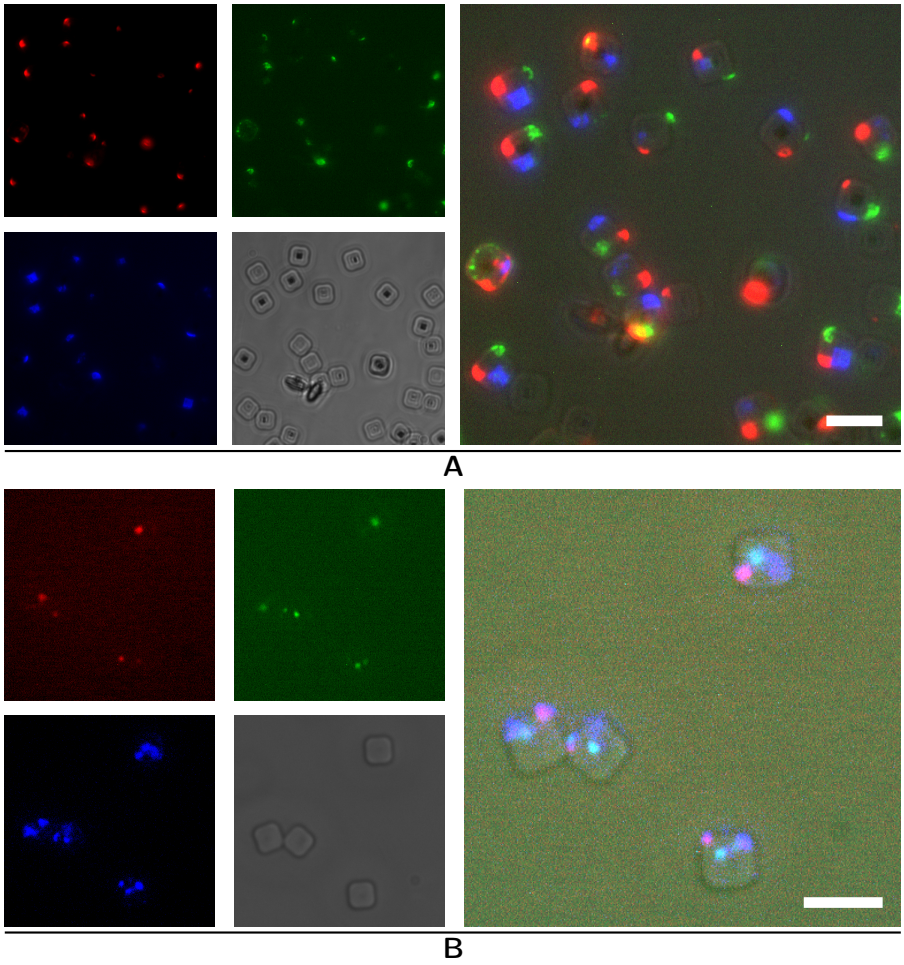

Figura 6.10: **Partículas multiplexadas liberadas.** Imágenes resultantes de los cuatro canales de emisión de los tres fluoróforos y luz visible. (A) WGA-TxR, WGA-OG488 y el anti-cabra conjugado con AMCA, representados en rojo, verde y azul respectivamente. (B) Micropartículas conjugadas con el anticuerpo secundario obteniendo la suma de emisiones en rojo y verde resultando en magenta y cian. Barras de escala = 5 µm.

Para confirmar la funcionalidad de las biomoléculas, se desarrolló un inmunoensayo que identificaría a los puntos impresos sólo si el anticuerpo era afín a la proteína inmovilizada. La suma de las emisiones de fluorescencia en la Figura 6.10B confirman la unión del anticuerpo marcado y la proteína impresa.

6.3.4 *Conclusiones*

En este capítulo se han combinado los desarrollos y protocolos estandarizados obtenidos en el primer capítulo para crear patrones miniaturizados sobre micropartículas de óxido de silicio. Se ha demostrado la compatibilidad de la máquina automatizada para crear patrones en

áreas muy reducidas. Posteriormente, se ha cimentado un protocolo de liberación para suspender las micropartículas manteniendo la función de las biomoléculas impresas.

6.4 REPLICACIÓN DE MICRO*ARRAYS* DE ADN POR CONTACTO

6.4.1 *Introducción*

Los micro*arrays* de DNA son las herramientas que presentan la mejor alternativa para el estudio y la caracterización de la expresión de genes, el genotipo, la búsqueda de polimorfismos de nucleótidos y mutaciones. Estas herramientas consisten en decenas hasta cientos de miles de puntos de sondas de ADN inmovilizadas en un sustrato. El gran número de puntos individuales permiten análisis paralelos y simultáneos para estudiar un gran número de genes o de varias regiones del genoma, dando paso a aplicaciones de alto rendimiento.[16]

La tecnología de micro*arrays* está basada en la combinación de varios campos de la investigación. Primero, mecánica, microfabricación y microfluídica son utilizados para fabricar los sustratos y posicionar las sondas en áreas definidas formando unidades discretas. Segundo, química, bioquímica y enzimología son necesarias para fijar y entender el comportamiento del ADN, incluyendo la preparación de la sonda y la diana. Finalmente, la óptica y la bioinformática son utilizadas para adquirir e interpretar los resultados.[17] El principio de funcionamiento de los micro*arrays* de ADN está cimentado en la interacción altamente específica entre la sondo inmovilizada y la diana, creando así un evento único de reconocimiento molecular, conocido como hibridación. Las secuencias diana están modificadas típicamente al incluir una molécula fluorescente o con alguna molécula de anclaje para detectar la hibridación.

De acuerdo con Dufva[18], los micro*arrays* de ADN son una alternativa mejor que la técnica de *Dot Blot* dónde las sondas son inmovilizadas en una membrana e hibridadas posteriormente con una sonda radioactiva. Primeramente, la miniaturización de los puntos mejora la sensibilidad del sistema al responder rápidamente a los cambios más sutiles. Esto también limita la cantidad de reactivos necesarios y los residuos generados. Otra ventaja es el uso de dianas marcadas con fluoróforos en lugar de moléculas radioactivas, dando paso así a estudios de hibridaciones múltiples al utilizar fluoróforos con emisiones a diferentes longitudes de onda. Finalmente, el uso de un sustrato rígido en lugar de membranas facilita el uso y manejo de las muestras.

Como lo presenta la Figura 6.11, los métodos para fabricar micro*arrays* de ADN recaen en dos categorías: *Ex situ* e *in situ*. El primer método utiliza algún medio mecánico para transportar las cadenas previamente ensambladas o sintetizadas a una posición exacta en un sustrato. La impresión por contacto cae en este método. En la categoría *in situ*, se utilizan ciclos de desprotección y reacción para unir oligonucleótidos libres en un orden específico. Principalmente se uti-

lizan métodos de radiación para eliminar el grupo protector. La luz pasa a través de una máscara o es dirigida a la posición con una matriz de microespejos. Ambos método presentan ventajas y desventajas.

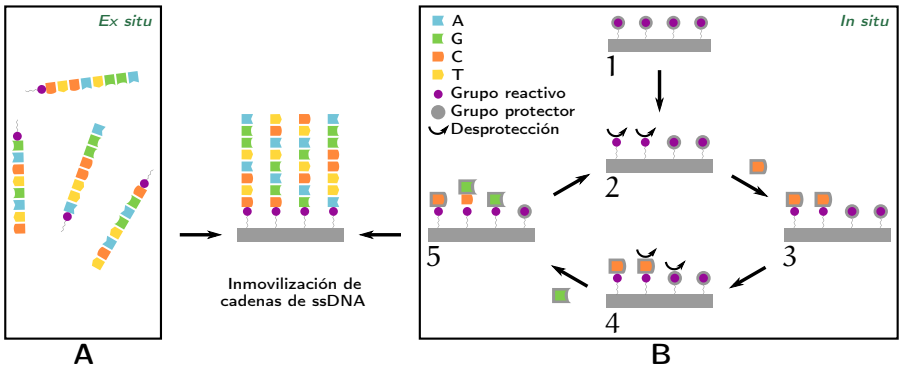

Figura 6.11: **Fabricación de *arrays* de ADN.** Dos métodos son utilizados para fabricar los micro*arrays* de ADN. (A) La propuesta *ex situ* utiliza un mecanismo para trasportar cadenas previamente ensambladas en la posición deseada. (B) El método *in situ* sintetiza en el lugar determinado la secuencia de ADN con la que se quiere trabajar. Un sustrato modificado (1), es expuesto a ciclos repetidos de desprotección selectiva, (2), seguido del ensamblado de un nucleótido, (3). La desprotección, (4), y ensamblado, (5), continua hasta obtener las cadenas completas.

Las técnicas de impresión por contacto publicadas transfieren una cadena hibridada a un nuevo sustrato, obteniendo un micro*array* formado solamente por cadenas complementarias. Para poder clonar toda la información presente en el *array* original, es necesario un segundo paso para transportar la nueva información a un tercer sustrato. El propósito de este trabajo es desarrollar un método de fabricación para crear micro*arrays* de ADN utilizando técnicas de inmovilización *ex situ* e *in situ*, superando las desventajas de ambos métodos.

6.4.2 *Metodología*

Se establecieron dos metodologías para fabricar nuevos micro*arrays*. Inicialmente se transportaron las dianas 5BT-3TR hibridadas al patrón de sondas de 5SH-3 inmovilizado a un sustrato de oro hacia un sustrato de PDMS modificado con NAV. Este paso intermedio utiliza la fuerte interacción entre la biotina presente en las cadenas 5BT-3TR para crear un enlace robusto. Posteriormente, este nuevo sustrato se expuso a una solución con las dianas 5SH-3. Después de la hibridación, se presionó hacia un nuevo sustrato de oro. El grupo tiol presente en las cadenas formaba un enlace dativo con la superficie del oro. Una separación mecánica controlada permitía el transporte de las cadenas a la posición definitiva. Ambos enlaces, el de biotina-NAV y el de tiol-

oro son lo suficientemente fuertes para dar paso a la ruptura de los puentes de hidrógeno que forman la doble cadena de ADN sin daño aparente. El resultado final permite crear micro*arrays* de oro que mantienen la distribución e información química del *array* original.

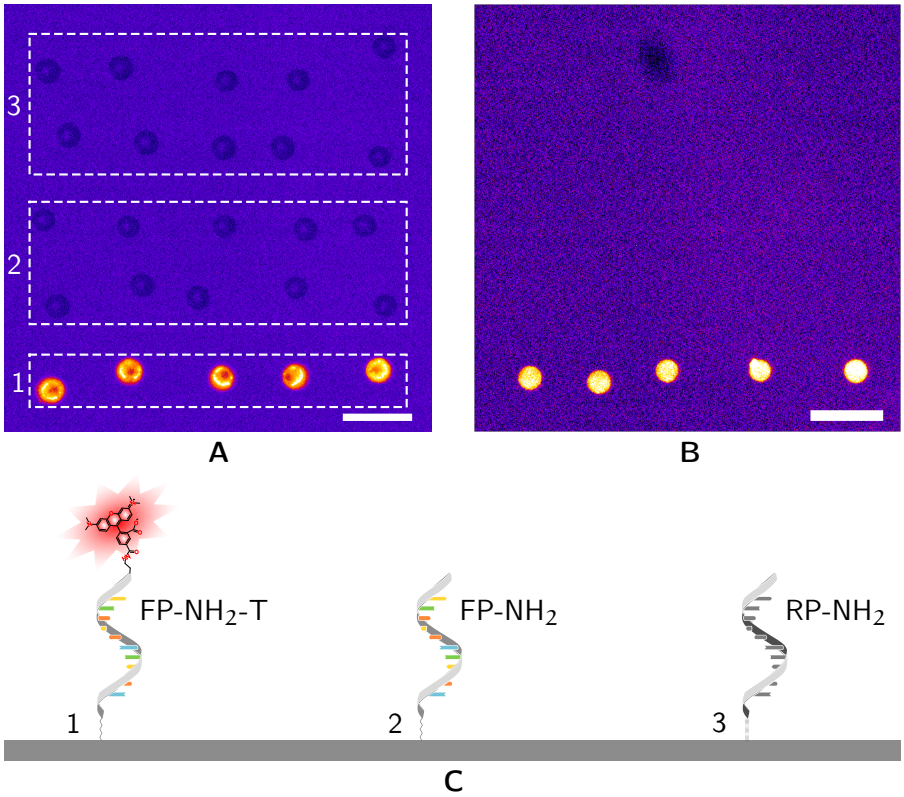

Figura 6.12: **Inmovilización de los cebadores de ADN.** imágenes de fluorescencia mostrando la posición de los puntos de los cebadores antes, (A), y después del lavado, (B). Los cebadores están representados en (C): FP-NH_2-T, FP-NH_2 y RP-NH_2, sobre PDMS funcionalizado. Barras de escala = 100 µm.

El principal límite presente en el método de replicación presentado recae en la longitud de la cadena que se desea replicar. El enlace biotina-NAV tiene un límite teórico que permitiría aguantar la fuerza de ruptura de hasta 50 bp.[19, 20] Para poder transportar cadenas más largas es necesario utilizar otro método de deshibridación. Por otro lado, este método está también limitado en el número de diferentes puntos que se quieren replicar. Para poder copiar el patrón, es necesario conocer la secuencia de los oligonucleótidos para poder transportarlos. Por esa razón, se ideó un sistema que sintetizaba las cadenas *in situ* sin depender de la secuencia. Se fabricaron una gran cantidad de sustratos con la distribución de cebadores de ADN mostrados en la Figura 6.12. La primera línea muestra puntos de cebadores marcados con el fluoróforo TAMRA para caracterizar el comportamiento durante la síntesis de las cadenas seleccionadas, seguidos de dos líneas de cebadores complementarios en dónde se dirigía el crecimiento de la cadena. En las últimas dos líneas de cebadores no complementarios,

es decir, en dónde la cadena de ADN no podría crecer. Todos los puntos fueron depositados con una impresora con un estilo.

Después de lavar y bloquear los sustratos, se expusieron a una solución con la enzima polimerasa, oligonucleótidos libres y una cadena complementaria de ADN para extender los puntos en dónde se depositaron los cebadores complementarios. Posteriormente, se introdujo a un termociclador para extender las cadenas. Seguidamente, un sustrato nuevo fue presionado sobre las cadenas para crear enlaces químicos. Después de una exposición a 95° C y separación mecánica, los sustratos fueron apartados. Una segunda extensión en el sustrato intermedio daba paso a la creación de cadenas doble de ADN, y su posterior transporte a un tercer sustrato. Este último mantenía la información química presente en el *array* original. Para confirmar la presencia de ADN inmovilizado en la superficie, se utilizaron ciclos de extensión de polimerasa para extraer la información a una solución que fue posteriormente caracterizada con electroforesis.

6.4.3 *Resultados y Discusión*

Todos los pasos necesarios para replicar el micro*array* de 5SH-3 se presentan en la Figura 6.13. Primero, en la Figura 6.13A se muestra el *array* original con la cadena complementaria 5BT-TR hibridada. Esto se confirma con la presencia de fluorescencia. Subsecuentemente, el *array* intermediario, la Figura 6.13B muestra las cadenas 5BT-TR que fueron separadas del primer *array*. La posición de los puntos refleja la posición original. Este *array* fue seguidamente expuesto a una solución con la caden 5SH-3, añadiendo un grupo activo tiol a cada una de las sondas inmovilizadas. El contacto conformal entre este sustrato intermedio y un sustrato nuevo de oro posiciona las cadenas en un unto específico. La distribución en el plano cartesiano es ahora una réplica exacta a la del *array* original. La información química se mantiene a través de todo el proceso, siendo esto comprobado con la hibridación de la cadena 5BT-TR mostrada en la Figura 6.13C. Ya que la emisión de fluorescencia es directamente proporcional a la cantidad de moléculas inmovilizadas, este parámetro puede ser utilizado para realizar una comparativa y calcular la eficiencia de transferencia entre cada paso. La intensidad promedio obtenida de los valores de emisión corresponden a 685.59 ± 34.28, 596.08 ± 14.78 y 523.87 ± 14.95 a.u. en cada un de los casos. Es evidente que hay pérdida de intensidad entre los pasos. En ambos casos, entre el sustrato original y el intermedio, y entre el intermedio y el último sustrato, la eficiencia de transferencia rondaba el ~87 %. Esto da una eficiencia total de ~76 % desde el original y el último.

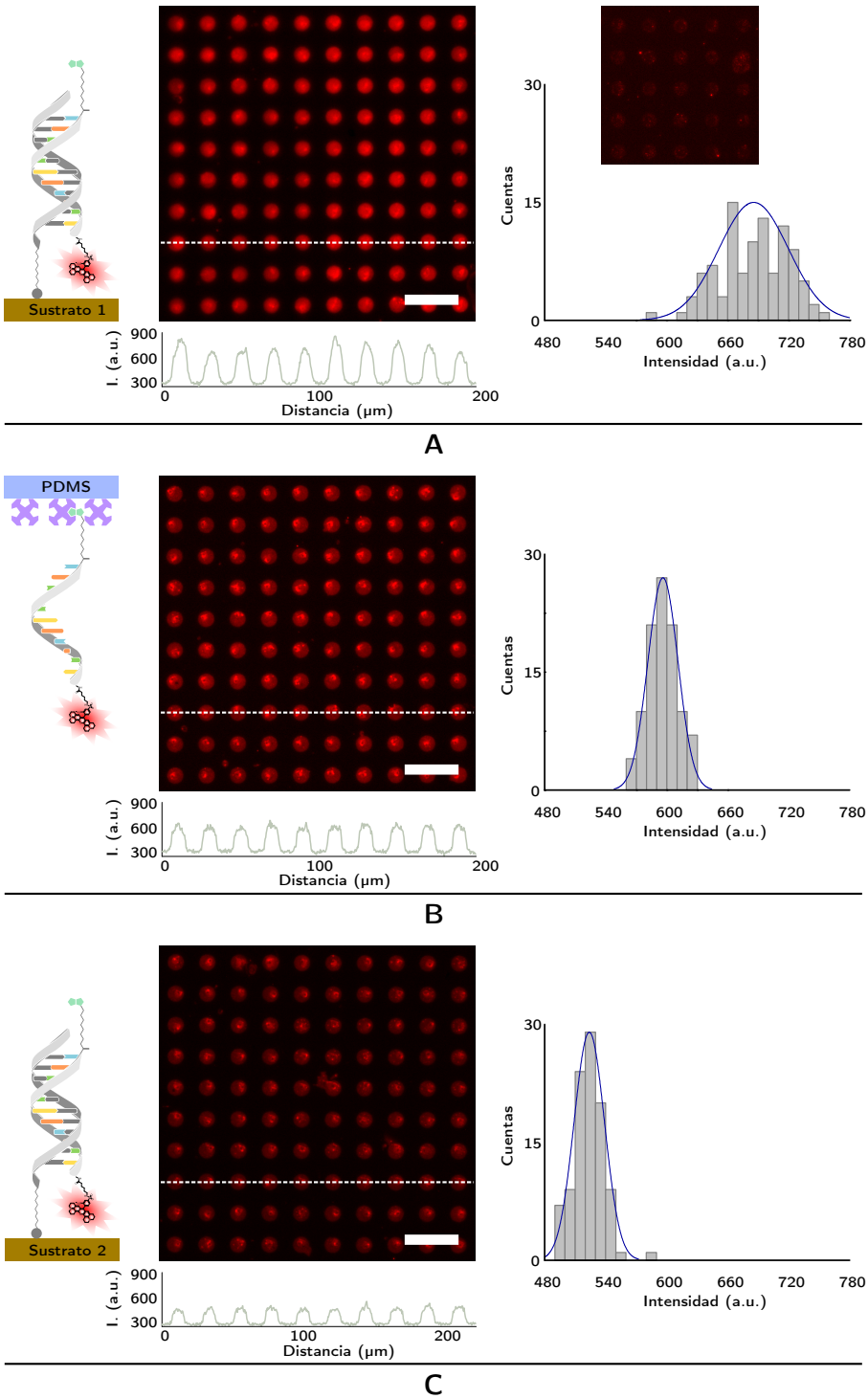

Figura 6.13: **Replicación por contacto de cadenas hibridadas.** Imágenes de microscopía de fluorescencia de los *arrays* fabricados y copiados. (A) Un *array* de las cadenas 5SH-3 inmovilizadas en oro e hibridadas con 5BT-3TR. (B) Muestra las cadenas previamente hibridadas ahora transferidas a un nuevo PDMS modificado con NAV. Este *array* fue posteriormente hibridado con 5SH-3 e impreso sobre un sustrato nuevo de oro. (C) Presenta este último patrón hibridado con 5BT-3TR. Los valores de la intensidad de los puntos representan una distribución Gaussiana ($n = 100$). Barras de escala = 50 μm.

Para la creación de micro*arrays* sintetizando las secuencias de ADN, se estudió la extensión de las moléculas a diferentes ciclos térmicos. Los sustratos con los cebadores y la emisión con el cebador de reversa dotado con el fluoróforo Cy3 se muestran en la Figura 6.14. Se puede ver claramente la influencia del número de ciclos necesarios para extender las cadenas en la superficie. Para poder comparar entre sustratos, se definió un sistema de normalización de valores de emisión. Primero, se midió la cantidad de cebadores que se perdían con los cíclos de temperatura. En la curva de la izquierda de la Figura 6.14 se muestra un resumen de las intensidades de los puntos control después de los ciclos de PCR. Es evidente una pérdida inicial de señal, pero afortunadamente se mantiene constante a través de los siguientes ciclos. La curva de la derecha muestra la intensidad normalizada de los puntos extendidos con respecto a la emisión de los puntos control. Se observa el crecimiento exponencial de la emisión fluorescente entre los ciclos 20 y 30, hasta llegar a una meseta después del ciclo 35, donde ya no hay más extensión de ADN.

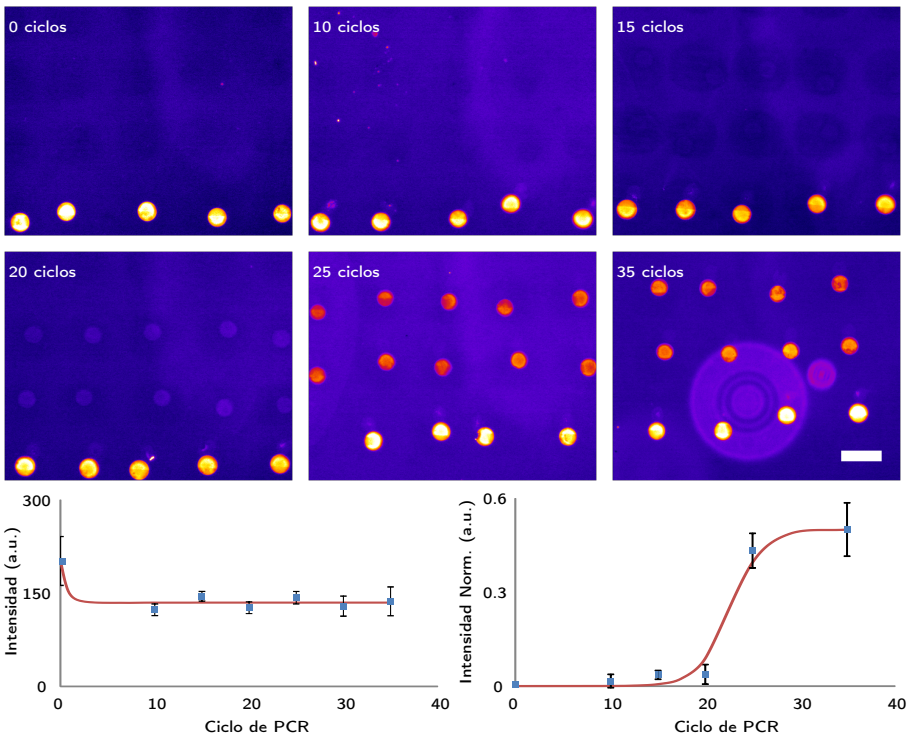

Figura 6.14: **Emisión de fluorescencia de los puntos después de SP-PCR.** Puntos de FP-NH_2-T impresos después de 0, 10, 15, 20, 25, 30, o 35 ciclos de SP-PCR. La curva de la izquierda muestra la emisión constante de fluorescencia después de una pérdida inicial. Por otro lado, la curva de la derecha muestra la emisión normalizada de los puntos tomando como referencia la emisión de los puntos de control, mostrando el crecimiento exponencial entre los ciclos 20 y 30, llegando a una meseta después de 35 ciclos. Barra de escala = 100 µm.

En lugar de utilizar cebadores marcados con un fluoróforo, se continuó con cebadores con un grupo amina que reaccionarían con el grupo epóxido presente en los sustratos de PDMS subsecuentes. Después de la extensión con los cebadores con amina, se produjo un contacto conformal con otro sustrato modificado. La transferencia del ADN se confirmó con la extracción de éste mostrado en las bandas presentes en el gel de electroforesis en la Figura 6.15A. Para la última réplica, se extendieron las cadenas presentes en la cadena intermedia y se transportaron al último sustrato. Las bandas que se observan claramente en la Figura 6.15B confirman el traspaso de información.

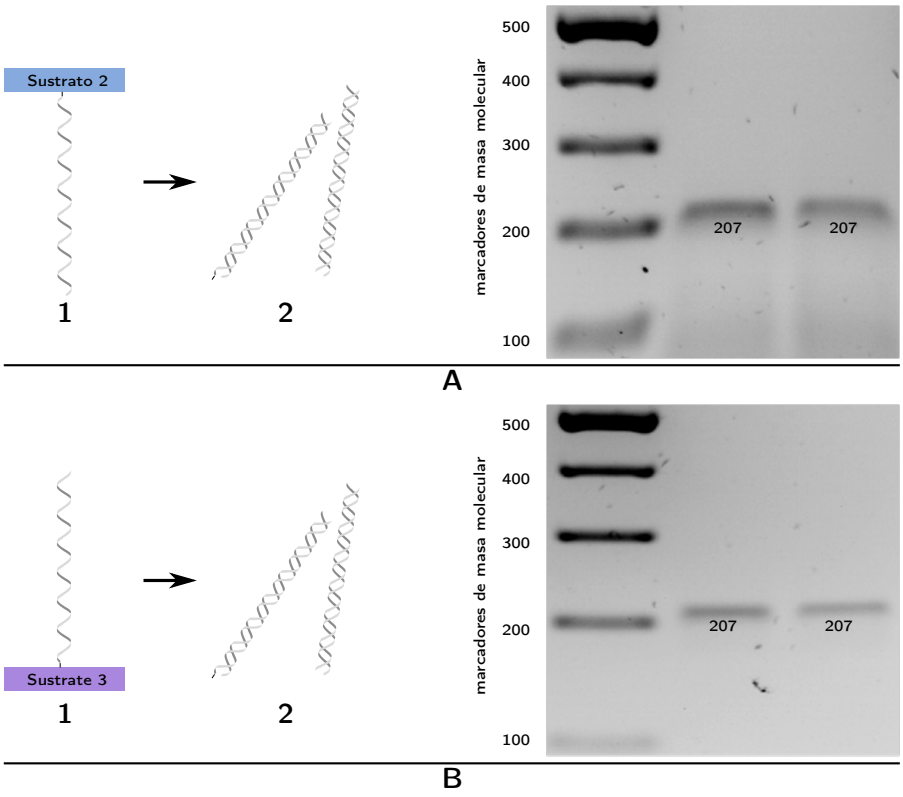

Figura 6.15: **Secuencia de ADN en el paso intermedio y final.** (A) La secuencia de ADN del sustrato 2 es multiplicada y posteriormente caracterizada por electroforesis para separar las cadenas replicadas. La presencia las bandas con una masa de 207 bp confirman la extracción de la información. (B) De la misma manera, la información presente en el último sustrato se caracterizó con electroforesis, en donde el ADN está presente en las bandas de 207 bp.

6.4.4 *Conclusiones*

En este capítulo se han demostrado dos métodos para fabricar *arrays* de ADN por replicación basada en contacto. El primer método está basado en la transferencia de cadenas por deshibridación mante-

niendo la localización e información presente en el *array* original. El segundo método utilizó el crecimiento enzimático para extender las cadenas de ADN que fueron posteriormente transferidas a sustratos nuevos. En ambos métodos, la información química almacenada en las superficies fue replicada íntegramente.

6.5 REFERENCIAS

[1] Kumar, A and Whitesides, GM. 'Features of gold having micrometer to centimeter dimensions can be formed through a combination of stamping with an elastomeric stamp and an alkanethiol "ink" followed by chemical etching'. *Applied Physics Letters*, 63 (14) (1993) 2002. URL http://link.aip.org/link/APPLAB/v63/i14/p2002/s1&Agg=doi

[2] Vericat, C; Vela, ME; Benitez, G; Carro, P; and Salvarezza, RC. 'Self-assembled monolayers of thiols and dithiols on gold: new challenges for a well-known system.' *Chemical Society reviews*, 39 (5) (2010) 1805–34. URL http://www.ncbi.nlm.nih.gov/pubmed/20419220

[3] Wang, M; Liechti, KM; Wang, Q; and White, JM. 'Self-assembled silane monolayers: fabrication with nanoscale uniformity.' *Langmuir*, 21 (5) (2005) 1848–57. URL http://www.ncbi.nlm.nih.gov/pubmed/15723481

[4] Liao, X; Braunschweig, AB; Zheng, Z; and Mirkin, CA. 'Force- and time-dependent feature size and shape control in molecular printing via polymer-pen lithography.' *Small*, 6 (10) (2010) 1082–6. URL http://www.ncbi.nlm.nih.gov/pubmed/19859944

[5] Johnston, ID; McCluskey, DK; Tan, CKL; and Tracey, MC. 'Mechanical characterization of bulk Sylgard 184 for microfluidics and microengineering'. *Journal of Micromechanics and Microengineering*, 24 (3) (2014) 035017. URL http://stacks.iop.org/0960-1317/24/i=3/a=035017?key=crossref.cf83b17be3210f20943ae0e9169fc9b8

[6] Barreiros dos Santos, M; Azevedo, S; Agusil, J; Prieto-Simón, B; Sporer, C; Torrents, E; Juárez, A; Teixeira, V; and Samitier, J. 'Label-free ITO-based immunosensor for the detection of very low concentrations of pathogenic bacteria'. *Bioelectrochemistry*, 101 (2015) 146–152. URL http://linkinghub.elsevier.com/retrieve/pii/S1567539414001558

[7] González, L; Otero, J; Agusil, JP; Samitier, J; Adan, J; Mitjans, F; and Puig-Vidal, M. 'Micropattern of antibodies imaged by shear force microscopy: comparison between classical and jumping modes.' *Ultramicroscopy*, 136 (2014) 176–84. URL http://www.ncbi.nlm.nih.gov/pubmed/24184681

[8] Pandey, A and Mann, M. 'Proteomics to study genes and genomes'. *Nature*, 405 (June) (2000) 837–46. URL http://www.nature.com/nature/journal/v405/n6788/abs/405837a0.html

[9] Kim, MS; Pinto, SM; Getnet, D; Nirujogi, RS; Manda, SS; Chaerkady, R; Madugundu, AK; Kelkar, DS; Isserlin, R; Jain, S; Thomas, JK; Muthusamy, B; Leal-Rojas, P; Kumar, P; Sahasrabuddhe, NA; Balakrishnan, L; Advani, J; George, B; Renuse, S; Selvan, LDN; Patil, AH; Nanjappa, V; Radhakrishnan, A; Prasad, S; Subbannayya, T; Raju, R; Kumar, M; Sreenivasamurthy, SK; Marimuthu, A; Sathe, GJ; Chavan, S; Datta, KK; Subbannayya, Y; Sahu, A; Yelamanchi, SD; Jayaram, S; Rajagopalan, P; Sharma, J; Murthy, KR; Syed, N; Goel, R; Khan, AA; Ahmad, S; Dey, G; Mudgal, K; Chatterjee, A; Huang, TC; Zhong, J; Wu, X; Shaw, PG; Freed, D; Zahari, MS; Mukherjee, KK; Shankar, S; Mahadevan, A; Lam, H; Mitchell, CJ; Shankar, SK; Satishchandra, P; Schroeder, JT; Sirdeshmukh, R; Maitra, A; Leach, SD; Drake, CG; Halushka, MK; Prasad, TSK; Hruban, RH; Kerr, CL; Bader, GD; Iacobuzio-Donahue, CA; Gowda, H; and Pandey, A. 'A draft map of the human proteome.' *Nature*, 509 (7502) (2014) 575–81. URL http://www.ncbi.nlm.nih.gov/pubmed/24870542

[10] Hall, DA; Ptacek, J; and Snyder, M. 'Protein microarray technology.' *Mechanisms of ageing and development*, 128 (1) (2007) 161–7. URL http://www.pubmedcentral.nih.gov/articlerender.fcgi?artid=1828913&tool=pmcentrez&rendertype=abstract

[11] Templin, MF; Stoll, D; Schrenk, M; Traub, PC; Vöhringer, CF; and Joos, TO. 'Protein microarray technology'. *TRENDS in Biotechnology*, 20 (4) (2002) 815–22. URL http://www.ncbi.nlm.nih.gov/pubmed/12546969

[12] Sun, H; Chen, GYJ; and Yao, SQ. 'Recent advances in microarray technologies for proteomics.' *Chemistry & biology*, 20 (5) (2013) 685–99. URL http://www.ncbi.nlm.nih.gov/pubmed/23706635

[13] Romanov, V; Davidoff, SN; Miles, AR; Grainger, DW; Gale, BK; and Brooks, BD. 'A critical comparison of protein microarray fabrication technologies.' *The Analyst*, 139 (6) (2014) 1303–26. URL http://www.ncbi.nlm.nih.gov/pubmed/24479125

[14] Nolan, JP and Sklar, LA. 'Suspension array technology: evolution of the flat-array paradigm.' *TRENDS in Biotechnology*, 20 (1) (2002) 9–12. URL http://www.ncbi.nlm.nih.gov/pubmed/11742671

[15] Huo, F; Zheng, Z; Zheng, G; Giam, LR; Zhang, H; and Mirkin, CA. 'Polymer pen lithography.' *Science*, 321 (5896) (2008) 1658–60. URL http://www.ncbi.nlm.nih.gov/pubmed/18703709

[16] Heise, C and Bier, FF. 'Immobilization of DNA on Microarrays'. In 'Immobilisation of DNA on Chips II', volume 261, pages 1–25. Springer-Verlag Berlin, Berlin (2006). URL http://link.springer.com/book/10.1007/11544432

[17] Dufva, M. *DNA Microarrays for Biomedical Research: Methods and Protocols*. Humana Press, Hatfield, Hertfordshire, UK (2009). URL http://link.springer.com/content/pdf/10.1007/978-1-59745-538-1.pdf

[18] Dufva, M. 'Fabrication of high quality microarrays.' *Biomolecular engineering*, 22 (5-6) (2005) 173–84. URL http://www.ncbi.nlm.nih.gov/pubmed/16242381

[19] Morfill, J; Kühner, F; Blank, K; Lugmaier, RA; Sedlmair, J; and Gaub, HE. 'B-S transition in short oligonucleotides.' *Biophysical journal*, 93 (7) (2007) 2400–9. URL http://www.pubmedcentral.nih.gov/articlerender.fcgi?artid=1965448&tool=pmcentrez&rendertype=abstract

[20] Severin, PMD; Ho, D; and Gaub, HE. 'A high throughput molecular force assay for protein-DNA interactions.' *Lab on a chip*, 11 (5) (2011) 856–62. URL http://www.ncbi.nlm.nih.gov/pubmed/21221429

A

APPENDIXES

A.1 FABRICATION AND CHARACTERIZATION TECHNIQUES

A.1.1 *Atomic force microscopy (AFM)*

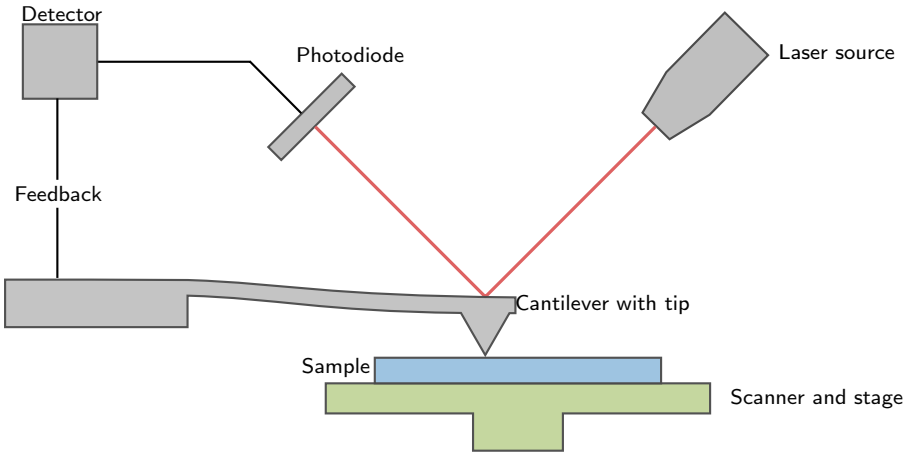

Figure A.1: **Schematic diagram of an AFM.** A microfabricated cantilever with a sharp tip on its underside is located on top of the sample to analyze. A laser is beamed at the backside of the cantilever and reflected towards a four quadrant photodiode. The sample is moved under the tip, any deflection of the tip following the surface of the sample translates on the change of the position of the reflected laser. The surface topography is measured by the deflection of the laser spot on the photodiode. A feedback system maintains the tip close enough to the sample.

A scanning probe microscope drags a micromachined sharp tip over a sample to study the topography of its surface and reconstructs it as image. Atomic force microscopy AFM is a high-resolution scanning probe microscope used to characterize the surfaces down to the nanoscale. A very sharp probe with a tip-radius of a few nm is raster-scanned across the surfaces. When the tip is lowered to the substrate, molecular interactions deflect the cantilever towards the surface. To measure the deflection, a laser spot is beamed at the back side of the cantilever and reflected to a set of photodiodes. Any change in the reflection is recorded to reconstruct a topographical image of the surface. To prevent damage to the fragile probe, a feedback systems is constantly monitoring the attractive and repulsive forces between

substrate and tip, raising or lowering the entire cantilever accordingly. The AFM set-up is presented in Figure A.1.

Two scanning modes are traditionally used: contact and tapping modes. Contact mode consists in recording the deflection of the tip by the direct interaction with the sample. Tapping mode requires the cantilever to be externally stimulated to oscillate at its resonance frequency. When the oscillating tip approaches the substrate, the amplitude of the oscillation changes. Anya change in contact or tapping mode is recorded by the displacement of the laser spot on the photodiode.

A Dimension 3100 equipment from Veeco Instruments (Plainview, NY, USA) was used to obtain all the AFM images.

A.1.2 *Direct write laser lithography (DWL)*

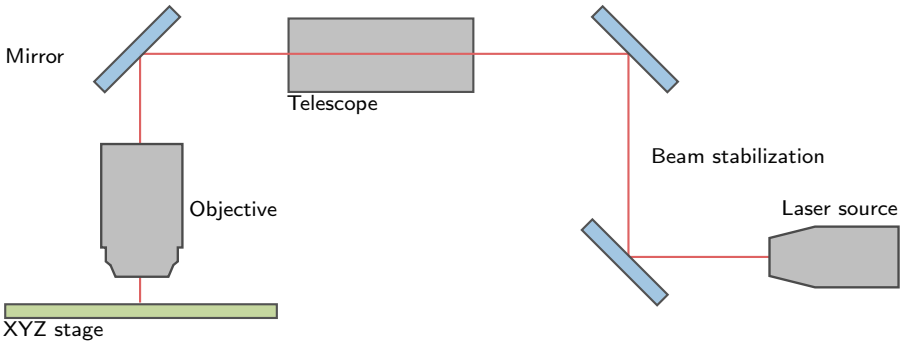

Figure A.2: **Schematic diagram of DWL.** A silicon wafer is coated with a thin photoresist film. A laser travels through an optical arrangement and changes the chemical composition of the film at the focusing point. The micropattern is resolved when the exposed resist is removed.

Direct write laser lithography was used to fabricate masters to replicate the PDMS stamps. Figure A.2 shows a schematic of the components of this equipment. Initially, a SiOx wafer was coated with 1.4 μm of AZ© 1512 positive photoresist from MicroChemicals GmbH (Ulm, Germany) using a spin coater at 2000 rpm for 30 s form Laurell Technologies Corp. (North Wales, PA, USA), and lastly baked at 95 °C for 2 min to evaporate any solvent left in the resist. Then, the wafer was placed on the XYZ-stage inside the DWL 66FS maskless lithography equipment from Heidelberg Instruments Mikrotechnik GmbH (Heidelberg, Germany). The stage positioned the spin-coated wafer to the desired location. Afterwards, the shutter was opened to let the 405 nm, 50 mW laser through a focusing lens, and illuminated the exposed photoresist. The movement of the stage follows a previously introduced design. After the illuminating process, the wafer was submerged in AZ© 726MIF developer from Microchemical GmbH (Ulm,

Germany) for 6 s and immediately afterwards rinsed with Milli-Q water. This process removes the resolved resist, leaving the wafer with microstructures. The exposed silicon was later etched and the rest of the photoresist washed away to reveal the final form of the master. This technique was used to fabricate the stamps described in Chapter 2.

A.1.3 *Scanning electron microscopy (SEM)*

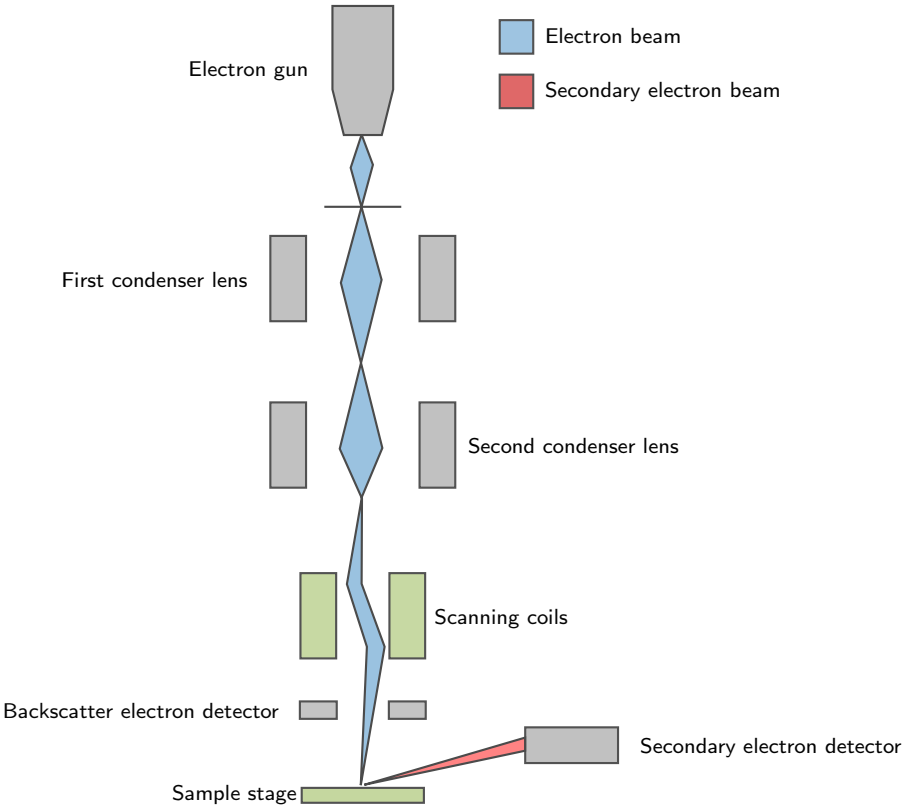

Figure A.3: **Schematic diagram of SEM.** An electron beam produced by and electron gun is condensed and directed towards a sample. The raster-scanned specimen produces secondary electrons which are captured by the detector and transformed into an image.

A method to characterize the surface of a sample with nanoscopic resolution is Scanning Electron Microscopy SEM. Instead of photons, this technique uses the interaction between an electron beam produced by a tungsten filament cathode and the atoms of the surface of the sample. The interaction between the electron beam and the substrate results in the emission of high energy electrons, secondary electrons and x-rays. These emissions are collected by dedicated detectors to obtain the surface information as topography, composition or electrical conductivity. As showin in Figure A.3, the electron beam

is accelerated and focused by two condenser lens and deflected to raster-scan a sample with a pair of scanning coils. A Nova NanoSEM 230 microscope from FEI Co. (Hillsboro, OR, USA) was used to characterize the SiOx masters used to fabricate the PDMS stamps used throughout the Thesis.

A.1.4 *Optical microscopy and fluorescence microscopy*

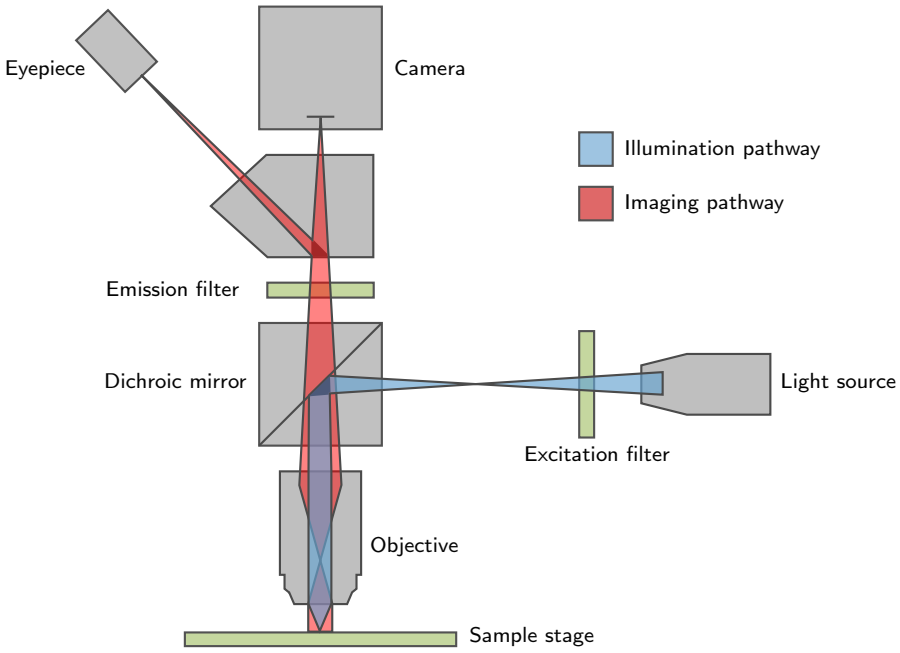

Figure A.4: **Schematic diagram of a fluorescence microscope.** A light beam generated from a Hg lamp crosses the excitation filter where only the chosen wavelengths pass. The beam is reflected towards the sample with a dichroic mirror. The light shines back to the microscope and is filtered through an emission filter to be directed towards the eyepiece or camera.

Figure A.4 presents and schematic view of the components of fluorescence microscopy. Initially, a full spectrum light beam is generated in a Hg lamp and directed towards an excitation filter. This filter permits the pass of a defined wavelength range. Later, the filtered light is reflected towards the sample placed below an objective with a dichroic mirror. The objective is a stack of lenses and its function is to collect the light from the sample. The light bounces from the sample and is directed back to the microscope. The optical path intersects the dichroic mirror, and the beam later crosses an emission filter. As in the excitation filter, it only allows a narrow band of light with the selected wavelength. The filtered light is then diverted towards the user through the eyepieces or at a camera to capture a photograph. An Eclipse E1000 Fluorescence microscope from Nikon

(Chiyoda, Tokyo, Japan) was used to capture the fluorescence images presented in the thesis.

A.1.5 *Confocal microscopy*

Another system, with higher resolution to characterize fluorescent samples is confocal microscopy. As presented in Figure A.5, a laser beam is directed towards the sample using point illumination as it crosses a pinhole. The light excites any fluorescent probe on the sample and the emission returns to the microscope through the objective. The addition of a pinhole at the confocal plane of the lens blocks any out-of-focus emission. This increases the optical resolution in the sample depth. The TCS SP2 confocal microscope from Leica Microsystems GmbH (Wetzlar, Germany) was used to obtain the confocal images presented in the this Thesis.

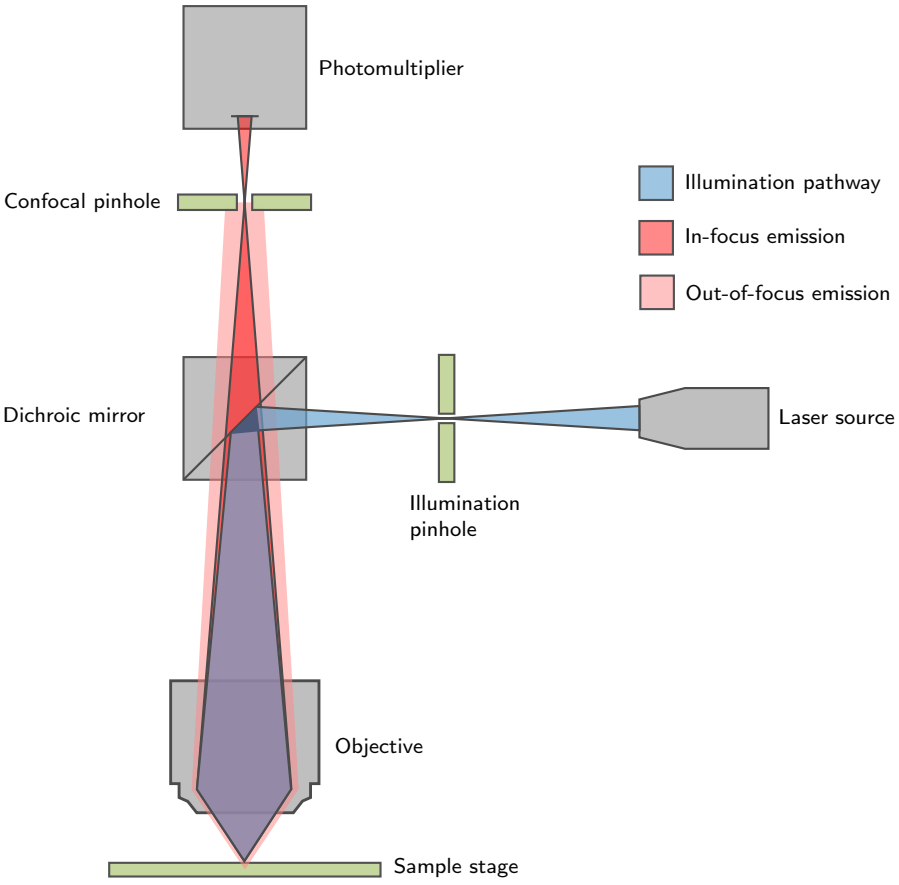

Figure A.5: **Schematic diagram of a confocal microscope.** A source emits a laser which passes through a pinhole, and it is later directed towards the sample. The emission from all the focal planes in the sample are returned to the system. Only the light from the desired focal plane is able to pass through the confocal pinhole and reach the photomultiplier.

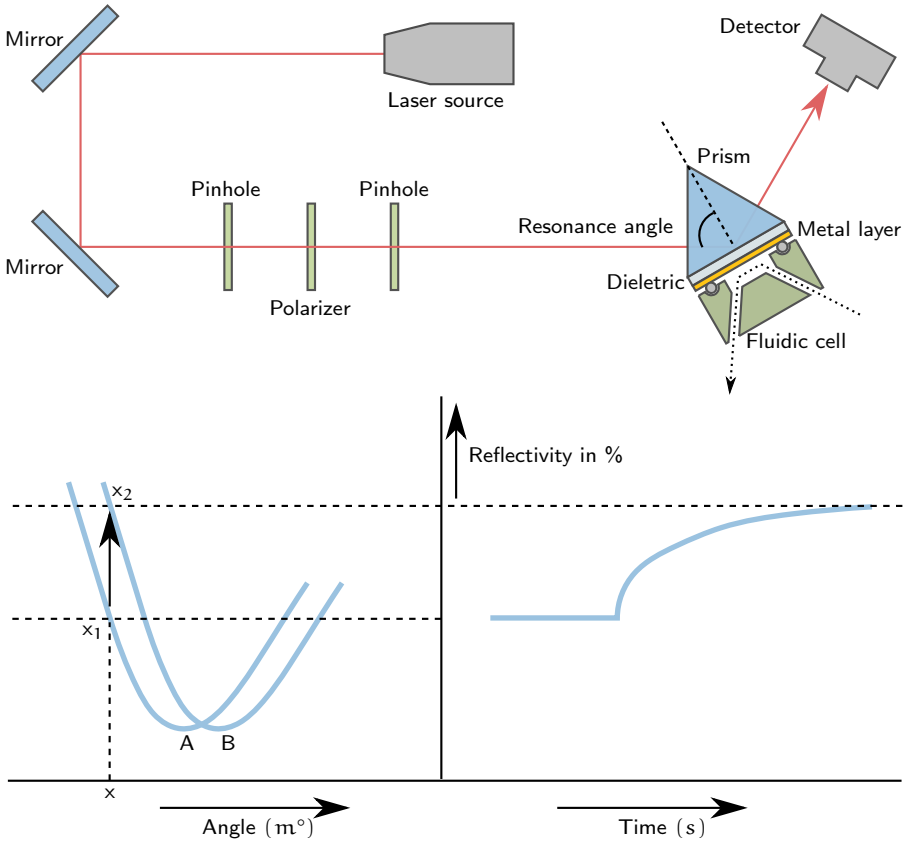

Figure A.6: **Schematic and principle of SPR.** A laser beam is polarized and directed towards a prism located on top of a specialized chip with a thin metal layer. The laser is absorbed at the resonance angle, which depends on the properties of the metal-dielectric interface. A fluidic cell changes the thickness the interface depositing matter on top of the chip.

Electrons oscillate collectively when stimulated by incident light. When the frequency of the incident photons matches the frequency of the electrons on the surface, a resonance condition is established producing surface plasmons. These are electromagnetic waves that travel parallel to a metal-dielectric interface and are very sensity to any change in this interface. The SPR equipment shown in Figure A.6 illuminates a thin metal layer with a laser. At a certain angle of incidence the light is adsorbed producing surface plasmons. This resonance angle depends on the refractive index of the dielectric, any adsorbed molecule in the interface produces a change on the refractive index, displacing the resonance angle which can be related to the thickness of the adsorbed layer. The Fresnel equations correlate the displacement of the resonance angle to the thickness of the adsorbed layer.[1] SPR was used in Chapter 4 to calculate the hybridization efficiency of immobilized DNA strands.

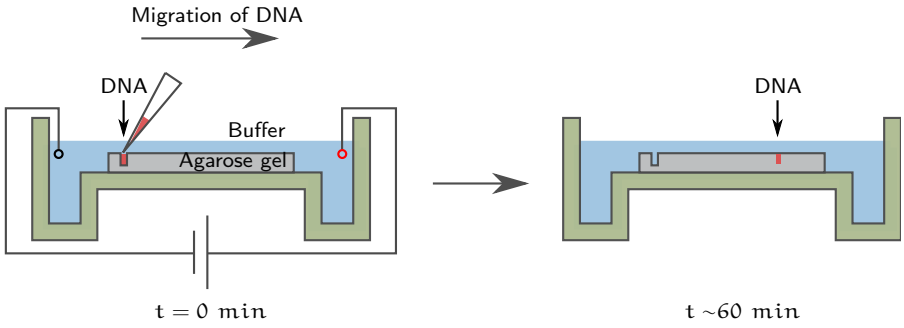

Figure A.7: **Schematic of DNA gel electrophoresis.** The negative nature of DNA allows the migration when subjected to an electric field.

DNA gel electrophoresis is a method to separate DNA strands based on their size. This technique uses an electric field to force the movement of DNA strands through a gel. The gel serves as an obstacle matrix where the negatively-charged strands are attracted towards the anode, while being repelled by the cathode. Initially, as presented in Figure A.7, the sample is loaded into an opening present at the beginning of the gel. The complete set-up is submerged in a conductive buffer and a D.C. electrical field is applied. Large DNA molecules move more slowly through the matrix while shorter molecules move faster. The SYBR© Safe fluorescent stain from Life Technologies (Carlsbad, CA, USA) is used to identify the separated bands along the gel. Gel electrophoresis was used in Chapter 4 first to separate and later to characterize the replication of DNA.

A.2 OLIGONUCLEOTIDE STRANDS

The oligonucleotides presented in Table A.1 were obtained from different suppliers. FP-NH_2-T, FP-NH_2, and RP-NH_2 were purchased from biomers.net GmbH, (Ulm, Germany), the 5BT-3TR, 5SH-3, and 5OG-3 strands from Metabion, GmbH (Planegg, Germany), and finally, the TB-ropB gene, and the FP1, FP2 and the RP-Cy3 strands from Bioneer (Daejeon, South Korea).

Table A.1: Reference to the identification and sequence of the oligonuclotide strands

CODE	SEQUENCE (5′ → 3′)
5BT-3TR	Biotin-AAG CCG TCA CGT AGT GCG CCA-TxR
5OG-3	OG_{488}-CAA GAC CGA GCT GAT CAA ACC
5SH-3	SH-TGG CGC ACT ACG TGA CGG CTT
FP1	GGT TTG ATC AGC TCG GTC TTG
FP-NH_2	NH_2-C_6-10(T) GGT TTG ATC AGC TCG GTC TTG
FP-NH_2-T	NH_2-C_6-10(T) GGT TTG ATC AGC TCG GTC TTG-TAMRA
RP1	CAT CTG GAC CCG CCA ACA AG
RP-Cy3	CAT CTG GAC CCG CCA ACA AG-Cy3
RP-NH_2	NH_2-C_6-10(T) CAT CTG GAC CCG CCA ACA AG

The oligonucleotides were dissolved in nuclease-free water from Thermo Fisher Scientific, Inc. (Rockford, IL, USA) to a final concentration of 100 µM and stored at −20 °C until used.

The extendable DNA strand (TB-ropB) was a sequence of 207 bp from the *rpoB* gene of *Mycobacterium tuberculosis*:

GGT TTG ATC AGC TCG GTC TTG TAT AGG CCG TTG
ATC GTC TCG GCT AGT GCA TTG TCA TAG GAG CTT
CCG ACC GCT CCG ACC GAC GGT TGG ATG CCT GCC
TCG GCG AGC CGC TCG CTG AAC CGG ATC GAT GTG
TAC TGA GAT CCC CTA TCC GTA TGG TGG ATA ACG
TCT TTC AGG TCG AGT ACG CCT TCT TGT TGG CGG
GTC CAG ATG

This *rpoB* site of mutation renders resistance to rifamycin antibacterial agents.[2]

A.3 SOFTWARE CODE

A.3.1 *Image analysis with ImageJ*

The following Macro was used to analyze each and every printed spot on the anchored microparticles on Section 3.5.2.2.

```
requires("1.48d");
Dialog.create("Max x Factor");
Dialog.addNumber("Factor:",
    0.5);
Dialog.show();
factor = Dialog.getNumber();
run("Clear Results");
result1 = getTitle;
run("Duplicate...", "title="+
    result1+" duplicate range =
    1-"+nSlices);
run("Flip Vertically");
run("Split Channels");

//+++++RED CHANNEL+++++
selectWindow("C1-"+result1);
title = getTitle;
run("8-bit");
run("Add...", "value=1");
open("/Users/Juan Pablo/Desktop
    /Macros/mask1.tif");
imageCalculator("Multiply
    create", title, "mask1.tif")
    ;
result = getTitle;
selectWindow("mask1.tif");
run("Close");
selectWindow(result);
w = getWidth;
h = getHeight;
counts = 0;
for (y=0; y<h; y++)
{
 for (x=0; x<w; x++)
 {
  if ((getPixel(x,y) == 0) && (
      getPixel(x+1,y) == 0) && (
      getPixel(x,y+1) == 0) && (
      getPixel(x+1,y+1) != 0))
  {
   counts++;
  }
 }
}
coord = newArray(counts*2);
Array.fill(coord, 0);
coord2 = newArray(counts*2);
Array.fill(coord2, 0);
a = 0;
b = 0;
for (y=0; y<h; y++)
{
 for (x=0; x<w; x++)
 {
  if ((getPixel(x,y) == 0) && (
      getPixel(x+1,y) == 0) && (
      getPixel(x,y+1) == 0) && (
      getPixel(x+1,y+1) != 0))
  {
   coord[a] = x+1;
   coord[a+1] = y+1;
   a+=2;
  }
  if ((getPixel(x,y) == 0) && (
      getPixel(x-1,y) == 0) && (
      getPixel(x,y-1) == 0) && (
      getPixel(x-1,y-1) != 0))
  {
   coord2[b] = x;
   coord2[b+1] = y;
   b+=2;
  }
 }
}
coord_f = newArray(counts*2);
thres_red = newArray(counts*2);
t = 0;
q = 1;
for (z=0; z<counts*2; z+=2)
{
 k=0; //contador tr+k
 selectWindow(result);
 run("Duplicate...", "title");
 makeRectangle(coord[z], coord[
     z+1], coord2[z]-coord[z],
     coord2[z+1]-coord[z+1]);
 run("Crop");
 rename("a"+q);
 title_crop = getTitle;
```

```
run("Enhance Contrast...", "
    saturated=0.5 normalize");
run("8-bit");
getRawStatistics(nPixels, mean
    , min, max);
run("Find Maxima...", "noise
    ="+max+" output=[Point
    Selection]");
getSelectionBounds(m, n, o, p)
    ;
coord_f[z] = m;
coord_f[z+1] = n;
tr = max*factor;
setThreshold(max/2, max, "B&W
    ");
run("Analyze Particles...", "
    size=0-Infinity circularity
    =0.00-1.00");
if (nResults == 0)
{
 thres_red[t] = 0;
 thres_red[t+1] = 0;
}
else
{
 if (nResults > 1)
 {
  while (nResults > 1)
  {
   run("Clear Results");
   setThreshold(tr+k, max, "B&
       W");
   run("Analyze Particles...",
        "size=0-Infinity
       circularity=0.00-1.00");
   k++;
  }
 }
 if (getResult("Area") > 2.5)
 {
  while (getResult("Area") >
      2.5)
  {
   run("Clear Results");
   setThreshold(tr+k, max, "B&
       W");
   run("Analyze Particles...",
        "size=0-Infinity
       circularity=0.00-1.00");
   k++;
  }
 }
  if (nResults > 1)
  {
   while (nResults > 1)
   {
    run("Clear Results");
    setThreshold(tr+k, max, "B&
        W");
    run("Analyze Particles...",
         "size=0-Infinity
        circularity=0.00-1.00");
    k++;
   }
  }
  thres_red[t] = tr+k;
  thres_red[t+1] = max;
 }
 t+=2; //contador array
     threshold
 q++;
}
t = 0;
q = 1;
selectWindow(title);
run("Close");
selectWindow(result);
run("Close");

//+++++GREEN CHANNEL+++++
selectWindow("C2-"+result1);
title = getTitle;
run("8-bit");
run("Add...", "value=1");
open("/Users/Juan Pablo/Desktop
    /Macros/mask1.tif");
imageCalculator("Multiply
    create", title, "mask1.tif")
    ;
result = getTitle;
selectWindow("mask1.tif");
run("Close");
selectWindow(result);
w = getWidth;
h = getHeight;
coord = newArray(counts*2);
Array.fill(coord, 0);
coord2 = newArray(counts*2);
Array.fill(coord2, 0);
a = 0;
b = 0;
for (y=0; y<h; y++)
{
 for (x=0; x<w; x++)
```

```
 {
  if ((getPixel(x,y) == 0) && (
      getPixel(x+1,y) == 0) && (
      getPixel(x,y+1) == 0) && (
      getPixel(x+1,y+1) != 0))
  {
   coord[a] = x+1;
   coord[a+1] = y+1;
   a+=2;
  }
  if ((getPixel(x,y) == 0) && (
      getPixel(x-1,y) == 0) && (
      getPixel(x,y-1) == 0) && (
      getPixel(x-1,y-1) != 0))
  {
   coord2[b] = x;
   coord2[b+1] = y;
   b+=2;
  }
 }
}
coord_v = newArray(counts*2);
t = 0;
q = 1;
for (z=0; z<counts*2; z+=2)
{
 k=0; //contador tr+k
 selectWindow(result);
 run("Duplicate...", "title");
 makeRectangle(coord[z], coord[
     z+1], coord2[z]-coord[z],
     coord2[z+1]-coord[z+1]);
 run("Crop");
 rename("b"+q);
 title_crop = getTitle;
 run("Enhance Contrast...", "
     saturated=0.5 normalize");
 run("8-bit");
 getRawStatistics(nPixels, mean
     , min, max);
 run("Find Maxima...", "noise
     ="+max+" output=[Point
     Selection]");
 getSelectionBounds(m, n, o, p)
     ;
 coord_v[z] = m;
 coord_v[z+1] = n;
 tr = max*factor;
 setThreshold(max/2, max, "B&W
     ");
 run("Analyze Particles...", "
     size=0-Infinity circularity
     =0.00-1.00");
 if (nResults == 0)
 {
  thres_red[t] = 0;
  thres_red[t+1] = 0;
 }
 else
 {
  if (nResults > 1)
  {
   while (nResults > 1)
   {
    run("Clear Results");
    setThreshold(tr+k, max, "B&
        W");
    run("Analyze Particles...",
         "size=0-Infinity
        circularity=0.00-1.00");
    k++;
   }
  }
  if ((getResult("Area") != 0)
      && (getResult("Area") >
      2.5))
  {
   while (getResult("Area") >
       2.5)
   {
    run("Clear Results");
    setThreshold(tr+k, max, "B&
        W");
    run("Analyze Particles...",
         "size=0-Infinity
        circularity=0.00-1.00");
    k++;
   }
  }
  if (nResults > 1)
  {
   while (nResults > 1)
   {
    run("Clear Results");
    setThreshold(tr+k, max, "B&
        W");
    run("Analyze Particles...",
         "size=0-Infinity
        circularity=0.00-1.00");
    k++;
   }
  }
```

```
  thres_red[t] = tr+k;
  thres_red[t+1] = max;
 }
 t+=2; //contador array
     threshold
 q++;
}
t = 0;
q = 1;
selectWindow(title);
run("Close");
selectWindow(result);
run("Close");

//+++++BLUE CHANNEL+++++
selectWindow("C3-"+result1);
title = getTitle;
run("8-bit");
run("Add...", "value=1");
open("/Users/Juan Pablo/Desktop
    /Macros/mask1.tif");
imageCalculator("Multiply
    create", title, "mask1.tif")
    ;
result = getTitle;
selectWindow("mask1.tif");
run("Close");
selectWindow(title);
run("Close");
selectWindow(result);
w = getWidth;
h = getHeight;
coord = newArray(counts*2);
Array.fill(coord, 0);
coord2 = newArray(counts*2);
Array.fill(coord2, 0);
a = 0;
b = 0;
for (y=0; y<h; y++)
{
 for (x=0; x<w; x++)
 {
  if ((getPixel(x,y) == 0) && (
      getPixel(x+1,y) == 0) && (
      getPixel(x,y+1) == 0) && (
      getPixel(x+1,y+1) != 0))
  {
   coord[a] = x+1;
   coord[a+1] = y+1;
   a+=2;
  }
  if ((getPixel(x,y) == 0) && (
      getPixel(x-1,y) == 0) && (
      getPixel(x,y-1) == 0) && (
      getPixel(x-1,y-1) != 0))
  {
   coord2[b] = x;
   coord2[b+1] = y;
   b+=2;
  }
 }
}
coord_a = newArray(counts*2);
t = 0;
q = 1;
for (z=0; z<counts*2; z+=2)
{
 k=0; //contador tr+k
 selectWindow(result);
 run("Duplicate...", "title");
 makeRectangle(coord[z], coord[
     z+1], coord2[z]-coord[z],
     coord2[z+1]-coord[z+1]);
 run("Crop");
 rename("c"+q);
 title_crop = getTitle;
 run("Enhance Contrast...", "
     saturated=0.5 normalize");
 run("8-bit");
 getRawStatistics(nPixels, mean
     , min, max);
 run("Find Maxima...", "noise
     ="+max+" output=[Point
     Selection]");
 getSelectionBounds(m, n, o, p)
     ;
 coord_a[z] = m;
 coord_a[z+1] = n;
 tr = max*factor;
 setThreshold(max/2, max, "B&W
     ");
 run("Analyze Particles...", "
     size=0-Infinity circularity
     =0.00-1.00");
 if ((nResults == 0) || (
     getResult("Area") == 0))
 {
  thres_red[t] = 0;
  thres_red[t+1] = 0;
 }
 else
 {
  if (nResults > 1)
```

```
  {
   while (nResults > 1)
   {
    run("Clear Results");
    setThreshold(tr+k, max, "B&
        W");
    run("Analyze Particles...",
         "size=0-Infinity
        circularity=0.00-1.00");
    k++;
   }
  }
  if ((getResult("Area") != 0)
      && (getResult("Area") >
      2.5))
  {
   while (getResult("Area") >
       2.5)
   {
    run("Clear Results");
    setThreshold(tr+k, max, "B&
        W");
    run("Analyze Particles...",
         "size=0-Infinity
    circularity=0.00-1.00");
    k++;
   }
  }
  if (nResults > 1)
  {
   while (nResults > 1)
   {
    run("Clear Results");
    setThreshold(tr+k, max, "B&
        W");
    run("Analyze Particles...",
         "size=0-Infinity
        circularity=0.00-1.00");
    k++;
   }
  }
  thres_red[t] = tr+k;
  thres_red[t+1] = max;
 }
t+=2; //contador array
    threshold
q++;
}
selectWindow(result);
run("Close");
t = 0;
q = 1;
run("Clear Results");
for (z=0; z<counts*2; z+=2)
{
 selectWindow("a"+q);
 run("Analyze Particles...", "
     size=0-Infinity circularity
     =0.00-1.00 display");
 run("Close");
 q++;
}
q = 1;
for (z=0; z<counts*2; z+=2)
{
 selectWindow("b"+q);
 run("Analyze Particles...", "
     size=0-Infinity circularity
     =0.00-1.00 display");
 run("Close");
 q++;
}
q = 1;
for (z=0; z<counts*2; z+=2)
{
 selectWindow("c"+q);
 run("Analyze Particles...", "
     size=0-Infinity circularity
     =0.00-1.00 display");
 run("Close");
 q++;
}
r = Array.concat(coord_f, coord
    _v);
R = Array.concat(r, coord_a);
b = 0;
for (g=0; g<2; g++) //numero de
     columnas
{
 for (j=0; j<counts*3; j++)
 {
  setResult(g, j, (R[b])*3/13);
  b+=2;
 }
 b=1;
}
updateResults();
```

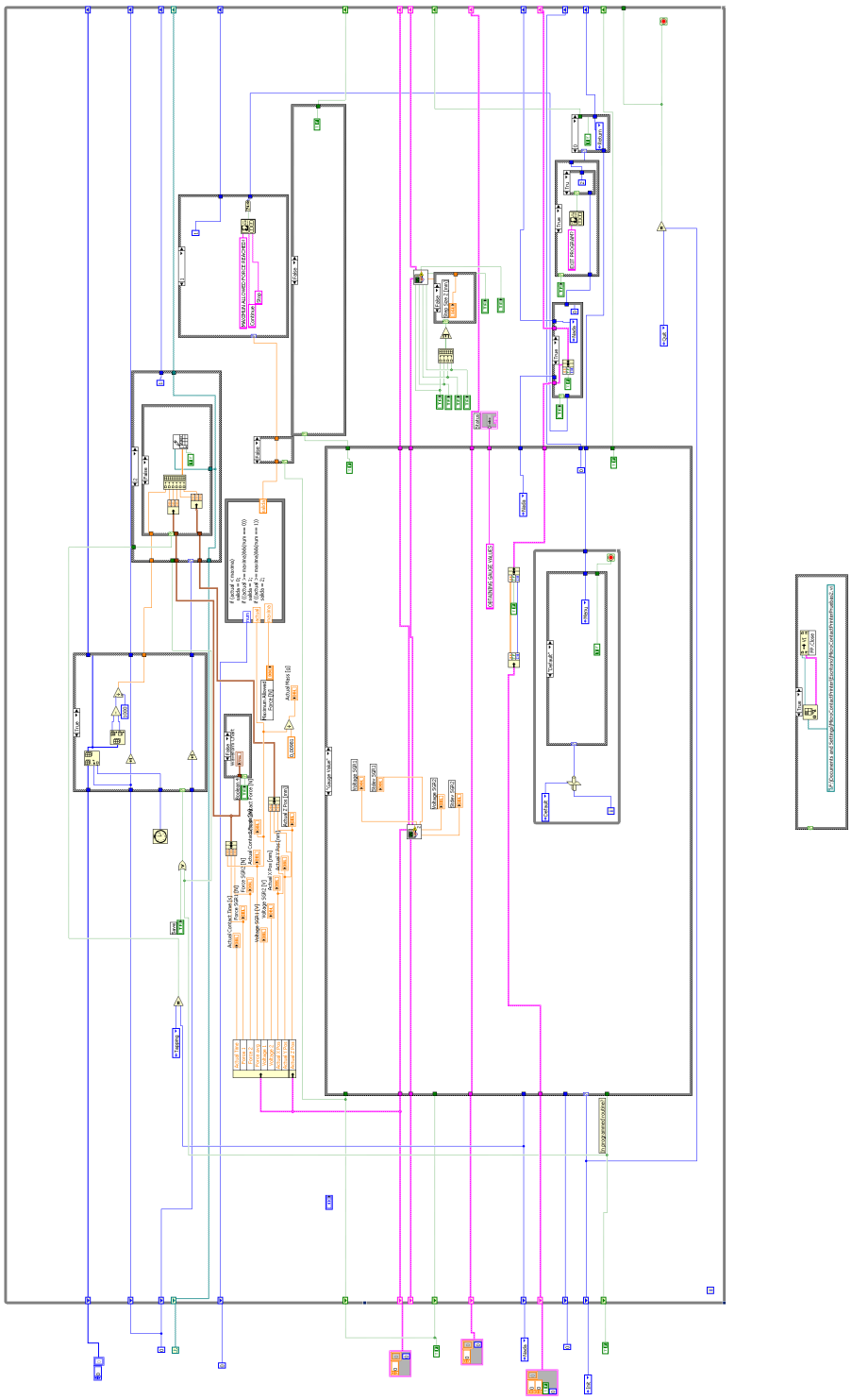

Figure A.8: **µCP tool block diagram.** Main virtual instrument (VI) from the LabVIEW© code running the sensors and actuators of the µCP tool program.

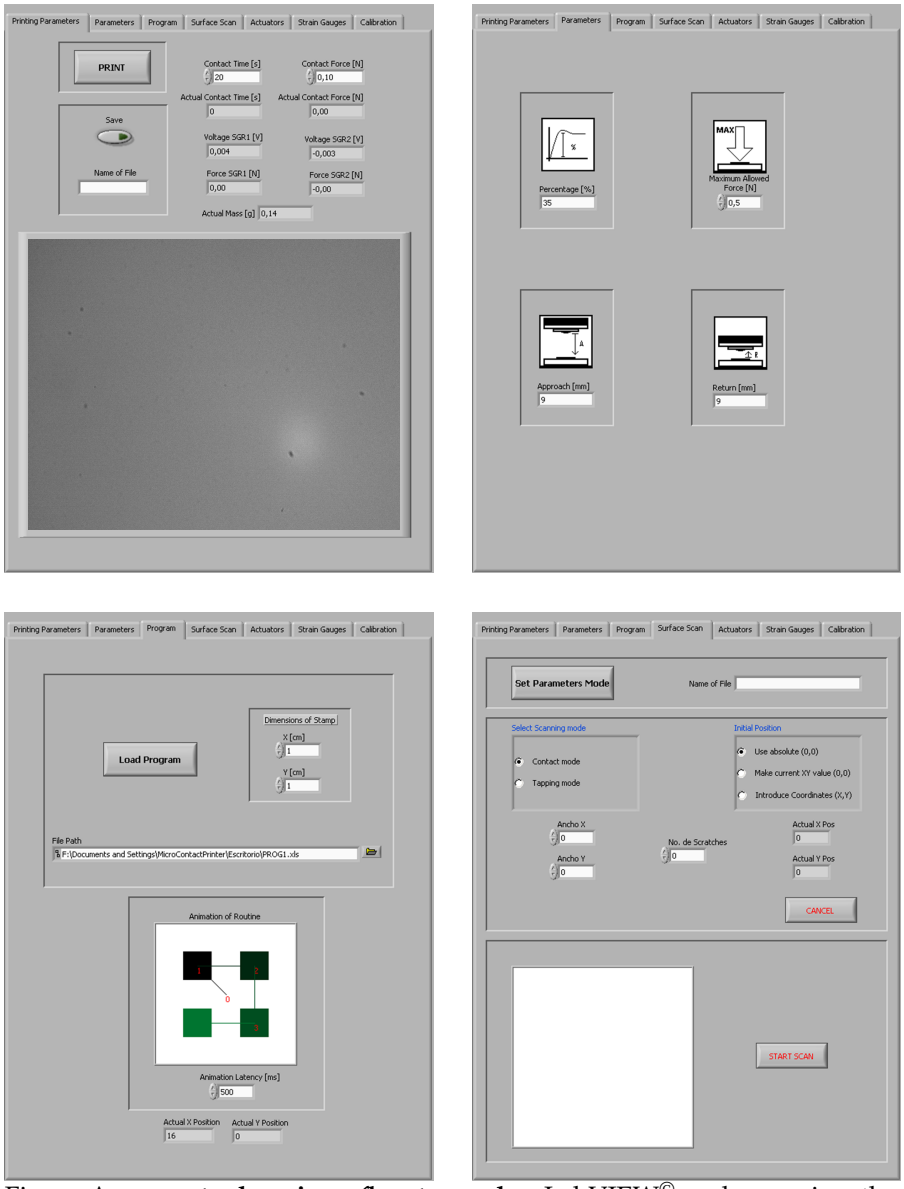

Figure A.9: **µCP tool various fIront panels.** LabVIEW© code running the sensors and actuators shown in the front panel of the µCP tool program.

The program controlling the µCP tool is based on a code written in LabVIEW©. Figure A.8 presents the internal connections between parts of the program. In Figure A.9, the top present two complementary tabs to that presented in Section 2.3.2.3. The controls and indicators on the panel on the left guide the user through the automatized printing cycle. The panel on the right contains several controls to define the maximum pressure and absolute travel distance used for the automatized printing. The bottom panels presents different controls and indicators. The panel on the left is used to insert the parameters required for the loading and correct function for multiple prints. On the right, the panel is used to introduce the parameters to fabricate micromachined substrates following a defined program.

The final μCP tool is presented in Figure A.10. In the digital photography, the components are omitted. The complete explanation follows the description shown in Figure 3.12.

Figure A.10: **Actual μCP tool.** Digital photograph of the final μCP tool.

A.4 REFERENCES

[1] Comelles Pujadas, J. *Biochemical gradients on Poly(methyl methacrylate) surfaces*. Ph.D. thesis, Universitat de Barcelona (2012)

[2] Campbell, EA; Korzheva, N; Mustaev, A; Murakami, K; Nair, S; Goldfarb, A; and Darst, SA. 'Structural mechanism for rifampicin inhibition of bacterial rna polymerase.' *Cell*, 104 (6) (2001) 901–12. URL http://www.ncbi.nlm.nih.gov/pubmed/11290327